MATHEMATICAL AND LABORATORY STUDIES OF DIFFUSION-LIMITED, ORGANIC SORPTION REACTIONS IN ATMOSPHERIC AND AQUEOUS SYSTEMS

Stewart Alan Rounds
B.S., University of Illinois, Champaign-Urbana, Illinois, 1985

A thesis submitted to the faculty of the
Oregon Graduate Institute of Science & Technology
in partial fulfillment of the requirements for the degree
of Doctor of Philosophy
in
Environmental Science and Engineering

July, 1992

The dissertation "Mathematical and laboratory studies of diffusion-limited, organic sorption reactions in atmospheric and aqueous systems" by Stewart A. Rounds has been examined and approved by the following Examination Committee:

James F. Pankow, Thesis Advisor
Professor

Terry F. Bidleman
Professor

Carl D. Palmer
Assistant Professor

William Fish
Assistant Professor

ACKNOWLEDGEMENTS

Throughout the time I spent in graduate school, many people helped to make my graduate school experience more rewarding, enlightening, productive, and enjoyable. Although too numerous to mention each of them here, I wish to express my thanks to all of those individuals.

I wish to thank my thesis advisor, Jim Pankow, for his insightful direction, encouragement, advice, financial support, patience, and friendship. His tolerance of my pursuit of tangentially-related and sometimes completely unrelated subjects was a valued gift of independence. I thank Jim for building a very strong department, always encouraging me to "take more math," and for teaching me the finer points of entering a river via a rope swing. I am truly grateful to have been a part of Jim's research group. I also thank the other members of my thesis committee, Carl Palmer, Bill Fish, and Terry Bidleman, for reviewing this work and offering insightful comments.

I thank the National Science Foundation for three years of financial support via a Graduate Fellowship. Thanks to the Oregon Department of Transportation, Sylvan Section, for access to the Vista Ridge Tunnel air sampling site. Special thanks to Bruce Tiffany, John Storey, and Lorne Isabelle for their roles in obtaining the experimental data used to examine gas/particle sorption kinetics. Thanks also to Rohm and Haas, Co. for providing XAD-7 sorbent for use in the aqueous kinetic studies. For letting me use his computers and for being NICE +0 to me, I thank Rick Johnson.

The staff at OGI truly live up to their motto of excellence (and humility). Thanks to Allan Ryall, Doug Davis, Judi Irvine, Pam Locke, Matt Perrott, Sandy Holt, Maureen Sloan, Chris Lightcap, Margaret Day, Gerry Boehme, Dave Duncan, and Donna Reed. Special thanks to Lorne Isabelle, whose experience, resourcefulness, and skill keeps the lab running, and whose sense of humor

enriches the lives of all around him. Hearty thanks also to Don Buchholz for his friendship and for patiently enduring hours of computer-related questions.

I will always be grateful to J. MacPherson for being a good friend and labmate, for showing me the ropes when I first started graduate school, for always inspiring me to work harder, and for teaching me the finer points of Ultimate frisbee. Many other students and former students also made graduate school more enjoyable, especially Bill Asher, Mike Rosen, Mike Anderson, Barbara Turpin, Ken Hart, Karel Mesuere, Mike Elovitz, John Storey, Chee Choy, Liannha Sa, Kathy McCarthy, Patty Toccalino, Leah Matheson, Tim Mayer, Jim Tesoriero, Brian Patterson, and Raimund Ege. For many hours of fun and competition, thanks to all of the members of my softball and Ultimate teams, even though nobody showed up on time and we never won any trophies.

Special thanks to my parents, who knew that I wouldn't be in school forever, even if it seemed that way. They may not understand all that I have accomplished in graduate school, but they are proud of me anyway.

Finally, the last and most important acknowledgement goes to my wife, Bernadine Bonn. She has been my colleague, companion, editor, and best friend. Her love, support, help, and encouragement was invaluable to the successful completion of this thesis.

TABLE OF CONTENTS

LIST OF FIGURES

LIST OF TABLES

ABSTRACT

Mathematical and Laboratory Studies of
Diffusion-Limited, Organic Sorption Reactions
in Atmospheric and Aqueous Systems

Stewart Alan Rounds, Ph.D.

Oregon Graduate Institute of Science & Technology, 1992
Supervising Professor: James F. Pankow

The partitioning of nonionic organic compounds in gas/particle and water/particle systems is of fundamental importance in determining their transport and ultimate fates in the environment. Knowledge of both the extent and rate of sorption reactions is necessary to properly assess the environmental behaviors of such compounds. Very little is known about the kinetics of gas/particle sorption reactions in the atmosphere. In aqueous systems, intraparticle diffusion is often implicated as a mechanism of rate-limited sorption, but previous studies have not determined the relative importance of intraparticle transport versus other diffusive processes.

The kinetics of sorption in gas/particle systems was investigated and evaluated for consistency with a diffusive rate limitation. Models of gas/particle sorption kinetics were developed using intraparticle diffusion as the rate-limiting mechanism and a porous shell/solid core representation of atmospheric particles. Sorption reactions were modeled for airborne particles and for particles captured on filters. Based on intraparticle pore diffusion, sorption reaction time scales were predicted to be on the order of minutes to hours for commonly determined compounds. The observed rates were significantly slower than predicted, although the results were consistent with intraparticle diffusion. Liquid-like

diffusion through an organic phase, solid phase diffusion, and dead-end pores were postulated as additional resistances to intraparticle transport.

Investigations of sorption kinetics in aqueous sorbent suspensions were conducted to discern the nature of the rate-limiting mechanisms. The characteristics of five mechanistic models were examined. Experiments were performed to determine the kinetics of adsorption for several chlorinated benzenes with a model sorbent (XAD-7). The ability of each of the models to describe the experimental data was assessed. A dual resistance model, coupling both external film diffusion and intraparticle diffusion in series, provided the best description of the data. External film diffusion was found to dominate the adsorption kinetics, while intraparticle diffusion contributed only a minor resistance. Prior to this work, film diffusion had been discounted as an important rate-limiting mechanism. These data suggest that film diffusion must be reconsidered as an important, and possibly dominating, mechanism of rate-limited sorption in natural waters.

CHAPTER I

Introduction

Background

Adsorption and desorption are fundamental processes that affect the transport and fate of almost all organic compounds in the environment. Because many processes in natural systems are coupled to partitioning processes, a clear understanding of the rates and equilibrium positions of sorption reactions will also contribute to the study of other important processes. Sorption can affect biodegradation rates (*1-2*), inhibit or accelerate chemical and photochemical reactions (*3-6*), retard or facilitate transport in groundwater (*7-8*), influence long range atmospheric transport and deposition (*9-10*), complicate site remediations (*11*), and affect estimates of the ecological and health effects of pollutants (*12-13*).

The factors that affect sorption equilibrium in aqueous and atmospheric environments have been characterized fairly well. Sorption of nonionic organic compounds in aqueous systems is dominated by a partitioning process in which the solute is proposed to actually dissolve into the organic fraction of the sorbent (*14-15*). The adsorption of such compounds on inorganic materials in soils or sediments is negligible because water easily displaces those solutes from mineral surfaces (*16*). According to partitioning theory, equilibrium concentrations of nonionic organic compounds in the solid phase are linearly related to their aqueous-phase concentrations. Linear partitioning theory also has been applied successfully to the distribution of organic compounds between the gas and

particulate phases in the atmosphere (*17*). A theoretical consideration of gas/particle partitioning (*18*) has shown that the linear partition coefficient is related to particle properties such as the aerosol surface area and compound properties such as the subcooled liquid vapor pressure and the difference between the enthalpies of desorption and vaporization.

Although important, knowledge of the equilibrium phase distribution of a particular compound may not be sufficient to fully describe its sorption behavior. To accurately predict the behavior of a compound in the environment, the mechanisms that control its approach to sorption equilibrium must also be characterized. Sorption kinetics in aqueous systems is often described by a fast initial exchange followed by a very slow uptake or release of sorbate. Time scales for the reaction can be very long, ranging from days to weeks or even years in certain cases (*1, 19-21*). Because the sorption of nonionic organic compounds in aqueous systems is characterized by very weak forces, it is generally recognized that chemical reactions such as chemisorption cannot be responsible for rate-limited sorption. In chemisorption, strong chemical bonds are formed between sorbate and sorbent. Consequently, diffusion-limited transport has been implicated as the slow step in sorption interactions. A moderate amount of success has been achieved by modeling aqueous sorption kinetics with intraparticle diffusion (e.g. 22-23).

Very little work has been done to characterize the time scales of sorption reactions in gas/particle systems of environmental significance. Reported results suggest that sorption to fly ash particles is quite rapid and requires only minutes to achieve equilibrium (*24*). The kinetics of sorption for urban particulate matter is expected to be slower due to the stronger partitioning to such particles. Kinetic studies using urban particles, however, have been limited to those concerned with desorption losses from filter-bound particles (e.g. *25*). In such systems, rate-limited sorption is partially masked by the kinetics associated simply with the capacity of the air flow to transport material to and from the filter; the data analysis required to isolate the sorption kinetics has never been

performed. A diffusive rate limitation was implicated in the previously-mentioned study of organic sorption to fly ash particles. For environmentally-significant particulate material, only one theoretical investigation of diffusion-limited sorption kinetics could be found. In that study, estimated reaction time scales were on the order of minutes to hours (*13*).

For many years, diffusion has been known to control the rates of many types of reactions. Ion exchange was shown to be a diffusion-limited reaction as long ago as 1947 by Boyd *et al.* (*26*). Chemical engineers have long studied the effect of diffusion on reaction rates in porous catalysts (*27*). Environmental engineers have known for forty years that the sorption rates of many organic compounds to activated carbon were controlled by diffusive intraparticle transport (*28-29*). The importance of diffusion in these very similar processes lends support for the idea of diffusive rate control for sorption in natural systems.

Although much support has been offered for a diffusive rate limitation, the nature of that process is still not clearly defined. Diffusive rate control can manifest itself in any of several different forms. Intraparticle diffusion, the most commonly implicated rate limitation, can be the result of diffusion both within the particle pores (pore diffusion) and along the walls of those pores (surface diffusion). Solid phase diffusion or diffusion through the polymer-like matrix of organic matter (intraorganic matter diffusion, *30*) might also significantly contribute to the intraparticle rate-limitation. External to the particles, diffusion across a boundary layer (film diffusion) at the particle surface can exert a significant resistance to mass transport.

Objectives

The objective of this research was to characterize the importance of diffusion as a rate-limiting mechanism of sorption in both atmospheric and aqueous systems. It was particularly important to assess the ability of each of the different types of diffusion to control the sorption rate. Because so little is

known about sorption kinetics in gas/particle systems, it was felt that it was valuable to show simply that a diffusive rate-limitation is consistent with experimental data. Speculations could then be made concerning the probable nature of that diffusive process. For aqueous suspensions of a sorbent, since intraparticle diffusion has so often been implicated in previous studies, the goal was to probe the exact nature of the rate-limiting mechanism. An assessment of the relative importance of intraparticle diffusion versus external film diffusion would provide valuable information upon which to build models of environmental fate and transport.

Models of diffusion-limited sorption were developed to provide theoretical predictions of sorption reaction time scales. The characteristics of the models were investigated. Experiments were conducted to determine the kinetics of sorption in selected atmospheric and aqueous systems. The ability of the sorption models to describe the experimental data was then assessed. Fitted rate parameters were probed for insight concerning the nature of the rate-limiting mechanisms at the microscopic level. Mechanistic information is extremely valuable and without a doubt will be the most important contribution of this work.

Overview

Chapter Two through Chapter Five were written in the form of research papers; each chapter contains an independent abstract, introduction, summary, and reference section. Chapter Two and Chapter Three consider the kinetics of sorption in gas/particle systems. Chapter Four develops the analytical methodology that is needed to perform the experiments discussed in Chapter Five. The kinetics of sorption in aqueous sorbent suspensions is the subject of Chapter Five.

In Chapter Two, a radial intraparticle diffusion model is adapted to describe gas/particle sorption kinetics for both airborne particles and particle-laden filters. A porous shell/solid core model is proposed as a rough description

of particles that are not completely porous. The characteristics of the intraparticle diffusion model are examined. Diffusion reaction time scales are estimated. Mass transfer time scales are defined. The probability and magnitude of sorption-related artifacts for field-derived values of the gas/particle partition coefficient are assessed for compounds of different volatility.

In Chapter Three, the filter-based intraparticle diffusion model is tested with experimental data. Particulate matter was collected on a filter. Organic compounds associated with the particulate phase were then desorbed over time in a controlled experiment. The experimental data were fitted to the model using two fitting parameters. The ability of the model to describe the data is discussed. The optimized fitting parameters are probed for insight concerning the possible rate-limiting processes and the physical properties of atmospheric particles. Estimates of diffusion reaction time scales are re-examined. The role of rate-limited sorption in the expression of sampling artifacts is explored.

Chapter Four describes the analytical method employed in Chapter Five to determine the concentrations of chlorinated benzenes in aqueous samples. This gas chromatographic method is an adaptation of the purge with whole column cryotrapping method (P/WCC, *31*) for use with an electron capture detector. Purge gas desiccation is effected with a glass-bead water trap (*32*). Theoretical purging efficiencies are analyzed and compared to experimentally obtained values. This method combines the simplicity and high reliability of the P/WCC method with the exceptional sensitivity of an electron capture detector.

In Chapter Five, various mechanistic and empirical models of sorption kinetics in aqueous sorbent suspensions are examined and compared. The characteristics of four diffusion-based models, a particle abrasion model, and two implementations of a first order reaction model are investigated. The kinetics for the adsorption of several chlorinated benzenes to a model sorbent (XAD-7) was measured experimentally. Each of the diffusion-based models and the particle abrasion model were fitted to the data to gain insight concerning the most important rate-limiting mechanisms. The relative importance of film

diffusion versus intraparticle diffusion in aqueous sorbent suspensions is assessed.

Chapter Six is a summary of the conclusions reached in each of the previous chapters. In addition, areas of further research are identified. In Appendices A and C, the experimental data from the filter desorption and the aqueous adsorption experiments, respectively, are presented. During this investigation of sorption kinetics, a great number of computer programs were developed. The source codes of the most important programs are listed in Appendices B and D.

The material discussed in Chapter Two was published in a modified form in the September, 1990 issue of *Environmental Science & Technology* (33). The filter desorption research presented in Chapter Three has been submitted to *Environmental Science & Technology* in a modified form (34). Bruce Tiffany is a co-author on that paper. A discussion of the analytical method presented in Chapter Four has been submitted to *Journal of High Resolution Chromatography* (35). The research presented in Chapter Five has not yet been prepared for publication.

Literature Cited

(1) Steinberg, S. M.; Pignatello, J. J.; Sawhney, B. L. *Environ. Sci. Technol.* **1987**, *21*, 1201-1208.

(2) Rijnaarts, H. H. M.; Bachmann, A.; Jumelet, J. C.; Zehnder, A. J. B. *Environ. Sci. Technol.* **1990**, *24*, 1349-1354.

(3) Fox, M. A.; Olive, S. *Science* **1979**, *205*, 582-583.

(4) Grosjean, D.; Fung, K.; Harrison, J. *Environ. Sci. Technol.* **1983**, *17*, 673-679.

(5) Yokley, R. A.; Garrison, A. A.; Wehry, E. L.; Mamantov, G. *Environ. Sci. Technol.* **1986**, *20*, 86-90.

(6) Kamens, R. M.; Karam, H.; Guo, J.; Perry, J. M.; Stockburger, L. *Environ. Sci. Technol.* **1989**, *23*, 801-806.

(7) Mackay, D. M.; Roberts, P. V.; Cherry, J. A. *Environ. Sci. Technol.* **1985**, *19*, 384-392.

(8) McCarthy, J. F.; Zachara, J. M. *Environ. Sci. Technol.* **1989**, *23*, 496-502.

(9) Kurtz, D. A., Ed. *Long Range Transport of Pesticides*; Lewis Publishers: Chelsea, MI, 1990.

(10) Bidleman, T. F. *Environ. Sci. Technol.* **1988**, *22*, 361-367.

(11) Mackay, D. M.; Cherry, J. A. *Environ. Sci. Technol.* **1989**, *23*, 630-636.

(12) Harris, H. J.; Sager, P. E.; Regier, H. A.; Francis, G. R. *Environ. Sci. Technol.* **1990**, *24*, 598-603.

(13) Gerde, P.; Scholander, P. *Environ. Health Perspectives* **1989**, *79*, 249-258.

(14) Chiou, C. T.; Peters, L. J.; Freed, V. H. *Science* **1979**, *206*, 831-832.

(15) Chiou, C. T.; Porter, P. E.; Schmedding, D. W. *Environ. Sci. Technol.* **1983**, *17*, 227-231.

(16) Chiou, C. T.; Shoup, T. D. *Environ. Sci. Technol.* **1985**, *19*, 1196-1200.

(17) Yamasaki, H.; Kuwata, K.; Miyamoto, H. *Environ. Sci. Technol.* **1982**, *16*, 189-194.

(18) Pankow, J. F. *Atmos. Environ.* **1987**, *21*, 2275-2283.

(19) Karickhoff, S. W. *J. Hydraul. Eng.* **1984**, *110*, 707-735.

(20) Karickhoff, S. W.; Morris, K. R. *Environ. Toxicol. Chem.* **1985**, *4*, 469-479.

(21) Coates, J. T.; Elzerman, A. W. *J. Contam. Hydrol.* **1986**, *1*, 191-210.

(22) Wu, S.-C.; Gschwend, P. M. *Environ. Sci. Technol.* **1986**, *20*, 717-725.

(23) Ball, W. P.; Roberts, P. V. *Environ. Sci. Technol.* **1991**, *25*, 1237-1249.

(24) Rothenberg, S. J.; Mettzler, G.; Poliner, J.; Bechtold, W. E.; Eidson, A. F.; Newton, G. J. *Environ. Sci. Technol.* **1991**, *25*, 930-935.

(25) Miguel, A. H.; de Andrade, J. B.; Hering, S. V. *Intern. J. Environ. Anal. Chem.* **1986**, *26*, 265-278.

(26) Boyd, G. E.; Adamson, A. W.; Meyers, L. S. *J. Am. Chem. Soc.* **1947**, *69*, 2836-2848.

(27) Satterfield, C. N. *Mass Transfer in Heterogeneous Catalysis*; R. E. Krieger Pub. Co.: Malabar, FL, 1981.

(28) Eagle, S.; Scott, J. W. *Ind. Eng. Chem.* **1950**, *42*, 1287-1294.

(29) Edeskuty, F. J.; Amundson, N. R. *Ind. Eng. Chem.* **1952**, *44*, 1698-1703.

(30) Brusseau, M. L.; Jessup, R. E.; Rao, P. S. C. *Environ. Sci. Technol.* **1991**, *25*, 134-142.

(31) Pankow, J. F.; Rosen, M. E. *Environ. Sci. Technol.* **1988**, *22*, 398-405.

(32) Pankow, J. F. *Environ. Sci. Technol.* **1991**, *25*, 123-126.

(33) Rounds, S. A.; Pankow, J. F. *Environ. Sci. Technol.* **1990**, *24*, 1378-1386.

(34) Rounds, S. A.; Tiffany, B. A.; Pankow, J. F. submitted to *Environ. Sci. Technol.* **1992**.

(35) Rounds, S. A.; Pankow, J. F. submitted to *J. High Res. Chromatog.* **1992**.

CHAPTER II

The Application of a Radial Diffusion Model to Describe Gas/Particle Sorption Kinetics

Abstract

A radial diffusion model is adapted to describe the kinetics of the exchange of organic compounds between the gas and particulate phases in the atmosphere. A Crank-Nicolson finite difference scheme with variable time stepping is used in applying the model to polydisperse particle size distributions. Two sets of conditions are simulated: (1) airborne particles, as in the ambient atmosphere, and (2) filter-bound particles, such as those found in an air filtration apparatus. The time scale of the intraparticle diffusion reaction, T_D, is greatly dependent upon the atmospheric partition coefficient of the compound, K_p ($m^3/\mu g$), and the particle size distribution of the aerosol. For most compounds typically determined in atmospheric samples, sorption equilibrium with airborne particles is approached rapidly. Sorption reactions that take place on/in filters are controlled not only by T_D but also by an equilibrium mass transfer time scale T_M which is a function of K_p, the amount of particulate mass M_p, and the volumetric flow rate f. The kinetics of sorption reactions on/in filters is predicted to play an important role in the determination of both the probability and the magnitude of sorption related artifacts within field-derived values of K_p.

Introduction

The transport, fate, and health effects of atmospheric pollutants depend in large part upon whether those pollutants are associated with the gas phase or with the particulate phase. In general, the distribution of a compound between the gas and particulate phases depends upon the vapor pressure of the compound, the ambient temperature, and the volume concentration of atmospheric particulate matter. For urban atmospheric particulate matter, the dependence on the latter two variables has been placed in the context of a linear Langmuir model by Yamasaki *et al.* (*1*), leading to

$$\log K = \log \frac{A \cdot TSP}{F} = \frac{m}{T} + b \qquad (2.1)$$

where K is an atmospheric partition coefficient ($\mu g/m^3$), A is the gas-phase concentration of the compound (ng/m^3), TSP is the total suspended particulate matter concentration ($\mu g/m^3$), F is the concentration of analyte associated with the particulate phase (ng/m^3), and T is the absolute temperature. The parameters m and b are compound-dependent constants. In a recent review of the theories of equilibrium partitioning in the atmosphere, Pankow (2) has shown that the parameter b includes the dependence of K on the compound's subcooled liquid vapor pressure, p_L^o.

The partition coefficient K as defined by Yamasaki *et al.* (*1*) is the inverse of the usual form for a distribution coefficient. Normally, gas/solid partition coefficients are defined such that an increase in the coefficient results in more "partitioning" to the solid phase. As defined in equation (2.1), an *increase* in the partition coefficient *decreases* the partitioning. To avoid this counterintuitive notation, Pankow (3) has proposed the use of a redefined partition coefficient K_p ($m^3/\mu g$) such that

$$K_p = \frac{F}{A \cdot TSP} = \frac{1}{K} \tag{2.2}$$

To emphasize the fact that equation (2.2) represents a simple distribution of a compound between two phases, K_p may be written as the ratio of the concentration of analyte in the particulate phase (F/TSP (ng/μg)) to its concentration in the gas phase (A (ng/m^3)).

$$K_p = \frac{F}{A \cdot TSP} = \frac{F/TSP}{A} \tag{2.3}$$

Recent work by Bidleman and co-workers (*4-6*) has supported the Yamasaki approach for a set of organochlorine compounds and polycyclic aromatic hydrocarbons (PAHs). Ligocki and Pankow (*7*) also used this model successfully to describe the equilibrium partitioning of PAHs. Furthermore, Bidleman and co-workers (*4,8*) and Ligocki and Pankow (*7*) have found that these compound-dependent partition coefficients are remarkably independent of the source of the particulate matter.

Although much support for the linear Langmuir model has been generated, some evidence suggests that deviations can occur, especially at low surface coverages. In a study of the distribution of PAHs between the gas and particulate phases in Portland, Oregon, Ligocki and Pankow (*7*) found that compounds with relatively high values of p_L^o exhibited significant positive deviations from the expected values of K_p. An identical behavior was observed by Hart (*9*) for a set of *n*-alkanes. As one possible explanation for this deviation, Ligocki and Pankow (*7*) and Pankow (*10*) have postulated that a fraction of the particle-associated compound may be "non-exchangeable," i.e., incapable of exchange with the gas phase. The amount of non-exchangeable material is expected to depend on the nature, source, and age of the particulate matter as well as the properties of the compound. This type of result is consistent with a classic two-site model in which the sorbed material is divided into two

fractions, one of which is assumed to exchange freely with the non-sorbed phase, while the other is assumed to be bound comparatively tightly to the particulate phase, and cannot desorb within the time scale of interest. The observed deviations may therefore be examples of non-equilibrium behavior.

Partition coefficients of the type discussed above are frequently calculated using values of *A*, *F*, and *TSP* measured by the simultaneous collection of particulate matter on filters, and gas-phase compounds on polyurethane foam (PUF) or another type of sorbent. During the time in which a sample is collected, however, several physical processes may act to modify the gas/particle distribution of the compounds within the sampling apparatus, thereby introducing artifacts into the measured values of *A* and *F*. Two such processes that have been hypothesized to cause sampling artifacts are the desorption of sorbed compounds from filter-bound particles (*11*), and the adsorption of gas-phase compounds onto collected particles (*4,6*) and filters (*12*). For example, during laboratory experiments in which constant concentrations of analytes were passed through particle-laden filters, Foreman and Bidleman (*5*) observed that the downstream gas-phase concentrations of some compounds did not stabilize rapidly. The observed stabilization time, up to 30 hours in one case, was attributed to slow adsorption of the compounds by filter-bound particles. Despite the frequency with which adsorption/desorption artifacts have been invoked to explain experimental data, however, no attempts have been made to determine the extent to which sorption kinetics might limit the rates of these processes.

This study is a first attempt to develop guidelines for predicting when the application of an equilibrium partitioning model is appropriate for atmospheric systems, and when sorption kinetics must be considered. The time scales of atmospheric sorption reactions are important to predictions of long-range transport, deposition and washout processes, reaction kinetics on/in particles, and the health effects of particle-associated compounds. To explore the time scales of atmospheric sorption reactions, the uptake and release of organic

compounds by atmospheric particles was simulated using a radial diffusion model. In addition, the kinetics of sorption reactions which may occur on/in the filters of air sampling equipment was investigated using a similar diffusion-based model together with face velocities and sampling times that are typical of high-volume air sampling. Finally, the implications of non-equilibrium sorption behavior during aerosol collection on the determination of ambient gas- and particulate-phase concentrations are discussed.

The Radial Diffusion Model

Development. The model used in this study describes the diffusive uptake or release of a gas-phase organic compound by atmospheric particles. Similar models were developed more than 35 years ago to describe the kinetics of ion exchange or absorption in batch reactors (*13*) and in fixed beds (*14-15*). The application of such models to environmental problems, however, has only recently received widespread attention (*16-18*), and then only in aqueous systems.

This study is the first to simulate general atmospheric sorption kinetics with a radial diffusion model. Many assumptions are inherent in the formulation of this model. Diffusion into and out of the particles is assumed to be the only rate-limiting process. Thus, mass transport in the air is assumed to be sufficiently rapid that the gas-phase concentration of the compound is uniform up to the external surfaces of the particles. In light of available specific surface area measurements for urban aerosols (*19*), most atmospheric particles are probably not fully porous. In addition, the consideration of particles that are only fractionally porous is more consistent with the appearance of scanning electron micrographs of aerosol particles (e.g. *20*). Therefore, the particles are assumed to be spherical and to have a nonporous, nonsorbing inner core surrounded by a uniformly porous, sorbing outer shell (Figure 2.1).

Given the fractional particle volume which is porous, α, the radius of the inner core is

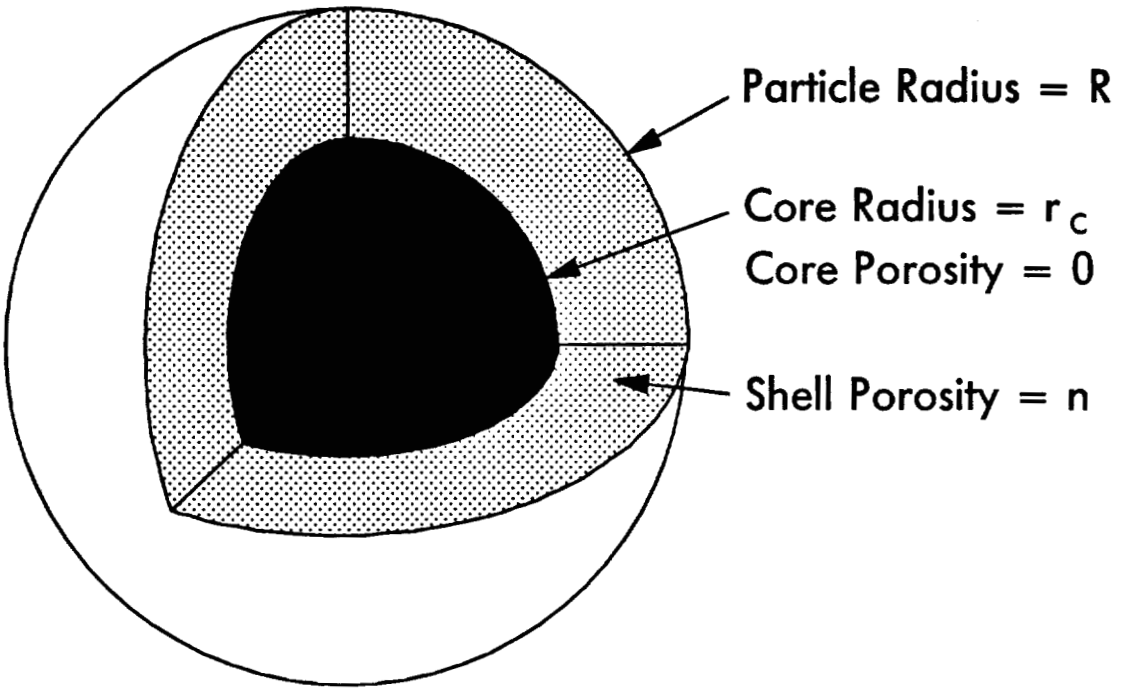

Figure 2.1. Cut-away drawing of a spherical particle characterized by a nonporous core and a porous outer shell.

$$r_c = R(1-\alpha)^{1/3} \tag{2.4}$$

where R is the radius of the particle. The value of α is nonzero, and is assumed to be constant for all particle sizes. All particles are assumed to have identical sorption properties; therefore, the K_p of a compound does not vary from one particle to another, regardless of size. Finally, sorption within the micropores of each particle is assumed to be reversible, instantaneous, and described by the linear Langmuir isotherm of Yamasaki *et al.* (*1*). Although this diffusion model is somewhat simplistic, and does not exactly describe the true shape, porosity, or heterogeneity of atmospheric particulate matter, the hope is that the model simulates reality *sufficiently closely* that its predictions can offer meaningful guidance.

The mathematical formulation of this model is similar to that of the radial diffusion model proposed by Wu and Gschwend (*16*) to describe the rate-limited sorption of hydrophobic organic compounds in soil/water and sediment/water systems. Because the particles in our model are not necessarily completely porous, however, a portion of the development of this model differs from that of Wu and Gschwend (*16*).

In spherical coordinates, the governing equation for diffusion is

$$\frac{\partial S(r)}{\partial t} = \frac{D_m n}{\tau}\left[\frac{\partial^2 A'(r)}{\partial r^2} + \frac{2}{r}\frac{\partial A'(r)}{\partial r}\right] \tag{2.5}$$

where $S(r)$ is the total volumetric concentration of the compound at a radial distance r from the center of a particle, $r > r_c$. The volumetric concentration of the compound in the micropores of a particle is $A'(r)$, D_m is the molecular diffusion coefficient of the compound in air, n is the intraparticle porosity of the porous shell (void volume in the shell per total volume of the shell), τ is a tortuosity factor that relates the actual diffusion length to the thickness of the porous shell, and t is the time. Gas-phase pore diffusion is assumed to be the

predominant mechanism for intraparticle transport. Transport due to surface diffusion is assumed to be negligible.

Local equilibrium is assumed to exist within the micropores of the particles. For linear equilibrium sorption, the concentration of analyte associated with the solid phase as a function of radial distance is given by

$$S'(r) = A'(r) \cdot K_p' \tag{2.6}$$

where $S'(r)$ is the concentration of analyte associated with the solid phase (mass/mass) at a distance r from the center of a particle and K_p' is a modified partition coefficient. Because only the outer shell of each particle is involved in sorption, the measured value of the partition coefficient K_p must be corrected to exclude the fraction of the total particulate mass which is nonporous and therefore not able to sorb. This correction is a simple function of α and n, and represents the ratio of the total particulate mass to the mass of the porous shell. The modified partition coefficient, then, is related to the measured value by

$$K_p' = K_p \frac{1-\alpha n}{\alpha(1-n)} \tag{2.7}$$

If the total volumetric concentration of the compound in the particle at radius r is defined as

$$S(r) = \rho_s(1-n)S'(r) + nA'(r) \tag{2.8}$$

where ρ_s is the specific density of the particulate matter, then $S(r)$ in terms of $A'(r)$ is

$$S(r) = \rho_s(1-n)K_p' A'(r) + nA'(r) = \left[\rho_s(1-n)K_p' + n\right]A'(r) \tag{2.9}$$

Substituting equation (2.7) into equation (2.9) gives

$$S(r) = \left[\rho_s K_p \frac{1-\alpha n}{\alpha} + n \right] A'(r) \tag{2.10}$$

Solving for $A'(r)$ and substituting into equation (2.5) yields

$$\frac{\partial S(r)}{\partial t} = \frac{D_m \alpha n / \tau}{\rho_s K_p (1-\alpha n) + \alpha n} \left[\frac{\partial^2 S(r)}{\partial r^2} + \frac{2}{r} \frac{\partial S(r)}{\partial r} \right] \tag{2.11}$$

$$\frac{\partial S(r)}{\partial t} = D_{eff} \left[\frac{\partial^2 S(r)}{\partial r^2} + \frac{2}{r} \frac{\partial S(r)}{\partial r} \right] \tag{2.12}$$

where D_{eff} is an effective diffusion coefficient. The tortuosity factor can be assumed to be equal to the inverse of the intraparticle porosity (*16*).

$$\tau \approx \frac{1}{n} \tag{2.13}$$

The effective diffusion coefficient, then, is constant within the porous shell and is given by

$$D_{eff} = \frac{D_m \alpha n^2}{\rho_s K_p (1-\alpha n) + \alpha n} \approx \frac{D_m \alpha n^2}{\rho_s K_p (1-\alpha n)} \tag{2.14}$$

If units of g/cm^3 are utilized for ρ_s, then

$$D_{eff} = \frac{D_m \alpha n^2}{\rho_s K_p (1-\alpha n) 10^{12} + \alpha n} \approx \frac{D_m \alpha n^2}{\rho_s K_p (1-\alpha n) 10^{12}} \tag{2.15}$$

where K_p is in m^3/μg, and D_m and D_{eff} are expressed in cm^2/s.

Solution Technique. Equation (2.12) can be solved analytically for a monodisperse particle size distribution. Solutions of this type for several sets of boundary conditions have been documented by Crank (*21*). For polydisperse particle size distributions such as those encountered in the atmosphere, however, a numerical solution is necessary. Wu and Gschwend (*22*) used an Euler explicit finite difference method to model polydisperse distributions

suspended in aqueous systems. In this study, a Crank-Nicolson (C-N) finite difference scheme was developed to solve the diffusion equation. Although the C-N method is computationally more intensive than the explicit technique, it possesses distinct advantages. In particular, the C-N method is unconditionally stable and has a truncation error on the order of $(\Delta t)^2$. Larger time steps can be used (23), and the time step can be increased as the simulation proceeds. The Crank-Nicolson formulation can complete a simulation with fewer time steps and in less CPU time than the explicit technique, and with no **significant** loss of accuracy.

Model Compounds and Parameter Estimation

The uptake and release kinetics of four model compounds characterized by a range of K_p values were simulated in this study. The four compounds are pyrene, chrysene, hexachlorobenzene (HCB), and 2,2-bis(4-chlorophenyl)-1,1-dichloroethene (p,p'-DDE). At typical urban *TSP* levels, HCB resides almost exclusively in the gas phase, while chrysene is predominantly associated with the particulate phase. Pyrene and DDE have intermediate partition coefficients, but are expected to be found primarily in the gas phase. Because K_p varies over several orders of magnitude within this group, the results of these simulations apply to compounds with a wide range of sorption properties.

Gas-phase molecular diffusion coefficients were estimated by the method of Wilke and Lee, as outlined by Lyman *et al.* (24). Values of K_p for HCB, DDE, and pyrene were taken from laboratory data (T = 20°C) compiled by Foreman and Bidleman (5). The K_p value for chrysene was estimated based on data from Ligocki and Pankow (7). Effective diffusion coefficients were calculated using equation (2.15), assuming ρ_s = 2.0 g/cm^3 and n = 0.50. Typical urban gas-phase concentrations for these compounds were used in the simulations, and were taken from Bidleman and co-workers (4-5) and from Ligocki and Pankow (7). These parameters are summarized in Table 2.1, where D_{eff} is given for fully porous particles (α = 1.0). The classic Pasadena aerosol, as described by Whitby

et al. (*25*), was used as the atmospheric particle size distribution. The volume distribution of this aerosol is depicted in Figure 2.2.

Table 2.1. Sorption Parameters for Model Compounds.

compound	K_p ($m^3/\mu g$)	D_m (cm^2/s)	D_{eff} (cm^2/s)	A (ng/m^3)
HCB	1.47×10^{-6}	0.058	9.8×10^{-9}	0.3
DDE	2.22×10^{-4}	0.050	5.6×10^{-11}	0.1
Pyrene	3.57×10^{-4}	0.058	4.1×10^{-11}	15.0
Chrysene	1.00×10^{-1}	0.049	1.2×10^{-13}	2.0

Model 1. Gas/Particle Distributions in the Atmosphere

Formulation. The first system of interest is that of particulate matter suspended in the atmosphere. In this model, a gas/particle system is allowed to proceed toward equilibrium for specific values of K_p, TSP, α, and initial values for A and F. Initially, the fraction of analyte which is particle-associated is assumed to be distributed uniformly throughout the particulate phase, and the sorbed fraction is assumed to be in equilibrium with an intraparticle gas-phase concentration A_o, where $A_o \neq A$. In other words, particles which initially are at sorption equilibrium with a compound whose gas-phase concentration is A_o are forced to adjust to a new gas-phase concentration A.

Verification. To ensure the predictive accuracy of the model, the results of simulations for a simple monodisperse aerosol were compared to the predictions of the analytical solution described by Crank (*21*). This comparison is shown in Figure 2.3 for $D_{eff} = 4.1 \times 10^{-11}$ cm^2/s, $K_p = 3.57 \times 10^{-4}$ $m^3/\mu g$, $TSP = 50$ $\mu g/m^3$, $\alpha = 1.0$, $A = 15$ ng/m^3, $A_o = 0$ ng/m^3, and $R = 0.375$ μm. The numerical solution used 21 nodes per particle. The curves in Figure 2.3 are plotted against the dimensionless time, t/T_D, where T_D is the diffusion reaction time scale and is defined as

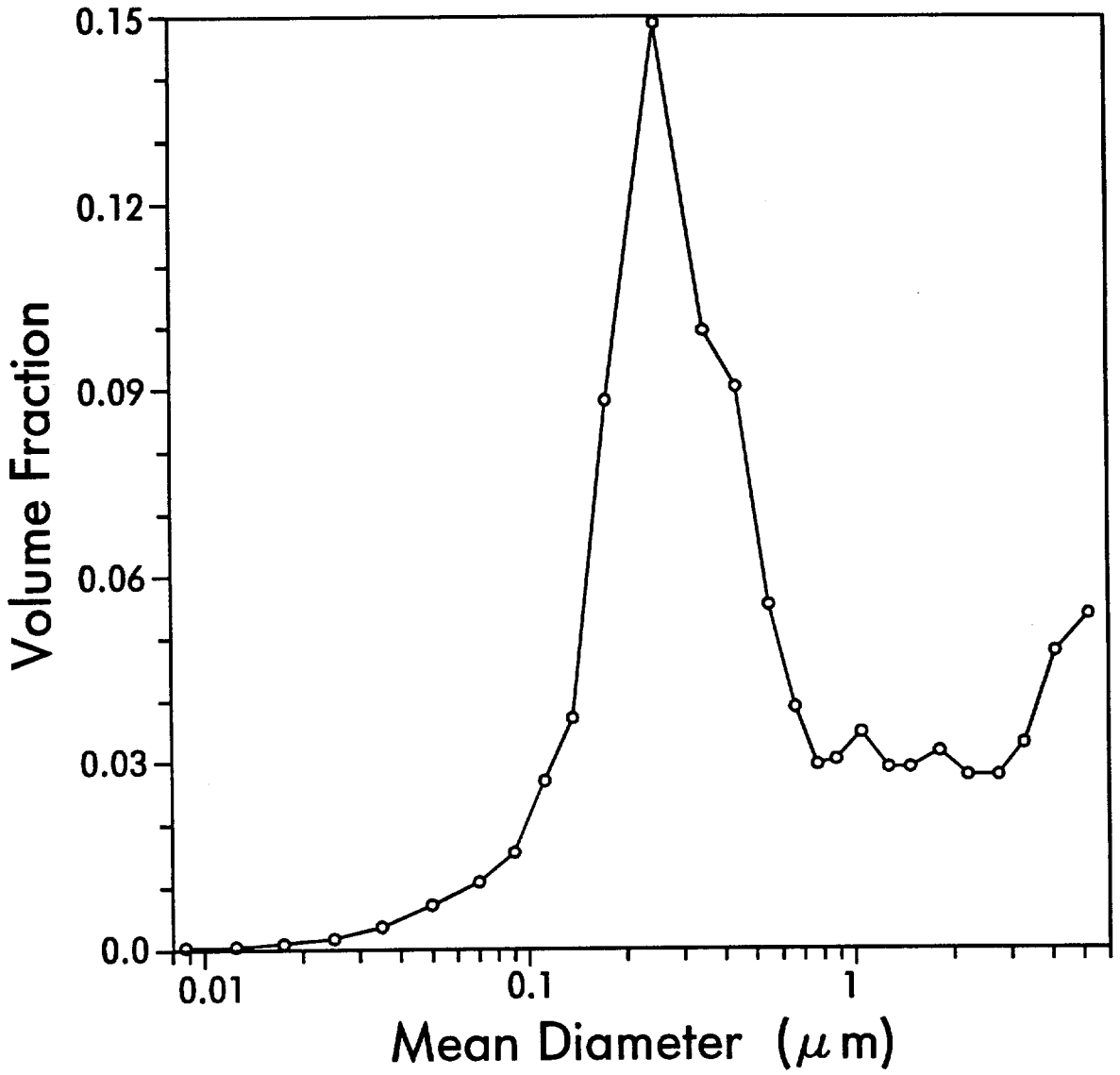

Figure 2.2. Volume distribution of particles in the classic Pasadena aerosol as described by Whitby *et al.* (25).

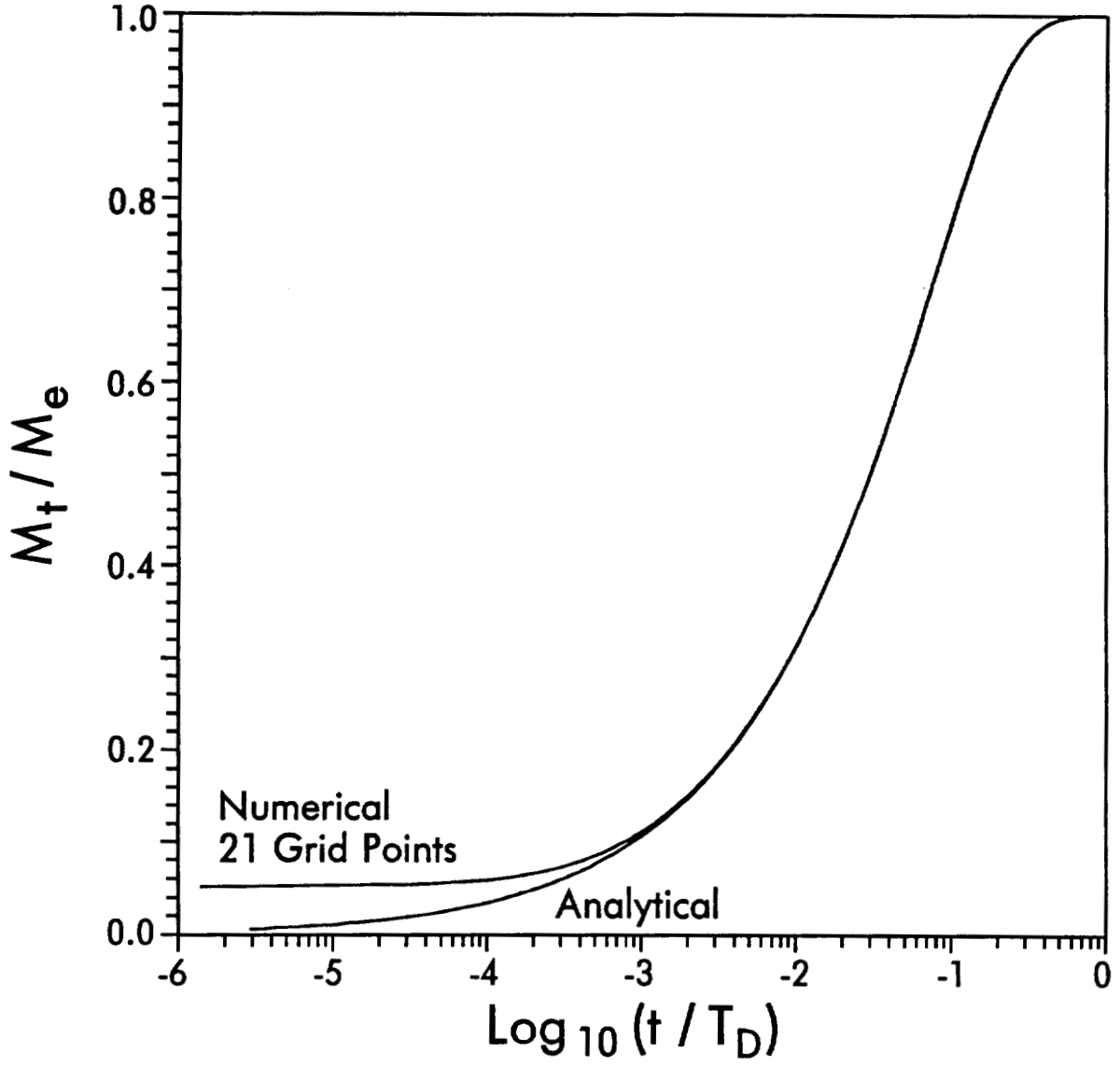

Figure 2.3. Numerical and analytical predictions of the fractional approach to equilibrium for model 1 using a monodisperse particle size distribution.

$$T_D = \frac{(diffusion\ length)^2}{D_{eff}} \tag{2.16}$$

When the factor α is 1.0, the diffusion length equals R. On the y axis, M_t is the total mass adsorbed or desorbed at time t, M_e is the corresponding amount at equilibrium, and M_t/M_e, therefore, is the fractional approach to equilibrium. Because a linear isotherm is assumed, the rate of approach to equilibrium is independent of the values of A and A_o.

The numerical method overestimates M_t/M_e at small t due to the fact that diffusion into or out of the particles is exaggerated during the first few time steps. This numerical error increases as the dimensionless parameter $K_p \cdot TSP$ increases. A finer spatial discretization can be used to more closely approximate the analytical solution at early times. Increasing the number of nodes per particle, however, also increases the computation time. For the cases discussed here, up to 201 nodes per particle were used when large values of $K_p \cdot TSP$ were studied, or when highly accurate curves were required. For most of the simulations, however, 51 nodes per particle were sufficient to keep the numerical error at an acceptable level.

Model 2. Gas/Particle Distributions for Filter-Bound Particles

Formulation. A model was constructed to simulate compound adsorption to and desorption from particles that are trapped on/in a filter, such as that which can occur in an air sampling apparatus containing a filter followed by an adsorbent. This model was developed specifically to simulate the processes of adsorption and desorption on/in filters and to predict the magnitude of the associated artifacts. In this system, particles are collected on a filter from an air parcel which contains a compound at a constant gas-phase concentration A_o. The particles are assumed to be in sorption equilibrium with A_o. The simulation is then started by passing a different, particle-free air parcel through the particle-laden filter. This new air parcel contains the compound at a concentration A,

where $A \neq A_0$. Adsorption or desorption, depending on whether $A > A_0$ or $A < A_0$, respectively, then occurs until the particles are in equilibrium with the new air parcel.

Over the course of a typical six hour aerosol collection period, the gas-phase concentration of a compound in the sampled air volume may vary greatly, causing the first particles collected to react to changes in the gas-phase concentrations to which they are exposed. The time scales of sorption reactions on filters can be expected to control the magnitude of the potential adsorption or desorption sampling artifacts. If the reaction time scale is short compared to the sampling period, then the artifacts in the determination of gas- and particulate-phase concentrations can be large.

The formulation of this model is fairly complex, since the concentration of the compound in the gas phase must be allowed to change (due to adsorption by, or desorption from the trapped particles) as the air passes through the filter. To allow such changes, the thickness of the filter was discretized into N layers such that the thickness of each layer is $1/N$th of the total thickness. An air parcel first enters layer 1, then passes to layer 2, and so on until exiting the filter after layer N. Each layer of the filter is assumed to contain $1/N$th of the total particulate mass, and to have a size distribution which is identical to the overall distribution (Pasadena aerosol (25)). This conceptual-ization is accurate for heavily-loaded filters. When the total mass of particles is low and glass fiber filters are used, the number of particles will drop off exponentially with distance into the filter. Including this level of complexity in the model, however, would not have changed the conclusions obtained here to a significant degree.

To start the simulation, an air parcel is sent into layer 1, where adsorption or desorption is allowed to occur for a specified period of time, and the gas- and particulate-phase concentrations are decreased or increased according to the radial diffusion model. The air parcel then moves into layer 2, where an identical period of time is allowed to elapse. The gas-phase concentration of the air parcel and the sorbed concentrations for each particle size are modified as the

air parcel moves through each layer of the filter. Upon leaving the filter, the exiting gas-phase concentration, A_{out}, is recorded, and the next air parcel is sent into layer 1 to repeat the process.

The magnitude of adsorption and desorption artifacts will be influenced by many factors including sorption kinetics and the variability of A, TSP, and temperature over the sampling period. In order to isolate the effects of sorption kinetics, several simplifying assumptions were made. Firstly, as discussed previously, the influent gas-phase concentration A was held constant during the simulation. The flow rate of air through the filter was also held constant and was typical of flow rates commonly used in hi-vol samplers. Secondly, the total particulate mass on the filter was fixed; no particles were added during the simulation. Finally, the temperature was assumed to be constant; thus the value of K_p did not change during the simulation.

Parameter Optimization. The sensitivity of the filter-based model to the number of filter layers, the number of nodes per particle (grid points), and an internal time step criterion was tested. Figure 2.4 illustrates the dependence of the normalized breakthrough curve on the number of layers used by the model, varying from five layers to sixty, with $\alpha = 1.0$, $A_0 = 0$ ng/m^3, 21 nodes/particle, and a Pasadena-type particle size distribution. The x axis in Figure 2.4 is a dimensionless time, t/T_M, where T_M is the time required for the influent gas to deliver/remove the mass of analyte that must be exchanged between the gas and particulate phases for sorption equilibrium to be achieved. This mass transfer time scale is

$$T_M = \frac{K_p M_p}{f} \tag{2.17}$$

where M_p is the mass of particles on the filter and f is the volumetric flow rate of gas through the filter. If the sorption kinetics were infinitely fast, then the particles would be in complete equilibrium with the influent concentration when $t = T_M$. The dependence of T_M upon $K_p \cdot M_p$ illustrates the similarity between

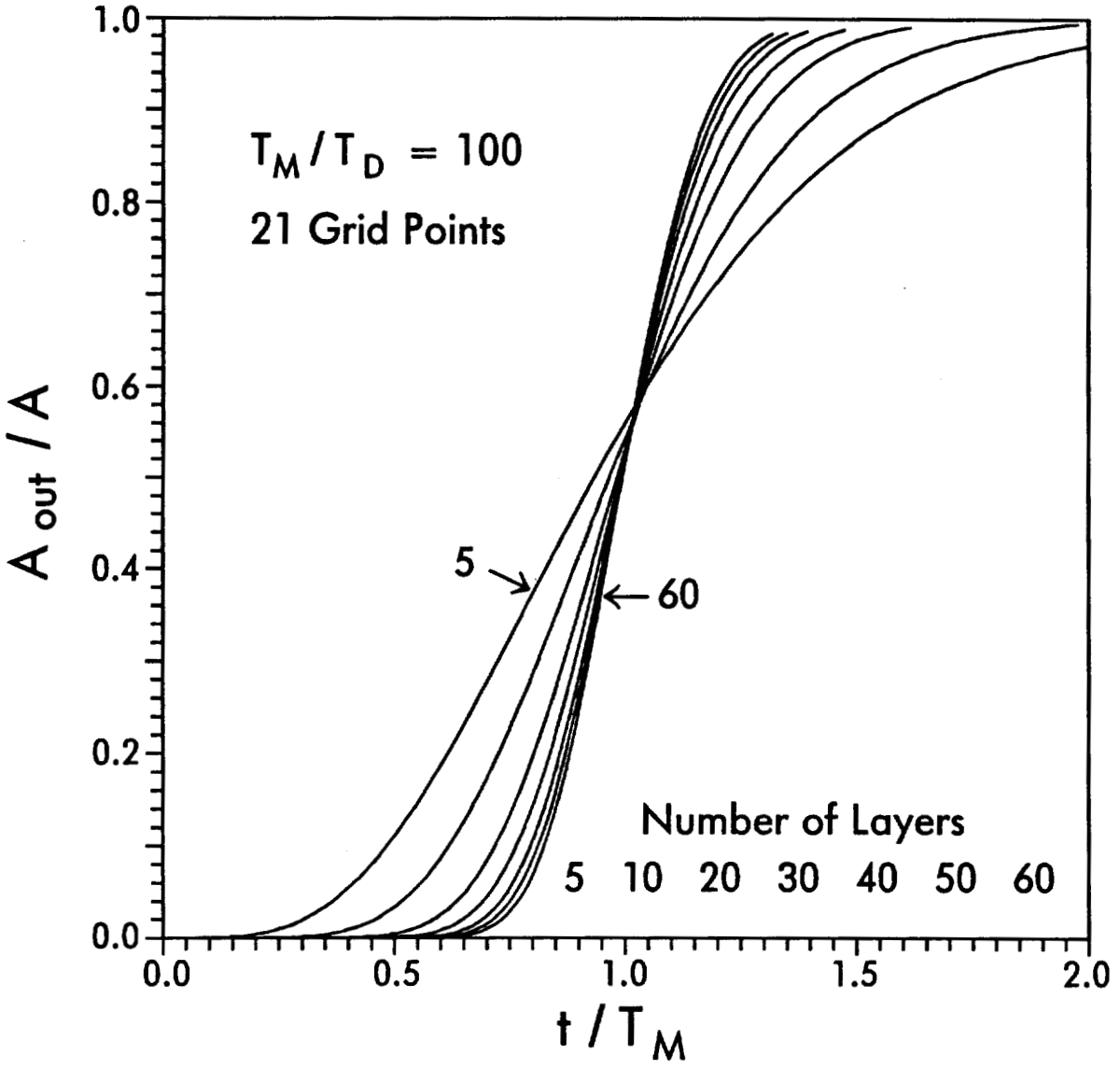

Figure 2.4. Dependence of the normalized breakthrough curve for model 2 on the number of layers within the filter. The ratio of the mass transfer time scale to the diffusion reaction time scale for these simulations is 100.

sorption processes on/in a filter and those in a PUF plug or a Tenax cartridge; it is the product of the partition coefficient and the mass that determines the retention volume (*26*). (This is just one of many examples of why K_p is a more intuitive type of partition coefficient than is K.) The dimensionless time, then, is

$$\frac{t}{T_M} = \frac{V/f}{K_p M_p/f} = \frac{V}{K_p M_p} \tag{2.18}$$

where V is the volume of air that has passed through the filter at time t. When the y axis is also non-dimensionalized, the breakthrough curve depends only upon the ratio T_M/T_D rather than the individual values of K_p, M_p, f, and A.

Figure 2.4 shows that the normalized breakthrough curve asymptotically approaches a final position as the number of layers is increased. Though not shown, the relationship between the normalized breakthrough curve and the number of layers depends upon the ratio T_M/T_D; the dependence becomes more pronounced as the ratio is increased. The largest ratio used in this study was 100; therefore, this ratio was used for the layer optimization. As the number of filter layers is increased, the computation time increases proportionally, but the incremental increase in accuracy decreases. Because of this trade-off, forty layers were considered to be adequate, and this number was used for the balance of the simulations.

The sensitivity of the model to the number of intraparticle grid points was investigated using 21, 41, and 61 grid points with $T_M/T_D = 100$, $\alpha = 1.0$, $A_o = 0$ ng/m^3, 40 filter layers, and the Pasadena size distribution. As illustrated in Figure 2.5, the normalized breakthrough curve shows virtually no dependence on the number of grid points. The dependence of the breakthrough curve on this parameter does not increase significantly for other values of T_M/T_D. In order to minimize computation time, therefore, 21 grid points were considered to be sufficient. Finally, the dependence of the normalized breakthrough curve on various types of internal time step criteria was studied. Again, no significant

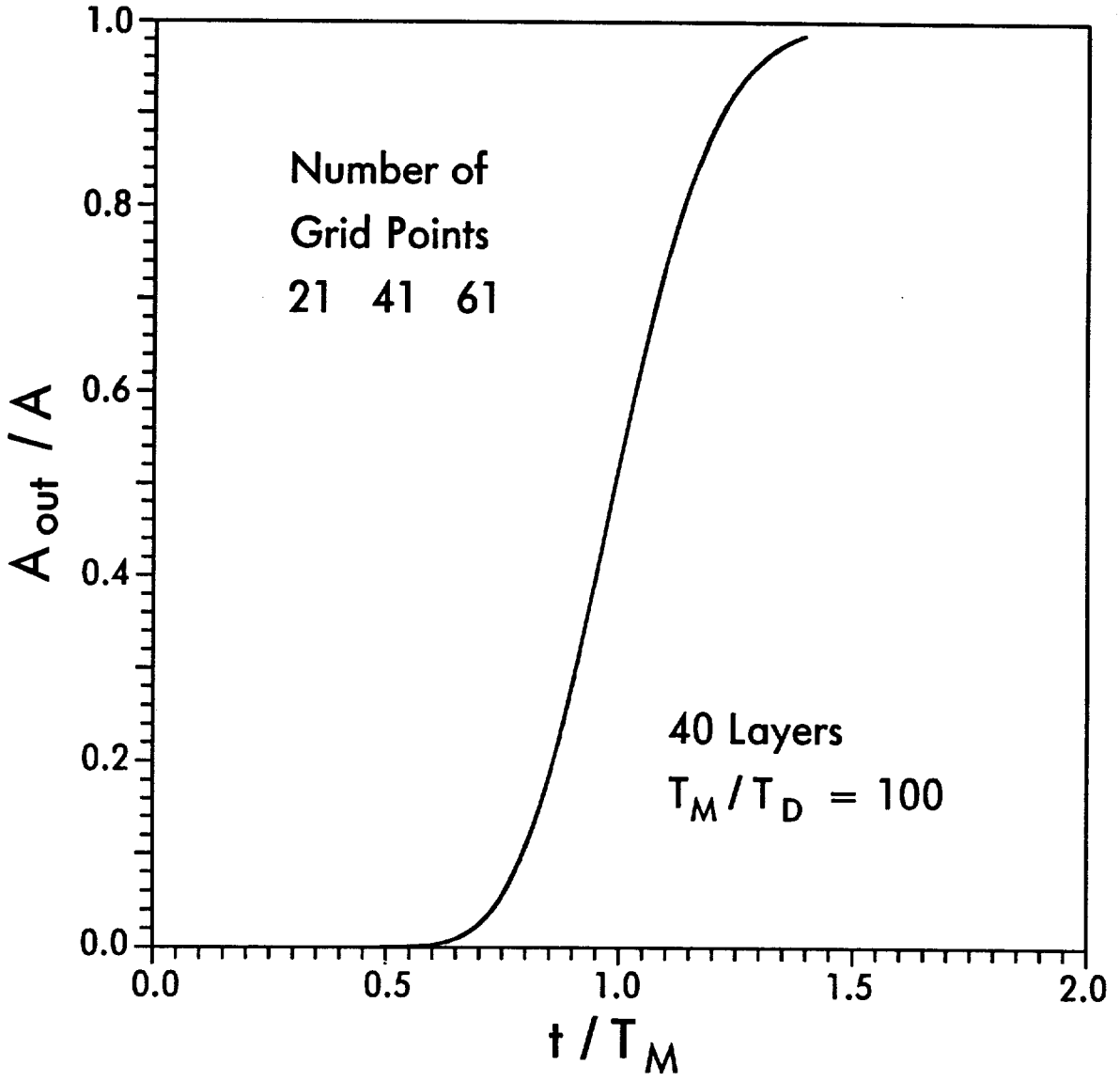

Figure 2.5. Dependence of the normalized breakthrough curve for model 2 on the number of nodes per particle. Curves are shown for 21, 41, and 61 nodes, using 40 filter layers and a T_M/T_D of 100.

dependence was observed, indicating that the variable time stepping algorithm used in this model did not lead to significant errors.

Results and Discussion

Model 1. Airborne Particles. Simulations were performed with model 1 to study the dependence of M_t/M_e on the dimensionless parameter $K_p \cdot TSP$. Fully porous particles were used in a Pasadena-type size distribution. When plotted against the dimensionless diffusion reaction time t/T_D, a family of curves is created that is compound-independent (Figure 2.6). The diffusion reaction time scale used in plotting the computed results for this polydisperse system was taken as the average T_D for all sizes, weighted by the mass fraction. The resulting value of T_D is the same as that which would result from a diffusion length (R) of 0.915 μm. Figure 2.6 describes the behavior for **any** K_p value and **any** concentration of airborne particles giving $K_p \cdot TSP$ in the range 0.001 to 100. The fractional approach to equilibrium depends on $K_p \cdot TSP$ because this value equals the equilibrium ratio F/A, and therefore determines the driving force for the final fractional uptake or release of a compound. The dependence of intraparticle transport rates on the equilibrium ratio F/A, a fundamental parameter which Crank unfortunately designates α, has been well documented (*21*).

Since specific surface area measurements of urban aerosols (*19*) indicate that atmospheric particles may not be fully porous, a set of simulations was performed to examine the dependence of the diffusion reaction time scale on the fractional particle volume that is porous, α. Porous fractions of 0.1, 0.2, 0.4, 0.6, and 1.0 were simulated using pyrene, an A_o of 0 ng/m^3, the Pasadena-type size distribution, and a TSP of 50 μg/m^3. The results are shown in Figure 2.7. As would be expected, particles which are only fractionally porous, and therefore have smaller diffusion lengths, are predicted to reach equilibrium more quickly than particles which are fully porous. The decrease in T_D caused by the change in diffusion length, however, is partially offset by a decrease in the effective

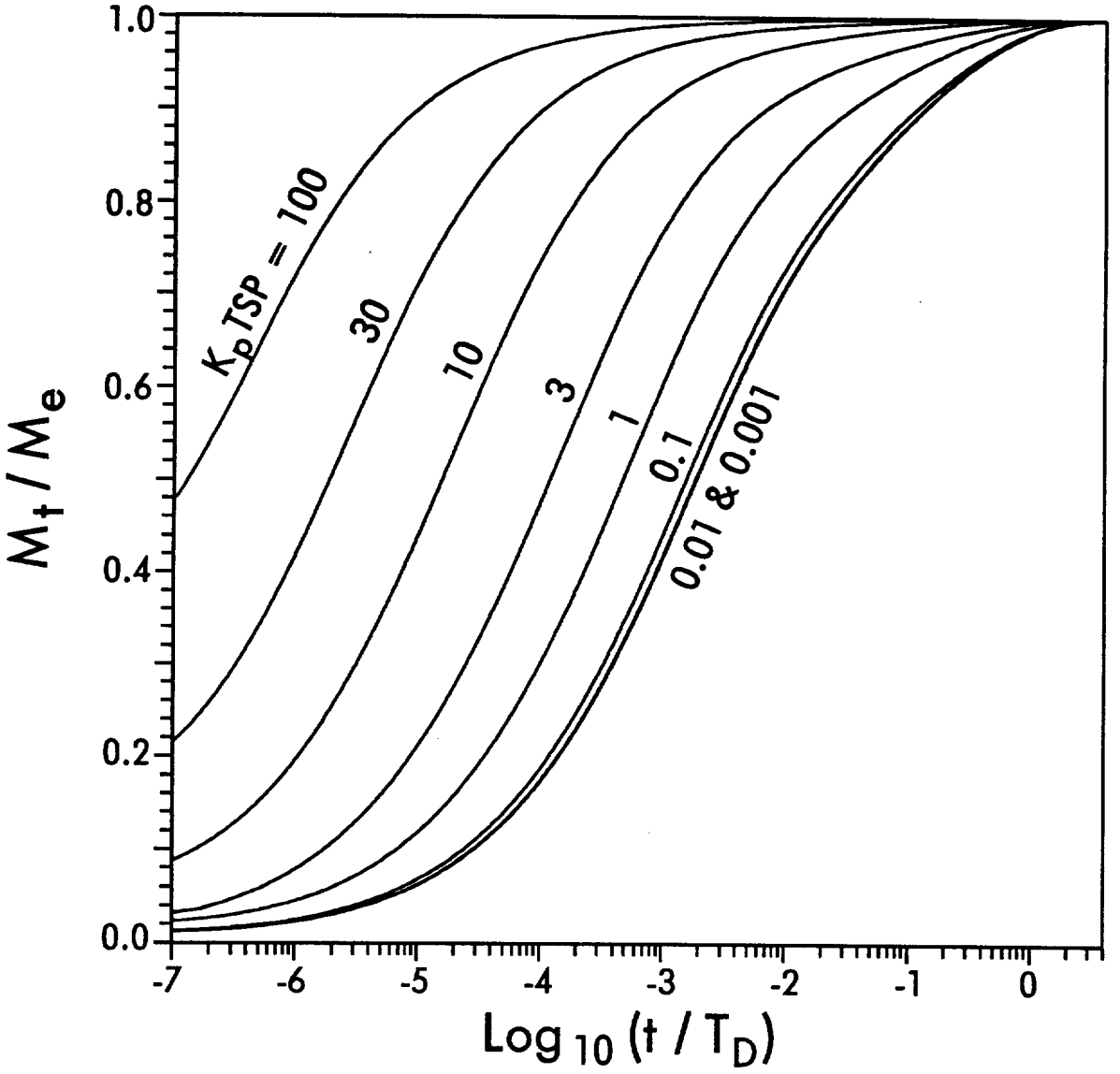

Figure 2.6. Normalized fractional approach to equilibrium curves as predicted by model 1 for fully porous particles. The characteristic parameter for each of these curves is the dimensionless parameter $K_p \cdot TSP$.

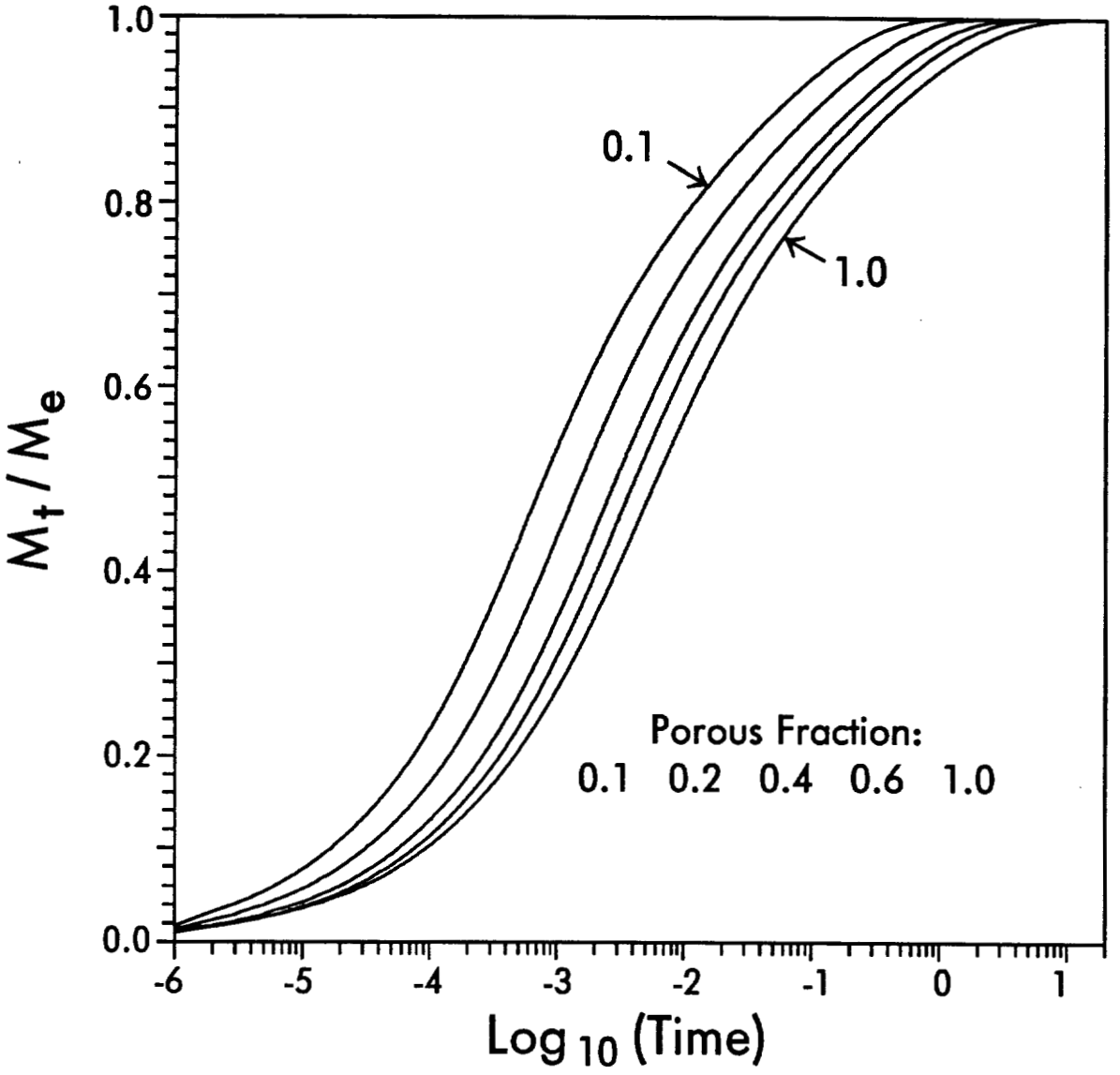

Figure 2.7. Dependence of the diffusion reaction time scale on α, the fractional particle volume that is porous. Curves are for pyrene, a *TSP* of 50 $\mu g/m^3$, and 101 nodes/particle. Time is expressed in minutes.

diffusion coefficient as calculated by equation (2.15). As a rule of thumb, particles that have a nonporous core such that only 10% of their volume is porous (α = 0.1) are predicted to reach sorption equilibrium in roughly 10% of the time required for fully porous particles in a system of the same $K_p \cdot TSP$.

The sensitivity of model results to changes in the intraparticle porosity and the specific particle density were explored. For a given value of α, a change in either the specific density or the porosity of the outer shell affects the amount of particulate mass that resides in the porous shell. This results in a small change in the value of D_{eff} and a corresponding shift in the diffusion reaction time scale. This effect, however, was found to be small.

The dependence of the diffusion reaction time scale on the atmospheric particle size distribution was also explored. The results are shown in Figure 2.8, where the sorption kinetics for a Pasadena-type distribution is compared to the kinetics that result from three different monodisperse distributions. For the sake of comparability of the results, the simulations for the monodisperse particles were performed with the numerical model. Particle diameters of 0.00875 μm, 0.25 μm, and 5.22 μm were chosen because they represent the measured lower limit, the maximum, and the upper limit, respectively, of the mass distribution of the Pasadena aerosol. All four simulations used fully porous particles. Since the Pasadena aerosol contains significant numbers of particles smaller than 0.25 μm in diameter, these results indicate that the larger particles in a polydisperse distribution tend to be more important than the smaller particles in determining the overall reaction time scale.

Predictions of the reaction time scales for each of the model compounds are shown in Figure 2.9. These curves were generated using the values listed in Table 2.1, fully porous particles, a Pasadena-type size distribution, TSP = 50 $\mu g/m^3$, A_0 = 0 ng/m^3, and 101 nodes/particle. As the value of the atmospheric partition coefficient increases from HCB to chrysene, the reaction time scale increases due to a corresponding decrease in D_{eff}. Equilibrium is achieved for each of these compounds very quickly relative to their residence times in the

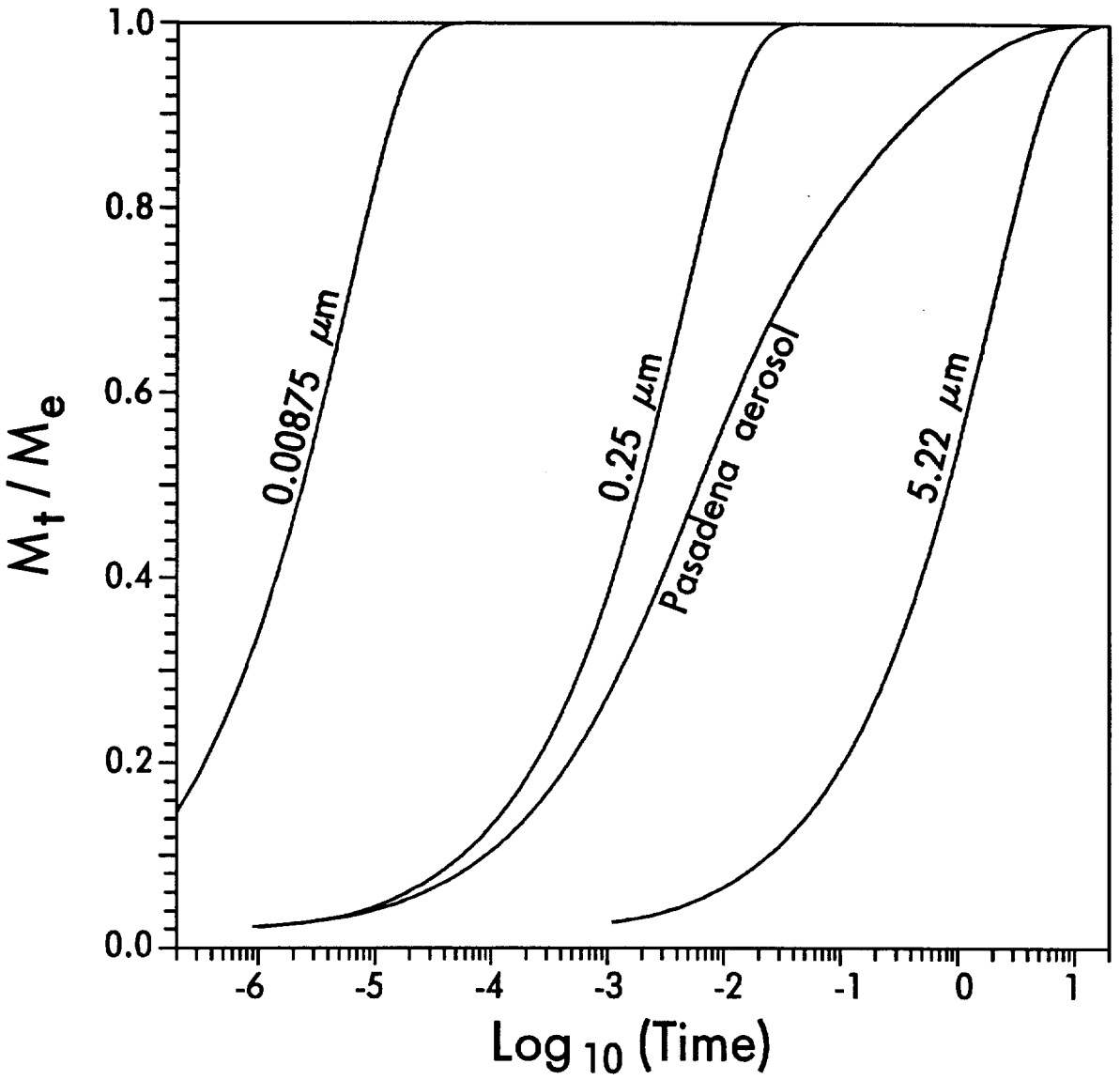

Figure 2.8. Dependence of the fractional approach to equilibrium for model 1 on the particle size distribution, using pyrene, 51 nodes/particle, fully porous particles, and a *TSP* of 50 $\mu g/m^3$. Curves for the three monodisperse size distributions are labeled with their diameters. Time is expressed in minutes.

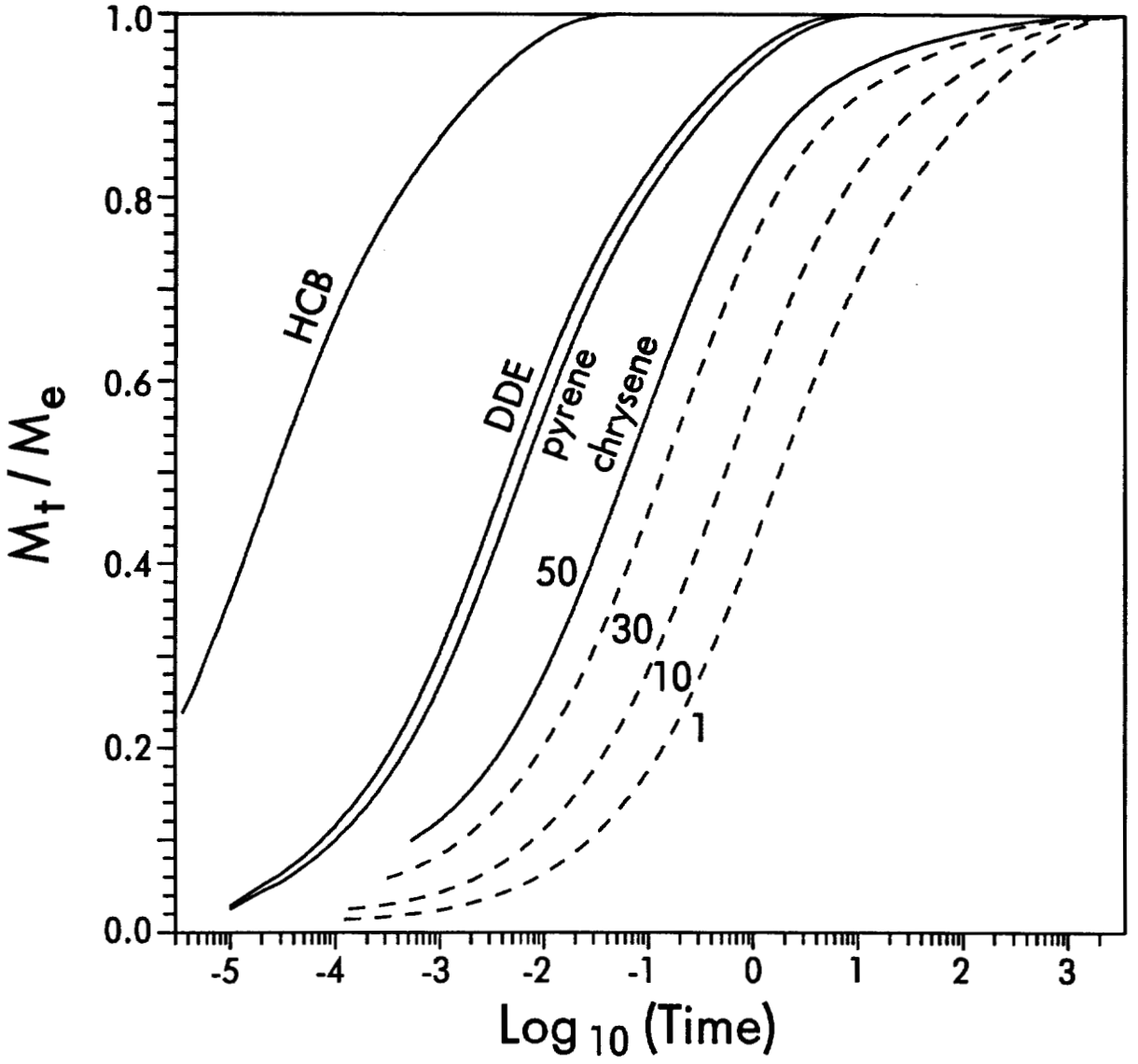

Figure 2.9. Predictions from model 1 of the fractional approach to equilibrium for each of the four model compounds. The solid lines were generated using a *TSP* value of 50 $\mu g/m^3$, while the dashed lines represent chrysene with *TSP* values of 30, 10, and 1 $\mu g/m^3$. Time is expressed in minutes.

atmosphere. Even chrysene, which has the largest K_p and therefore the smallest D_{eff} of the model compounds, is predicted to approach sorption equilibrium in approximately one hour under these conditions.

Figure 2.9 also illustrates the dependence of the reaction time scale on the value of $K_p \cdot TSP$. Chrysene exhibits a significant dependence on the value of *TSP*. The other three compounds, however, show such weak dependence on *TSP* in the range 1 to 50 $\mu g/m^3$ that the effects are not visible in a plot over this time range. The rate of reaction for chrysene is particularly sensitive to a change in the value of *TSP* because, for this range of *TSP*, the partition coefficient is of sufficient magnitude to dictate that a significant fraction of the compound is associated with the particulate phase at equilibrium. As mentioned previously, the equilibrium fraction of analyte associated with the particulate phase affects intraparticle transport rates. The equilibrium values of *F/A* for pyrene, DDE, and HCB, however, are too small for the kinetics to be significantly affected by changes in *TSP* within this range.

Model 2. Filter-Bound Particles. The filter-based model is designed to predict the time required for trapped particles initially in equilibrium with one air parcel, perhaps a relatively clean one, to react to the arrival of a second, possibly polluted air parcel, or vice versa. The gas-phase concentration differences used for these simulations are identical to those listed in Table 2.1. Because linear isotherms are used, however, the magnitude or sign of the gas-phase concentration change is not of fundamental importance in determining the shape or position of the breakthrough curve.

The shape and position of the normalized breakthrough curve are determined by the relationship between the intraparticle diffusion reaction time scale and the equilibrium mass transfer time scale. Simulations were performed to determine the dependence of the output of model 2 on the ratio T_M/T_D using forty layers, 21 nodes/particle, fully porous particles, and a Pasadena-type size distribution. The results are plotted as A_{out}/A versus t/T_M in Figure 2.10, and as M_t/M_e versus t/T_M in Figure 2.11. As the ratio T_M/T_D decreases, the diffusion

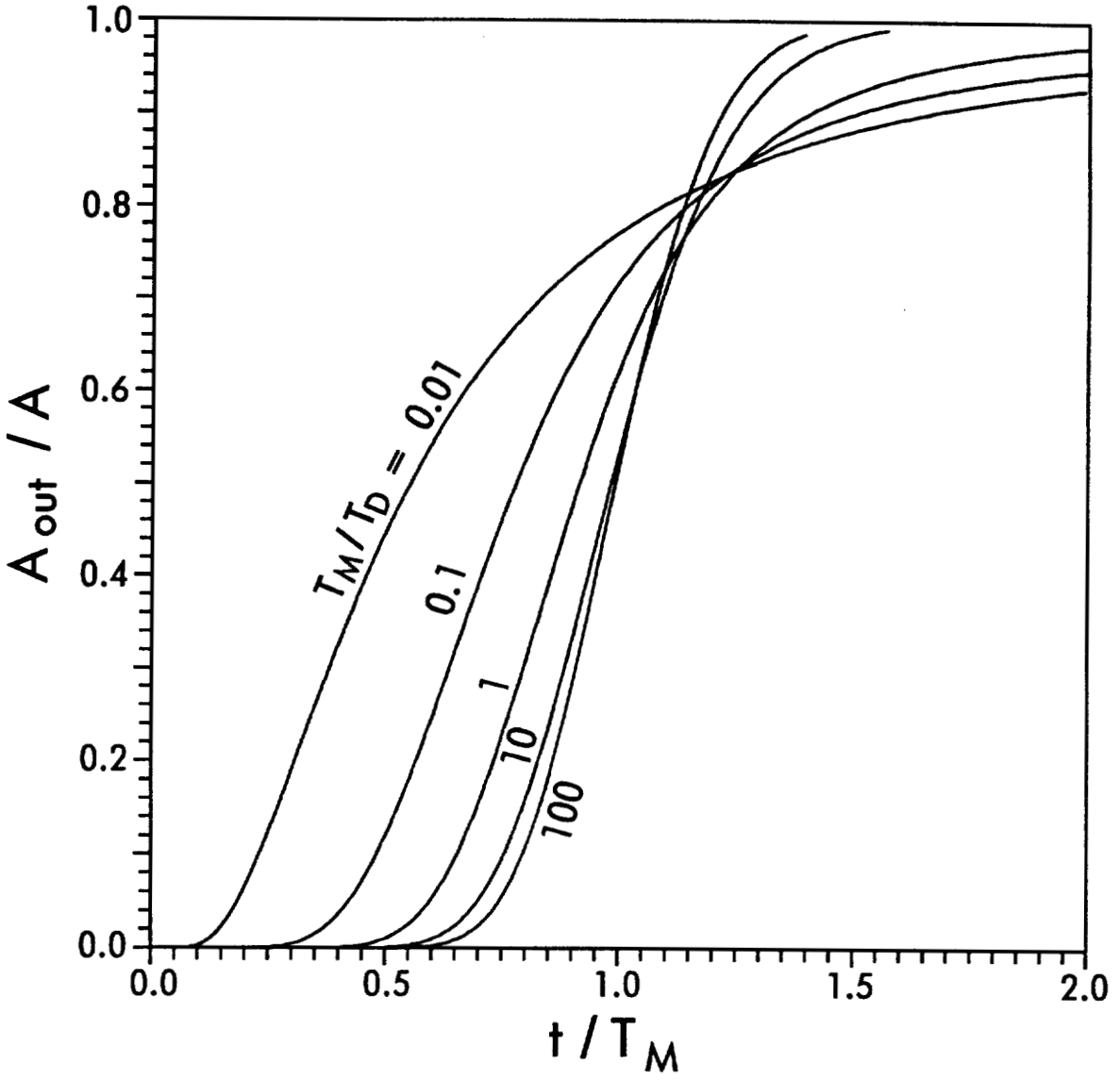

Figure 2.10. Normalized breakthrough curves for model 2, using forty layers, 21 nodes/particle, and fully porous particles in a Pasadena-type size distribution. The characteristic parameter for each curve is the ratio T_M/T_D.

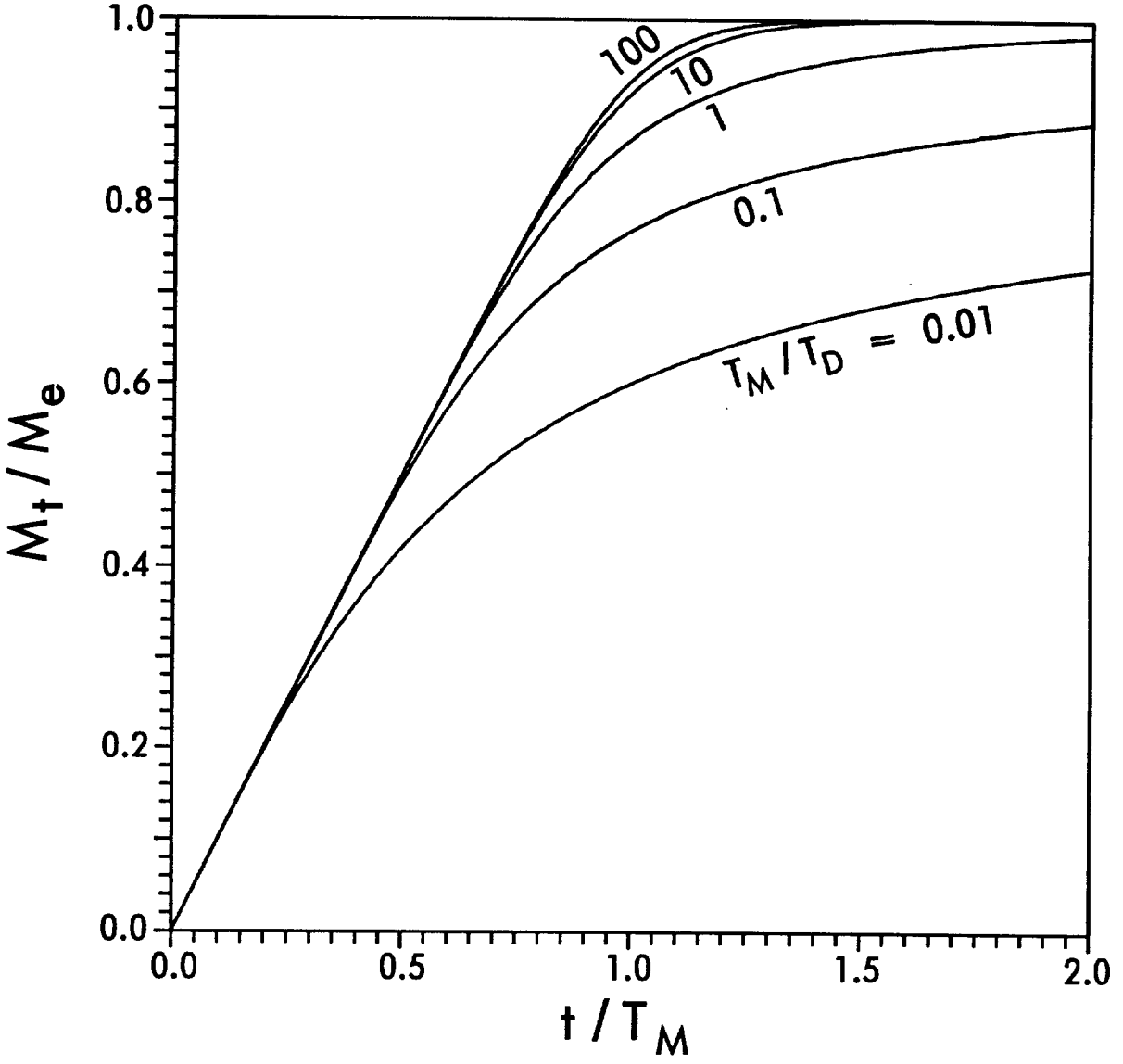

Figure 2.11. Normalized fractional approach to equilibrium curves for model 2, using forty layers, 21 nodes/particle, and fully porous particles in a Pasadena-type size distribution. The characteristic parameter for each curve is the ratio T_M/T_D.

kinetics becomes more limiting. Conversely, as T_M/T_D increases, diffusion kinetics becomes less limiting. The kinetics of intraparticle diffusion is important everywhere in the range of T_M/T_D from 0.01 to 100. If it were unimportant, the breakthrough curve would be a step function. Indeed, as the ratio T_M/T_D increases from 0.01 to 100, Figure 2.10 shows that the simulated breakthrough curve becomes more, but not completely, vertical. The relative importance of intraparticle diffusion versus equilibrium mass transfer is illustrated well in Figure 2.11. If diffusion were not limiting ($T_M/T_D = \infty$), then the curve would be a straight line from (0,0) to (1,1). Because the small particles on the filter react rapidly to changes in A, every curve starts on the $T_M/T_D = \infty$ line. The extent of the deviation from that line depends on the relative importance of the intraparticle diffusion reaction.

The dependence of the normalized breakthrough curve on α was also explored. Simulations with 40 layers, 21 nodes/particle, and the Pasadena size distribution were performed. The ratio T_M/T_D for the case of fully porous particles was set equal to 10. Figure 2.12 illustrates the results. Essentially, as the fraction of porous particulate volume decreases from 1.0 to 0.01, the reduction in the diffusion length causes a decrease in the diffusion reaction time scale which in turn results in a larger ratio of T_M/T_D.

Simulations for each of the four model compounds were performed using the parameters in Table 2.1, fully porous particles, a Pasadena-type size distribution, and 21 nodes/particle. The flow rate through the filter was fixed at 0.43 m^3/min, corresponding to a face velocity of approximately 14 cm/sec in a high-vol with a 20 cm by 25 cm filter. The results are shown in Figure 2.13 for particulate masses of 240 mg (solid lines) and 130 mg (dashed lines). Under these conditions, the T_M values for HCB are quite small. Values of T_M for DDE and pyrene are larger, but still less than a typical 6 hour sampling period. Chrysene, however, has a T_M that is much larger than typical sampling times. The ratio T_M/T_D for these simulations is fairly large for all of the model compounds, averaging $\sim$54 for M_p = 240 mg and $\sim$29 for M_p = 130 mg.

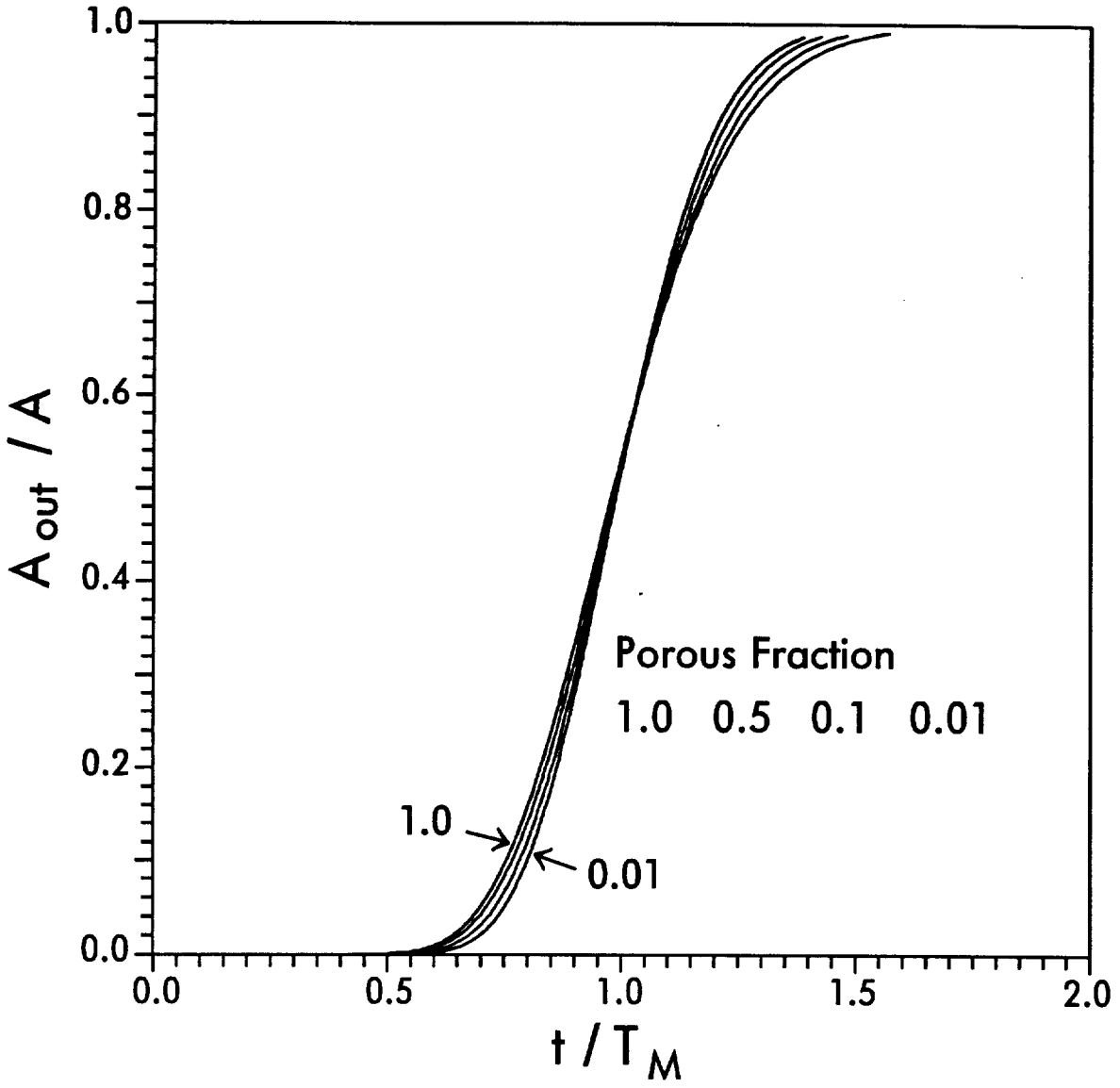

Figure 2.12. Dependence of the normalized breakthrough curve for model 2 on α, the fractional particle volume that is porous, using forty layers and 21 nodes/particle. The ratio T_M/T_D = 10 for the curve where α = 1.0.

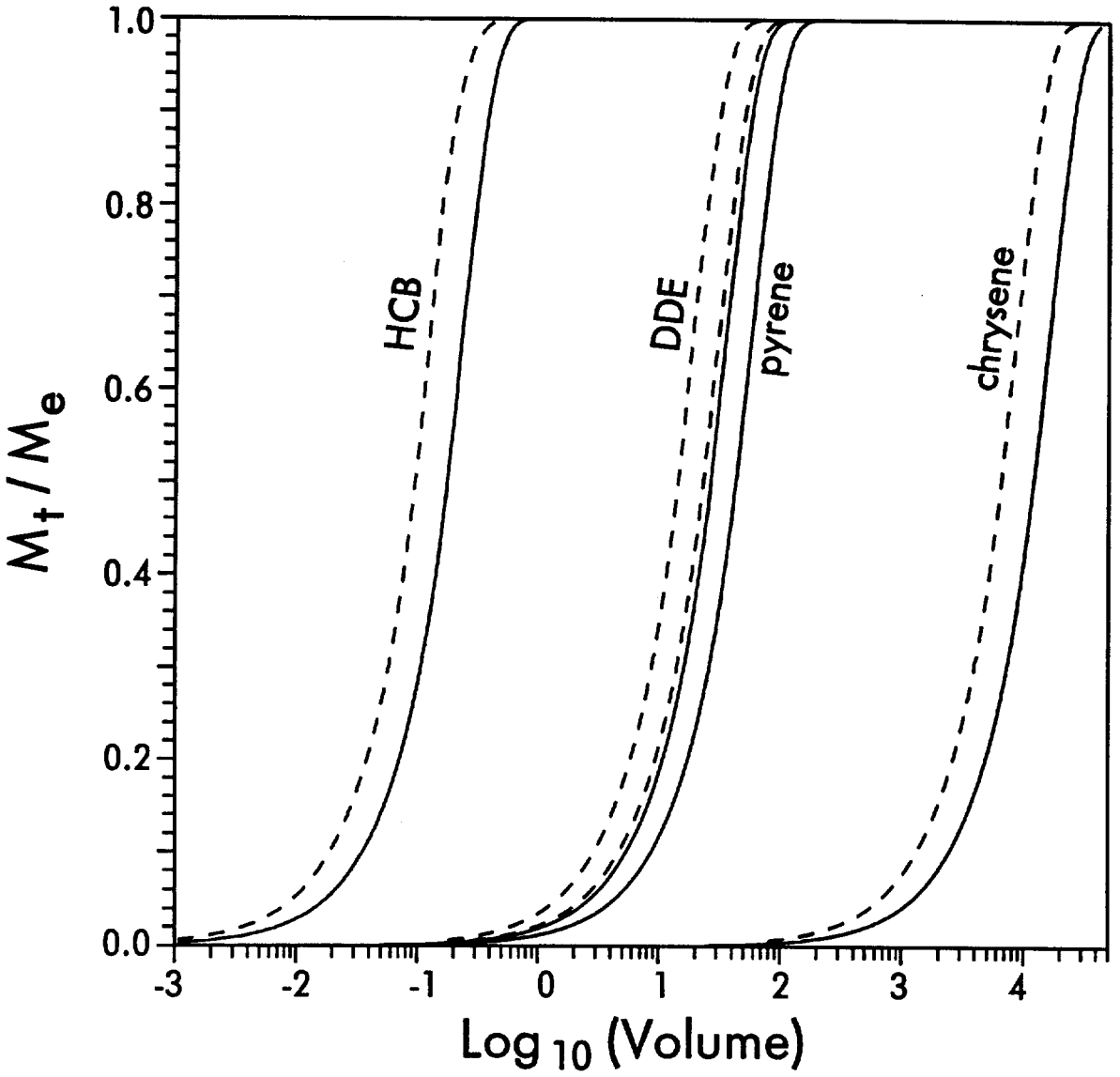

Figure 2.13. Predictions from model 2 of the time required for filter-bound particles to react to a change in a compound's influent concentration, using fully porous particles in a Pasadena-type size distribution. Solid lines are for 240 mg of particulate mass; dashed lines are for 130 mg. The volume of air is expressed in m^3.

Simulations with less particulate mass on the filter (smaller T_M/T_D) would produce curves that are shifted to smaller times and more affected by intraparticle diffusion, as in Figure 2.11.

The potential artifacts caused by adsorption to and desorption from trapped particles on/in a filter depend upon many factors including the reaction time scales and the variability of *A*, *TSP*, and temperature over the course of the sampling period. To extend the results of this study to the description of adsorption and desorption artifacts within a hi-vol sampler is not straightforward. During the course of particle collection, T_D may vary somewhat with temperature, but T_M increases linearly with M_p. In fact, the ratio T_M/T_D is essentially a function of M_p/f. Therefore, the ratio T_M/T_D will increase as the sampling event progresses. Particles collected at different times and from different air parcels will proceed toward sorption equilibrium along different interdependent paths.

The above caveats notwithstanding, some general statements concerning the probability and magnitude of adsorption and desorption sampling artifacts may be made. They are grouped into three categories according to the magnitude of K_p. For compounds that react quickly (small K_p, large D_{eff}), the measured particulate-phase concentration will reflect the last gas-phase concentration to which the particles were exposed. The measured gas-phase concentration will represent the sample volume average of A_{out}. Because K_p is small, the measured value of *A* will be largely unaffected by any exchange of the compound between the gas phase and filter-bound particles. The value of *A* for the last air parcel, however, is not likely to be equal to the average value of *A* for the entire sampling event. Therefore, the potential for significant artifacts in the calculation of K_p for these compounds is high. For compounds which react on time scales much longer than the sampling period (very large K_p, small D_{eff}), the measured gas- and particulate-phase concentrations are more likely to reflect the true volume average of *A* and *F* over the course of sampling. Consequently, the potential for the above artifacts is low. Finally, for

compounds which have diffusion reaction time scales on the same order as the sampling time (chrysene, for example), a significant amount of analyte may exchange between phases, but the exchange will probably be incomplete. The potential for significant artifacts is present, but at a lower probability than for compounds that react very quickly.

The implications of these predictions on sample collection and handling are serious. In order to increase the probability that only one air parcel is sampled, collection times should be kept at a minimum as allowed by analytical method detection limits and the need to minimize sorption directly to the filter. Alternative sampling methods which have the potential to average or eliminate adsorption and desorption artifacts should be investigated. The determination of partition coefficients for highly volatile compounds may need to be made in the laboratory, where better control over conditions can be exercised. In addition, filter samples must be handled with care during their transport and subsequent analysis. Exposure to laboratory air, even over a short period of time, may cause sorbed compounds to redistribute between the collected particles and the air in the laboratory.

Summary and Conclusions

An intraparticle diffusion model was adapted to describe sorption kinetics both in the atmosphere and on particle-laden filters. Both systems were simulated for a series of model compounds whose partitioning properties vary over a large range. The radial diffusion model predicts the rapid attainment of equilibrium for most compounds typically determined in atmospheric samples. For compounds with K_p values smaller than 0.10 $m^3/\mu g$, reaction time scales in the atmosphere are expected to be on the order of several hours or less, depending on the particular compound. Particles which are only porous in the outer portion of their structure are predicted to approach equilibrium faster than their fully porous counterparts. During aerosol filtration, the potential for adsorption and desorption artifacts is controlled in part by the kinetics of

sorption processes. The magnitude of the artifact will depend upon the variability of A, TSP, and temperature during the sampling event as well as the diffusion and mass transfer reaction time scales. For compounds possessing small K_p values, adsorption to and desorption from filter-bound particles is predicted to be rapid. Consequently, the potential is high for significant artifacts in the measurement of A and F and in the subsequent calculation of K_p. Compounds that have large values of K_p are predicted to react more slowly and therefore are less likely to display artifacts of the same magnitude as those that have small values of K_p. The predictions of these models, however, only provide rough guidelines. The radial diffusion model requires calibration and verification for actual atmospheric particles. The implications of these predictions are serious enough to merit further investigation.

Glossary

A	gas-phase concentration (ng/m^3)
A_o	gas-phase concentration in sorption equilibrium with particles before a simulation is started (ng/m^3)
A_{out}	gas-phase concentration leaving the filter (ng/m^3)
$A'(r)$	gas-phase concentration in micropores at a radial distance r from the center of the particle (ng/m^3)
b	constant in equation for log K
D_{eff}	effective diffusion coefficient (cm^2/s)
D_m	gas-phase molecular diffusion coefficient (cm^2/s)
f	volumetric flow rate through the filter (m^3/min)
F	particulate-phase concentration (ng/m^3)
K	sorption equilibrium constant ($\mu g/m^3$)
K_p	sorption equilibrium constant ($m^3/\mu g$)
K_p'	sorption equilibrium constant corrected for the fractional particle mass in the porous shell ($m^3/\mu g$)
m	compound-dependent slope of log K versus $1/T$

M_e	mass exchanged between phases at equilibrium
M_p	mass of particulate matter on the filter
M_t	mass exchanged between phases at time t
M_t/M_e	fractional approach to equilibrium
n	intraparticle porosity
N	number of filter layers
p_L^o	subcooled liquid vapor pressure
r	radial distance
r_c	radius of the nonporous inner core (μm)
R	particle radius (μm)
$S'(r)$	sorbed-phase concentration of analyte at a radial distance r from the center of the particle (ng/μg)
$S(r)$	total volumetric concentration of analyte at a radial distance r from the center of the particle (ng/m^3)
t	time (min)
T	absolute temperature (K)
T_D	diffusion reaction time scale (min)
T_M	mass transfer time scale (min)
TSP	total suspended particulate matter concentration (μg/m^3)
t/T_D	dimensionless diffusion reaction time
t/T_M	dimensionless mass transfer time
V	volume of air (m^3)
α	fractional particle volume that is porous
ρ_s	specific particle density (g/cm^3)
τ	tortuosity factor

Registry No. Chrysene, 218-01-9; Hexachlorobenzene, 118-74-1; p,p'-DDE, 72-55-9; Pyrene, 129-00-0.

Literature Cited

(1) Yamasaki, H.; Kuwata, K.; Miyamoto, H. *Environ. Sci. Technol.* **1982**, *16*, 189-194.

(2) Pankow, J. F. *Atmos. Environ.* **1987**, *21*, 2275-2283.

(3) Pankow, J. F. *Atmos. Environ.* **1991**, *25A*, 2229-2239.

(4) Bidleman, T. F.; Billings, W. N.; Foreman, W. T. *Environ. Sci. Technol.* **1986**, *20*, 1038-1043.

(5) Foreman, W. T.; Bidleman, T. F. *Environ. Sci. Technol.* **1987**, *21*, 869-875.

(6) Bidleman, T. F.; Foreman, W. T. In *The Chemistry of Aquatic Pollutants*; Hites, R. A., Eisenreich, S. J., Eds.; Advances in Chemistry 216; American Chemical Society: Washington, DC, 1987; p. 27.

(7) Ligocki, M. P.; Pankow, J. F. *Environ. Sci. Technol.* **1989**, *23*, 75-83.

(8) Keller, C. D.; Bidleman, T. F. *Atmos. Environ.* **1984**, *18*, 837-845.

(9) Hart, K. M. Ph.D. Thesis, Oregon Graduate Institute, 1990.

(10) Pankow, J. F. *Atmos. Environ.* **1988**, *22*, 1405-1409.

(11) Van Vaeck, L.; Van Cauwenberghe, K.; Janssens, J. *Atmos. Environ.* **1984**, *18*, 417-430.

(12) McDow, S. Ph.D. Thesis, Oregon Graduate Center, 1986.

(13) Eagle, S.; Scott, J. W. *Ind. Eng. Chem.* **1950**, *42*, 1287-1294.

(14) Rosen, J. B. *J. Chem. Phys.* **1952**, *20*, 387-394.

(15) Rosen, J. B. *Ind. Eng. Chem.* **1954**, *46*, 1590-1594.

(16) Wu, S-C.; Gschwend, P. M. *Environ. Sci. Technol.* **1986**, *20*, 717-725.

(17) Rao, P. S. C.; Rolston, D. E.; Jessup, R. E.; Davidson, J. M. *Soil Sci. Soc. Amer. J.* **1980**, *44*, 1139-1146.

(18) Miller, C. T.; Weber, W. J. *J. Contam. Hydrol.* **1986**, *1*, 243-261.

(19) Corn, M.; Montgomery, T. L.; Esmen, N. A. *Environ. Sci. Technol.* **1971**, *5*, 155-158.

(20) Hallett, J.; Hudson, J. G.; Rogers, C. F. *Aerosol Sci. Technol.* **1989**, *10*, 70-83.

(21) Crank, J. *The Mathematics of Diffusion*, 2nd ed.; Clarendon: Oxford, England, 1975; 89-96.

(22) Wu, S-C.; Gschwend, P. M. *Water Res. Res.* **1988**, *24*, 1373-1383.

(23) Carnahan, B.; Luther, H. A.; Wilkes, J. O. *Applied Numerical Methods*; John-Wiley: New York, NY, 1969; p. 451.

(24) Lyman, W. J.; Reehl, W. F.; Rosenblatt, D. H. *Handbook of Chemical Property Estimation Methods*; McGraw-Hill: New York, NY, 1982; pp. 17-13 to 17-17.

(25) Whitby, K. T.; Husar, R. B.; Liu, B. Y. H. *J. Colloid Interface Sci.* **1972**, *39*, 177-204.

(26) Pankow, J. F. *Anal. Chem.* **1988**, *60*, 950-958.

CHAPTER III

Description of Gas/Particle Sorption Kinetics with an Intraparticle Diffusion Model: Desorption Experiments

Abstract

An intraparticle diffusion model was successfully used to describe the desorption of a wide range of *n*-alkanes and polycyclic aromatic hydrocarbons (PAHs) from a particle-laden filter. Aerosol particles from a highway tunnel were collected using standard techniques. Sorbed organic compounds were then desorbed for 28 days by passing clean nitrogen through the filter. Volatile compounds were liberated from the filter quickly; only a small fraction of the less volatile compounds were desorbed. A non-linear least squares method was used to fit the diffusion model to the experimental data. Two fitting parameters were used: the gas/particle partition coefficient (K_p), and an effective intraparticle diffusion coefficient (D_{eff}). Optimized values of K_p are in agreement with previously reported values. The slope of a correlation between the fitted values of D_{eff} and K_p agrees well with theory, but the absolute values of D_{eff} are a factor of $\sim 10^6$ smaller than predicted for sorption-retarded, gaseous diffusion. Slow transport through an organic or solid phase within the particles or preferential flow through the bed of particulate matter on the filter might be the cause of these very small effective diffusion coefficients.

Introduction

Theoretical models that describe the equilibrium distribution of organic compounds between the gas and particulate phases in the atmosphere are often based upon linear sorption isotherms (*1-4*). For a given compound and temperature, the linear model defines the ratio of particulate- and gas-phase concentrations in terms of a partition coefficient K_p ($m^3/\mu g$), given as

$$K_p = \frac{F \,/\, TSP}{A} \tag{3.1}$$

where F is the concentration of analyte associated with the particulate phase (ng/m^3), TSP is the total suspended particulate matter concentration ($\mu g/m^3$), and A is the gas-phase concentration of the compound (ng/m^3). The partition coefficient varies with the absolute temperature T (K) according to

$$\log K_p = \frac{m_p}{T} + b_p \tag{3.2}$$

where m_p and b_p are constants that depend upon the compound and the nature of the particulate matter. This temperature dependence was first proposed by Yamasaki *et al.* (*3*) and later modified and given a theoretical foundation by Pankow (*1, 5*). In addition, Pankow (*1*) has shown why the magnitude of the linear partition coefficient K_p is expected to be proportional to the inverse of the compound's subcooled liquid vapor pressure, p_L^o. Linear partitioning theory has been applied successfully to a wide range of organic compounds in both field (*3, 6-10*) and laboratory (*11-13*) experiments.

Although the characterization of gas/particle sorption equilibrium has been met with a considerable amount of success, relatively little is known about the kinetics of gas/particle interactions. Studies of the kinetics of these interactions are important in the elucidation of the mechanisms that control such processes. In turn, a better understanding of the physical nature of gas/particle partitioning will provide an improved foundation upon which to build models

of long range atmospheric transport, deposition and washout processes, reaction kinetics on/in particles, and the health effects of particulate-bound compounds. Much disagreement exists, for example, concerning the ability of atmospheric particles to catalyze reactions or, in contrast, to protect sorbed compounds from reaction (*14-19*). Kinetic investigations can also provide critical insight into the microscopic physical properties of atmospheric particles. Sorption kinetics may be an important factor in the aging of particulate materials as they are transported from their sources. In addition, adsorption and desorption processes that occur on/in filters as a result of concentration gradients or temperature changes are often cited as the cause of artifacts in high-volume air samplers (*6, 14, 20-21*). The extent to which sorption kinetics might limit the rates of these processes and the magnitude of the associated artifacts, however, is not yet well understood. Because gas/particle partitioning affects so many important processes, knowledge of the mechanisms that control sorption kinetics in atmospheric systems will be of great benefit.

Only a few attempts have been made to model sorption kinetics in atmospheric systems. Natusch and Tomkins (*22*) developed a predictive model for gas/particle adsorption kinetics based on a Langmuirian isotherm with activation energies for adsorption and desorption. Kittelson and Barris (*23*) extended the model of Natusch and Tomkins (*22*) to include diffusion-limited transport across a boundary layer around the sorbent particles. Neither of these groups, however, expanded their studies to describe experimental data. Rothenberg and Cheng (*24*) applied a first order rate model to the adsorption of water on fly ash particles. The obtained rate data did not follow the predictions of the model of Natusch and Tomkins (*22*), but could be explained in the context of intraparticle diffusion. Experiments concerning the adsorption kinetics of *m*-xylene on coal fly ash gave similar results (*25*). Miguel *et al.* (*26*) collected particles on a filter, then passed clean air through the filter and measured the desorption of PAHs from that filter. No attempt was made to correlate the results with a mechanistic model. Gerde and Scholander (*27*) applied diffusion-

based analytical models to predict the adsorption rates of gas-phase PAHs by individual porous particles and fibers. Recently, Rounds and Pankow (*28*) developed a radial intraparticle diffusion model for the description of sorption kinetics both in the atmosphere and on particle-laden filters, and discussed the implications for sampling.

In this study, the intraparticle diffusion model of Rounds and Pankow (*28*) is used to describe the desorption of a set of *n*-alkanes and PAHs from a particle-laden filter. The ability of the model to describe the observed behavior is discussed in terms of diffusion/partitioning theory. Values of the fitted diffusion coefficients are probed for implications concerning the nature of atmospheric particles and the gas/particle partitioning process. The significance of the observed diffusion reaction time scales is assessed. In addition, the limits placed on the magnitude of adsorption/desorption sampling artifacts by intraparticle diffusion are briefly discussed.

This filter desorption experiment was a group effort. The people involved in the project were Stewart A. Rounds, James F. Pankow, John M. E. Storey, Lorne M. Isabelle, and Bruce A. Tiffany. All worked on the experimental design. Bruce collected the particles and performed the bulk of the experimental work with the assistance of John and Lorne. Bruce, Jim, and Stewart worked up the raw data. The data analysis and modelling were performed by Stewart and are the subject of this chapter.

Experimental

Sampling Site. Particulate matter was collected from air in the eastbound tube of the Vista Ridge Tunnel (U.S. Route 26) in Portland, Oregon. The Vista Ridge Tunnel is a 306-meter, two-tube tunnel that conveys a moderate to heavy vehicular load; each tube contains three lanes of traffic. Tunnel air was sampled from a room above the eastbound traffic tube by positioning the sampler intake line through an open ventilation grate 30 meters from the eastern end of the tunnel.

Filter Loading. Particles were collected on a Teflon membrane filter (TMF) (Gelman Sciences, Inc., Ann Arbor, MI) which had been cleaned via Soxhlet extraction with methylene chloride (EM Science, Gibbstown, NJ, chromatography grade) for 18 hours. The tared filter was then mounted in the sampling system, consisting of a ⅜ inch copper intake tube followed by a 71 mm filter holder (Model 710, Environmental Research Corp.) and a carbon-vane, oil-less pump (Model 1022, Gast Mfg., Benton Harbor, MI). Air from the tunnel was sampled continuously from May 3rd, 1990 (10:30 am) to May 23rd, 1990 (10:15 am) with an average flow rate of 173 m^3/day and an average pressure drop of 230 mm Hg across the filter. The total volume of air sampled was 3460 m^3. The mass of particulate matter was 96.73 mg (average TSP = 28.0 $\mu g/m^3$). After replacing the loaded filter in the filter holder, the inlet and outlet ports of the holder were capped and the assembly was stored in a refrigerator.

Desorption Apparatus. A schematic of the filter desorption apparatus is shown in Figure 3.1. The same filter holder that was used to collect the particles was used for the desorption. Clean, humidified N_2 was passed through the filter at a controlled rate, thereby inducing sorbed compounds to desorb from the particle-laden filter. The lab-grade compressed N_2 (Air Products) was cleaned with a hydrocarbon trap containing 50:50 activated carbon and molecular sieve 13X (Chemical Research Supplies, Addison, IL). The trap was conditioned prior to use by heating it for several hours at 300°C with concomitant throughput of ultra-high purity He (Air Products). A humidifier downstream of the hydrocarbon trap maintained an environment of constant relative humidity to prevent the particles from drying out during the desorption. Ports in the N_2 line both before ("system blank") and after ("sample") the filter allowed the gas stream to be sampled with adsorption/thermal-desorption (ATD) cartridges packed with 0.9 grams of 35/60 mesh Tenax-TA (Alltech Associates, Inc., San Jose, CA). Needle valves regulated the flow through each cartridge. Approximately 20% of the flow through the filter passed through the sample ATD cartridge. The balance of the flow ("waste") was vented to a hood. Flow

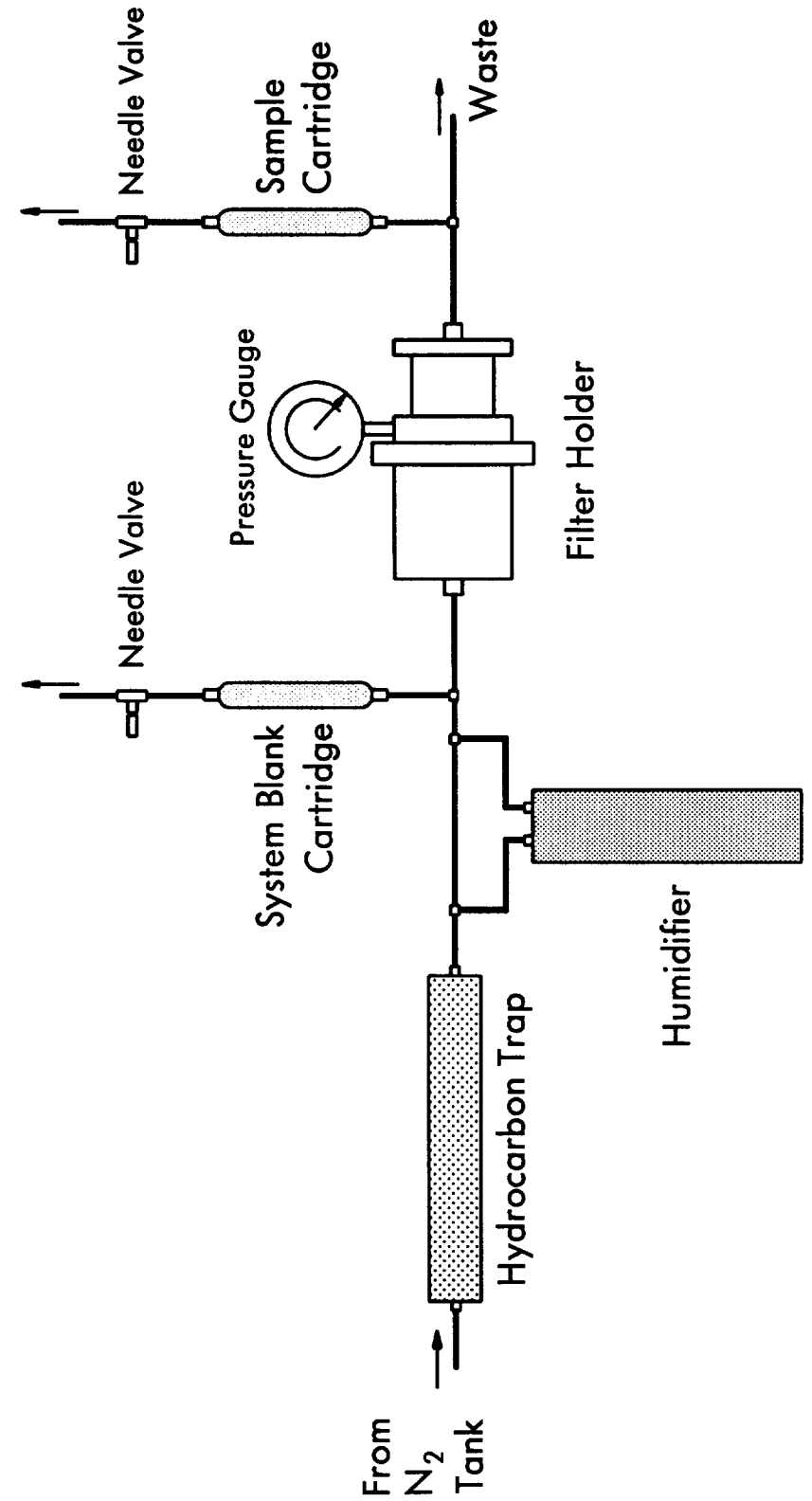

Figure 3.1. Schematic of the experimental filter desorption apparatus.

rates were measured with a calibrated wet test meter (Precision Scientific, Chicago, IL). Relative humidity measurements were made with a dew point hygrometer (Model 880, EG&G Thermoelectric, Idaho Falls, ID). Teflon tubing was used throughout the system.

Procedure. The desorption experiment took place over a period of 28 days. Except for very brief periods when it was necessary to replace cartridges or N_2 cylinders, a continuous flow of N_2 through the filter and the ATD cartridges was maintained. Because the gas-phase concentrations of the more volatile compounds were expected to decrease rapidly over time, the ATD cartridges were initially replaced after short time intervals, and thereafter at increasingly longer intervals. The system blank and sample cartridges were always replaced simultaneously. Each used ATD cartridge was capped, sealed in a screw cap tube, and stored in a refrigerator. Ten sets of system blank and sample cartridges were collected over the course of the experiment.

The total flow rate through the filter was measured periodically and averaged 3.30 L/min, giving an average filter face velocity of 1.5 cm/sec (Figure 3.2). The average flow rates through the system blank, sample, and waste lines were 0.63, 0.69, and 2.61 L/min, respectively. A total of 131.5 m^3 of N_2 was passed through the filter during the experiment. The mean relative humidity of the exit gas was 53%. The experiment was conducted at ambient laboratory temperature (22°-24°C).

Compounds. A suite of *n*-alkanes and PAHs were selected as representative compounds with a range of gas/particle partitioning properties. The *n*-alkanes used were hexadecane (C16), octadecane (C18), nonadecane (C19), eicosane (C20), heneicosane (C21), docosane (C22), tricosane (C23), tetracosane (C24), and pentacosane (C25). The PAHs used were acenaphthene (ACE), acenaphthylene (ACY), benz(a)anthracene (BaA), chrysene (CHR), fluoranthene (FLA), fluorene (FLU), 9-fluorenone (9FL), 2-methylphenanthrene (2ME), phenanthrene (PHE), and pyrene (PYR). Compounds with relatively high vapor pressures (e.g. naphthalene) were excluded from the group because they were

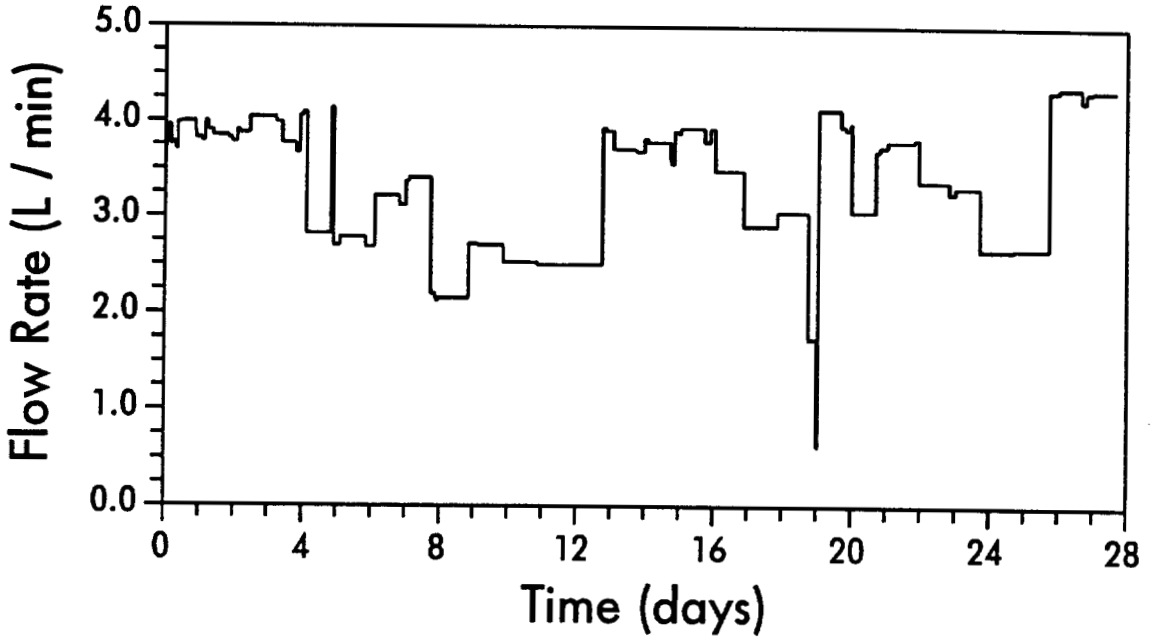

Figure 3.2. Flow rates measured during the desorption experiment.

not likely to be present in the particulate phase at measurable levels. Similarly, compounds with extremely low vapor pressures were not included since the desorption rates of those compounds would be immeasurably low and therefore unsuitable for a kinetic study. Standard materials were obtained from various suppliers and used without further purification.

Analytical Methods. All analyses were performed with a Hewlett-Packard 5790A GC (Palo Alto, CA) interfaced to a Finnigan 4000 mass spectrometer/data system (MS/DS) (Sunnyvale, CA). Chromatographic separation was achieved with a 30 m, 0.32 mm i.d. DB-5 capillary column with a 0.25 μm film thickness (J&W Scientific, Folsom, CA). ATD cartridges were analyzed in the manner of Pankow *et al.* (*29*). Prior to the analysis, each cartridge was spiked with an internal standard. Cartridges were desorbed with ultra-high purity He for 30 minutes at 270°C. Whole column cryotrapping at 0°C was employed during the thermal desorption step, followed by a temperature program of: 0°-150°C @ 25°C/min, 150°-310°C @ 10°C/min, hold @ 310°C for 2 minutes. Standard m/z values were used for quantitation.

Immediately upon completion of the experiment, the filter was removed from its holder and extracted to determine the concentrations of all compounds that were incompletely desorbed. A blank TMF was similarly extracted to determine procedural blank levels. Each filter was spiked with a surrogate standard, then Soxhlet-extracted with 325 mL methylene chloride for 5½ hours. The extract volume was reduced to between 2 and 3 mL via evaporation using 3-ball Snyder columns. Upon cooling, each extract was passed through a clean-up/drying column packed with 0.6 grams of activated silica gel (J.T. Baker, Phillipsburg, NJ, 60-200 mesh, chromatography grade) and 0.4 grams of anhydrous sodium sulfate (Mallinckrodt, Inc., St. Louis, MO, analytical grade) to remove polar compounds and traces of water. The silica gel was conditioned prior to use at 400°F for over 16 hours; the Na_2SO_4 was conditioned at 800°F for the same period of time. Each column was rinsed with 100 mL of methylene chloride before use. After passage through the cleanup columns, the treated

extracts were gently blown down to ~400 μL with N_2. The columns were then rinsed with ~3 mL aliquots of methylene chloride. These rinses were combined with the extracts, and the volume was again blown down. This rinse/blow-down cycle was repeated a total of three times. The extracts were stored in vials in a freezer.

Immediately prior to analysis, the extract vials were weighed and spiked with an internal standard. Analysis was performed with the previously described GC/MS/DS, equipped this time with an on-column injector (J&W Scientific, Folsom, CA). Injections of 1.0 μL of each extract were analyzed using a temperature program of: hold 60°C for 0.5 min, 60°-150°C @ 20°C/min, 150°-300°C @ 10°C/min.

The gas-phase concentrations determined downstream of the filter represent averages over their respective sampling periods. Because the observed concentrations were not associated with precise points in time, the experimental data were most conveniently represented as

$$\frac{\left(\textit{cumulative mass desorbed}\right)_t}{\textit{total mass of compound}} \tag{3.3}$$

The subscript t is the total elapsed time at the end of a given sampling period; the total mass includes the total amount desorbed during the experiment as well as the mass extracted from the filter. This ratio is the fractional approach to equilibrium. At equilibrium with the clean N_2, the cumulative mass desorbed will equal 100% of the total mass of the compound.

Intraparticle Diffusion Model

Formulation. The filter-based intraparticle diffusion model used in this work is the one discussed by Rounds and Pankow (*28*). This version, however, is modified to accept a variable flow rate through the filter. Many assumptions are inherent in the formulation of this model. Intraparticle diffusion is assumed to be the only process that limits the exchange of compounds between the gas

and particulate phases. Particles are assumed to be spherical and to have a nonporous, nonsorbing inner core surrounded by a uniformly porous, sorbing outer shell. The radius of the solid core is given by

$$r_c = R(1-\alpha)^{1/3} \tag{3.4}$$

where R is the radius of the entire particle and α is the fractional particle volume that is porous. Alpha is nonzero and assumed to be constant, regardless of particle size. It is assumed that sorption within each particle is reversible, instantaneous, and follows the linear isotherm represented by equation (3.1). Each particle in the size distribution is assumed to have identical, uniform sorption properties; that is, K_p and D_{eff} are constant both within the particles and from particle to particle. These assumptions may oversimplify the shape and uniformity of atmospheric particulate matter, but they do constitute a workable set of approximations.

The governing equation for intraparticle diffusion in spherical coordinates is given by

$$\frac{\partial S(r)}{\partial t} = D_{eff}\left[\frac{\partial^2 S(r)}{\partial r^2} + \frac{2}{r}\frac{\partial S(r)}{\partial r}\right] \tag{3.5}$$

where $S(r)$ is the total volumetric concentration of the compound at a radial distance r from the center of a particle ($r > r_c$), D_{eff} is the effective intraparticle diffusion coefficient, and t is the time. The effective diffusion coefficient is defined by Rounds and Pankow (*28*) as

$$D_{eff} = \frac{D_m \alpha n^2}{\rho_s K_p (1-\alpha n) 10^{12} + \alpha n} \approx \frac{D_m \alpha n^2}{\rho_s K_p (1-\alpha n) 10^{12}} \tag{3.6}$$

where D_m is the molecular diffusion coefficient in air, n is the intraparticle porosity of the porous shell (void volume in the shell per total volume of the shell), and ρ_s is the specific density of the particulate matter (g/cm^3). For the

purposes of this study, the values of ρ_s and n are assumed to be 2.0 g/cm^3 and 0.5, respectively.

This model represents the thickness of the filter (or the deposit of particles on/in the filter) as a series of N layers, each of which is equally populated with $1/N$th of the total particulate mass. Air parcels proceed through the filter one layer at a time, pausing for a time interval (Δt) to interact with the particles in each layer before moving through to the next layer. The filter, therefore, acts very much like a chromatographic column; N is the number of theoretical plates. At the beginning of a simulation, it is assumed that gas/particle partitioning equilibrium exists for each of the sorbed compounds; that is, $S(r)$ is constant with respect to r for $r > r_c$. As long as partitioning equilibrium exists at the start of the desorption, any phase redistribution problems that may have occurred during the collection of particles are irrelevant.

The size distribution of the collected particles was not measured. Rather, the classic Pasadena aerosol as measured by Whitby *et al.* (*30*) was used as an estimate of the actual size distribution. That distribution has 27 size fractions. The computation time required to utilize a 27-bin distribution when the diffusion model is coupled to an optimization routine, however, is enormous, even on a computer such as the IBM RISC System/6000 (model 320, ~8 Mflops). Consequently, size fractions from the 27-bin size distribution were combined to create a 6-bin size distribution that still retains the basic character of the original distribution (Figure 3.3). The diameter for each bin of the 6-bin distribution is the average of the combined bins, weighted by volume fraction. When a uniform specific density is assumed, the volume fraction is identical to the mass fraction.

General Characteristics. The general behavior of the filter-based intraparticle diffusion model is characterized by three parameters: the number of filter layers, N; the mass-transfer time scale, T_M; and the diffusion reaction time scale, T_D. The physical significance of T_M can be conceptualized by considering the effect of an instantaneous change in gas-phase concentration

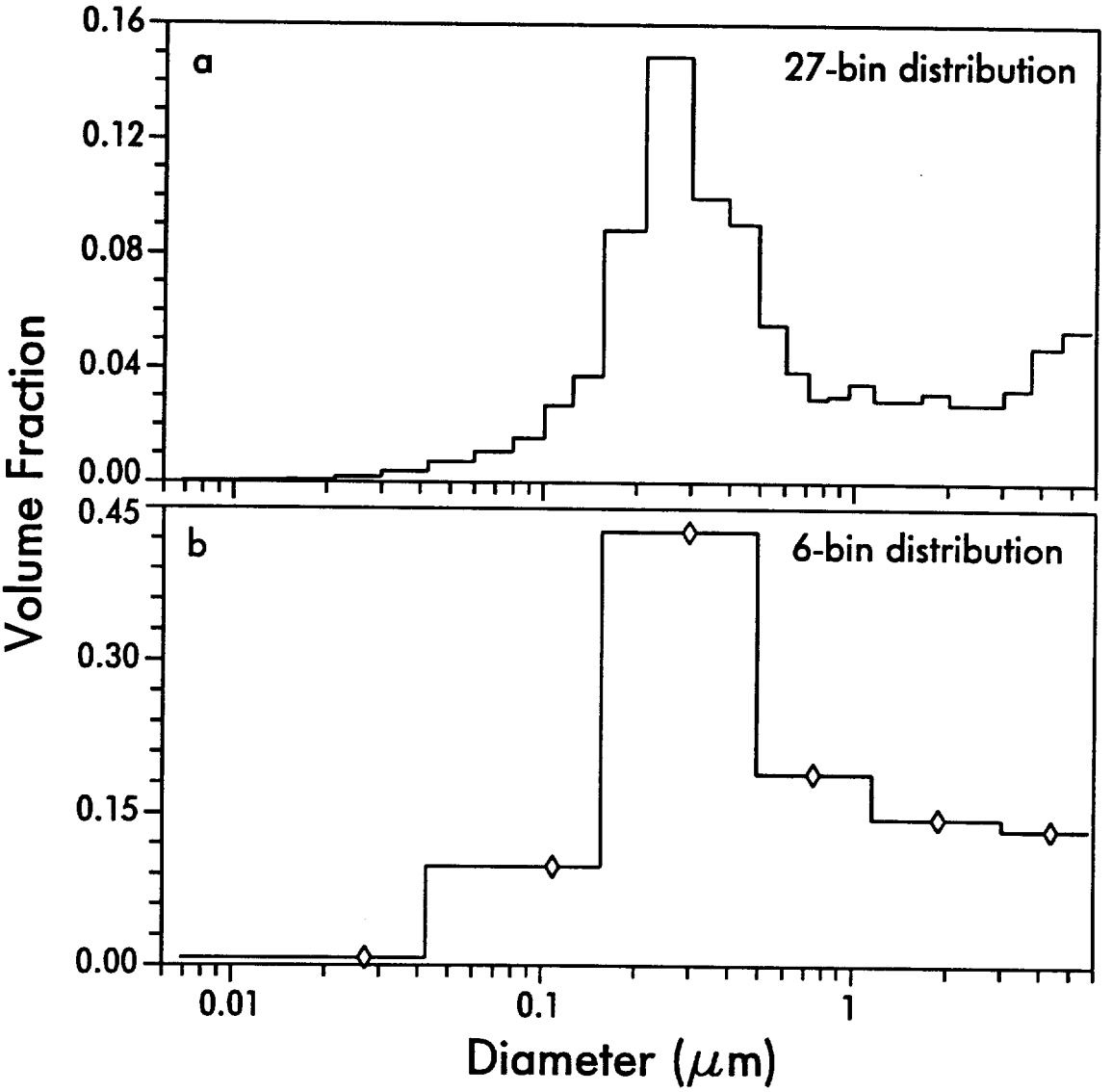

Figure 3.3. Volume distribution of aerosol particles in a 27-bin (a) and a 6-bin (b) distribution. The 27-bin distribution is the classic Pasadena aerosol as described by Whitby *et al.* (*30*). The 6-bin distribution is a coarser, volume-averaged version of the Pasadena aerosol. Diamonds on the 6-bin plot denote the volume-averaged diameter of each bin.

upon a particle-laden filter originally at sorption equilibrium with the influent gas phase. For equilibrium to be re-established, a finite mass of analyte must be exchanged between the gas and particulate phases; T_M is the time required for the influent gas stream to deliver/remove that mass of analyte. Regardless of the rate of the exchange process, equilibrium cannot be re-achieved in a time less than T_M. Mathematically, T_M and T_D are given as

$$T_M = \frac{K_p M_p}{f} \quad , \qquad T_D = \frac{(diffusion\ length)^2}{D_{eff}} \tag{3.7}$$

where M_p is the mass of particles on the filter (μg), and f is the **constant** flow rate through the filter (m^3/min). For a general analysis, it is convenient to consider a system with a constant flow rate. The diffusion reaction time scale for polydisperse size distributions can be defined as an average of T_D for each size, weighted by the mass fraction. For fully porous particles (α = 1.0), the diffusion length is equal to the particle radius.

The normalized breakthrough curve predicted by this model is determined almost entirely by the number of filter layers and the relative magnitudes of T_M and T_D. Consider first the base case in which diffusion is instantaneous (T_M/T_D = ∞). The dependence of the normalized breakthrough curve and the fractional approach to equilibrium on the number of filter layers is illustrated in Figures 3.4 and 3.5, respectively. The gas-phase concentration exiting the filter is A_{out}, and the fractional approach to equilibrium is M_t/M_e, where M_t is the mass exchanged between phases at time t and M_e is the corresponding amount at equilibrium. Characteristic curves are plotted in each graph for N = 1, 2, 4, 8, 16, 32, 64, 128, 256, 512, and ∞. The x axis is a dimensionless mass-transfer time, t/T_M. As the number of layers is increased, the breakthrough (desorption) curve more closely approximates a step function, and equilibrium is achieved at times closer to T_M. For the one layer case, all of the particles on the filter are exposed to the same air parcel simultaneously. Consequently, the gas-phase concentration at any given time cannot vary with depth in the filter. As more

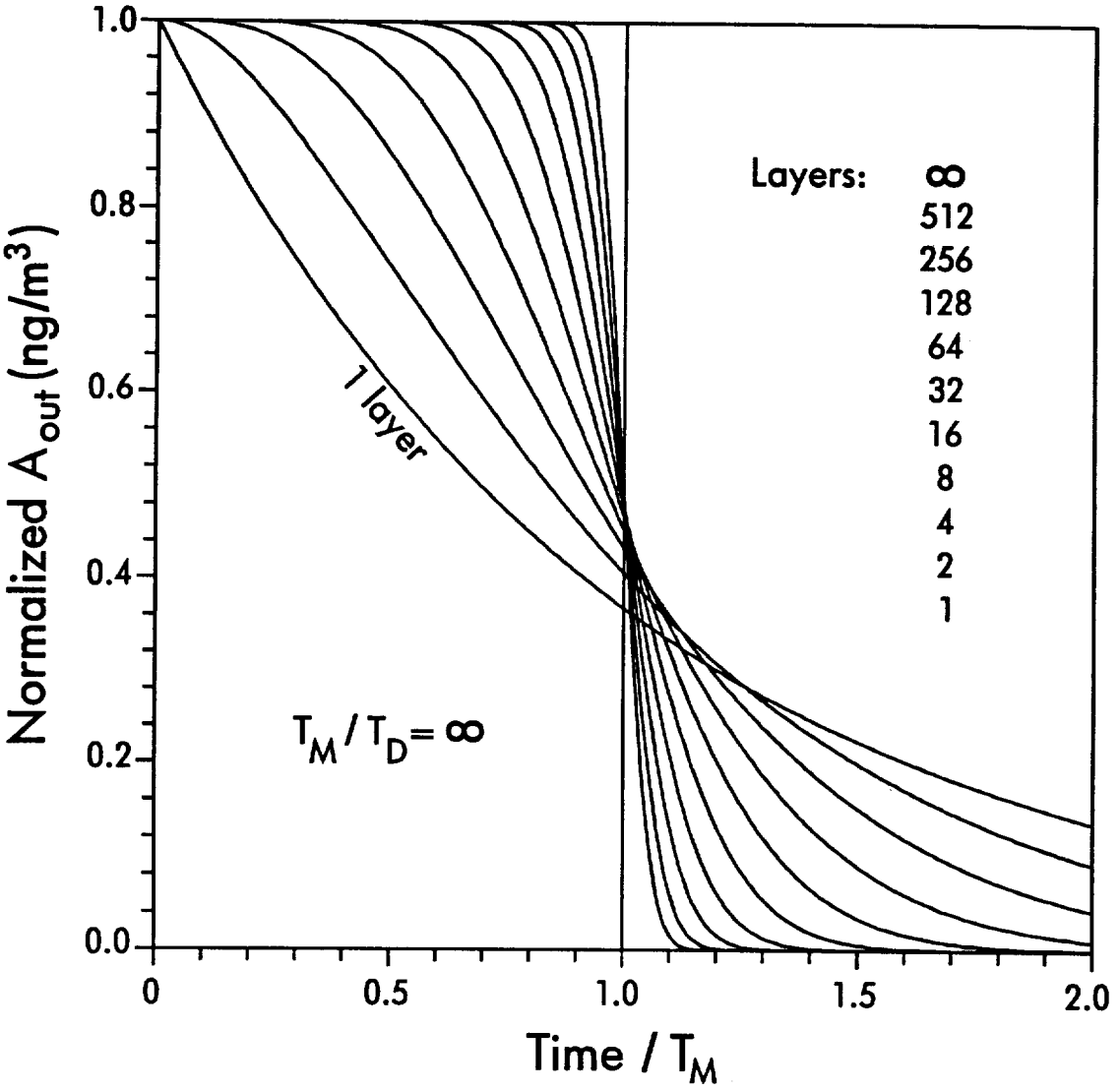

Figure 3.4. Dependence of the normalized breakthrough curve on the number of theoretical plates (layers) in the filter when intraparticle diffusion is infinitely fast ($T_D = 0$). Time on the x-axis is normalized to the mass-transfer time scale.

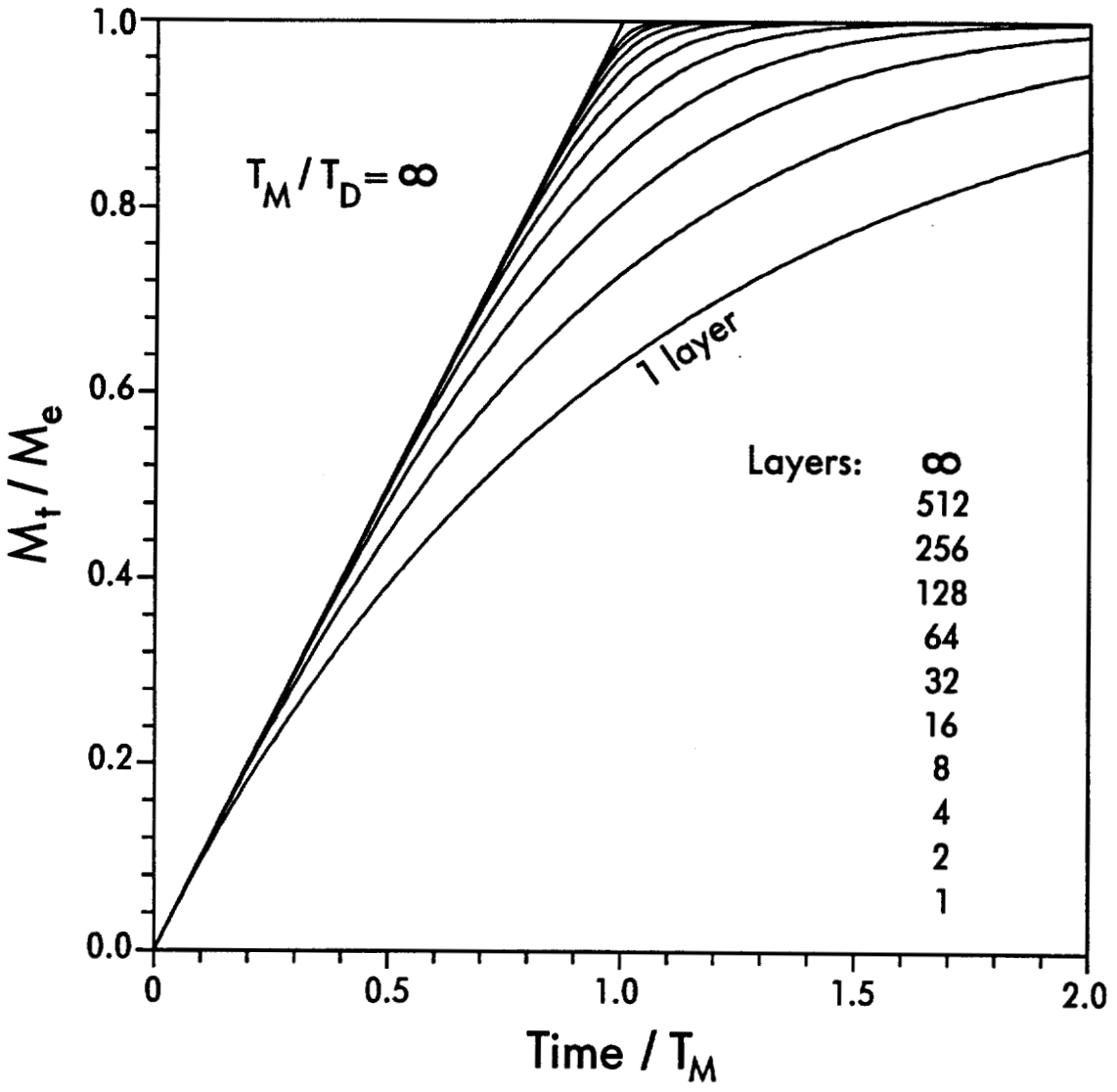

Figure 3.5. Dependence of the fractional approach to equilibrium on the number of theoretical plates (layers) in the filter when intraparticle diffusion is infinitely fast ($T_D = 0$). Time on the x-axis is normalized to the mass-transfer time scale.

layers are added, the gas-phase concentration of an air parcel is allowed to change in an increasingly smooth fashion as it traverses the filter.

In attempting to model a real system, the selection of a number for N reflects a fundamental decision concerning the physical processes that are at work in the filter. Clearly, the gas-phase concentrations in each air parcel must change as it travels through the filter. The question is whether or not the particles embedded deep in the filter (or the particle bed) are exposed to a significantly different environment than those on the leading edge. Both extrema were investigated in this work; simulations were performed with both 1 and 40 filter layers. Forty layers were chosen as an approximation to the infinite layer case because of the dramatic rise in computation time with increasing N.

The ratio of the mass-transfer and diffusion reaction time scales is a good measure of the relative importance of intraparticle diffusion in determining the shape of the normalized breakthrough curve. The dependence of A_{out} and M_t/M_e on the ratio of time scales is illustrated in Figures 3.6 and 3.7 for the case of 1 filter layer and in Figures 3.8 and 3.9 for 40 layers. In both cases, an increase in the diffusion reaction time scale (a decrease in T_M/T_D) causes the exchange of analyte between phases to become slower. This is reflected by a downward shift in the M_t/M_e curves and an increase in the time needed to reach equilibrium. For the base case of instantaneous diffusion ($T_M/T_D = \infty$), no concentration gradients exist inside the particles. Deviations from this base case are caused by the creation of such gradients. Note that the curve families for the 1 and 40 layer cases have characteristically different shapes. While the same trends are visible within each family, the curvature of lines with identical T_M/T_D are markedly different. Simulations from one family, therefore, may fit the experimental data better than those from the other.

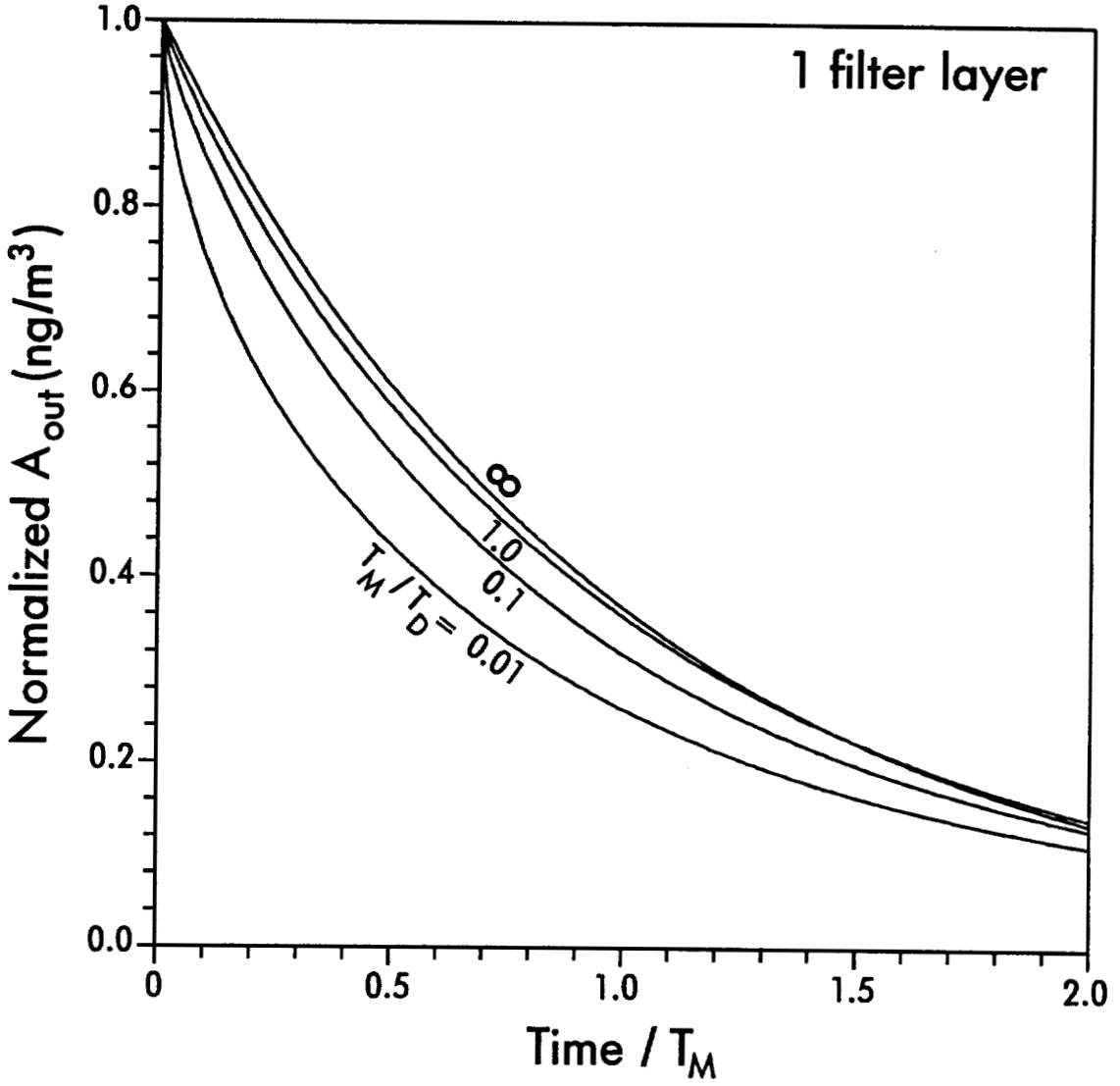

Figure 3.6. Simulated, normalized breakthrough curves for 1 filter layer, 51 nodes/particle, and fully porous particles in the 6-bin size distribution. The value of the characteristic parameter T_M/T_D is noted next to each curve. The base case is represented by the $T_M/T_D = \infty$ curve, which was calculated analytically.

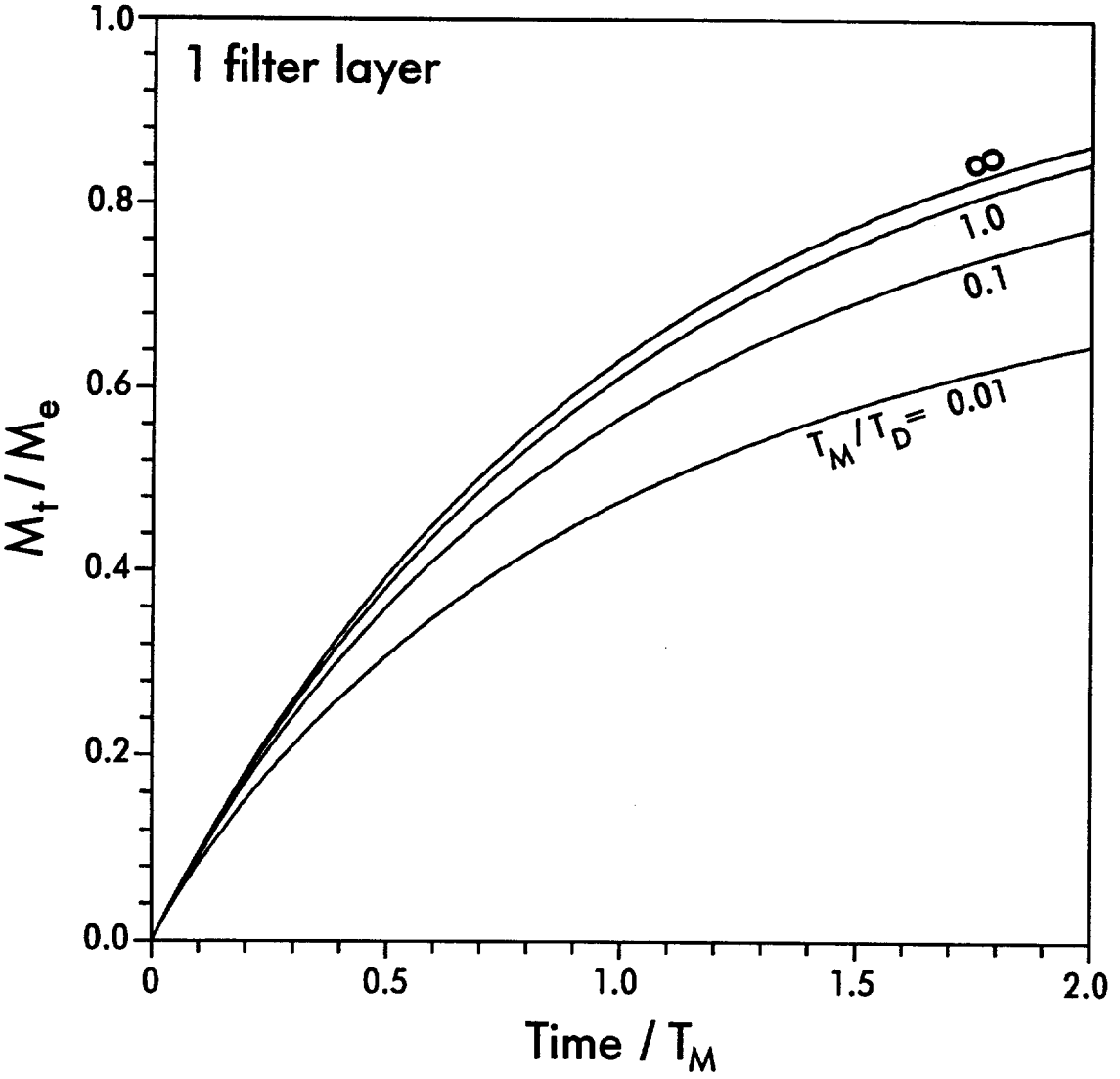

Figure 3.7. Simulated, normalized fractional approach to equilibrium curves for 1 filter layer, 51 nodes/particle, and fully porous particles in the 6-bin size distribution. The value of the characteristic parameter T_M/T_D is noted next to each curve. The base case is represented by the $T_M/T_D = \infty$ curve, which was calculated analytically.

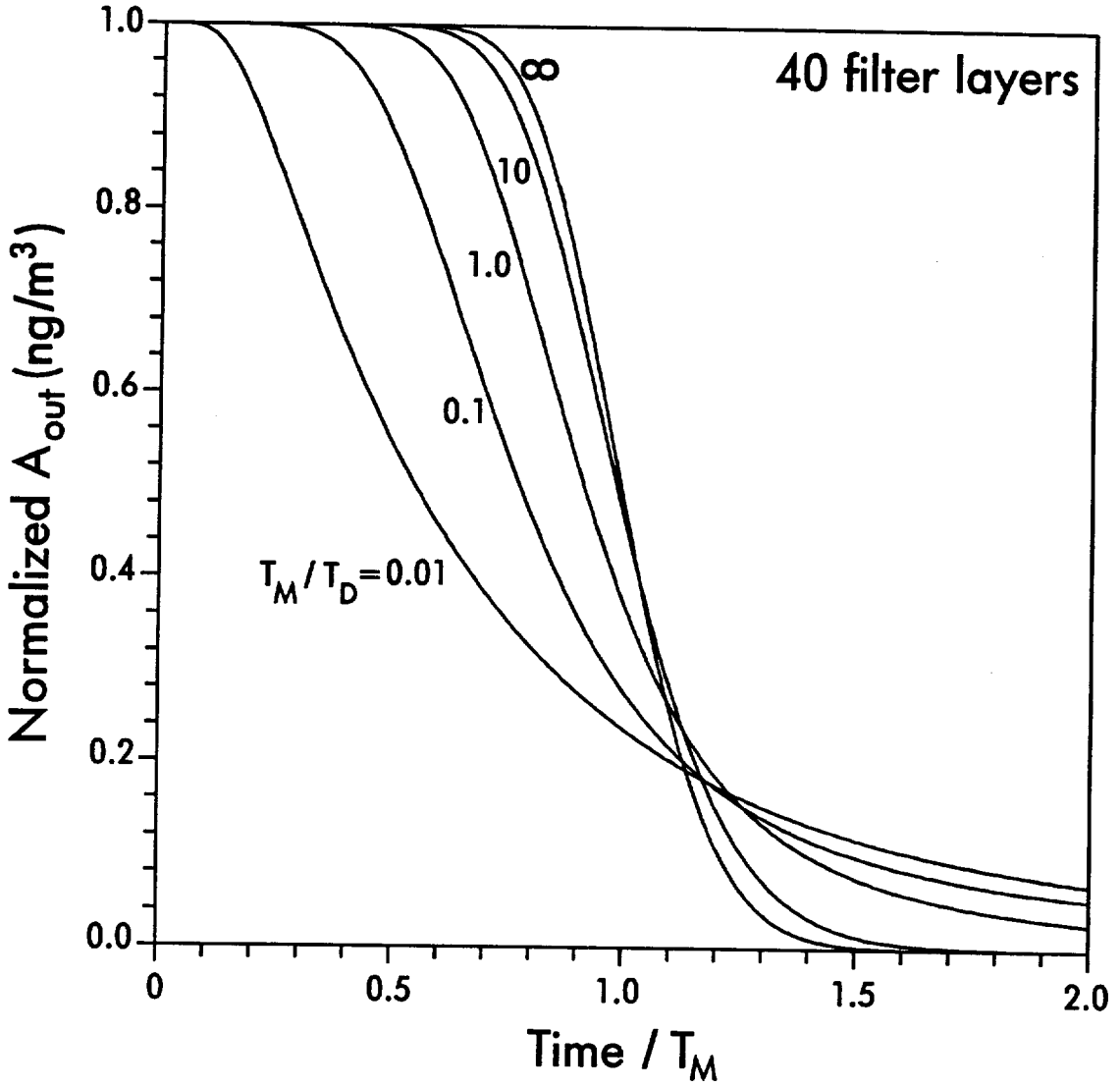

Figure 3.8. Simulated, normalized breakthrough curves for 40 filter layers, 51 nodes/particle, and fully porous particles in the 6-bin size distribution. The value of the characteristic parameter T_M/T_D is noted next to each curve. The base case is represented by the $T_M/T_D = \infty$ curve, which was calculated analytically.

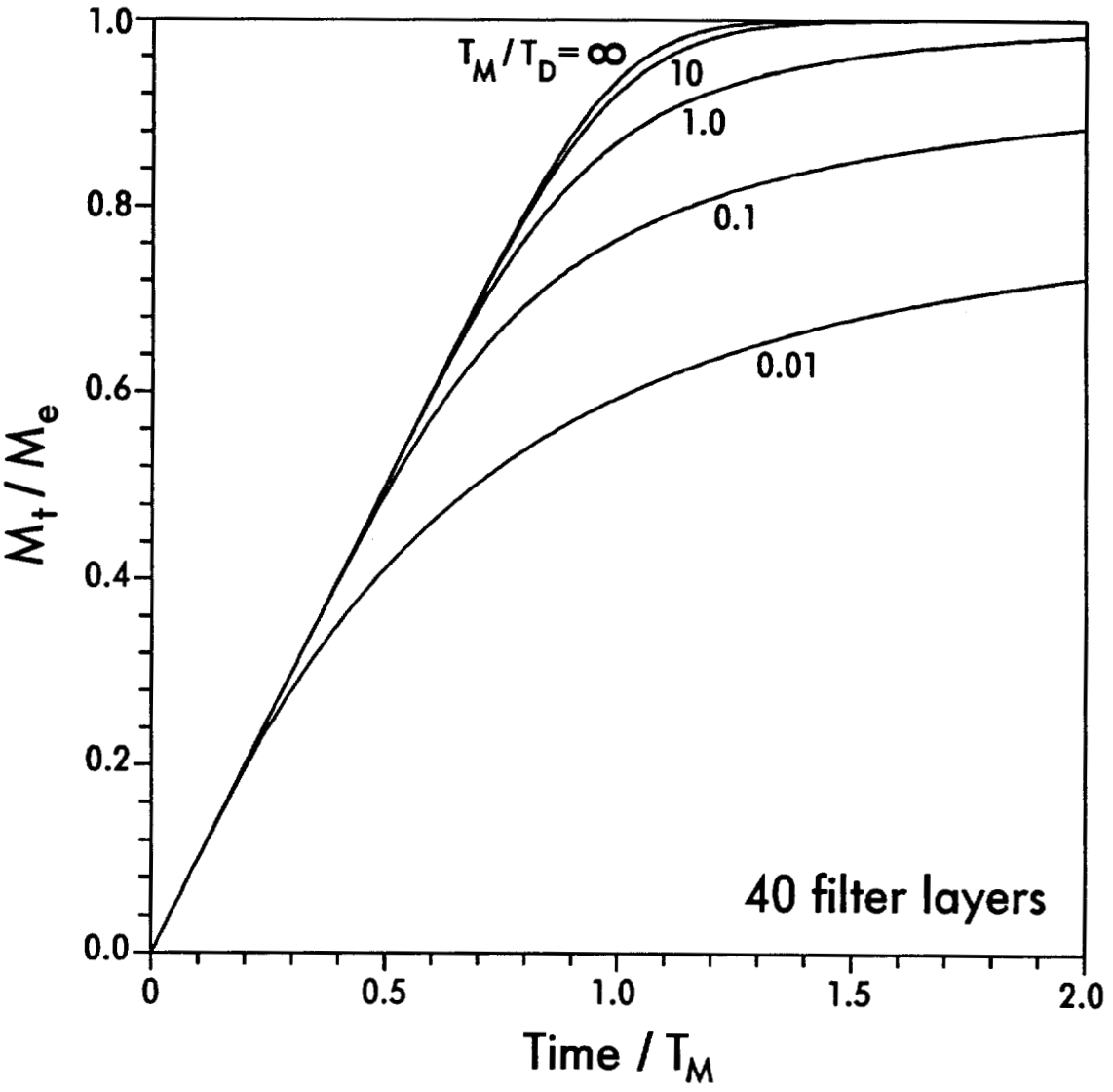

Figure 3.9. Simulated, normalized fractional approach to equilibrium curves for 40 filter layers, 51 nodes/particle, and fully porous particles in the 6-bin size distribution. The value of the characteristic parameter T_M/T_D is noted next to each curve. The base case is represented by the $T_M/T_D = \infty$ curve, which was calculated analytically.

Optimization Method

The filter-based intraparticle diffusion model was fitted to the experimental M_t/M_e data through the use of a non-linear least squares optimization routine. Two independent fitting parameters were used: the partition coefficient (K_p) and the effective diffusion coefficient (D_{eff}). The best fit was defined as that which minimized the sum of squared residuals (*SSR*), calculated as

$$SSR = \sum_{i=1}^{10} \left[\left(M_t/M_e \right)_{calc,i} - \left(M_t/M_e \right)_{expt,i} \right]^2 \qquad (3.8)$$

where $(M_t/M_e)_{calc,i}$ and $(M_t/M_e)_{expt,i}$ are the calculated and experimental values of M_t/M_e at the end of sampling period i. The downhill simplex method as described by Press *et al.* (*31*) was used as the optimization technique. Although this routine might be characterized as inefficient, in this instance it was more robust and faster than the more elegant conjugate direction set method of Powell (as described by Press *et al.* (*31*)). For each optimization, the simplex routine was started from at least four different positions in the K_p-D_{eff} domain. Except in cases where one of the parameters was found to be indeterminate, runs from different starting positions always converged to the same point.

Estimated confidence limits were determined for each of the optimized values of K_p and D_{eff}. Standard statistics texts carefully point out that confidence limits cannot be precisely defined for the parameters of a non-linear system (*32-33*). For two fitted variables in such a system, confidence *regions* can be created in the parameter domain by plotting contours of constant *SSR*, but the level of confidence, again, is not rigorously defined. The confidence level can be estimated, however, using known theoretical relationships developed for linear systems. An approximate 95% joint confidence region for K_p and D_{eff}, then, is bounded by a *SSR* contour whose value is given by (*32-33*)

$$SSR_{crit} = SSR_{min}\left[1 + \frac{p}{N_p - p}\,\mathbf{F}(p, N_p - p, 0.95)\right] \qquad (3.9)$$

where SSR_{crit} is the critical sum of squares, SSR_{min} is the minimum sum of squares given by the best fit, p is the number of fitted parameters, N_p is the number of data points used in the fit, and $\mathbf{F}(p, N_p\text{-}p, 0.95)$ refers to an F distribution with p and $N_p\text{-}p$ degrees of freedom. Given this approximate confidence region, Olmstead and Weber (*34*) proposed that individual confidence limits can be obtained by holding one parameter constant and moving to the edge of the region with the other parameter. These estimated limits do not have a rigorous theoretical basis, but they are useful in conveying an understanding of the goodness-of-fit. A typical contour map of the sum of squared residuals is shown in Figure 3.10. The shaded portion of the graph is the approximate 95% confidence region. The best-fit point is denoted by a diamond, and the error bars about that point are the estimated 95% confidence limits on each parameter.

Results and Discussion

The filter desorption experiment was designed to ensure that the release of compounds from the particles was caused only by the imposed concentration gradients. Processes that we sought to avoid were: desorption rate changes due to temperature fluctuations (*14, 20-21*), volatilization due to a pressure drop across the filter (*35*), chemical reactions with reactive gases or sunlight (*14-19*), and sorption of compounds to the filter media (*36-37*). Temperature fluctuations in the laboratory were small; therefore, desorption rates for each compound were not significantly affected by such variations. The pressure drop across the filter and the resulting face velocity were small, thus minimizing any volatilization problems. Chemical reactions were avoided by using clean nitrogen to desorb compounds from the filter. The use of a Teflon membrane filter minimized the sorption of gas-phase compounds to the filter medium.

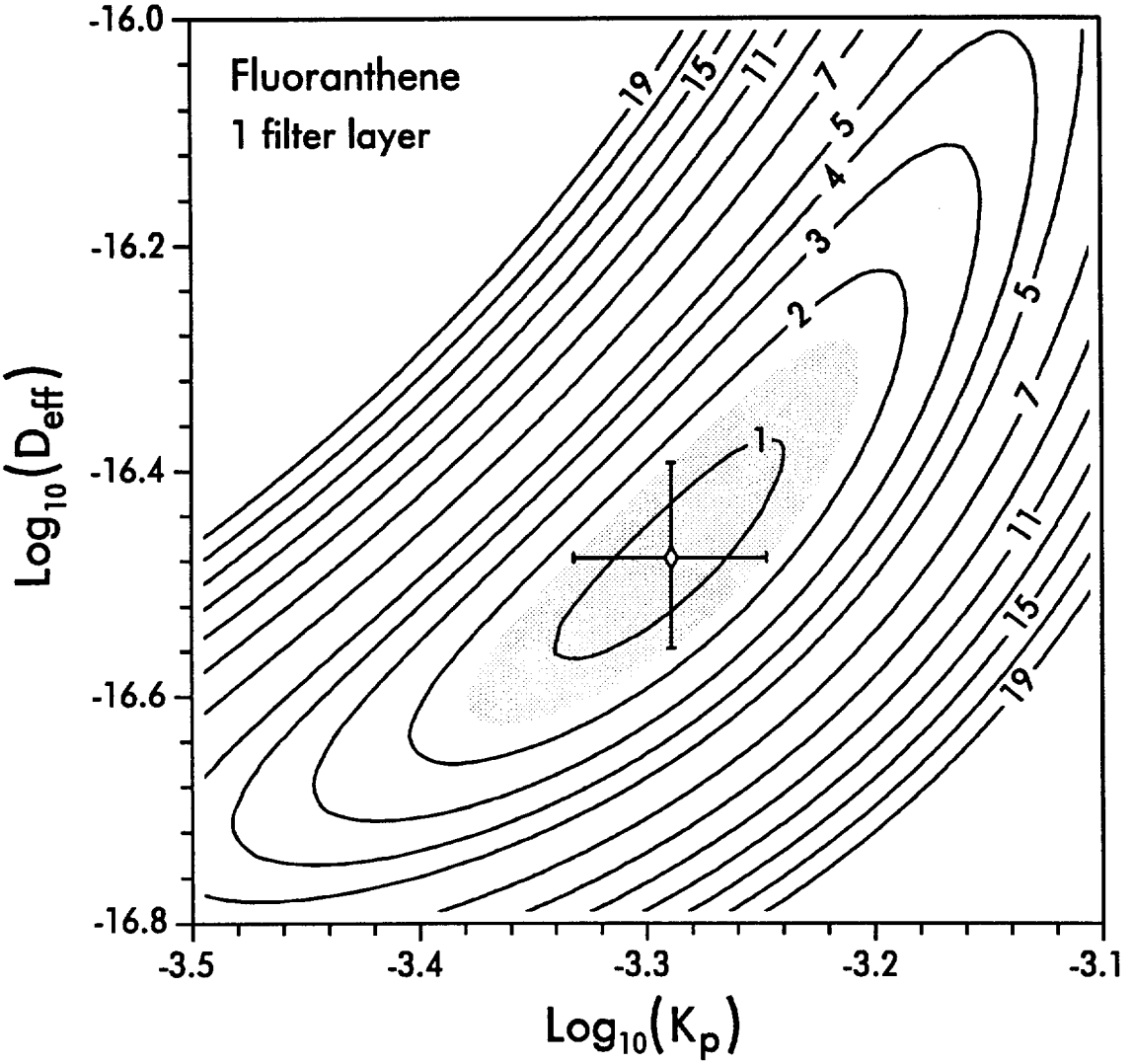

Figure 3.10. Contour map of the sum of squared residuals (times 1000) for fluoranthene using 1 filter layer, 51 nodes/particle, and fully porous particles in the 6-bin size distribution. The shaded area is the 95% confidence region. The best-fit point is represented by the diamond, and the error bars about that point are the estimated 95% confidence limits on each parameter.

Because the effects of other processes were minimized or eliminated, the experimental release data represent the effects of primarily one process: desorption due to an imposed concentration gradient.

It is impossible to extract any specific kinetic information from a visual examination of the experimental M_t/M_e versus volume (V) data for a given compound. The M_t/M_e data for most compounds were characterized by a curvature of generally decreasing slope similar to some of the curves in Figures 3.5, 3.7, and 3.9. A visual analysis of the relative importance of kinetic and equilibrium processes is not possible, however, because significant curvature is expected even for the equilibrium case ($T_M/T_D = \infty$) when the number of filter layers is small. Therefore, an analysis of the desorption kinetics can only be performed by fitting the diffusion model to the data and examining the magnitudes of the optimized parameters. For example, if the fitted values of D_{eff} are very large, then the kinetics of diffusion are very fast and are not rate-limiting, and *vice versa*.

Best-fit values of the partition coefficient and the effective diffusion coefficient for each of the compounds were obtained through the use of the non-linear least squares optimization routine described previously. Optimizations were performed for both 1 and 40 filter layers. Fully porous particles ($\alpha = 1.0$) and the 6-bin particle size distribution were used in both cases. Due to computation time constraints as outlined by Rounds and Pankow (*28*), 21 nodes per particle were used in the 40 layer case. Because the 1 layer case is intrinsically less demanding of computation time, the number of nodes per particle for those runs was increased to 51. Sensitivity tests showed that this increase was expected to change the values of the best-fit parameters by less than 3 percent. All optimizations were performed on an IBM RISC System/6000 (model 320). Despite the speed of that machine ($\sim$8 Mflops), runs for the 40 layer case required between 3 and 4 hours of computation time; 1 layer optimizations were faster, requiring $\sim$45 minutes per compound. Estimation of

individual 95% confidence limits for the best-fit values via the relationship in equation (3.9) took only 10 to 30 minutes of computation time per compound.

Excellent agreement was obtained between experimental and predicted curves for most of the compounds. Fits of the *n*-alkane data were found to be especially good, while those for a few of the PAHs do not match as well. The optimized breakthrough and fractional approach to equilibrium curves are plotted with the experimental data in Figures 3.11 and 3.12 for nonadecane and in Figures 3.13 and 3.14 for fluoranthene. These fits are representative of the agreement obtained for most of the compounds. The small "blips" on the predicted breakthrough curves in Figures 3.11 and 3.13, most noticeable at ~ 23, ~ 40, and ~ 87 m^3, are real and caused by corresponding decreases in the flow rate at ~ 4, ~ 8, and ~ 19 days (Figure 3.2). The best-fit K_p and D_{eff} values are listed in Table 3.1. For all compounds, the optimized values of K_p and D_{eff} for the 40 layer case are larger and smaller, respectively, than for the 1 layer case. In general, a comparison of the estimated 95% confidence intervals on K_p for the 1 and 40 layer cases shows very little overlap. In contrast, overlap of the intervals is common for D_{eff}. While it is clear that the 1 and 40 layer cases give different best-fit values for K_p and D_{eff}, these differences may not be statistically significant, given the estimated nature of the confidence intervals.

The determination of the best overall choice for the number of filter layers was not possible with this data set. Best-fit predictions using 1 filter layer and 40 filter layers both agree well with the experimental data. Figures 3.11 through 3.14 illustrate the high degree of similarity between the two cases. By far the greatest difference between the 1 and 40 layer cases is their behavior at the beginning of the desorption. For some compounds such as nonadecane (Figure 3.11), the use of 1 layer results in a more accurate description of desorption early in the experiment. For other compounds such as fluoranthene (Figure 3.13), the differences are not as obvious. An examination of the residuals for all of the compounds revealed no systematic misrepresentations by the use of either 1 or 40 layers. Excluding the three PAHs that were not fitted well by either case, the

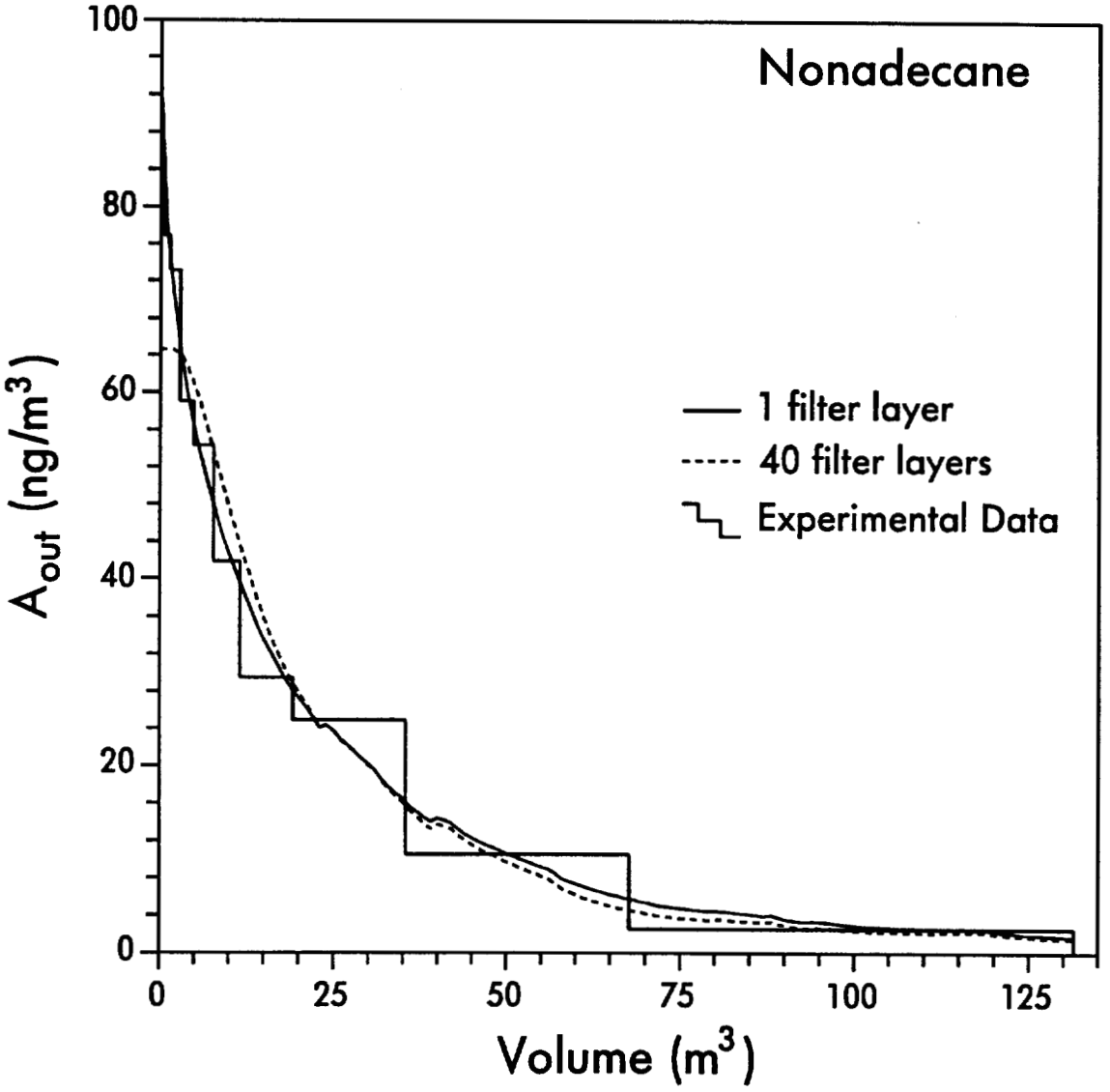

Figure 3.11. Fitted breakthrough curves for nonadecane. The solid curve represents the optimal fit for the 1 layer model, while the dashed line is the best fit using 40 filter layers. The experimental data are represented by a stairstep function. Fully porous particles in the 6-bin size distribution were used, with 51 and 21 nodes/particle in the 1 and 40 layer models, respectively.

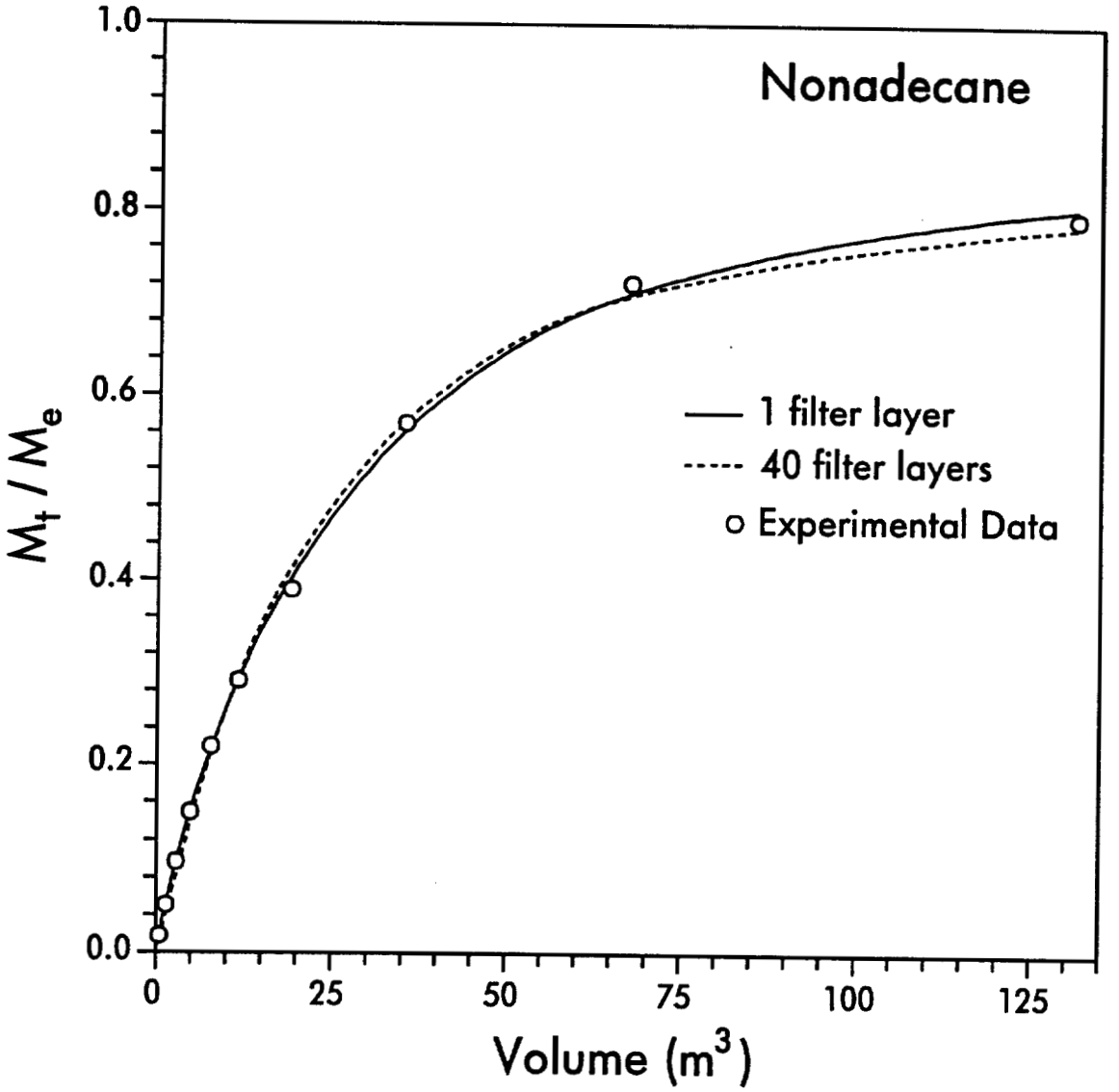

Figure 3.12. Fitted fractional approach to equilibrium curves for nonadecane. The solid curve represents the optimal fit for the 1 layer model, while the dashed line is the best fit using 40 filter layers. The experimental data are represented by open circles. Fully porous particles in the 6-bin size distribution were used, with 51 and 21 nodes/particle in the 1 and 40 layer models, respectively.

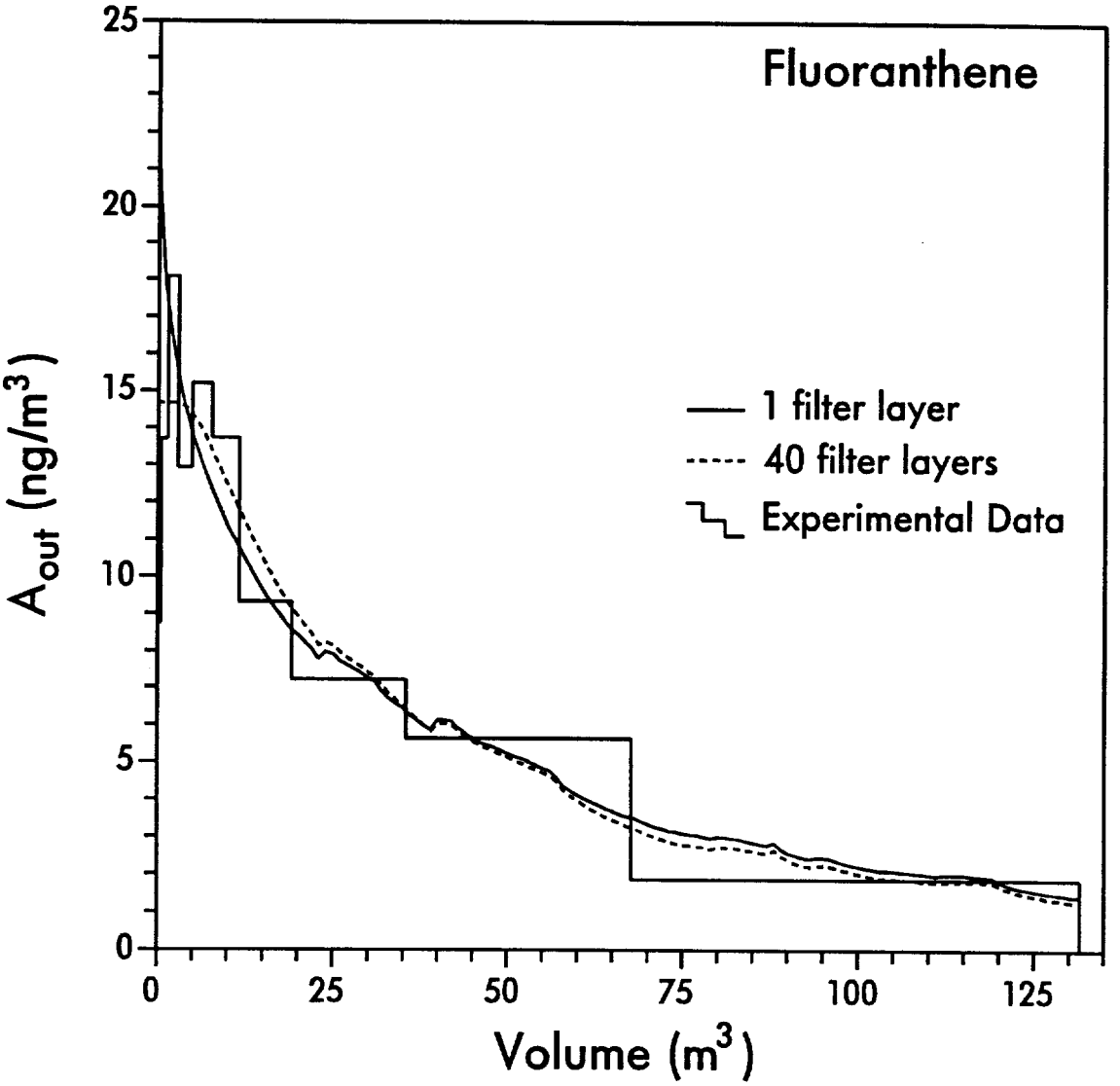

Figure 3.13. Fitted breakthrough curves for fluoranthene. The solid curve represents the optimal fit for the 1 layer model, while the dashed line is the best fit using 40 filter layers. The experimental data are represented by a stairstep function. Fully porous particles in the 6-bin size distribution were used, with 51 and 21 nodes/particle in the 1 and 40 layer models, respectively.

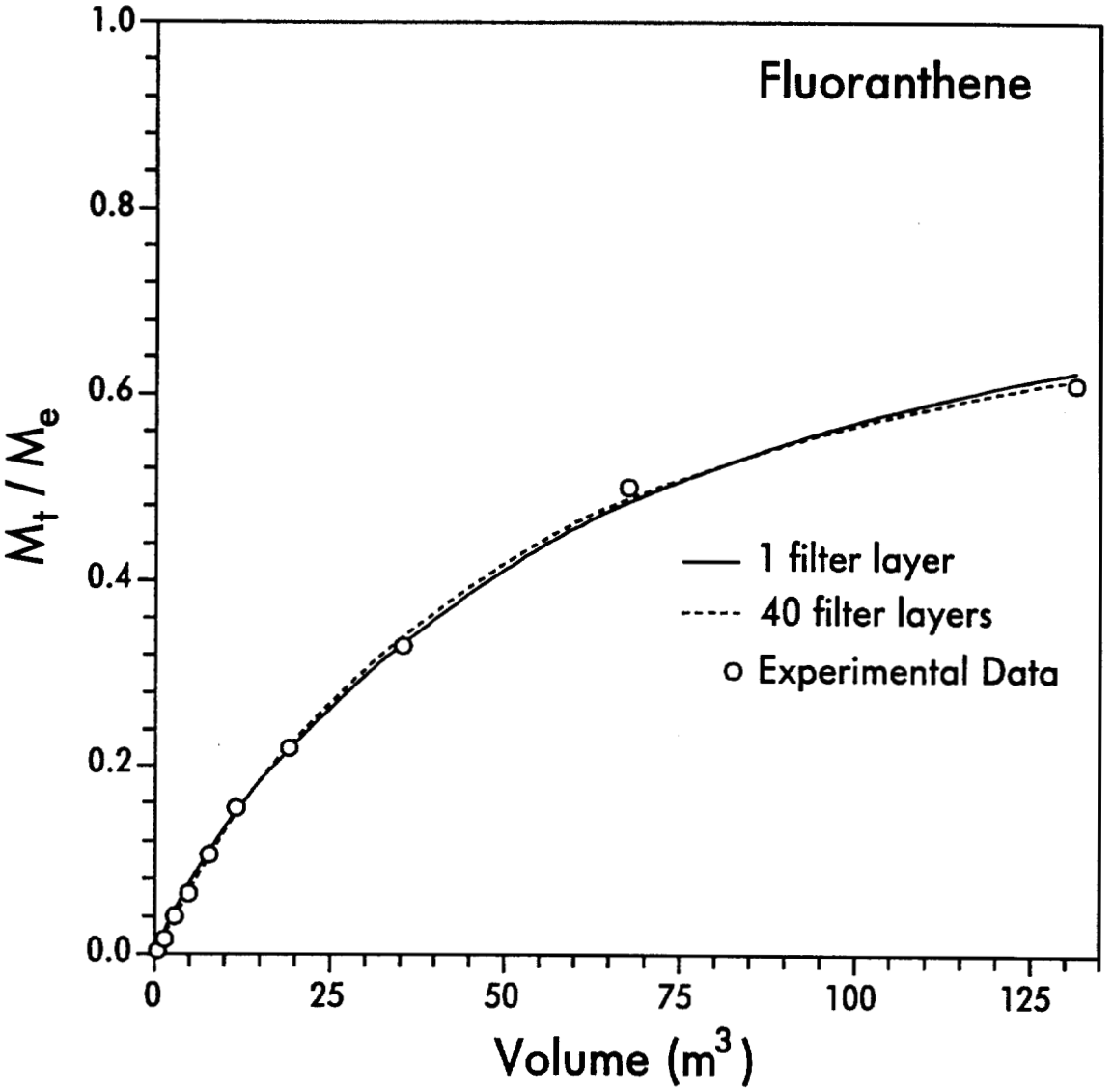

Figure 3.14. Fitted fractional approach to equilibrium curves for fluoranthene. The solid curve represents the optimal fit for the 1 layer model, while the dashed line is the best fit using 40 filter layers. The experimental data are represented by open circles. Fully porous particles in the 6-bin size distribution were used, with 51 and 21 nodes/particle in the 1 and 40 layer models, respectively.

Table 3.1. Best-Fit Values and Estimated 95% Confidence Intervals for K_p and D_{eff}.

compound	code	N	log K_p $m^3/\mu g$	log D_{eff} cm^2/s	C.I. for log K_p high – low	C.I. for log D_{eff} high – low
Hexadecane	C16	1	-4.160	-14.806	-4.059 – -4.268	-14.444 – -15.104
		40	-4.009	-15.093	-3.844 – -4.210	-14.660 – -15.444
Octadecane	C18	1	-3.939	-15.864	-3.875 – -4.008	-15.771 – -15.954
		40	-3.749	-15.953	-3.671 – -3.835	-15.850 – -16.052
Nonadecane	C19	1	-3.611	-15.804	-3.585 – -3.638	-15.736 – -15.870
		40	-3.445	-15.979	-3.399 – -3.492	-15.880 – -16.073
Eicosane	C20	1	-3.339	-15.652	-3.309 – -3.370	-15.506 – -15.786
		40	-3.202	-16.017	-3.159 – -3.246	-15.883 – -16.142
Heneicosane	C21	1	-3.038	-16.147	-3.010 – -3.065	-16.009 – -16.272
		40	-2.919	-16.549	-2.897 – -2.942	-16.489 – -16.606
Docosane	C22	1	-2.659	-17.308	-2.626 – -2.691	-17.218 – -17.396
		40	-2.522	-17.541	-2.497 – -2.547	-17.485 – -17.597
Tricosane	C23	1	-2.202	-19.103	-2.133 – -2.274	-19.010 – -19.202
		40	-1.928	-19.601	-1.868 – -1.987	-19.372 – -19.922
Tetracosane	C24	1	-1.728	-19.528	-1.699 – -1.758	-19.438 – -19.620
		40	-1.453	-26.128 [a]	-1.368 – -1.535	∞ – -∞
Pentacosane	C25	1	-0.954	-19.159	-0.926 – -0.980	-18.334 – -19.758
		40	-0.910	-21.492 [a]	-0.883 – -0.936	∞ – -∞

[a] Optimization did not give a precise value. This value is an average.

Table 3.1 (*continued*). Best-Fit Values and Estimated 95% Confidence Intervals for K_p and D_{eff}

compound	code	N	log K_p $m^3/\mu g$	log D_{eff} cm^2/s	C.I. for log K_p high – low	C.I. for log D_{eff} high – low
Acenaphthene	ACE	1	-5.205	-15.565	-4.303 – -∞	-15.198 – -15.896
		40	-4.965	-15.578	-4.093 – -∞	-15.214 – -15.908
Acenaphthylene	ACY	1	-4.526	-15.648	-4.048 – -∞	-15.243 – -15.998
		40	-4.471	-15.744	-3.882 – -∞	-15.389 – -16.071
9-Fluorenone	9FL	1	-11.015 [a]	-16.851	-4.074 – -∞	-16.703 – -17.006
		40	-4.830	-16.862	-3.726 – -∞	-16.708 – -17.025
Fluorene	FLU	1	-11.372 [a]	-17.033	-3.663 – -∞	-16.694 – -17.428
		40	-15.687 [a]	-17.067	-3.545 – -∞	-16.750 – -17.438
Phenanthrene	PHE	1	-11.403 [a]	-16.915	-3.868 – -∞	-16.663 – -17.190
		40	-16.473 [a]	-16.941	-3.634 – -∞	-16.698 – -17.208
2-Methylphenanthrene	2ME	1	-4.028	-16.743	-3.890 – -4.203	-16.688 – -16.798
		40	-3.711	-16.746	-3.609 – -3.835	-16.696 – -16.796
Fluoranthene	FLA	1	-3.289	-16.478	-3.247 – -3.332	-16.394 – -16.558
		40	-3.123	-16.620	-3.092 – -3.154	-16.571 – -16.667
Pyrene	PYR	1	-3.173	-17.013	-3.082 – -3.271	-16.894 – -17.132
		40	-2.970	-17.085	-2.904 – -3.040	-16.999 – -17.170
Benz(a)anthracene	BaA	1	-2.755	-17.576	-2.729 – -2.782	-17.533 – -17.620
		40	-2.581	-17.712	-2.548 – -2.614	-17.661 – -17.763
Chrysene	CHR	1	-2.233	-18.056	-2.206 – -2.261	-17.968 – -18.143
		40	-2.097	-18.364	-2.069 – -2.125	-18.270 – -18.456

[a] Optimization did not give a precise value. This value is an average.

use of 1 filter layer resulted in a lower SSR_{min} for 10 of the remaining 16 compounds. In particular, the 1 layer case gave smaller SSR_{min} values for 7 of the 9 *n*-alkanes.

The best choice for N should not be determined solely on the basis of fit; the physical characteristics of the particle load on the filter should also be considered. If a quartz fiber filter (QFF) were used in such an experiment, particles would be characteristically distributed throughout the thickness of the filter as well as on its front surface. This spatial separation of particles leads to the hypothesis that particles deeper in the filter might be exposed to a gas-phase concentration that is different from that which interacts with particles on the front edge of the filter. For a QFF, then, the choice of more than one filter layer seems logical. On the other hand, particle penetration into a Teflon membrane filter is less likely. This does not mean, however, that a choice of one filter layer should automatically be made for a TMF. A rough calculation of the volume of the particles on our TMF (M_p = 96730 μg) indicates that the particles are stacked on the filter in a layer tens of microns thick. Therefore, heavily loaded filters also have a spatial separation of particles that may allow those at the back of the bed to be exposed to a different gas-phase concentration than those on the leading edge. Given these considerations and the similar predictions of the 1 and 40 layer cases, it is not clear which is the better choice.

The three PAHs whose behavior defied description by the intraparticle diffusion model are 9-fluorenone, fluorene, and phenanthrene. In each case, the desorption data appear typical of other experiments; a rapid initial release is followed by a gradual decrease in the desorption rate. The confounding problem is that, despite very low desorption rates at the end of the experiment, considerable amounts of these three compounds were released during the filter extraction. As a result, the M_t/M_e versus V graphs are almost flat during the latter stages of the experiment, and yet the values of M_t/M_e at the end are only 0.53, 0.42, and 0.47 for 9FL, FLU, and PHE, respectively. The diffusion model cannot match this kind of curvature. Best-fit predictions underestimated the

initial release rates and overestimated the rates near the end of the experiment. It is possible that some fraction of the mass released during the Soxhlet extraction was either held tightly to specific sorption sites, or bound inside the solid matrix of the particles. In either case, this fraction may not desorb under the mild conditions of this experiment. The presence of specific sorption sites is unlikely, given the generally nonspecific nature of the partitioning process. Therefore, some fraction of the Soxhlet-extracted mass may have been "non-exchangeable" (*8, 10, 38-40*). Assuming that the fraction could be large, optimizations were rerun for these compounds neglecting the Soxhlet-extracted mass. In contrast to the first optimizations, the resulting predictions overestimated the initial release rates and underestimated the rates later in the experiment. Therefore, if a portion of the mass of these compounds was non-exchangeable, the non-exchangeable fraction was only part of that which was Soxhlet-extracted from the filter after the desorption experiment was terminated.

Partition Coefficients. An assessment of the accuracy of the best-fit K_p values can be attempted in many ways. Internal to the data set, the optimized values of K_p can be compared to estimates of K_p obtained from the initial slopes of M_t/M_e versus V graphs. All of the curves in Figures 3.5, 3.7, and 3.9 have an initial slope of 1.0. Since t/T_M is equal to $V/(K_pM_p)$ in the general case, experimental plots of M_t/M_e versus V will have initial slopes equal to $1/(K_pM_p)$. A least squares regression through the first two data points, forcing a zero intercept, was used to obtain initial slopes for each of the compounds. Given the mass of particles on the filter (M_p = 96730 μg), estimates of K_p were calculated. The correlation between the optimized (K_p^{opt}) and estimated (K_p^{init}) values is excellent and is shown in Figures 3.15 and 3.16 for 1 and 40 filter layers, respectively. The values of K_p^{opt} obtained from the diffusion model, therefore, are internally consistent with the values of K_p^{init}. Note that because only two data points were used, the errors associated with the initial slope estimates are large. These errors could have been decreased by gathering more data early in the experiment.

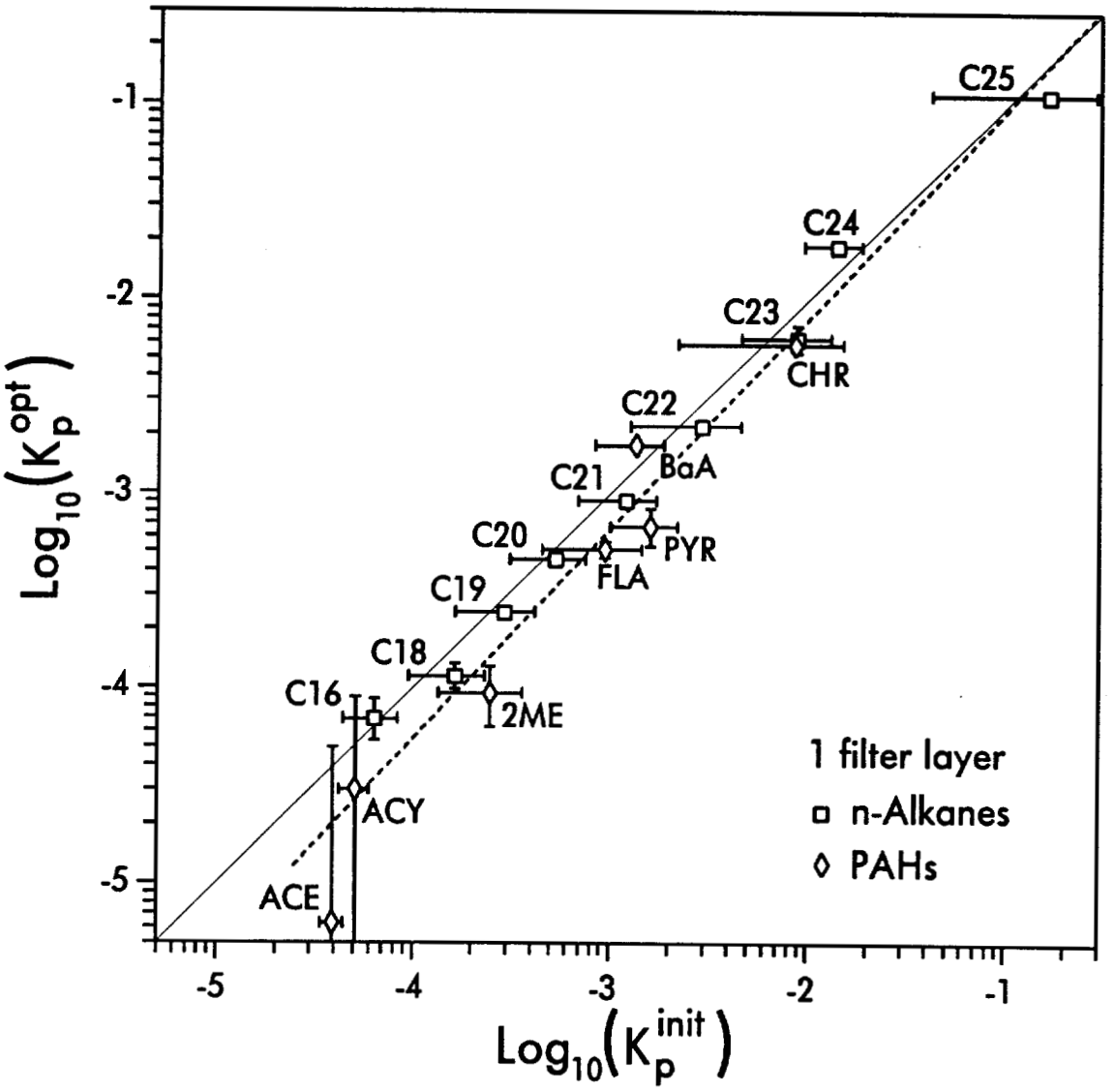

Figure 3.15. Correlation between the initial slope estimates of K_p ($m^3/\mu g$) and the optimized values of K_p ($m^3/\mu g$) for 1 layer simulations. Error bars on the initial slope K_p values represent one standard deviation while those on the optimized values of K_p are the estimated 95% confidence limits. The solid 1:1 line is plotted to show the expected dependence while the dashed line was obtained via linear regression. Slope = 1.078, intercept = 0.057.

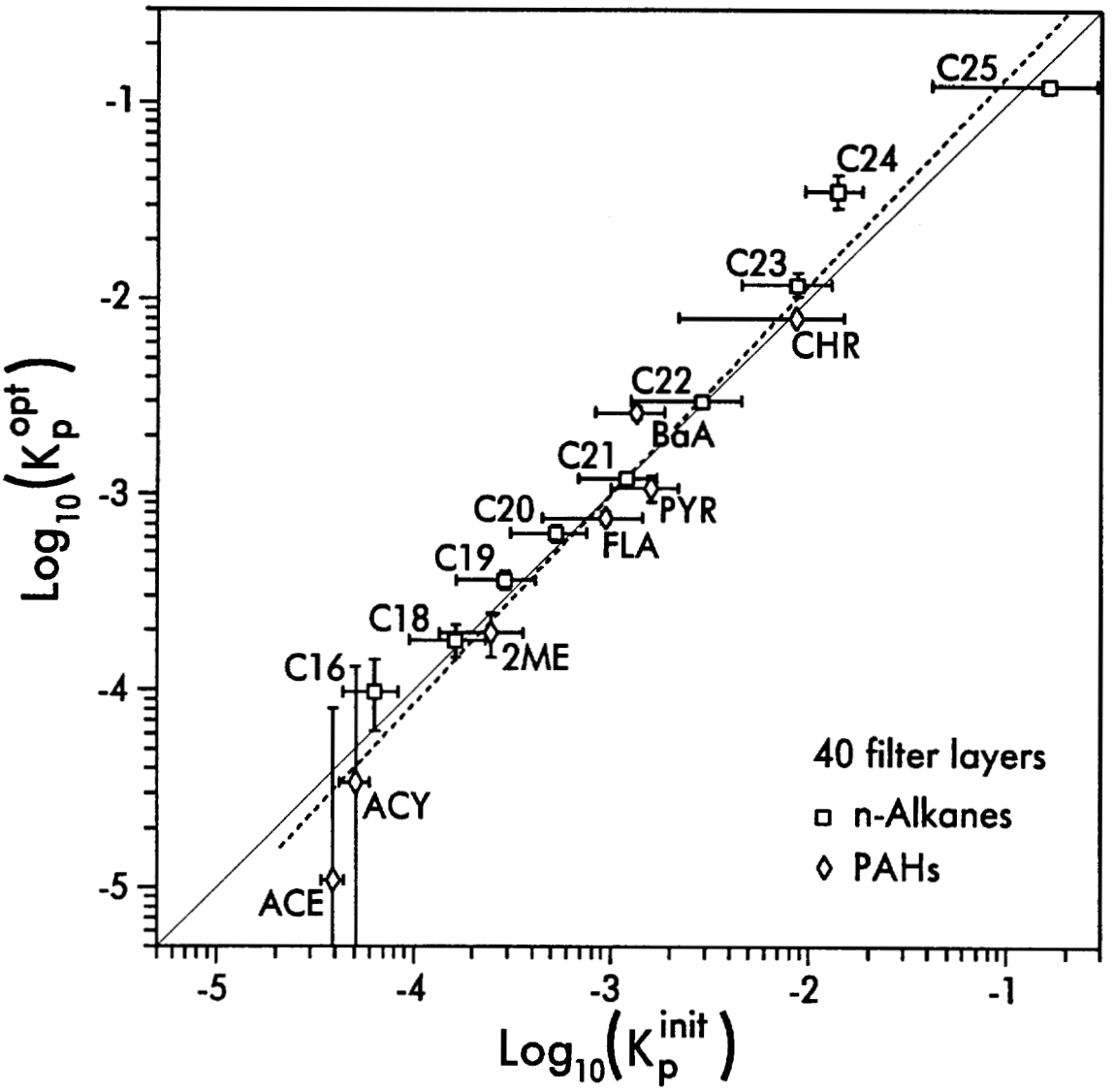

Figure 3.16. Correlation between the initial slope estimates of K_p ($m^3/\mu g$) and the optimized values of K_p ($m^3/\mu g$) for 40 layer simulations. Error bars on the initial slope K_p values represent one standard deviation while those on the optimized values of K_p are the estimated 95% confidence limits. The solid 1:1 line is plotted to show the expected dependence while the dashed line was obtained via linear regression. Slope = 1.070, intercept = 0.206.

The magnitude of the optimized partition coefficients can also be correlated with the subcooled liquid vapor pressure (p_L^o) of each compound. Recently, Pankow (*1, 5*) showed that a log K_p versus log p_L^o plot is expected to give a slope near -1.0 and an intercept that depends largely on the nature of the particulate matter and the enthalpies of desorption and vaporization of each compound. Within a given compound class, this intercept can be assumed to be constant. The correlation between log K_p and log p_L^o is illustrated in Figures 3.17 and 3.18 for most of the compounds. Slopes of -0.74 and -0.73 were obtained by linear regression for the 1 layer and 40 layer cases, respectively. While not equal to -1.0, the slopes do fall within the range of values determined in other studies (*5-8, 10-11, 13*). A similar statement may be made concerning the intercepts. Because the optimized values of K_p agree well with those calculated by others, they are more than just fitting parameters.

Effective Diffusion Coefficients. The theoretical relationship between D_{eff} and K_p is given in equation (3.6). Assuming the gas-phase molecular diffusion coefficient to be largely invariant from compound to compound, a plot of log D_{eff} versus log K_p should yield a slope of -1.0 according to

$$\log D_{eff} = -\log K_p + \log \left[\frac{D_m \alpha n^2}{\rho_s (1-\alpha n) 10^{12}} \right] \qquad (3.10)$$

Using D_m = 0.05 cm^2/s, α = 1.0, n = 0.5, and ρ_s = 2.0 g/cm^3, the expected value of the intercept is roughly -13.9. Correlations between the optimized values of D_{eff} and K_p are shown in Figures 3.19 and 3.20 for the 1 and 40 layer cases. Tetracosane and pentacosane are not included in the 40 layer graph because not enough curvature was evident in their M_t/M_e versus V graphs for those optimizations to determine a D_{eff} value. Linear regression gives slopes of -1.16 and -1.22 and intercepts of -20.6 and -20.7 for the 1 and 40 layer cases, respectively. If the slope is forced to be -1.0, the intercepts become -20.1 and -20.0. Considering the small amount of scatter in the data, the calculated slopes

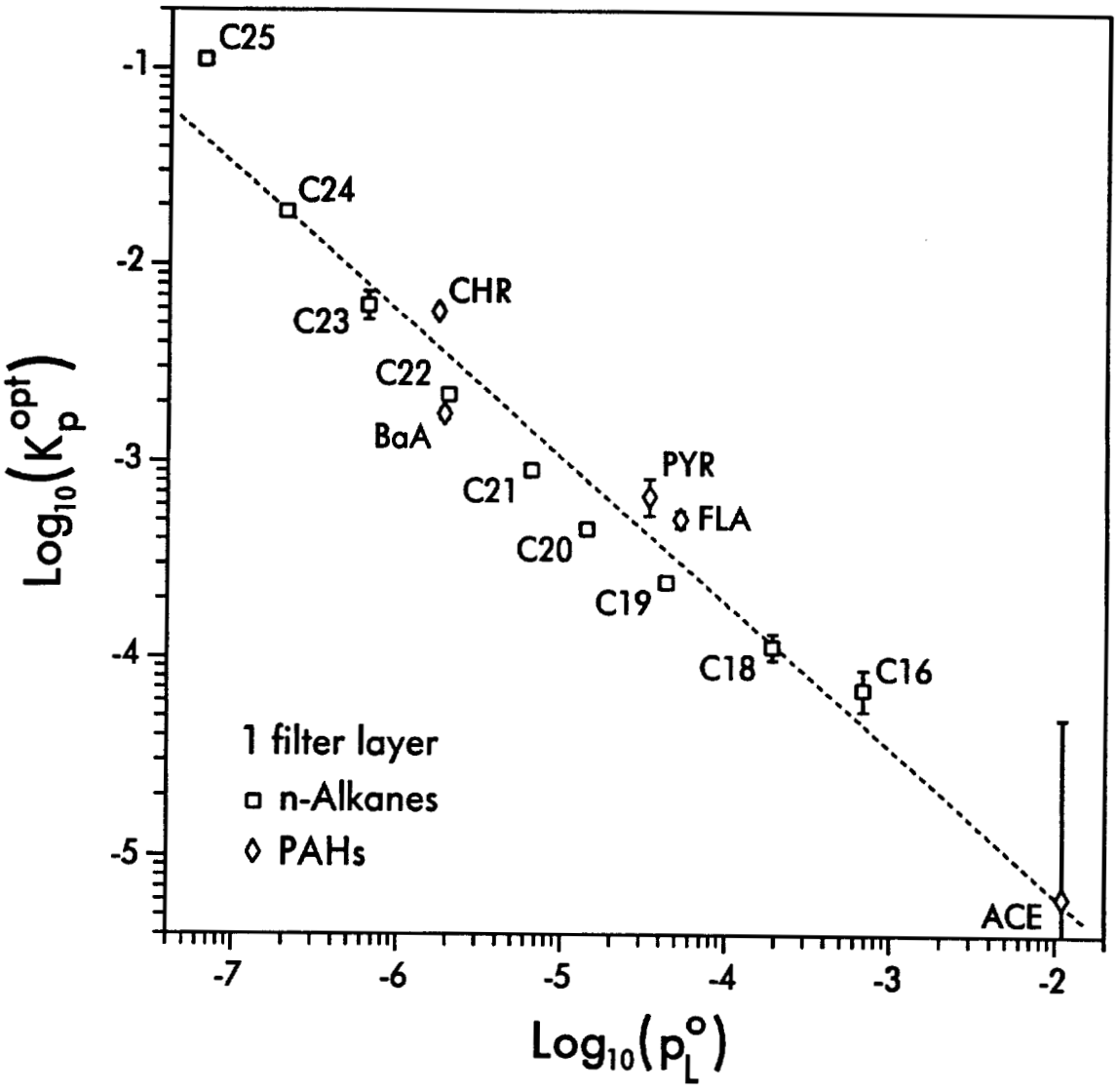

Figure 3.17. Correlation between the subcooled liquid vapor pressure, p_L^o (torr), and the optimized values of K_p ($m^3/\mu g$) for 1 layer simulations. Error bars on K_p are the estimated 95% confidence limits. The dashed line was obtained via linear regression, pooling all data points for the *n*-alkanes and the PAHs. Slope = -0.741, intercept = -6.681.

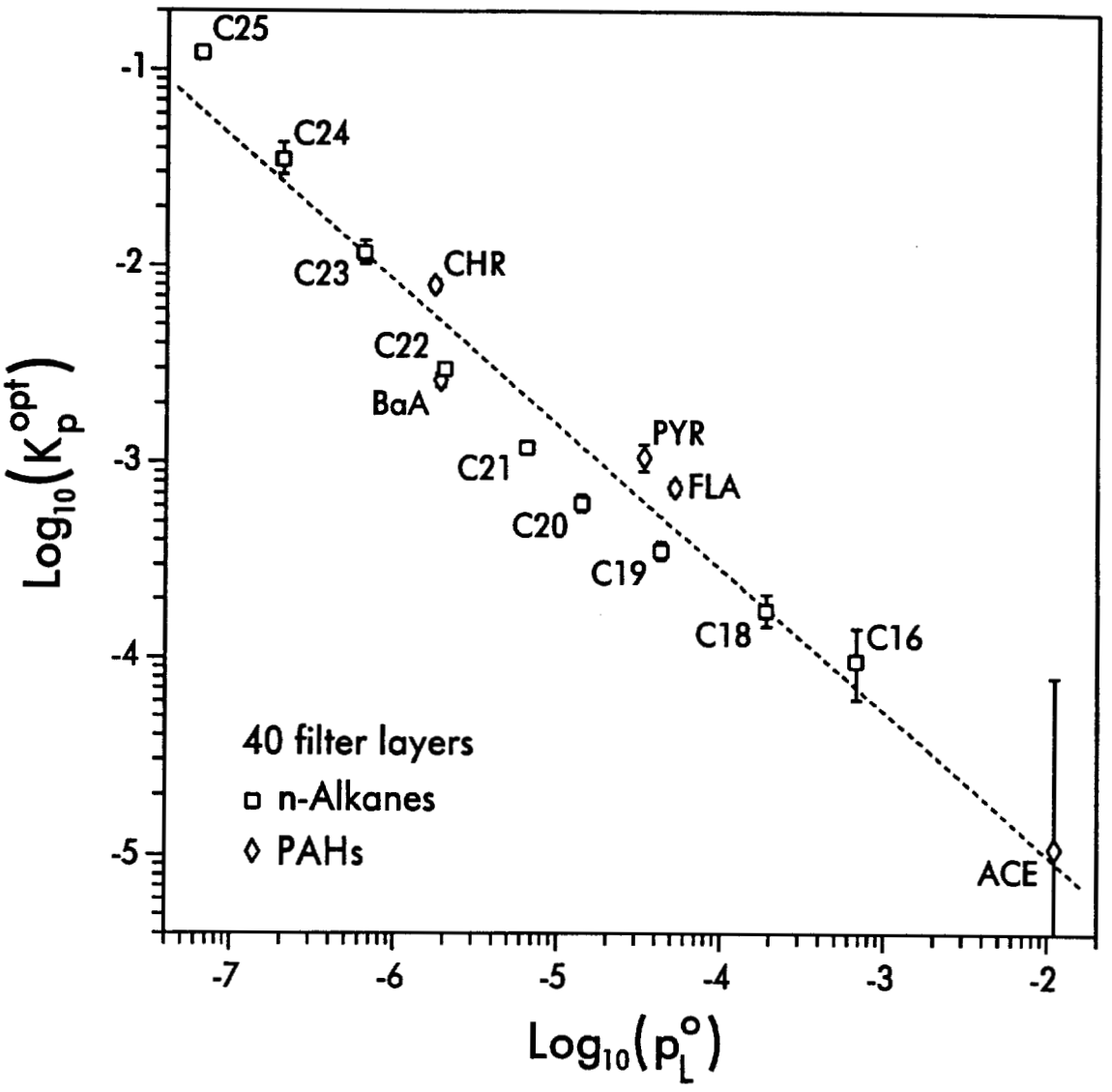

Figure 3.18. Correlation between the subcooled liquid vapor pressure, p_L^o (torr), and the optimized values of K_p ($m^3/\mu g$) for 40 layer simulations. Error bars on K_p are the estimated 95% confidence limits. The dashed line was obtained via linear regression, pooling all data points for the *n*-alkanes and the PAHs. Slope = -0.731, intercept = -6.464.

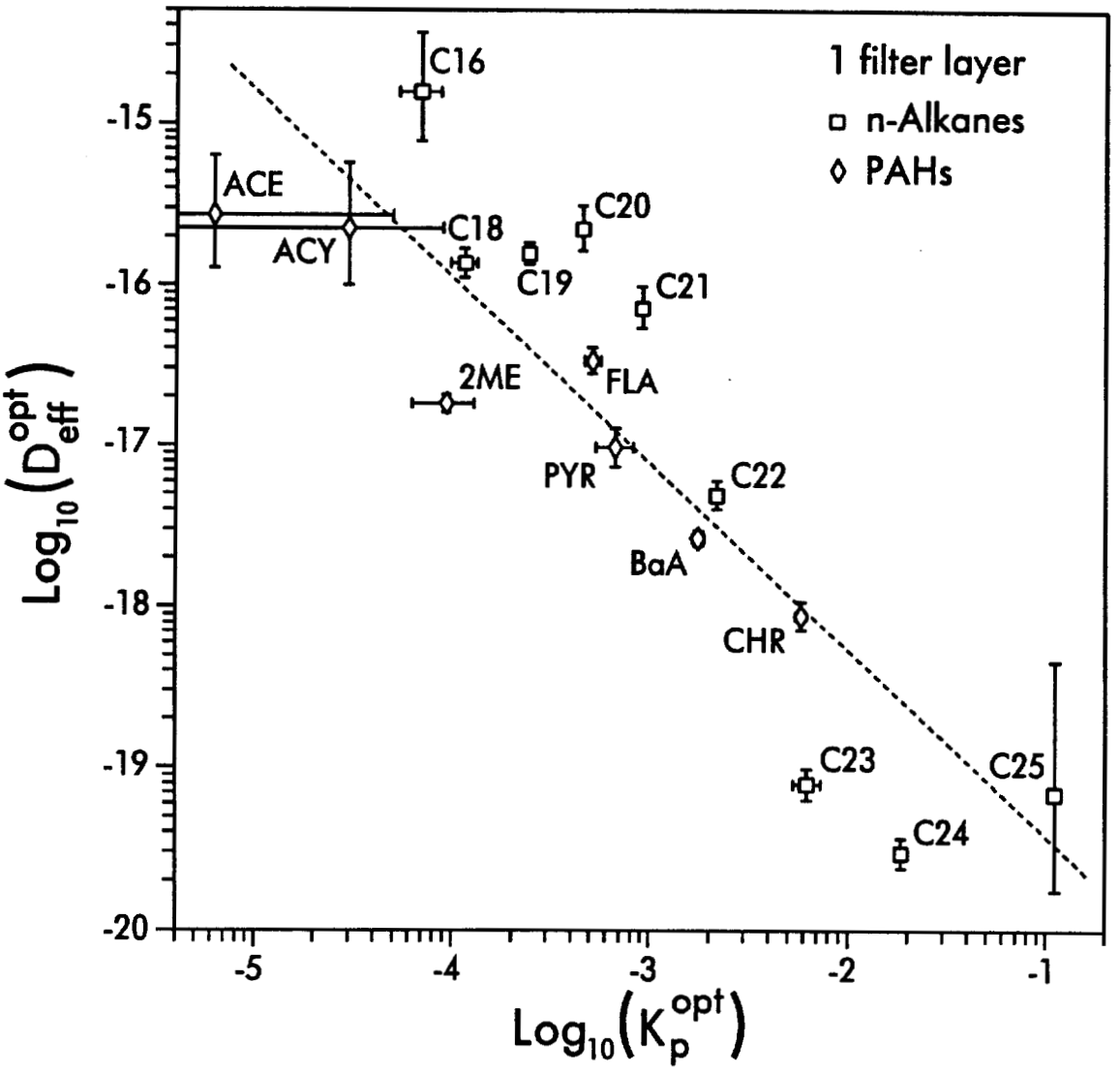

Figure 3.19. Correlation between the optimized values of D_{eff} (cm^2/s) and K_p ($m^3/\mu g$) for 1 layer simulations. Error bars on each point are the estimated 95% confidence limits for each parameter. The dashed line was obtained via linear regression. Slope = -1.157, intercept = -20.578.

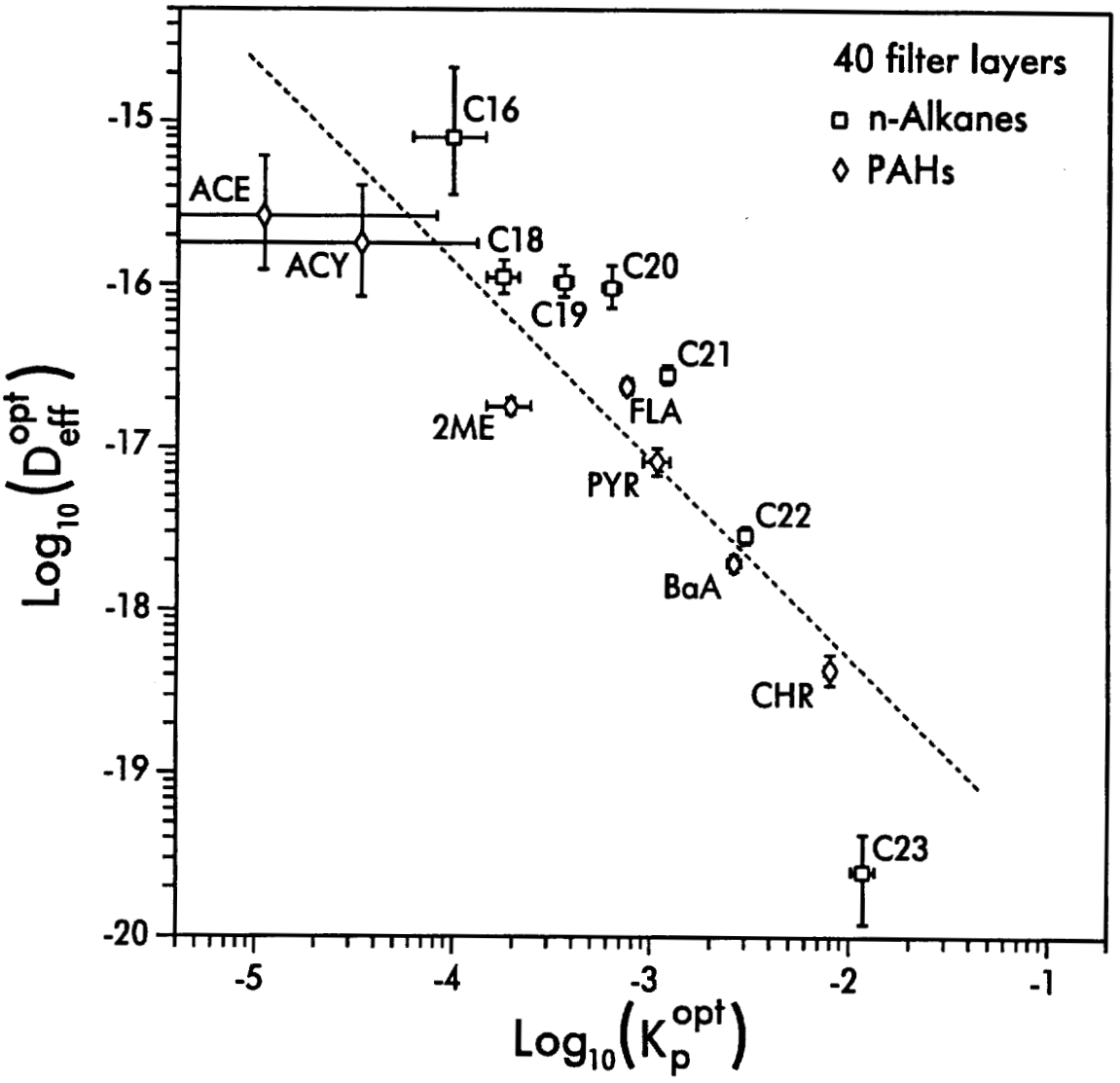

Figure 3.20. Correlation between the optimized values of D_{eff} (cm^2/s) and K_p ($m^3/\mu g$) for 40 layer simulations. Error bars on each point are the estimated 95% confidence limits for each parameter. The dashed line was obtained via linear regression. Slope = -1.216, intercept = -20.724.

are clearly not statistically different from -1.0. The intercepts, however, are about six log units lower than expected from equation (3.10). That is, the best-fit values of D_{eff} are roughly six orders of magnitude smaller than would be expected on the basis of sorption-retarded gaseous diffusion.

The small effective diffusion coefficients indicate that equilibrium conditions are not being achieved as the gas stream flows through the filter. Some process is slowing the desorption of compounds from the filter. This model assumes that the rate-limiting process is intraparticle diffusion, but other processes could contribute to or control the desorption rate. The optimized D_{eff} values, therefore, are an overall measure of the effect of all mechanisms affecting the desorption rate. A discussion of the possible rate processes may help to explain the discrepancy between the predicted and observed D_{eff} values.

Consider first the possibility that the rate-limiting process is *not* intraparticle diffusion. If this were true, then desorption from the particles would have to be fast, and concentration gradients must be present between adjacent particles in the bed. Given that gaseous molecular diffusion is rapid, with the small distances between particles on a highly loaded filter and a low average face velocity of 1.5 cm/s, it is unlikely that mass transport outside of the particles was in fact limiting. In addition, Gerde and Scholander (27) predicted that the time scale of diffusion external to a particle is two orders of magnitude smaller than the time scale of intraparticle diffusion. Since it is improbable that processes external to the particles are slow enough to produce the observed kinetics, some process or group of processes **inside** the particles must control the desorption rate. To reconcile the observed and predicted D_{eff} values within the context of an internal diffusive rate limitation, the influence of the physical properties of the particles (e.g., particle size, α, and tortuosity) on D_{eff} must be examined. If that fails to close the gap, the nature of the partitioning process itself may need to be re-evaluated. Finally, the impact of coupled processes must be considered.

While the effective diffusion coefficient was used as a fitting parameter in these simulations, the actual parameter being fit was T_D. The diffusion reaction time scale is related to D_{eff} through the square of the diffusion length (equation 3.7). By using an assumed particle size distribution, a diffusion length was also assumed. If particles on the filter were aggregated to a significant extent, or if preferential flow paths through the filter existed, then the effective diffusion length would be larger than that assumed in these simulations. Given fitted values of T_D, an increased diffusion length would result in increased values of D_{eff}. In order to account for a six order of magnitude difference between the expected and observed values of D_{eff}, however, the effective diffusion length must be **1000 times** larger than assumed. While no data are available to support or refute this possibility, it seems unlikely that a larger diffusion length is the sole reason for these small D_{eff} values.

An examination of equation (3.10) reveals several other variables that may be able to account for the difference between the predicted and observed D_{eff} values. Consider now the impact of a change in the value of α. A decrease in α would result in a decrease in the predicted value of D_{eff}. Recall, however, that the best-fit for any set of experimental data is controlled by the number of filter layers and the ratio of time scales T_M/T_D. The number of filter layers is constant. To preserve the fit, a change in the value of α cannot change the ratio T_M/T_D. The value of T_M is determined by K_p, which is set by the initial slope of the M_t/M_e versus V graph. The partition coefficient is a macroscopic quantity that does not depend upon α. Only one pair of values for T_M/T_D and T_M will provide the best fit for a given set of experimental data; T_D, therefore, must also remain constant. A reduction in α is reflected by a decrease in the effective diffusion length. By equation (3.7), such a decrease must be accompanied by a coincident decrease in the value of D_{eff}. This is, in fact, observed. The functionality of the relationship is such that a decrease in the value of α cannot narrow the gap between the predicted and observed D_{eff} values.

Consider next the impact of the tortuosity factor on the predicted D_{eff}. In the development of the intraparticle diffusion model, Rounds and Pankow (*28*) noted that one of the factors in the numerator of equation (3.6) acts in part as a surrogate for the tortuosity factor. The tortuosity factor accounts for the increase in diffusive path length caused by irregular and twisting pores inside the particles. If the micropores were extremely tortuous, the tortuosity factor would be smaller than the value used here, resulting in a small decrease in the predicted value of D_{eff}. The maximum reduction in the predicted value, however, is probably only 0.3 log units. The impact of other physical parameters such as ρ_s and n are also small. Dead-end pores might have a larger effect.

Perhaps a better explanation for the disparity between the predicted and observed D_{eff} values is obtained by examining the transport processes that may act within the particles. Experiments by McDow (*36*) and Cotham (*13*) demonstrated the ability of clean glass fiber filters situated behind particle-laden filters to become coated by organic compounds. An analysis of this coating revealed a suite of alkanes in addition to a complex mixture of chromatographically unresolved compounds. These researchers suggested that the particles on the front filter must also be coated with this material. In addition, Cotham (*13*) demonstrated that this coating can enhance sorption, and proposed that sorption to some atmospheric particles might be better described by the partitioning of compounds into a liquid film rather than adsorption to a solid surface. If intraparticle transport involves the diffusion of compounds through a liquid-like organic phase, however intermittently, then the magnitude of D_m in equations (3.6) and (3.10) should be more representative of molecular diffusion in a liquid rather than in air. Molecular diffusion coefficients in liquids are approximately four orders of magnitude smaller than those in air. Solid-phase diffusion may also play a role in intraparticle transport. The use of a solid- or liquid-phase D_m significantly reduces the discrepancy between the predicted and observed values of D_{eff}.

Several processes may act in concert to slow the kinetics of gas/particle exchange. The coupling of several rate-limiting transport phenomena inside the particles can slow the overall mass transport more than any one process acting alone. Processes that may couple in this way are: diffusion through a liquid-like organic phase, solid-phase diffusion, and sorption-retarded gaseous diffusion in the micropores of the particles. The model used in this study was not designed to describe such coupled processes. Consequently, such interactions are averaged in the application of the model. Despite this averaging effect caused by the use of only one kinetic parameter, the observed magnitudes of D_{eff} have provided insight into the rate-limiting processes at the microscopic level.

Constancy of T_M/T_D. Interestingly, each of the best-fit predictions gives a similar value for T_M/T_D. This is not surprising, since both T_M and T_D are expected to be linearly dependent upon the value of K_p. The value of T_M/T_D is expected to depend primarily on the mass of particles (M_p) and the properties of those particles. A weak compound-dependence is expected due to D_m. Therefore, T_M/T_D should be roughly compound-independent for a system with fixed values of M_p and f, and a plot of all M_t/M_e data versus a normalized axis ($V/(K_pM_p) \approx t/T_M$) should cause the data to collapse to one line. Figures 3.21 and 3.22 illustrate this normalization for the *n*-alkanes. The best-fit curves in Figure 3.21 are derived from the use of 1 filter layer, and those K_p^{opt} values were used for the normalization in Figure 3.22. The small amount of scatter in the normalized plot is due to the scatter in the observed relationship between D_{eff}^{opt} and K_p^{opt}.

Diffusion Time Scales. Rounds and Pankow (*28*) recently discussed the predicted diffusion reaction time scales of this model. They concluded that sorption equilibrium with airborne particles is rapidly approached for most of the compounds typically determined in atmospheric samples. If both preferential flow and particle aggregation on the filter are insignificant and values of D_{eff} are truly six orders of magnitude smaller than first predicted, then

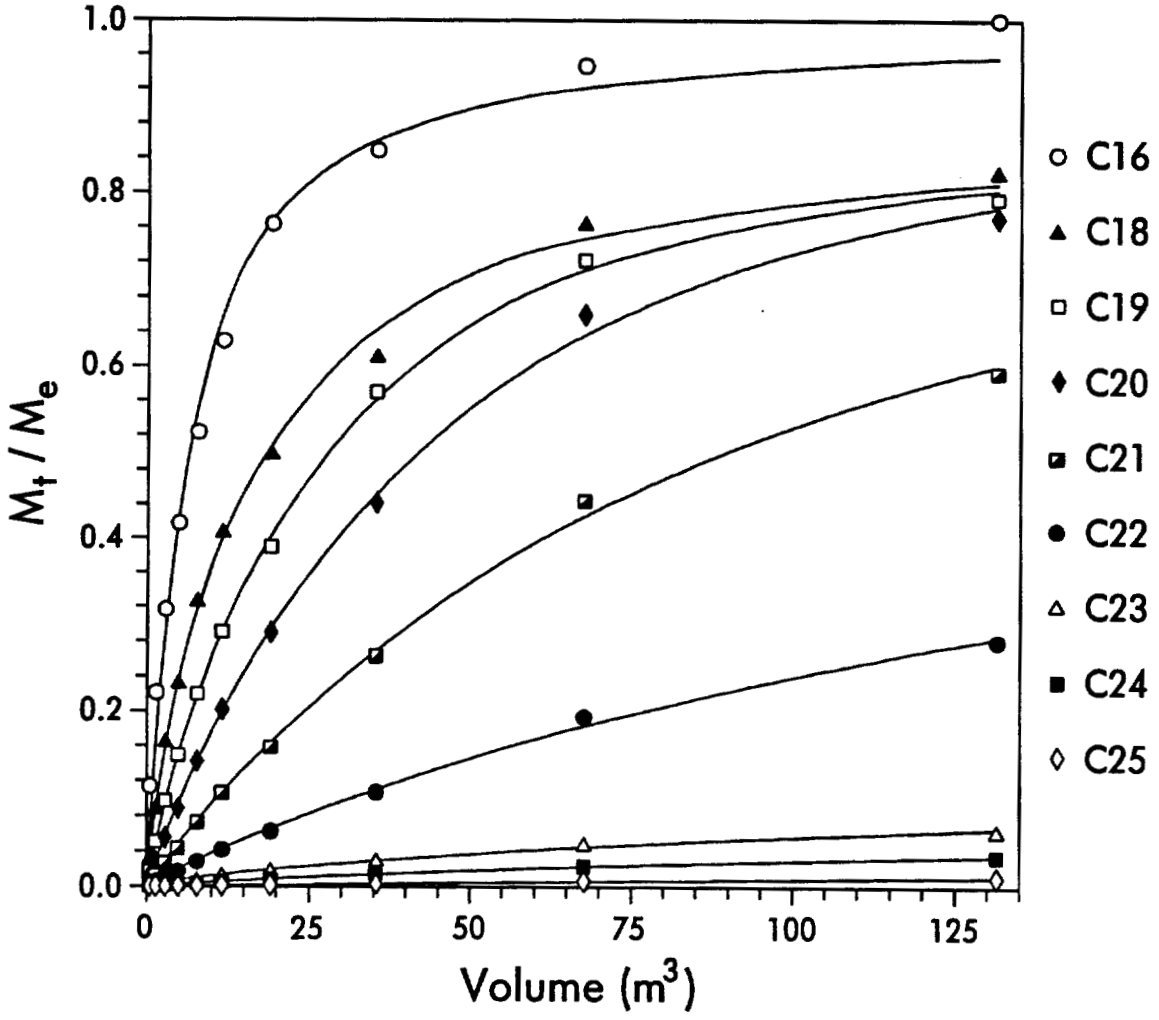

Figure 3.21. Best-fit fractional approach to equilibrium curves for each of the *n*-alkanes. The best-fit curves were obtained using 1 filter layer, 51 nodes/particle, and fully porous particles in the 6-bin size distribution.

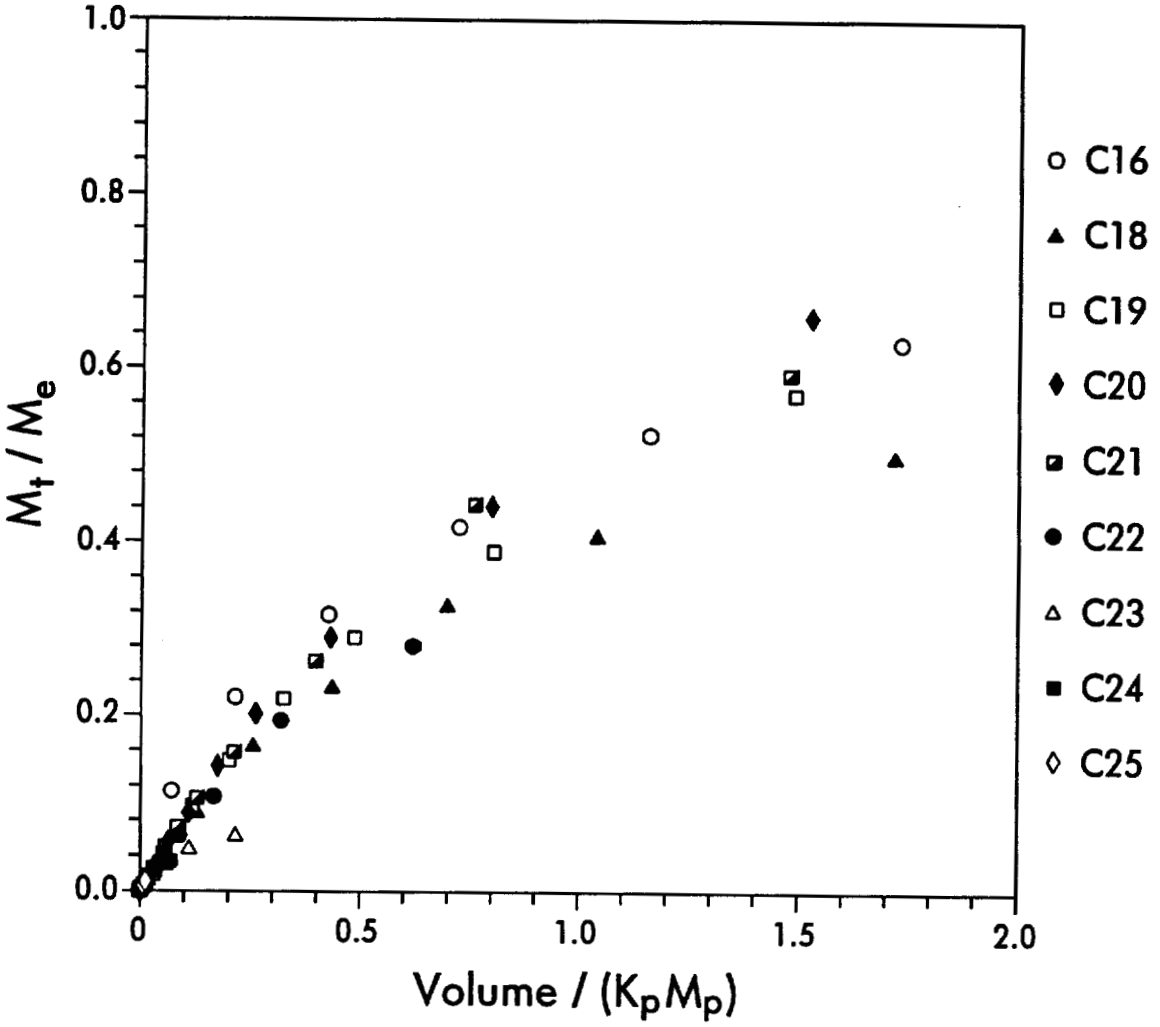

Figure 3.22. Normalized fractional approach to equilibrium data for each of the *n*-alkanes. The optimized values of K_p from the 1 layer model were used to normalize each data set.

values of T_D would be six orders of magnitude larger than those used previously. Therefore, the intraparticle diffusion model would now predict that strict gas/particle equilibrium with airborne particulate matter is *rarely* achieved for those compounds typically determined in atmospheric samples. In fact, most compounds would be unable to respond to the changes in equilibrium position caused by diurnal temperature variations. The actual deviation from equilibrium would depend upon the atmospheric residence time of the aerosol and the compositional history of the air parcel as it ages. Theoretically, long diffusion reaction time scales mean that the probability of an air parcel ever being in true gas/particle equilibrium is slight. The effects of diurnal temperature changes may average over time, but sorption kinetics will be important when the particles are exposed to different gas-phase concentrations as they are transported far away from their sources. More work must be performed to determine these diffusion reaction time scales.

Sampling Artifacts. Partition coefficients are routinely calculated via equation (3.1) with field-derived values of *A*, *F*, and *TSP*. In a high volume (hi-vol) sampler, particulate matter is collected on a filter while compounds in the gas phase are trapped on a sorbent such as polyurethane foam (PUF) or Tenax. Due to the low concentrations of some compounds and the constraints of analytical detection limits, six or more hours are commonly required for the collection of one sample. During that time, many processes can act to modify the measured gas- and particulate-phase concentrations, changing them from their actual average values in the atmosphere. Several air parcels of different compositions may be encountered during one sampling event, causing concentration gradients around the collected particles and a resultant redistribution via adsorption or desorption (e.g. *6*, *20*). An increase in temperature during the sampling period can cause compounds sorbed to filter-bound particles to desorb and be trapped on the PUF or Tenax; a decrease in sampling temperature can cause incoming gas-phase compounds to adsorb onto previously-collected particles (*14*, *20-21*). These processes are often cited as

sources of sampling artifacts, but the limits placed upon these processes by sorption kinetics is not yet well understood.

Assuming for the moment that the sampled air parcels are internally at sorption equilibrium, the potential for adsorption/desorption sampling artifacts is controlled by variations in A and T over the sampling period. The kinetics of gas/particle interactions is important only in limiting the rate of mass exchange once a driving force for that exchange is present. For any compound, adsorption/desorption sampling artifacts will be greatest for the case of instantaneous phase redistribution ($T_D = 0$, $T_M/T_D = \infty$). An in-depth analysis of this worst case scenario has been performed by Buchholz and Pankow (*41*). As T_M/T_D decreases, the magnitude of those artifacts will become limited by the kinetics of intraparticle diffusion.

The ability of a compound to re-achieve gas/particle equilibrium on/in a filter is constrained by the realities of equilibrium (as manifested in T_M) as well as those of kinetics (T_D). As noted previously, it is the ratio T_M/T_D that determines the relative importance of equilibrium and kinetic processes. Given the fact that T_M/T_D is roughly compound-independent (Figure 3.22), an examination of the magnitude of T_M for each compound can be used to determine the kinetic limitations for re-equilibration. Figure 3.21 illustrates this type of examination. Compounds such as hexadecane (C16) that have relatively high vapor pressures (small values of K_p and T_M) react quickly to gas-phase concentration changes. Because T_M is small and D_{eff} values for these compounds are relatively large, the curvature in the M_t/M_e versus V graph caused by rate-limited desorption may be entirely revealed within the time frame of interest. Consequently, compounds of high volatility are likely to re-achieve equilibrium on/in filters despite the constraints of kinetics. Compounds such as pentacosane (C25), on the other hand, are characterized by very small D_{eff} values, but T_M is so large that a plot of M_t/M_e versus V would have to extend to very large volumes to observe any curvature. The magnitude of adsorption/desorption artifacts for such compounds will in no way be limited by kinetics. Compounds

of intermediate volatility will be most affected by the limitations of intraparticle diffusion. Values of T_M for these compounds are small enough for the kinetics to affect the desorption within the time frame of interest, and yet not so small that the exchange is complete. If the time frame of interest changes, the range of volatility for which kinetics is important shifts accordingly.

Summary and Conclusions

The desorption kinetics of a suite of *n*-alkanes and PAHs from a particle-laden filter was observed in a laboratory experiment. The desorption data were successfully described with a filter-based intraparticle diffusion model. The values of the optimized partition coefficients are internally consistent, agree well with literature values, and correlate favorably with the subcooled liquid vapor pressure according to a theoretical relationship. Best-fit values of the effective diffusion coefficient correlate well with the partition coefficients. The relationship between these parameters agrees with that predicted by theory. The magnitudes of the optimized diffusion coefficients, however, are much lower than expected on the basis of sorption-retarded, gaseous diffusion. Diffusion through a liquid-like organic film and/or the solid particulate matrix is proposed as one possible explanation of this discrepancy. Dead-end pores may also contribute to the difference. Therefore, the rate-limitation for intraparticle diffusion may result from the coupling of several diffusional processes: transport through/within a liquid-like organic film, diffusion through the solid phase, and gaseous diffusion within the micropores. The effective diffusion coefficient in this study is an overall measure of the effects of these rate-limiting processes. Particle aggregation or preferential flow through the filter may also contribute to artificially low values of the fitted effective diffusion coefficient. If preferential flow was negligible, then diffusion reaction time scales would be much longer than first predicted. Strict gas/particle sorption equilibrium with airborne particulate matter would be achieved only rarely for most compounds typically determined in atmospheric samples. The ability of

intraparticle diffusion kinetics to limit the magnitude of adsorption and desorption sampling artifacts is greatest for compounds of intermediate volatility, and depends on the time frame of the experiment. Efforts by many researchers to understand gas/particle partitioning equilibrium have been largely successful. Taking the next step to understand the kinetics of gas/particle interactions will require more information concerning the microscopic physical properties of atmospheric particulate matter.

Glossary

A	gas-phase concentration (ng/m^3)
A_{out}	gas-phase concentration leaving the filter (ng/m^3)
b_p	constant in equation for log K_p
D_{eff}	intraparticle effective diffusion coefficient (cm^2/s)
D_m	gas-phase molecular diffusion coefficient (cm^2/s)
f	volumetric flow rate through the filter (m^3/min)
F	particulate-phase concentration (ng/m^3)
$\mathbf{F}(,,)$	the statistical **F** distribution at the 95% level
K_p	gas/particle partition coefficient (m^3/μg)
M_e	mass exchanged between phases at equilibrium
m_p	compound-dependent slope of log K_p versus $1/T$
M_p	mass of particulate matter on the filter
M_t	mass exchanged between phases at time t
M_t/M_e	fractional approach to equilibrium
n	intraparticle porosity of the porous shell
N	number of filter layers
N_p	number of experimental data points
p	number of fitted model parameters
p_L^o	subcooled liquid vapor pressure
r	radial distance
r_c	radius of the nonporous core (μm)

R	particle radius (μm)
$S(r)$	total volumetric concentration of analyte at a radial distance r from the center of the particle (ng/m^3)
SSR	sum of squared residuals
SSR_{crit}	critical sum of squared residuals
SSR_{min}	minimum sum of squared residuals
t	time (min)
T	absolute temperature (K)
T_D	diffusion reaction time scale (min)
T_M	mass-transfer time scale (min)
TSP	total suspended particulate matter concentration (μg/m^3)
V	volume of gas (m^3)
α	fractional particle volume that is porous
ρ_s	specific particle density (g/cm^3)

Registry No. Hexadecane, 544-76-3; Octadecane, 593-45-3; Nonadecane, 629-92-5; Eicosane, 112-95-8; Heneicosane, 629-94-7; Docosane, 629-97-0; Tricosane, 638-67-5; Tetracosane, 646-31-1; Pentacosane, 629-99-2; Acenaphthene, 83-32-9; Acenaphthylene, 208-96-8; Benz(a)anthracene, 56-55-3; Chrysene, 218-01-9; Fluoranthene, 206-44-0; Fluorene, 86-73-7; 9-Fluorenone, 486-25-9; 2-Methylphenanthrene, 2531-84-2; Phenanthrene, 85-01-8; Pyrene, 129-00-0.

Literature Cited

(1) Pankow, J. F. *Atmos. Environ.* **1987**, *21*, 2275-2283.

(2) Junge, C. E. In *Fate of Pollutants in the Air and Water Environments, Part I*; Suffet, I. H, Ed.; John Wiley: New York, 1977; pp 7-26.

(3) Yamasaki, H.; Kuwata, K.; Miyamoto, H. *Environ. Sci. Technol.* **1982**, *16*, 189-194.

(4) Bidleman, T. F.; Foreman, W. T. In *The Chemistry of Aquatic Pollutants;* Hites, R. A., Eisenreich, S. J., Eds.; Advances in Chemistry 216; American Chemical Society: Washington, DC, 1987; p 27.

(5) Pankow, J. F. *Atmos. Environ.* **1991**, *25A*, 2229-2239.

(6) Bidleman, T. F.; Billings, W. N.; Foreman, W. T. *Environ. Sci. Technol.* **1986**, *20*, 1038-1043.

(7) Foreman, W. T. Ph.D. Thesis, University of South Carolina, 1986.

(8) Ligocki, M. P.; Pankow, J. F. *Environ. Sci. Technol.* **1989**, *23*, 75-83.

(9) Eitzer, B. D.; Hites, R. A. *Environ. Sci. Technol.* **1989**, *23*, 1389-1395.

(10) Hart, K. M. Ph.D. Thesis, Oregon Graduate Institute, 1990.

(11) Foreman, W. T.; Bidleman, T. F. *Environ. Sci. Technol.* **1987**, *21*, 869-875.

(12) Storey, J. M. E.; Pankow, J. F. *Atmos. Environ.* **1992**, *26A*, 435-443.

(13) Cotham, W. E. Ph.D. Thesis, University of South Carolina, 1990.

(14) Coutant, R. W.; Brown, L.; Chuang, J. C.; Riggin, R. M.; Lewis, R. G. *Atmos. Environ.* **1988**, *22*, 403-409.

(15) Fox, M. A.; Olive, S. *Science* **1979**, *205*, 582-583.

(16) Peters, J.; Seifert, B. *Atmos. Environ.* **1980**, *14*, 117-119.

(17) Grosjean, D.; Fung, K.; Harrison, J. *Environ. Sci. Technol.* **1983**, *17*, 673-679.

(18) Yokley, R. A.; Garrison, A. A.; Wehry, E. L.; Mamantov, G. *Environ. Sci. Technol.* **1986**, *20*, 86-90.

(19) Kamens, R. M.; Karam, H.; Guo, J.; Perry, J. M.; Stockburger, L. *Environ. Sci. Technol.* **1989**, *23*, 801-806.

(20) Van Vaeck, L.; Van Cauwenberghe, K.; Janssens, J. *Atmos. Environ.* **1984**, *18*, 417-430.

(21) Coutant, R. W. *Environ. Sci. Technol.* **1991**, *25*, 1649.

(22) Natusch, D. F. S.; Tomkins, B. A. In *Carcinogenesis, Vol. 3: Polynuclear Aromatic Hydrocarbons;* Jones, P. W., Freudenthal, R. I., Eds.; Raven Press: New York, 1978; pp 145-153.

(23) Kittelson, D. B.; Barris, M. A. In *Aerosols: Science, Technology, and Industrial Applications of Airborne Particles;* Liu, B. Y. H., Pui, D. Y. H., Fissan, H. J., Eds.; Elsevier Science Publishing Co., Inc.: New York, 1984; pp 770-774.

(24) Rothenberg, S. J.; Cheng, Y. S. *J. Phys. Chem.* **1980**, *84*, 1644-1649.

(25) Rothenberg, S. J.; Mettzler, G.; Poliner, J.; Bechtold, W. E.; Eidson, A. F.; Newton, G. J. *Environ. Sci. Technol.* **1991**, *25*, 930-935.

(26) Miguel, A. H.; de Andrade, J. B.; Hering, S. V. *Intern. J. Environ. Anal. Chem.* **1986**, *26*, 265-278.

(27) Gerde, P.; Scholander, P. *Environ. Health Perspectives* **1989**, *79*, 249-258.

(28) Rounds, S. A.; Pankow, J. F. *Environ. Sci. Technol.* **1990**, *24*, 1378-1386.

(29) Pankow, J. F.; Ligocki, M. P.; Rosen, M. E.; Isabelle, L. M.; Hart, K. M. *Anal. Chem.* **1988**, *60*, 40-47.

(30) Whitby, K. T.; Husar, R. B.; Liu, B. Y. H. *J. Colloid Interface Sci.* **1972**, *39*, 177-204.

(31) Press, W. H.; Flannery, B. P.; Teukolsky, S. A.; Vetterling, W. T. *Numerical Recipes: The Art of Scientific Computing;* Cambridge University Press: New York, 1989; pp 289-301.

(32) Box, G. E. P.; Hunter, W. G.; Hunter, J. S. *Statistics for Experimenters;* John Wiley & Sons, Inc.: New York, 1978; ch 14.

(33) Draper, N. R.; Smith, H. *Applied Regression Analysis;* John Wiley & Sons, Inc.: New York, 1966; ch 10.

(34) Olmstead, K. P.; Weber, W. J. *Environ. Sci. Technol.* **1990**, *24*, 1693-1700.

(35) Zhang, X.; McMurry, P. H. *Environ. Sci. Technol.* **1991**, *25*, 456-459.

(36) McDow, S. R. Ph.D. Thesis, Oregon Graduate Center, 1986.

(37) McDow, S. R.; Huntzicker, J. J. *Atmos. Environ.* **1990**, *24A*, 2563-2571.

(*38*) Pankow, J. F. *Atmos. Environ.* **1988**, 22, 1405-1409.

(*39*) Pankow, J. F. In *Long Range Transport of Pesticides*; Kurtz, D. A., Ed.; Lewis Publishers: Chelsea, MI, 1990; pp 97-103.

(*40*) Pankow, J. F.; Bidleman, T. F. *Atmos. Environ.* **1991**, *25A*, 2241-2249.

(*41*) Buchholz, D. A.; Pankow, J. F.; unpublished work, Oregon Graduate Institute, **1992**.

CHAPTER IV

Determination of Chlorinated Benzenes in Water by Purging Directly to a Capillary Column with Whole Column Cryotrapping and Electron Capture Detection

Abstract

The purge with whole column cryotrapping (P/WCC) method for the determination of volatile organic compounds (VOCs) in aqueous samples is adapted for use with an electron capture detector (ECD). In this method, VOCs are stripped from an aqueous sample with an inert purge gas and transferred directly to the head of a capillary column for subsequent GC analysis. To prevent the column from plugging with ice during the purge step, and to reduce the chromatographic interference caused by the reaction of small amounts of water with thermal electrons in the detector, a glass-bead water trap is placed in-line between the purge vessel and the gas chromatograph. The water trap is constructed of a short length of ⅛ inch o.d. stainless steel tubing filled with 0.5 mm diameter glass beads. By maintaining the trap at -10°C during the purge, most of the water can be removed from the purge gas. Efficient transmission of the analytes to the column is then achieved with a subsequent, short purge of the trap at 25°C. The method was tested with the chlorinated benzenes. Despite their high molecular weights, the more chlorinated members of this group have large enough Henry's law constants that they **can** be determined with a purging technique. Purging efficiencies were determined and compared to theoretical values. This method allows the simplicity and the high reliability

of the P/WCC method to be combined with the exceptionally high sensitivity of an electron capture detector.

Introduction

The EPA purge and trap (P&T) method (*1, 2*) is the standard technique for the determination of volatile organic compounds (VOCs) in aqueous samples. In the P&T method, VOCs are stripped from the aqueous phase with an inert gas and transferred to a sorbent bed. Analytes trapped on the bed are then thermally desorbed to the column of a gas chromatograph for analysis. Recently, Pankow (*3*) and Pankow and Rosen (*4*) introduced the purge with whole column cryotrapping (P/WCC) method, in which analytes purged from the aqueous phase are transferred immediately to the head of a capillary GC column, eliminating the need for an intermediate sorbent trap. Due to its inherent simplicity, the P/WCC method offers a variety of advantages over conventional P&T (*3, 4*), including improved detection of very volatile compounds, lower background contamination, shorter analysis times, and lower capital costs.

Due to the finite vapor pressure of water, a small amount of water is transferred to the GC column during the purge step of the P/WCC method. Applying the ideal gas law, 0.023 μL of water is expected to be removed from solution per mL of purge gas at 25°C. The presence of water in the purge gas is a potential problem. Purging for long periods of time can transfer enough water that a small-bore capillary column held at cryotrapping temperature can become plugged with ice. Too much water on the column can cause chromatographic problems such as peak-splitting (*4*). In addition, water can interfere with the response of some types of detectors. The electron capture detector (ECD) is particularly sensitive to trace amounts of water. Indeed, a few microliters of water passing through an ECD can produce a very large, asymmetrical peak that can completely obscure a portion of the chromatogram. In order to combine the simplicity and reliability of the P/WCC method with the

selectivity and extreme sensitivity of the electron capture detector, most of the water in the purge gas must be removed before it is allowed to reach the gas chromatograph.

Purge gas desiccation is commonly effected by forcing the gas to pass through a short length of polar tubing such as Nafion (*5, 6*). Transmission of analytes through Nafion tubing, however, has been found to be less than quantitative for some compounds, causing unacceptable memory effects (*6, 7*). Alternatively, a simple cold-zone, glass-bead water trap has been developed by Rosen (*7*) and Pankow (*8*). A schematic of the glass-bead water trap is illustrated in Figure 4.1. The water trap consists of a 6.5 cm length of ⅛ inch stainless steel tubing packed with 0.5 mm diameter glass beads to provide a large, inert surface area. The trap is encased in an aluminum block whose temperature can be regulated with coolant or with a cartridge heater and thermocouple. In the first part of the purge (phase I), the water trap is held at a subambient temperature such as -10°C with a liquid coolant. Because the vapor pressure of ice at -10°C (0.00257 atm) is substantially lower than that of water at 25°C (0.0313 atm), most of the water purged from solution will be retained in the cold trap. By rapidly raising the temperature of the trap to 25°C during the last minute or so of the purge (phase II), any analytes retained in the trap during phase I are quickly and efficiently removed and focussed on the GC column (*8*). By minimizing the phase II purge time, the amount of water transferred to the column is also minimized. The theoretical desiccation efficiency of the water trap has been discussed in detail by Pankow (*8*).

In this study, the P/WCC method is adapted for use with an electron capture detector and tested with each of the chlorinated benzenes. Purge gas desiccation is effected with the glass-bead water trap. Theoretical purging efficiencies are calculated and compared to experimentally determined values.

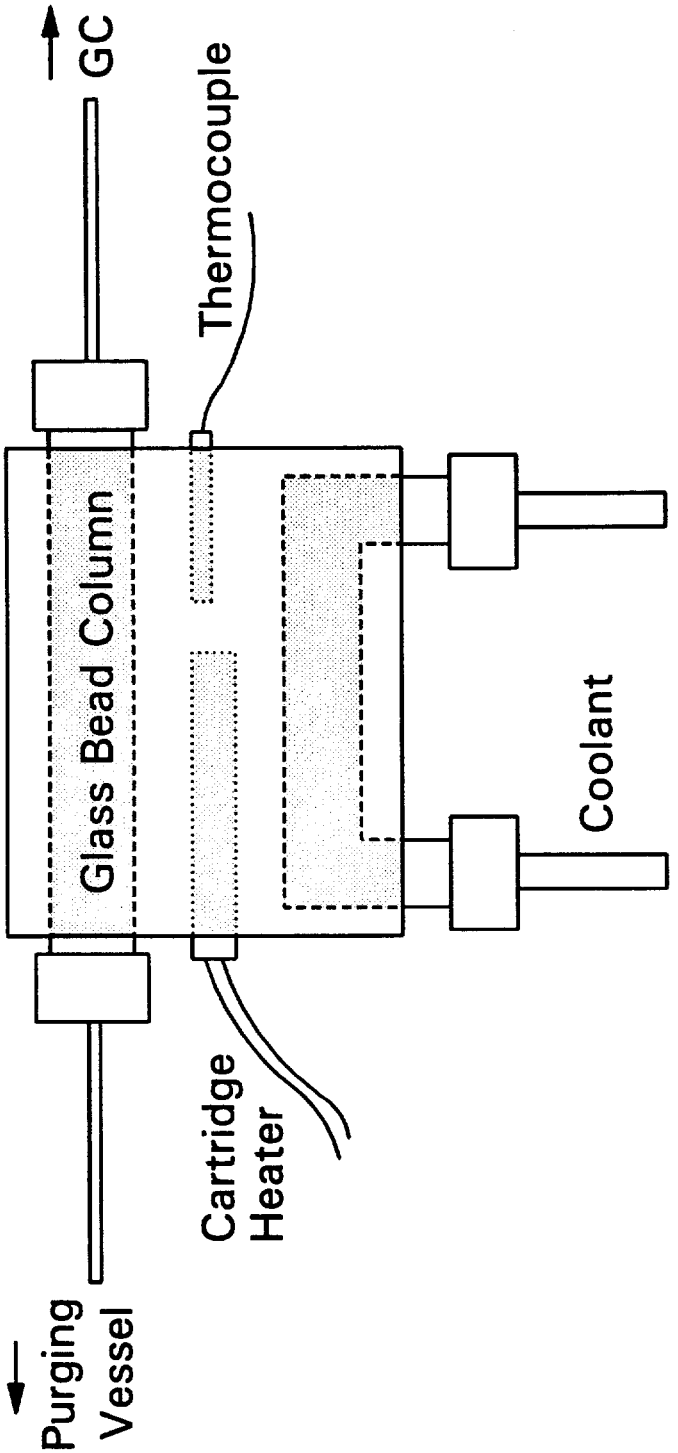

Figure 4.1. Schematic of the glass-bead water trap.

Theory

When a clean, inert gas is bubbled at a flow rate F (mL/min) through a volume of water V_{s1} (mL) for a period of time t_1 (min), the removal of a volatile analyte from aqueous solution is given by (*9*)

$$\frac{c_1}{c_{1,0}} = \exp\left[-\left(\frac{H}{RT_1}\right)\frac{F}{V_{s1}}t_1\right] \tag{4.1}$$

where c_1 is the aqueous concentration of the analyte at time t_1, $c_{1,0}$ is the initial aqueous concentration, H (atm·m^3/mol) is the Henry's law constant of the analyte at temperature T_1 (K), and R is the gas constant (8.205x10^{-5} atm·m^3/mol·K). The derivation of equation (4.1) involves a number of assumptions. The temperature and aqueous volume are assumed to be constant during the purge. The liquid phase is considered to be well mixed, and the gas phase is assumed to behave ideally. The partial pressure of the analyte must be small compared to the total pressure, and Henry's Law must apply over the concentration range of interest. In addition, the distribution of analyte between the gas and liquid phases is assumed to reach equilibrium by the time the bubbles leave the liquid phase.

Because the bubbles are in contact with the solution for a limited amount of time, full gas/liquid equilibrium will probably not be achieved before the bubbles exit the liquid phase (*10*). Equation (4.1), therefore, may slightly overpredict the removal of analyte from the aqueous phase. Despite this possibility, Pankow and Rosen (*4*) obtained excellent agreement with equation (4.1) for all of the purgeable priority pollutants. With $c_1/c_{1,0}$ given by equation (4.1), the maximum possible efficiency (fractional removal) of the purging process e_{p1} is defined as

$$e_{p1} = 1 - c_1/c_{1,0} \tag{4.2}$$

For a given compound, purging efficiency increases with t_1 and is largely a function of V_{g1}/V_{s1} ($= F \cdot t_1/V_{s1}$), where V_{g1} is the total volume of purge gas bubbled through the solution at time t_1.

The transfer efficiency of analytes through the water trap during phase II of the purge can also be modeled as a purging process. Some portion of each analyte will probably be transmitted to the GC column when the trap is cold (temperature T_2). In the worst case, the analytes purged from solution during phase I are fully retained in the water trap. The concentration of analyte in the water trap at the beginning of phase II, then, is given by

$$c_{2,0} = \frac{c_{1,0} V_{s1}}{V_{s2}} \left\{ 1 - \exp \left[- \left(\frac{H}{RT_1} \right) \frac{F}{V_{s1}} t_c \right] \right\} \tag{4.3}$$

where t_c is the time during which the trap is cold (phase I purge time, minutes), and V_{s2} is the volume of water retained in the trap during phase I. The magnitude of V_{s2} is easily calculated by considering the vapor pressures of ice and water at T_2 and T_1, respectively (*8*).

Taking into account the fact that the purge gas entering the water trap is not necessarily free of analyte, the concentration in the trap during phase II is given by

$$c_2 = \frac{c_{1,0} V_{s1}}{V_{s2}} \left[\lambda_{2,2} - \frac{\lambda_{1,c}}{V_{s1} - V_{s2}} \left(V_{s1} \lambda_{2,2} - V_{s2} \lambda_{1,2} \right) \right] \tag{4.4}$$

$$\lambda_{i,j} = \exp \left[- \left(\frac{H}{RT_1} \right) \frac{F}{V_{si}} t_j \right] \tag{4.5}$$

where t_2 is the phase II purge time ($t_2 = t_1 - t_c$, minutes). Following Pankow (*8*), the purging efficiencies for the water trap e_{p2} and for the overall purge $E_{overall}$ are defined as

$$e_{p2} = 1 - c_2/c_{2,0} \tag{4.6}$$

$$E_{overall} = e_{p1}e_{p2} \times 100\% \quad (4.7)$$

Given sufficient time to strip analytes from the water trap, e_{p2} will approach 100% and e_{p1} will approximate $E_{overall}$. The correspondence between e_{p1} and $E_{overall}$ is illustrated in Figure 4.2 as a function of t_2, using V_{s1} = 5 mL, V_{s2} = 4.23 μL, F = 20 mL/min, t_c = 10 min, T_1 = 298 K, and various values of H. Even for compounds with H values as low as 0.0001 atm·m^3/mol, theory predicts that a phase II purge time of 0.5 minutes is sufficient to efficiently transfer analytes from the water trap to the GC column. Because the experimental application of this method will require ~0.5 min to warm the trap from T_2 to T_1, a phase II purge time of 1 to 2 minutes should be adequate to prevent significant retention of analytes in the trap.

Experimental

A schematic of the P/WCC apparatus with incorporation of the water trap is illustrated in Figure 4.3. Notable modifications made after those discussed by Pankow (*8*) are the use of a 6-port Carle valve (Hach Co., Loveland, CO) to control carrier gas pressure and flow direction, and the use of heating tape on the transfer line between the purge vessel and the GC. The Carle valve provides a simple method to start and stop the purge, while the heated transfer line eliminates cold spots near the water trap and increases the transmission efficiency of the less volatile analytes to the GC. The basic operating procedures of both the P/WCC method and the water trap have been described elsewhere (*3*, *4*, *8*).

The P/WCC apparatus was connected to a Varian 3400 gas chromatograph equipped with an electron capture detector. The ECD temperature was set at 350°C, and the most sensitive range was used. Ultra-high purity N_2 was used as detector make-up gas at a flow rate of 28.5 mL/min. The GC column was a 27 m long, 0.32 mm i.d. DB-624 fused-silica capillary column with a 1.8 μm film thickness manufactured by J&W Scientific (Folsom, CA). To further reduce the

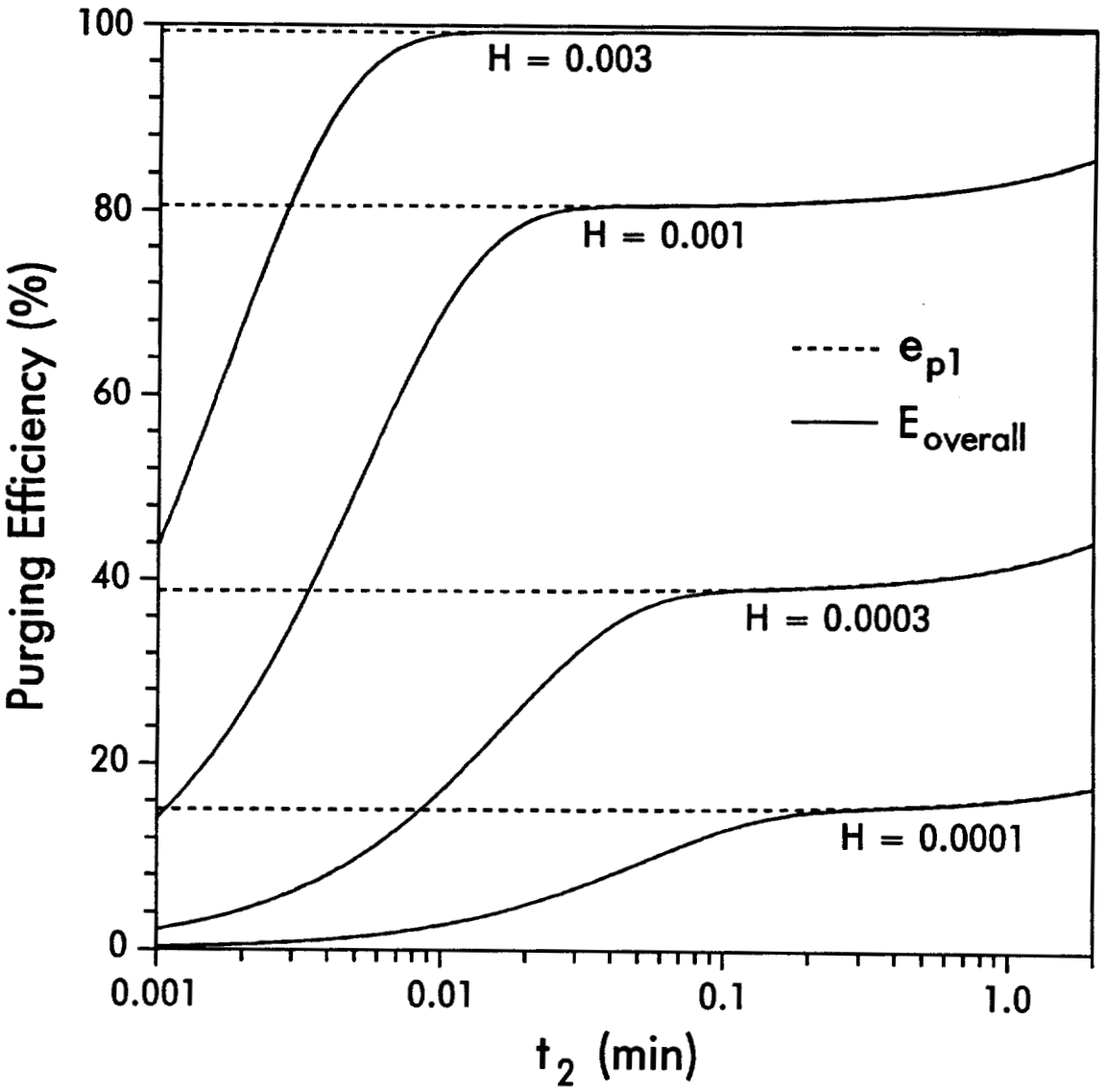

Figure 4.2. Theoretical purging efficiencies as a function of t_2 for a range of H values. The dashed lines represent e_{p1}, the maximum possible purging efficiency, while the solid lines denote $E_{overall}$, the overall purging efficiency when all analytes are assumed to be retained completely in the water trap during phase I of the purge. Conditions: V_{s1} = 5 mL, V_{s2} = 4.23 μL, F = 20 mL/min, t_c = 10 min, T_1 = 298 K, T_2 = 263 K.

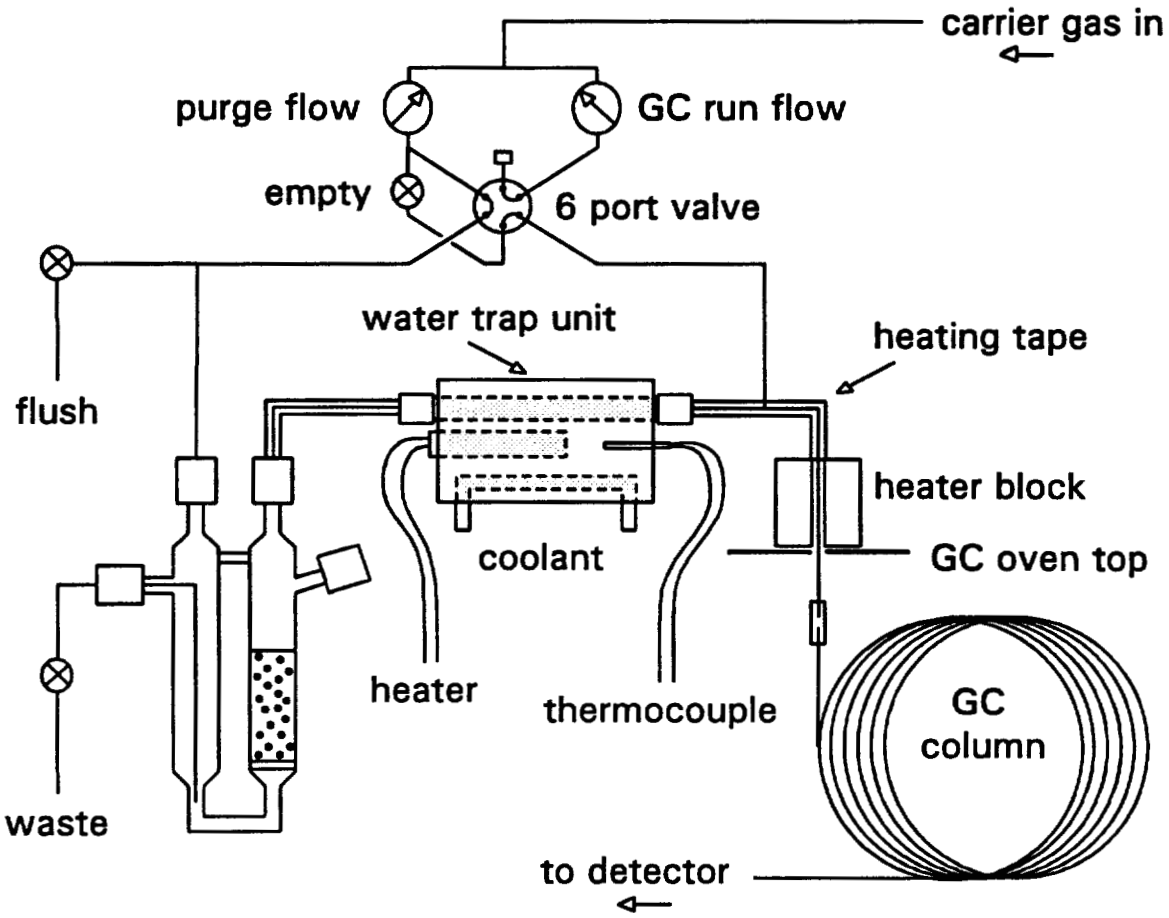

Figure 4.3. Schematic of the P/WCC apparatus with the glass-bead water trap. Snap valves are denoted by cross-hatched circles.

ability of ice to plug the column, a 0.5 m length of 0.53 mm i.d. DB-624 column with a 3.0 μm film thickness was installed in front of the main column. The two columns were joined with a universal press-fit connector (Restek Corp., Bellefonte, PA). The head of the column was connected to the transfer line in a "non-ice-trap" configuration (4); the column was extended through the transfer line union and into the heated zone above the GC oven. The temperatures of the transfer line and the GC interface heater block were both 220°C.

Ultra-high purity He was used as the purge and carrier gas. A purge gas flow rate of 20 mL/min was maintained with a purge pressure of 39 psig. The carrier gas pressure for the GC run was 13 psig. To prevent overpurging and erratic flow rates at both the start and end of the purge, precautions were taken to equalize the gas pressure across the purge vessel at those times. Such equalization was achieved before the start of the purge by selecting the purge position on the 6-port valve and opening the "empty" snap valve. The purge was then started by closing the "empty" valve. At the end of the purge, the 6-port valve was turned to the GC run position, and the excess pressure upstream of the purge vessel was vented by temporarily opening the "flush" snap valve.

The total purge time (t_1) for all analyses was 12 min. All were performed at ambient laboratory temperature ($T_1 \approx 298$ K). During phase I of the purge, the water trap was held at -10°C ($T_2 = 263$ K) with a liquid coolant composed of 50:50 (v/v) ethylene glycol and water. The phase I purge time (t_c) was 10 min. Phase II of the purge was 2 min (t_2) and was performed at 298 K. Whole column cryotrapping was performed at -30°C. The GC temperature program was ballistic from -30°C to 50°C, then at 5°C/min to 250°C. After the GC run was completed, the water trap was backflushed at 100°C to remove the trapped water, and the sample was drained from the purge vessel through the waste line. The three characteristic modes of the water trap are summarized in Table 4.1.

Table 4.1. Characteristics of the Three Water Trap Modes.

	Phase I Purge	Phase II Purge	Backflush
Coolant	ON	OFF	OFF
Heater	OFF	ON	ON
Temperature	-10°C	25°C	100°C
Flow	to GC	to GC	to PV [a]
Duration	10 min	2 min	4 min

[a] PV = purge vessel

Results and Discussion

The glass-bead water trap effectively reduced the amount of water transmitted to the GC column. When the water trap was in use, the column never plugged with ice. Purge times of up to 17 min were tested (t_2 = 2 min, V_{g1} = 340 mL). Not only did the column never plug with ice under these conditions, but no measurable decrease in the purge flow rate was observed. Without the water trap, purge volumes of approximately 100 mL were sufficient to plug the column, even when the column was installed in the "ice-trap" configuration (see 4). Moreover, the water trap reduced the chromatographic interference of water to a manageable level. Unlike flame ionization detectors, electron capture detectors are extremely sensitive to relatively small amounts of water. In the absence of a water trap, enough water was transmitted to the column to create a very large, asymmetric peak that obscured several minutes of the chromatogram. The use of the water trap, therefore, was key to the successful coupling of an ECD to P/WCC.

This method was tested with a standard containing each of the chlorinated benzenes. ECD response is quite sensitive to the degree of chlorination; in general, the detection limit for a given compound class will decrease as the number of chlorines increases. Consequently, the chlorobenzenes in the aqueous standard were at different concentrations: ϕCl

(3.7 ng/mL), each ϕCl_2 (0.11 ng/mL), each ϕCl_3 (0.028 ng/mL), each ϕCl_4 (0.019 ng/mL), ϕCl_5 (0.011 ng/mL), and ϕCl_6 (0.011 ng/mL). Figure 4.4a shows the chromatogram that results from purging 5.0 mL of the standard, while Figure 4.4b is the result of repurging the same standard. Both chromatograms are plotted on identical scales. The ECD was not very sensitive to chlorobenzene, and hexachlorobenzene behaved erratically; neither is shown in Figure 4.4. Good resolution was obtained for all but two of the remaining compounds. Figure 4.5 illustrates the overlap of the 1,2,3,5- and 1,2,4,5-tetrachlorobenzene peaks. For a 5.0 mL sample, representative method detection limits are 0.01 ng/mL for 1,2-ϕCl_2, 0.003 ng/mL for 1,2,4-ϕCl_3, and 0.0006 ng/mL for 1,2,4,5-ϕCl_4.

Experimental purging efficiencies were calculated by (*4*)

$$E_{obs} = \frac{A_i - A_r}{A_i} \times 100\% \tag{4.8}$$

where A_i is the peak area resulting from the initial purge and A_r is the corresponding peak area from the repurge. Values of E_{obs} were obtained for both 1.0 and 5.0 mL samples. The results are compared to theoretical values of $E_{overall}$ in Table 4.2. $E_{overall}$ represents the maximum possible purging efficiency because e_{p2} is approximately 100% and e_{p1} is known to be a theoretical maximum. All experimental values are lower than expected on the basis of theory. Portions of the discrepancies might be due to errors in the values of H. In addition, if gas/liquid equilibrium was not fully achieved as each gas parcel contacted the liquid phase, then negative deviations in the values of E_{obs} would be expected.

If the degree to which gas/liquid equilibrium is achieved is constant throughout the purge, then better predictions of $E_{overall}$ might be obtained through the use of an *effective* Henry's law constant, where the effective value of H is given by

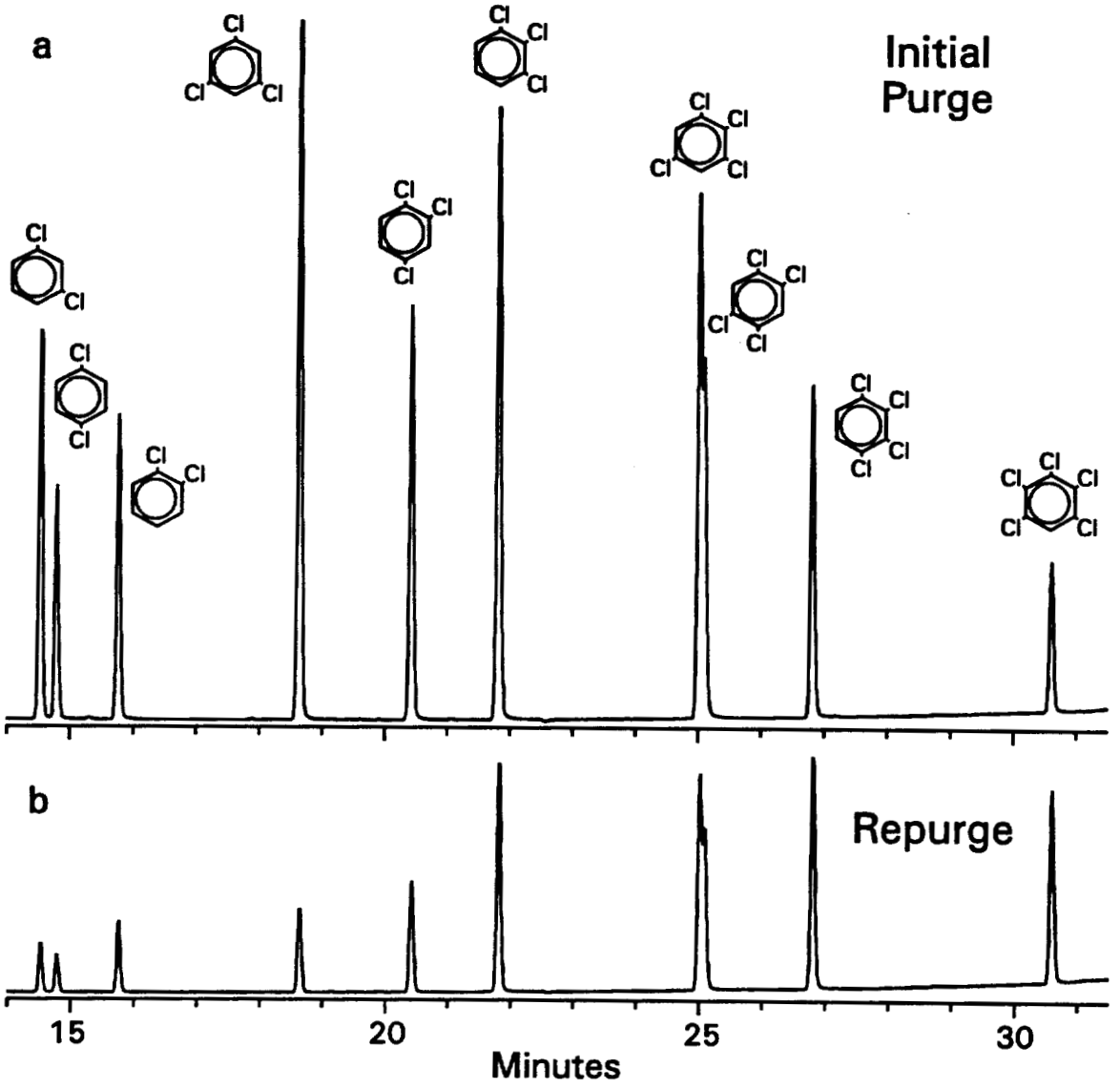

Figure 4.4. Initial (a) and repurge (b) chromatograms of a 5 mL water sample spiked with each of the chlorinated benzenes. Temperature program: 50°C to 250°C at 5°C/min.

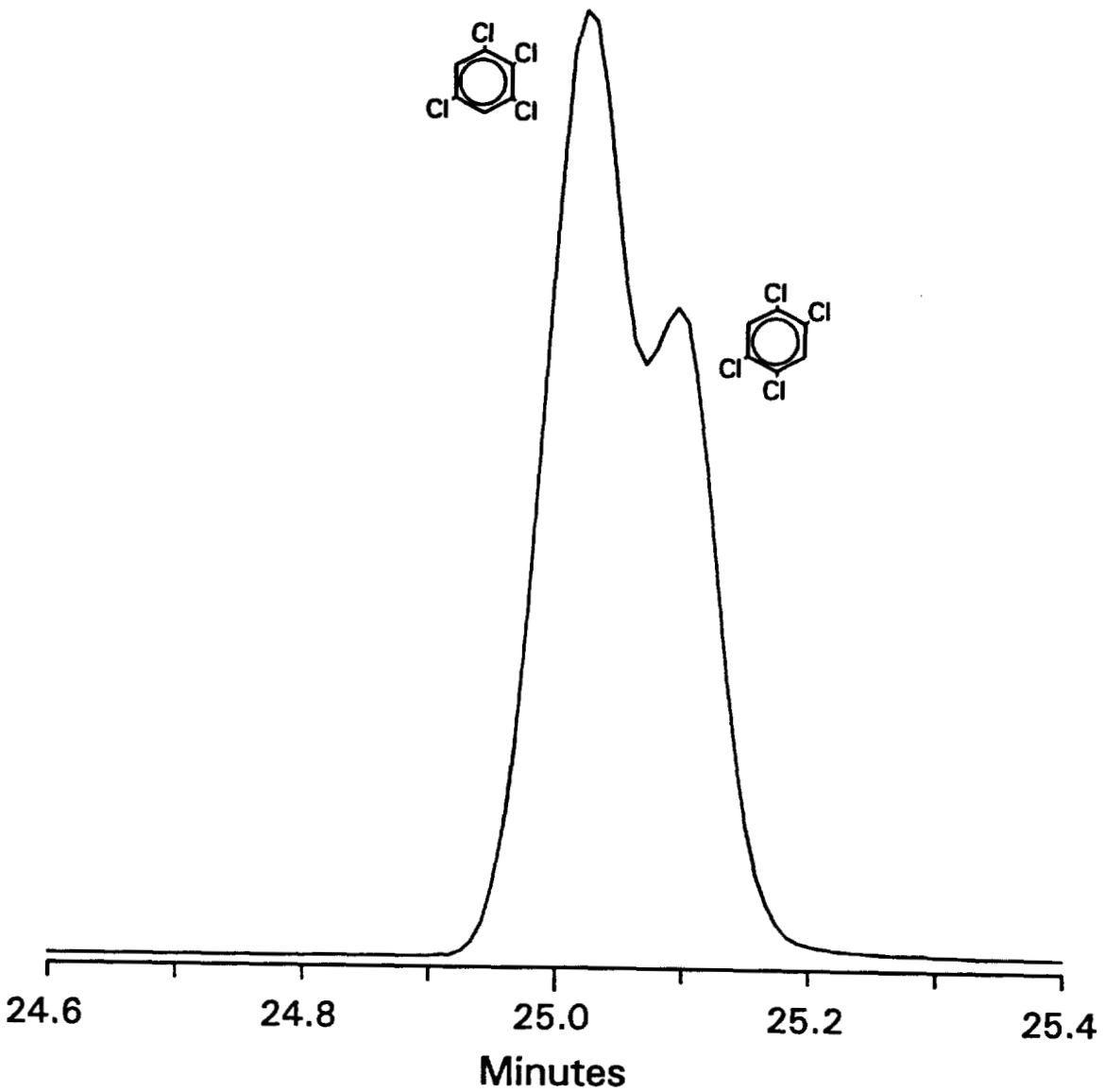

Figure 4.5. Representative section of a chromatogram showing the superposition of peaks for 1,2,3,5- and 1,2,4,5-tetrachlorobenzene.

Table 4.2. Henry's Law Constants (H), Predicted Purging Efficiencies ($E_{overall}$), and Observed Purging Efficiencies (E_{obs}) for the Chlorinated Benzenes.

Compound	H [a] (atm·m^3/mol)	5 mL sample $E_{overall}$ [b] (%)	5 mL sample E_{obs} [c] (%)	1 mL sample $E_{overall}$ [b] (%)	1 mL sample E_{obs} [c] (%)
Chlorobenzene	0.0036	99.9	ND [d]	100.0	ND
1,2-Dichlorobenzene	0.0019	97.6	77.6	100.0	92.7
1,3-Dichlorobenzene	0.0036	99.9	88.0	100.0	94.4
1,4-Dichlorobenzene	0.0031	99.8	85.1	100.0	94.0
1,2,3-Trichlorobenzene	0.0013 [e]	92.2	62.8	100.0	82.8
1,2,4-Trichlorobenzene	0.0023	98.9	73.4	100.0	88.6
1,3,5-Trichlorobenzene	0.0023 [e]	98.9	88.5	100.0	94.3
1,2,3,4-Tetrachlorobenzene	0.0026 [e]	99.4	30.7	100.0	30.4
1,2,3,5-Tetrachlorobenzene	0.0016 [e]	95.7	61.3	100.0	63.9
1,2,4,5-Tetrachlorobenzene	0.0026 [e]	99.4	52.7	100.0	54.8
Pentachlorobenzene	0.0016 [f]	95.7	NA [g]	100.0	NA
Hexachlorobenzene	0.00082 [h]	80.0	NA	100.0	NA

[a] H data from Mabey *et al.* (*11*) except as noted (T_1 = 298 K).

[b] $E_{overall}$ was calculated from equations (4.1-4.7), using T_1 = 298 K, R = 8.205x10^{-5} atm·m^3/mol·K, F = 20 mL/min, t_c = 10 min, t_2 = 2 min, and V_{s2} = 4.23 μL.

[c] E_{obs} was calculated using equation (4.8).

[d] ND = not detected.

[e] H data from Mackay and Shiu (*12*).

[f] Vapor pressure estimated from a vapor pressure versus boiling point regression; H estimated using that vapor pressure and solubility data from Verschueren (*13*).

[g] NA = not available. Results were inconsistent.

[h] H estimated using vapor pressure and solubility data from Verschueren (*13*).

$$H_{eff} = \gamma H \tag{4.9}$$

and γ is the fraction of equilibrium attained. The value of γ is expected to be smaller for a 1.0 mL sample than for a 5.0 mL sample due to the shorter contact time with the liquid phase. Using this approach, the differences between E_{obs} and $E_{overall}$ in Table 4.2 for the di- and trichlorobenzenes can be reconciled using a single value of γ for each value of V_{s1}. Those γ values, however, are not small enough to explain the low E_{obs} values of the less volatile compounds. Given that the transfer line had to be heated to 220°C to maximize throughput of the heavier compounds, and the fact that E_{obs} values for the tetrachlorobenzenes were found to be independent of V_{s1}, the lower than expected purging efficiencies might be due to hold-up in the transfer line or in the water trap. A higher phase II water trap temperature or a longer phase II purge time might increase these purging efficiencies.

Summary and Conclusions

The purge with whole column cryotrapping method of Pankow and Rosen (4) was adapted for use with an electron capture detector and tested with a set of chlorinated benzenes. Purge gas desiccation with a simple glass-bead water trap allowed the use of large purge gas volumes, prevented the GC column from plugging with ice, and reduced the interference of water in the chromatogram. Good chromatographic resolution was obtained. Despite smaller than expected purging efficiencies, compounds such as tetra- and pentachlorobenzene can be analyzed quickly and effectively with this simple P/WCC method. Purging methods can be successfully used for compounds with a wide range of Henry's law constants.

Glossary

A_i	peak area from initial purge
A_r	peak area from repurge

c_1	concentration of analyte in aqueous sample (ng/mL)
$c_{1,0}$	initial concentration of analyte in sample (ng/mL)
c_2	concentration of analyte in water trap during phase II purge (ng/mL)
$c_{2,0}$	concentration of analyte in water trap at beginning of phase II (ng/mL)
e_{p1}	maximum possible purging efficiency of the sample
e_{p2}	purging efficiency of analytes in the water trap
E_{obs}	observed purging efficiency (%)
$E_{overall}$	overall efficiency (%) for purging of analytes from a sample to the GC column
F	flow rate of purge gas through the purge vessel (mL/min)
H	Henry's law constant (atm·m^3/mol) for the analyte at T_1
H_{eff}	effective Henry's law constant (atm·m^3/mol)
R	gas constant (8.205x10^{-5} atm·m^3/mol·K)
t_c	time during which the water trap is cold (min)
t_1	total purge time (min)
t_2	phase II purge time (min)
T_1	temperature in the purge vessel and in the warm trap (K)
T_2	temperature in the cold trap (K)
V_{g1}	volume of purge gas bubbled through the sample (mL)
V_{s1}	volume of sample (mL)
V_{s2}	volume of liquid water in the trap (mL)
γ	fraction of gas/liquid equilibrium attained

Registry No. Chlorobenzene, 108-90-7; 1,2-Dichlorobenzene, 95-50-1; 1,3-Dichlorobenzene, 541-73-1; 1,4-Dichlorobenzene, 106-46-7; 1,2,3-Trichlorobenzene, 87-61-6; 1,2,4-Trichlorobenzene, 120-82-1; 1,3,5-Trichlorobenzene, 108-70-3; 1,2,3,4-Tetrachlorobenzene, 634-66-2; 1,2,3,5-Tetrachlorobenzene,

634-90-2; 1,2,4,5-Tetrachlorobenzene, 95-94-3; Pentachlorobenzene, 608-93-5; Hexachlorobenzene, 118-74-1.

Literature Cited

(1) Longbottom, J. E.; Lichtenberg, J. J. (eds), *Test Methods for Organic Chemical Analysis of Municipal and Industrial Wastewater;* EPA-600/4-82-057, U.S. EPA, Washington, DC, 1982.

(2) U.S. EPA, *Methods for the Determination of Organic Compounds in Finished Drinking Water and Raw Source Water;* Physical and Chemical Methods Branch, EMSL, Cincinnati, OH, 1986; Method 524.2.

(3) Pankow, J. F. *HRC & CC* **1987,** *10,* 409-410.

(4) Pankow, J. F.; Rosen, M. E. *Environ. Sci. Technol.* **1988,** *22,* 398-405.

(5) Simmonds, P. G. *J. Chromatogr.* **1984,** *289,* 117-127.

(6) Cochran, J. W. *HRC & CC* **1988,** *11,* 663-665.

(7) Rosen, M. E. Ph.D. Thesis, Oregon Graduate Center, 1988.

(8) Pankow, J. F. *Environ. Sci. Technol.* **1991,** *25,* 123-126.

(9) Pankow, J. F. *Anal. Chem.* **1986,** *58,* 1822-1826.

(10) Mackay, D.; Shiu, W. Y.; Sutherland, R. P. *Environ. Sci. Technol.* **1979,** *13,* 333-337.

(11) Maybey, W. R.; Smith, J. H.; Podoll, R. T.; Johnson, H. L.; Mill, T.; Chou, T.; Gates, J.; Partridge, I. W.; Jaber, H.; Vandenberg, D. *Aquatic Fate Process Data for Organic Priority Pollutants;* EPA-440/4-81-014, U.S. EPA, Washington, DC, 1982.

(12) Mackay, D.; Shiu, W. Y. *J. Phys. Chem. Ref. Data* **1981,** *10,* 1175.

(13) Verschueren, K. *Handbook of Environmental Data on Organic Chemicals,* 2nd ed.; Van Nostrand Reinhold, New York, NY, 1983.

CHAPTER V

Rate-Controlling Mechanisms of Organic Sorption in Aqueous Systems

Abstract

Experiments were conducted to investigate the rate-limited sorption of several chlorinated benzenes in an aqueous system. A model sorbent with well-defined physical properties (XAD-7) was used to allow the resulting data to be related to one or several specific rate-controlling mechanisms. Adsorption data were fitted to five different models of sorption kinetics: external film diffusion, first order particle abrasion, intraparticle diffusion, coupled intraparticle diffusion and particle abrasion, and coupled film and intraparticle diffusion (dual resistance). Each model is characteristically different in its predictions; the film diffusion and intraparticle diffusion models represent two extremes. Overall, the experimental data were best described by the dual resistance model. Film diffusion was found to be more important than intraparticle diffusion in determining the adsorption rate. When used alone, the intraparticle diffusion model consistently overpredicted the extent of adsorption early in each experiment and underpredicted adsorption at later times. Values of the fitted film mass-transfer coefficient agreed well with previously reported values. Hydrodynamic film thicknesses were calculated to be $\sim 11\ \mu m$, or about 1/25th of the particle radius. For particle suspensions in moving waters such as rivers,

lakes, and oceans, film diffusion is likely to be an important rate-controlling mechanism of organic adsorption and desorption.

Introduction

An accurate assessment of the transport and fate of a chemical species in natural systems can only be made with a knowledge of the mechanisms that control the behavior of that species. The ultimate fate of a particular compound is dependent upon many interrelated processes. Some of the most important processes are sorption, volatilization, dissolution, and biodegradation. Rate-limited sorption can greatly affect the behavior of organic compounds in aqueous systems, and can greatly retard transport and increase the time and complexity of remediation projects in groundwater systems (*1*). Slow sorption processes can decrease biodegradation rates by reducing the bioavailability of the compound (*2-5*). Numerous investigations have shown that sorption reaction time scales can be on the order of weeks to months, or longer in some cases (*3, 6-11*). Models of transport, biodegradation, and ecological impact, therefore, can potentially benefit from an accurate description of rate-limited sorption.

The sorption of nonionic, organic compounds to soils, sediments, and many common sorbents in aqueous systems is generally recognized to be nonspecific and reversible (*12-18*). Because sorption reactions are characterized by relatively weak forces, rate-limited sorption is expected to be due to some form of physical transport limitation rather than a slow chemical reaction. Numerous studies of organic sorption kinetics with soils have implicated a diffusive transport process as the rate-limiting mechanism (*3, 9, 10, 19-26*). Several types of diffusive rate control have been postulated, including diffusion across a boundary layer at the sorbent surface (film diffusion), intraparticle pore diffusion, intraparticle surface diffusion, intraorganic matter diffusion, and various combinations of these processes. For well over forty years, diffusion has been known to be the rate-limiting mechanism for ion exchange (*27-32*), certain types of catalysis (*33*), and organic sorption on activated carbon (*34-36*). The use

of these well-developed models to describe sorption kinetics in natural systems, however, was not pursued aggressively until about ten years ago.

Studies of diffusion-controlled sorption kinetics are complicated by the fact that the nature of the rate-limiting process can change depending upon the specific reaction conditions. Consider, for example, the kinetics of ion exchange in a batch system. Under rapid mixing conditions, intraparticle diffusion is expected to control the rate; film diffusion should be dominant at slow mixing speeds (*31-32*). Therefore, intraparticle diffusion can only be isolated for further study if film diffusion is minimized by vigorous mixing. Violent mixing conditions, however, can cause particles to break or abrade and that, in turn, can significantly affect the observed reaction rates (*21, 32*). In addition, particle radius and solution concentration might influence the type of diffusion control that predominates (*32*). An analysis of rate-controlling mechanisms must consider each of these competing processes.

The application of a diffusion model often requires detailed information concerning the physical properties of the sorbent, such as the particle radius or size distribution, particle porosity (void volume per total particulate volume), and/or pore size. Soils and sediments are very heterogeneous materials and are characterized by a wide range of properties. Because soils are complex mixtures, several physical processes might be expected to contribute to sorption kinetics. As a result, the assignment of one or several rate-limiting mechanisms can be difficult. In an attempt to avoid these complications, several investigators have chosen to use somewhat generic models of rate-limited sorption (*23, 25, 37-38*). First order reaction and two-site or bicontinuum models are the most commonly used of these empirical models.

In this study, the characteristics of five different mechanistic models of organic sorption kinetics were investigated and compared. Four of the models are diffusion-based; the fifth represents the competing process of particle abrasion. The ability of each model to describe the adsorption of a set of chlorinated benzenes to a model sorbent was assessed. Complexities caused by

sorbent heterogeneities were avoided by using XAD-7, a sorbent with well-defined physical properties. The most probable rate-controlling mechanisms are discussed. Implications for the representation of sorption kinetics in natural systems are explored. The relationships between first order, two-site, and diffusion-based models are considered.

Theory

Five mechanistic and two empirical models that describe sorption kinetics in batch systems were examined. The mechanistic models considered in this study are: external film diffusion, first order particle abrasion, intraparticle diffusion, coupled intraparticle diffusion and particle abrasion, and coupled film and intraparticle diffusion (dual resistance). Empirical first order reaction and two-site models were also assessed and compared to the diffusion-based models. Each mechanistic model is different in its description of the concentration gradients in the solution and the sorbent particles. Figures 5.1 and 5.2 illustrate the concentration profiles that are postulated by each of the mechanistic models. In all cases, sorbent particles are assumed to be spherical. In addition, only linear sorption isotherms are considered, defined as

$$K = S / C \tag{5.1}$$

where K is a linear partition coefficient (mL/g), S is the concentration of analyte in the solid phase (ng/g), and C is the bulk aqueous concentration of analyte (ng/mL).

First Order Reaction Model. The description of sorption kinetics with a first order reaction model is a generic approach that can represent either a chemical or a physical rate limitation. First order models are attractive because they provide the easiest method of incorporating an estimation of rate-limited sorption into larger transport models. If sorption kinetics are important and the first order reaction model is used, then the underlying mechanism for the rate-limitation is not as important as the attempt to include some form of sorption

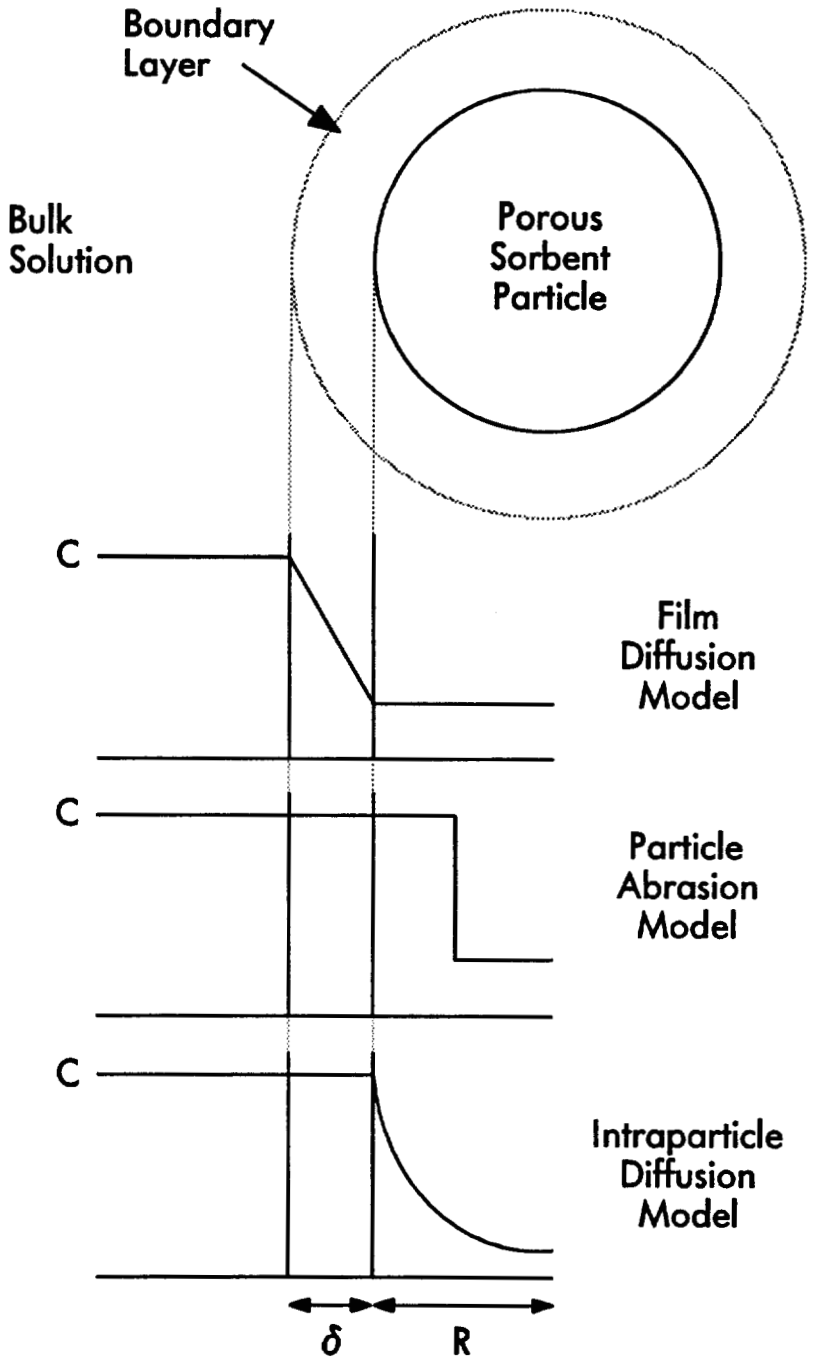

Figure 5.1. Postulated transient concentration profiles in the sorbent particle and the hydrodynamic boundary layer for the film diffusion, particle abrasion, and intraparticle diffusion models.

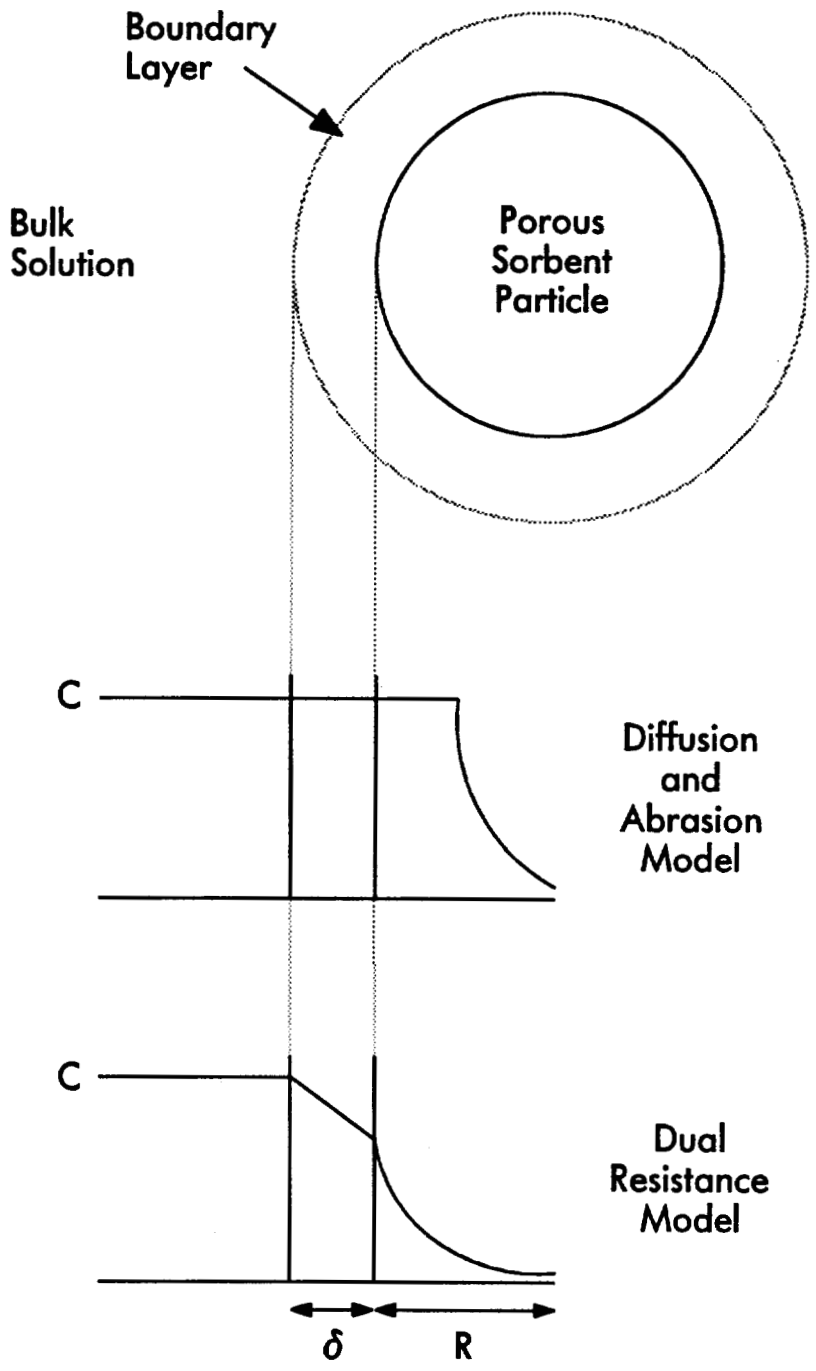

Figure 5.2. Postulated transient concentration profiles in the sorbent particle and the hydrodynamic boundary layer for the coupled intraparticle diffusion/particle abrasion model and the dual resistance model.

kinetics in the model. The governing equation for a first order reaction model is

$$\frac{dS}{dt} = k_d(KC - S) \tag{5.2}$$

where t is time (min) and k_d is a first order sorption rate constant (min^{-1}). Equation (5.2) is easily combined with a mass balance equation and then integrated to obtain an equation for C in terms of time. The result is

$$C = \frac{C_o V + mS_o}{V + mK} + \frac{m(KC_o - S_o)}{V + mK} \exp\left[-k_d\left[1 + \frac{mK}{V}\right]t\right] \tag{5.3}$$

where C_o is the initial aqueous concentration (ng/mL), V is the solution volume (mL), m is the mass of sorbent (g), and S_o is the initial concentration of analyte in the solid phase (ng/g).

Simulations were performed to determine the general characteristics of the first order reaction model. The sorption rate constant was varied over seven orders of magnitude. Figure 5.3 illustrates the normalized aqueous concentration versus log(t) for m = 0.117 g, V = 2350 mL, K = 500,000 mL/g, S_o = 0 ng/g, and C_o = 0.4 ng/mL. Curves (a) to (g) represent successive order of magnitude decreases in the value of k_d, from 10^{-1} min^{-1} to 10^{-7} min^{-1}, respectively.

Two-site or Bicontinuum Models. In a two-site model, the sorbent is divided into two fractions, one of which is considered to be in instantaneous equilibrium with the aqueous phase; the other fraction interacts via first order kinetics. This model retains the relative simplicity of the first order model while adding another parameter, the fraction of equilibrium sites F_e. This additional parameter improves the ability of the model to fit experimental data. When F_e is zero, the two-site model collapses to the first order model. Because all equilibrium sites are occupied at t = 0, a nonzero F_e value causes the fractional approach to equilibrium to start at F_e rather than at 0.0. The time scale of the

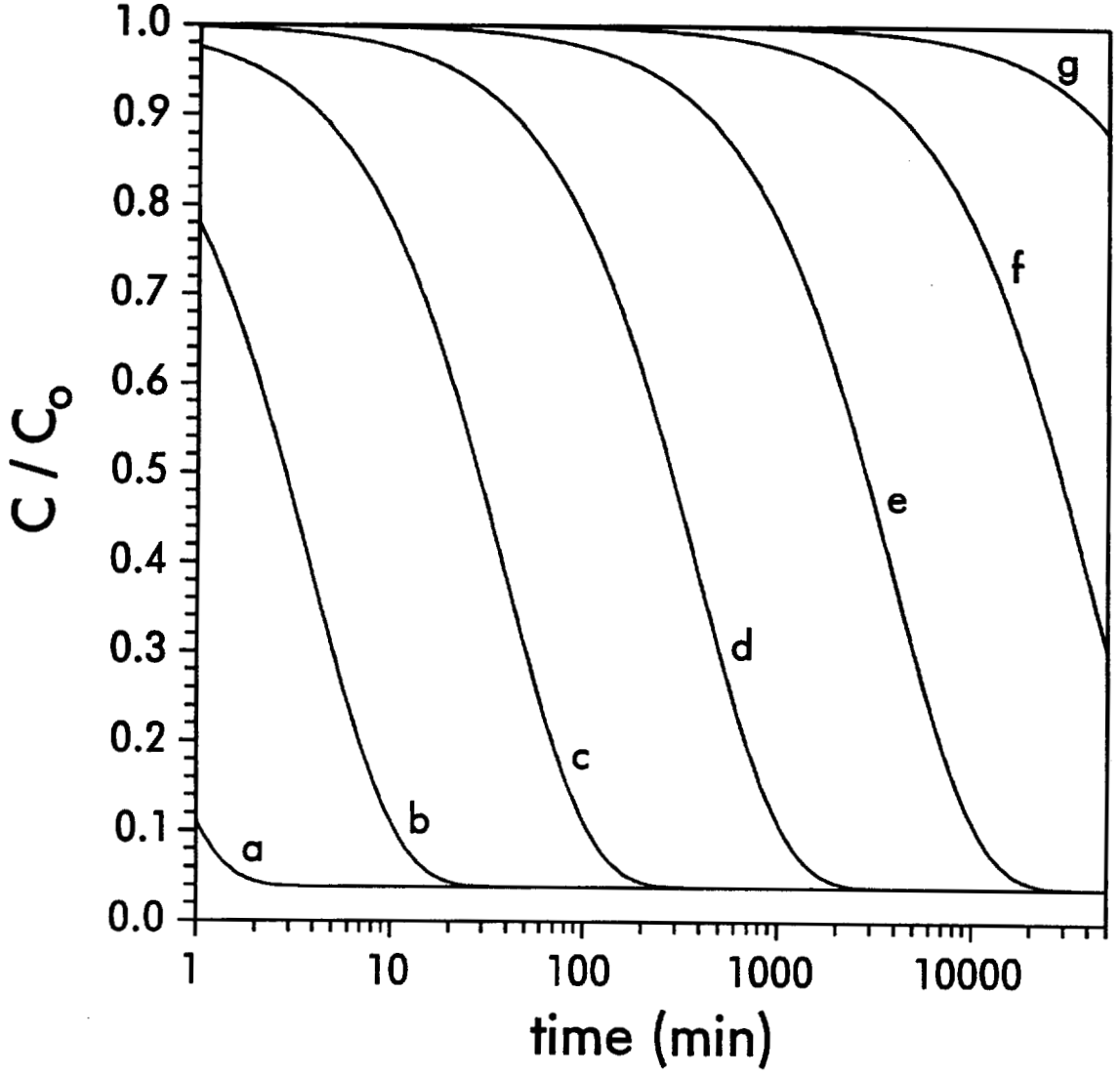

Figure 5.3. Normalized aqueous concentrations predicted by the first order reaction model. Values of k_d are 10^{-1}, 10^{-2}, 10^{-3}, 10^{-4}, 10^{-5}, 10^{-6}, and 10^{-7} min^{-1} for curves a-g, respectively. Other input parameters: m = 0.117 g, V = 2350 mL, K = 500000 mL/g, C_o = 0.4 ng/mL, and S_o = 0 ng/g.

reaction is unaffected by F_e. With respect to Figure 5.3, a nonzero F_e causes the C/C_o curve to proportionally contract in the y-direction and effectively decreases the characteristic slope.

Film Diffusion Model. If the only rate-controlling process is diffusion across a stagnant film surrounding each spherical sorbent particle, then the governing equation for the concentration change is

$$\frac{dS}{dt} = \frac{3D_m}{R\rho_b\delta}(C - C_s) = \frac{3D_m}{KR\rho_b\delta}(KC - S) \tag{5.4}$$

where D_m is the molecular diffusion coefficient in water (cm^2/s), R is the particle radius (cm), ρ_b is the bulk density of the sorbent (g/mL), δ is the hydrodynamic film thickness (cm), and C_s is the aqueous concentration at the particle surface (ng/mL). The ratio of the molecular diffusion coefficient to the film thickness is often represented by a film mass-transfer coefficient k_f (cm/s). The governing equations for film diffusion (5.4) and for first order reaction (5.2) are identical in form. Therefore, equation (5.3) is the solution for both models, and Figure 5.3 also represents the characteristics of the film diffusion model. Despite the simple approach of the first order and two-site models, both are closely related to the film diffusion model. The mass transfer coefficient k_f is related to the first order sorption rate constant by

$$k_f = \frac{D_m}{\delta} = \frac{KR\rho_b k_d}{3} \tag{5.5}$$

The hydrodynamic film thickness will depend upon the mixing rate of the solution and the viscosity of water. As the mixing rate increases, the film thickness decreases, thereby causing an increase in both k_f and the transport rate. If film diffusion is the rate-controlling mechanism and a first order reaction model is used, then the first order sorption rate "constant" k_d is not constant at all. Rather, it is dependent upon the compound, particle size, and mixing rate.

First Order Particle Abrasion Model. Particle abrasion is not a simple process to represent. If it is assumed that abrasion decreases the particle radius according to first order kinetics, then the particle radius r (cm) is given by

$$r = R \exp(-k_{ab} t) \tag{5.6}$$

where R is the original radius (cm) and k_{ab} is a first order abrasion rate constant (min^{-1}). Then, assuming that the particulate mass removed by abrasion reaches sorption equilibrium with the aqueous phase instantly, the change in the aqueous concentration is given by

$$C = \frac{C_o V + m S_o (1 - \eta)}{V + mK(1 - \eta)} \quad , \quad \eta = \exp(-k_{ab} t) \tag{5.7}$$

The characteristic predictions of this model are illustrated in Figure 5.4 for the same conditions as in Figure 5.3. The value of k_{ab} successively decreases by a factor of ten from 10^{-1} min^{-1} for curve (a) to 10^{-7} min^{-1} for curve (g). While the film diffusion and particle abrasion models give similar predictions, curves from the film diffusion model have steeper slopes. The model developed here, of course, is only one hypothetical representation of the abrasion process. In addition, even when particle abrasion is important, it is unlikely that sorbent particles will be completely destroyed ($r = 0$). Nevertheless, this model provides an instructive approximation of this competing process.

Intraparticle Diffusion Model. The governing equation for diffusion in spherical coordinates is

$$\frac{\partial S(r)}{\partial t} = D_{eff} \left[\frac{\partial^2 S(r)}{\partial r^2} + \frac{2}{r} \frac{\partial S(r)}{\partial r} \right] \tag{5.8}$$

where $S(r)$ is the total volumetric concentration of analyte (ng/mL) at a radial distance r (cm), and D_{eff} is an effective diffusion coefficient (cm^2/s). Equation (5.8) can represent either pore diffusion, or surface diffusion, or both; the definition of D_{eff} incorporates both processes. An analytical solution to equation

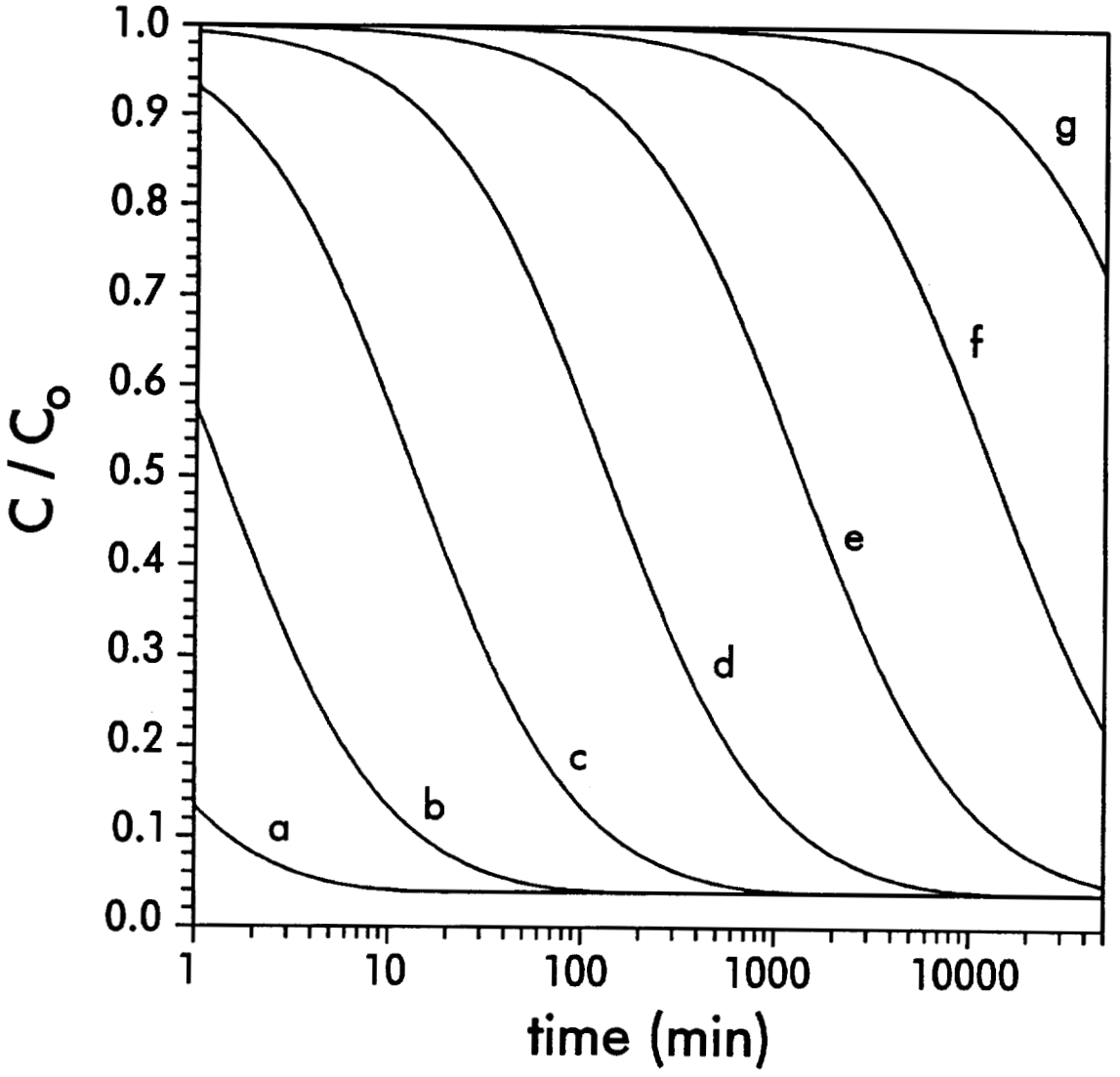

Figure 5.4. Normalized aqueous concentrations predicted by the first order particle abrasion model. Values of k_{ab} are 10^{-1}, 10^{-2}, 10^{-3}, 10^{-4}, 10^{-5}, 10^{-6}, and 10^{-7} min^{-1} for curves a-g, respectively. Other input parameters: m = 0.117 g, V = 2350 mL, K = 500000 mL/g, C_o = 0.4 ng/mL, and S_o = 0 ng/g.

(5.8) is given by Crank (39) for particles that are initially free of analyte ($S_o = 0$) and in a monodisperse particle size distribution. That series solution is

$$C = C_o - \frac{C_o}{1+\alpha_c}\left[1 - \sum_{n=1}^{\infty} \frac{6\alpha_c(\alpha_c+1)}{9+9\alpha_c+\alpha_c^2 g_n^2} \exp\left[\frac{-g_n^2 D_{eff} t}{R^2}\right]\right] \quad (5.9)$$

where α_c is related to the final (equilibrium) fractional uptake and is defined as

$$\alpha_c = \frac{V}{mK} \quad (5.10)$$

The values of g_n in equation (5.9) are the nonzero roots of

$$\frac{\tan g_n}{g_n} = \frac{3}{3+\alpha_c g_n^2} \quad (5.11)$$

In the implementation of this model, the series is truncated when the addition of the next term is no longer significant. Simulations with this model were performed with eight different values of D_{eff}/R^2, ranging from 10^{-3} min^{-1} to 10^{-10} min^{-1} and decreasing by a factor of 10 for each simulation. Other input was identical to that used previously. The results are illustrated in Figure 5.5. The general slope of these curves is much smaller than that observed for either the film diffusion or particle abrasion models. Recalling that the two-site model can effect a decrease in the normally steep slope of the first order curves when $F_e > 0$, it is not surprising that two-site models have been successful in representing the kinetics of diffusion-controlled processes.

Coupled Intraparticle Diffusion and Particle Abrasion Model. The mechanisms of intraparticle diffusion and first order particle abrasion were coupled and incorporated into a numerical model. In coupled models such as this one, the relative rates of the two processes will dictate which process dominates the observed kinetics. A dimensionless number ψ can be defined to represent the ratio of the abrasion rate to the intraparticle diffusion rate

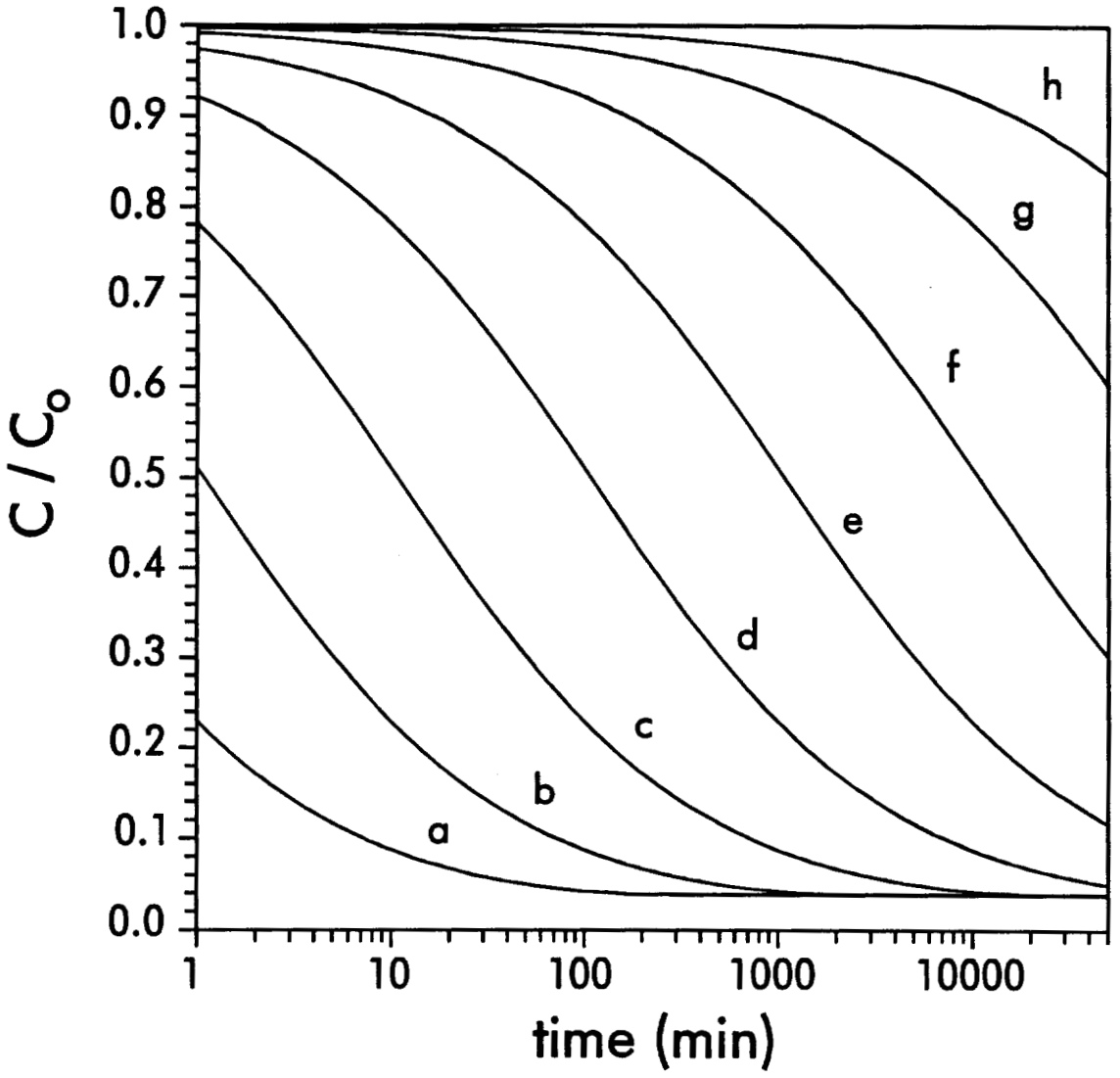

Figure 5.5. Normalized aqueous concentrations predicted by the intraparticle diffusion model. Values of D_{eff}/R^2 are 10^{-3}, 10^{-4}, 10^{-5}, 10^{-6}, 10^{-7}, 10^{-8}, 10^{-9}, and 10^{-10} min^{-1} for curves a-h, respectively. Other input parameters: m = 0.117 g, V = 2350 mL, K = 500000 mL/g, C_o = 0.4 ng/mL, and S_o = 0 ng/g.

$$\psi = \frac{k_{ab} R^2}{D_{eff}} \tag{5.12}$$

When ψ is less than ~10, intraparticle diffusion dominates, while for ψ values greater than ~100, abrasion is the rate-controlling mechanism. Between 10 and 100, both processes are important. These characteristics are illustrated in Figure 5.6 for various values of ψ, using a constant value of k_{ab} (10^{-5} min^{-1}) and the previous values of m, V, etc. The stairstep behavior evident for ψ = 100 and 1000 is the result of the numerical implementation of the abrasion model. Each step is the result of the abrasive loss of one layer. Smoother curves could be obtained with finer spatial discretization. The number of nodes/particle used in these simulations was 1501.

Coupled Film and Intraparticle Diffusion Model (Dual Resistance). The dual resistance model couples both film and intraparticle diffusion. Huang and Li (*31*) derived an analytical solution for this coupled model, assuming a monodisperse particle size distribution and S_o = 0. That series solution is

$$C = C_o - \frac{C_o}{1 + \alpha_c}\left[1 - \sum_{n=1}^{\infty} \Omega_n \exp\left[\frac{-g_n^2 D_{eff} t}{R^2}\right]\right] \tag{5.13}$$

$$\Omega_n = \frac{6\xi^2 \alpha_c(\alpha_c + 1)}{\left(9 + 9\alpha_c + \alpha_c^2 g_n^2\right)\xi^2 - (6 + \alpha_c)\alpha_c g_n^2 \xi + \alpha_c^2 g_n^4} \tag{5.14}$$

where ξ is a dimensionless number that relates the film diffusion rate to the intraparticle diffusion rate

$$\xi = \frac{R k_f}{K \rho_b D_{eff}} \tag{5.15}$$

and the values of g_n are the nonzero roots of

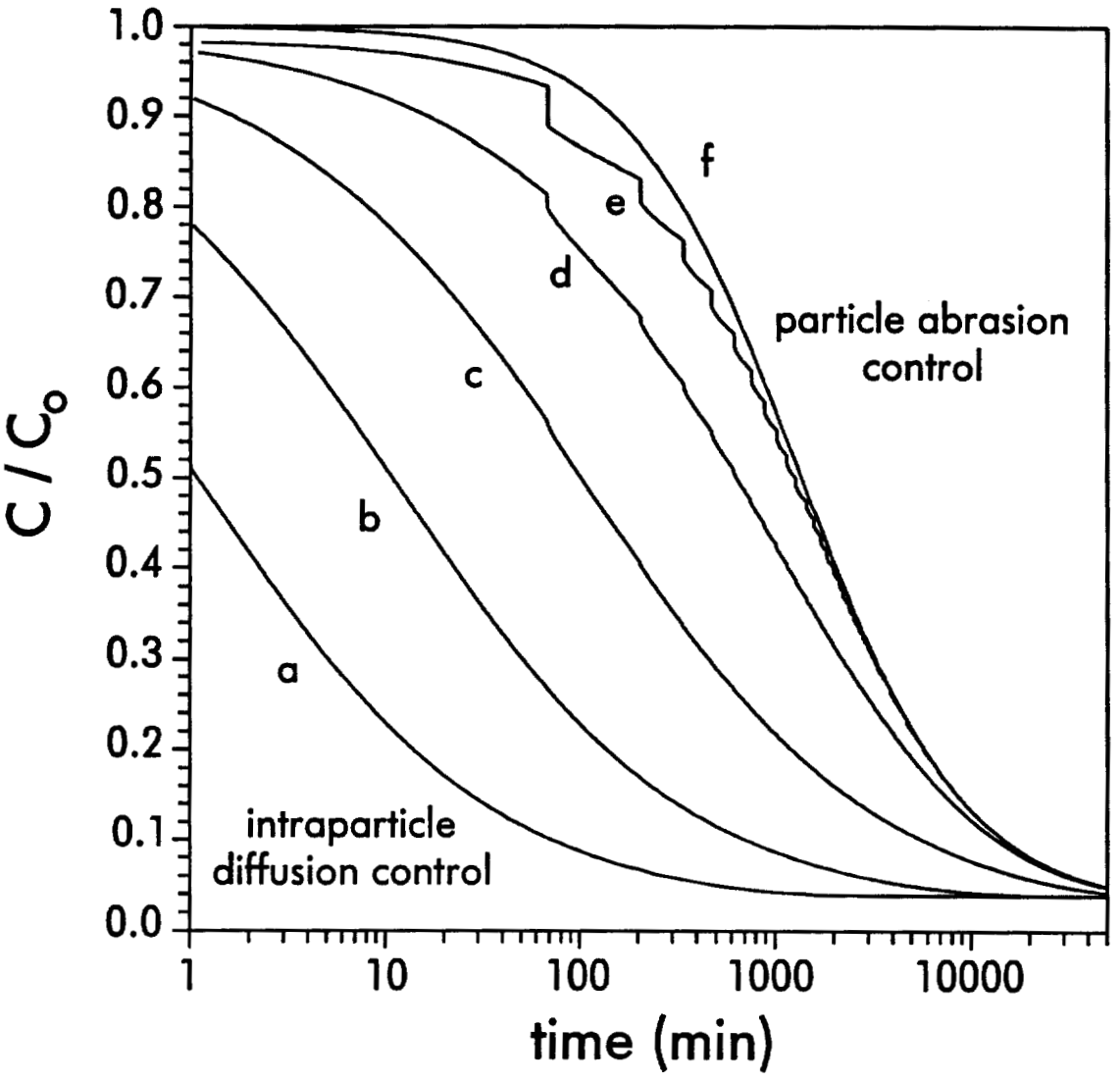

Figure 5.6. Representative normalized aqueous concentrations predicted by the coupled intraparticle diffusion/particle abrasion model. Values of ψ are 0.1, 1.0, 10, 100, 1000, and ∞ for curves a-f, respectively. Other input parameters: k_{ab} = 10^{-5} min^{-1}, m = 0.117 g, V = 2350 mL, K = 500000 mL/g, C_o = 0.4 ng/mL, and S_o = 0 ng/g.

$$\frac{\tan g_n}{g_n} = \frac{3\xi - \alpha_c g_n^2}{(\xi - 1)\alpha_c g_n^2 + 3\xi} \tag{5.16}$$

For ξ values less than ~10, film diffusion is the dominant mechanism, while intraparticle diffusion controls the rate for ξ values greater than ~100. Figure 5.7 shows the general characteristics of the dual resistance model for a wide range of ξ values, using $D_{eff}/R^2 = 10^{-5}$ min^{-1}, R = 0.01 cm, ρ_b = 0.558 g/mL, and other input as given previously. The shift in the rate-controlling mechanism from film diffusion (ξ = 0.01) in curve (a) to intraparticle diffusion ($\xi = \infty$) in curve (g) is clearly illustrated. This shift was effected by increasing the value of k_f and theoretically could be accomplished by dramatically increasing the mixing rate.

Sorption Reaction Time Scales. An interesting property of the dual resistance model is revealed when simulations are run with identical values of ξ and different sorbent to water ratios. Figure 5.8 shows the dependence of C/C_o versus log(t) curves on the value of m using ξ = 1.0, D_{eff}/R^2 10^{-5} min^{-1}, R = 0.01 cm, ρ_b = 0.558 g/mL, V = 2350 mL, K = 500,000 mL/g, S_o = 0 ng/g, and C_o = 0.4 ng/mL. Values of m ranged from 0.1 to 10 g. Because ξ is constant, all curves in Figure 5.8 show the characteristic slope of film diffusion. As the amount of sorbent is increased, the curves shift to earlier times due to the increased surface area for mass flux. If the same data are plotted as $(S/C)/K$ versus log(t), however, an altogether different picture appears (Figure 5.9). The dashed line in Figure 5.9 was obtained using m = 10 g and $\xi = \infty$. Despite the fact that the kinetics of curves (a)-(e) are dominated by film diffusion, the values of $(S/C)/K$ are increasingly controlled by intraparticle diffusion as the sorbent to water ratio is increased. From the appearance of curve (e) in Figure 5.8, the sorption reaction seems to be complete at t = ~200 minutes. At that time, however, $(S/C)/K$ is only ~0.2, and the reaction is far from complete.

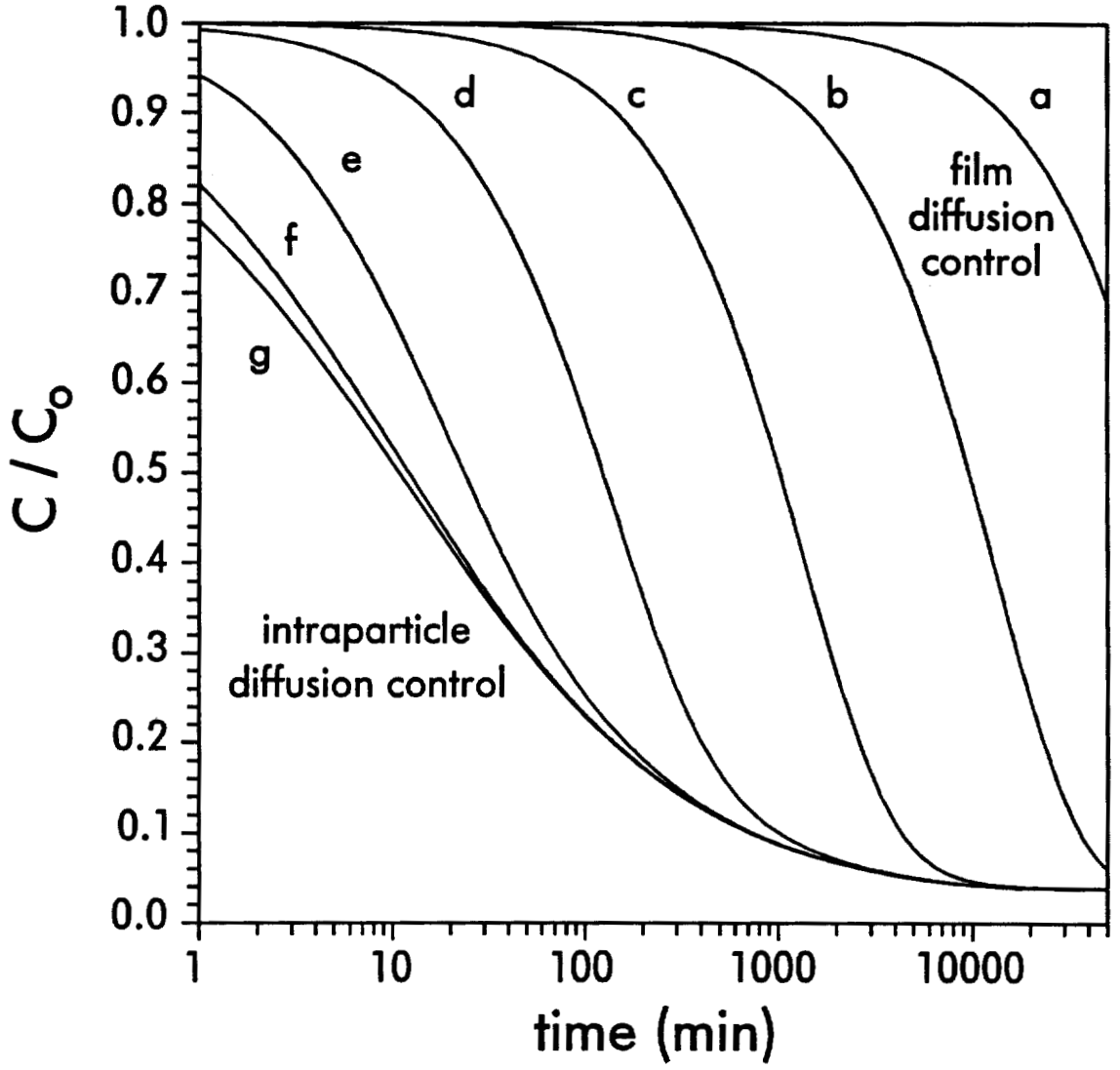

Figure 5.7. Representative normalized aqueous concentrations predicted by the dual resistance model. Values of ξ are 0.01, 0.1, 1.0, 10, 100, 1000, and ∞ for curves a-g, respectively. Other input parameters: $D_{eff}/R^2 = 10^{-5}$ min^{-1}, $R = 0.01$ cm, $m = 0.117$ g, $\rho_b = 0.558$ g/mL, $V = 2350$ mL, $K = 500000$ mL/g, $C_o = 0.4$ ng/mL, and $S_o = 0$ ng/g.

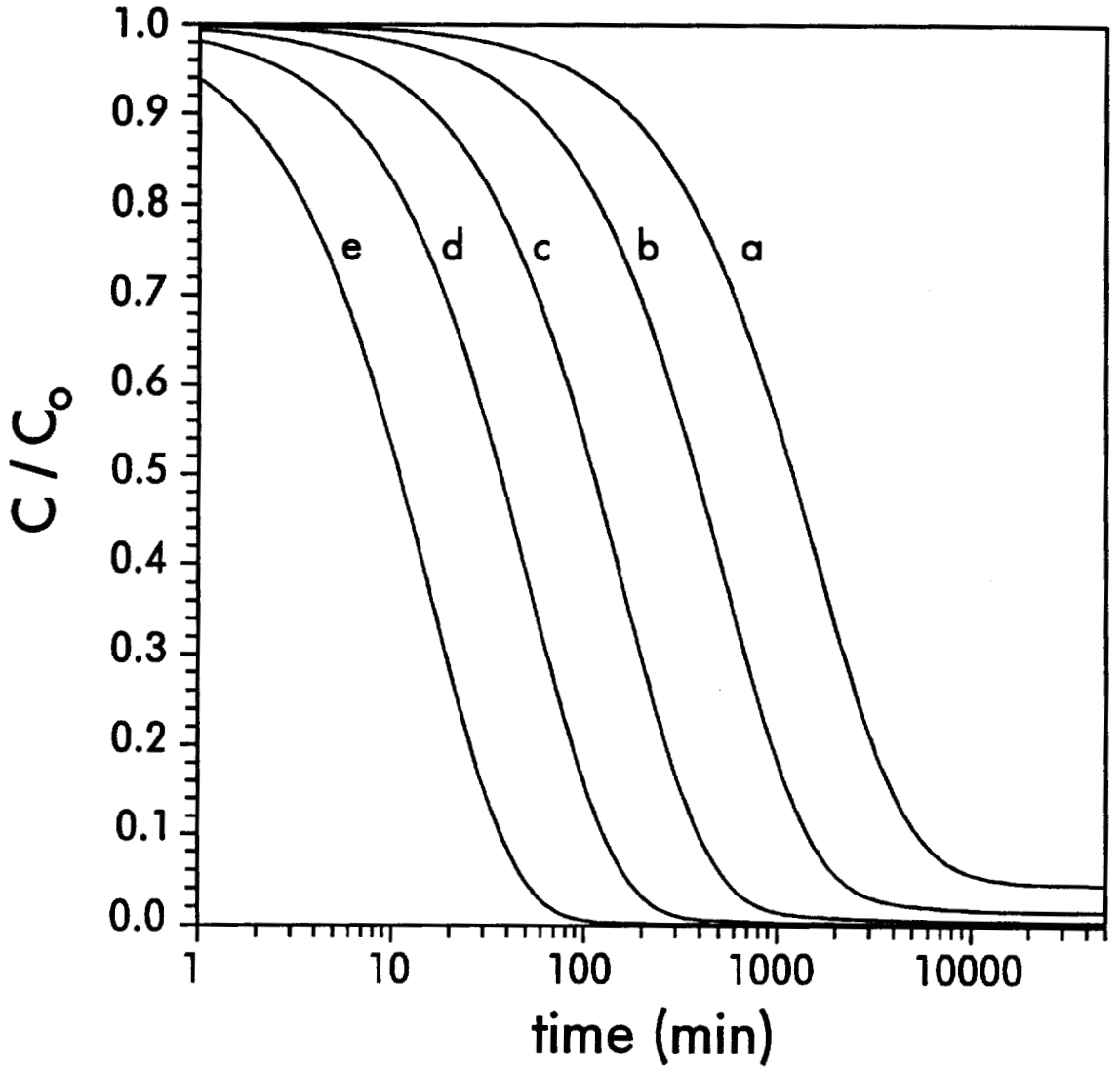

Figure 5.8. Sorbent mass dependence of the normalized aqueous concentration curves as predicted by the dual resistance model. Values of m are 0.1, 0.3, 1.0, 3.0, and 10 for curves a-e, respectively. Other input parameters: ξ = 1.0, $D_{eff}/R^2 = 10^{-5}$ min^{-1}, R = 0.01 cm, ρ_b = 0.558 g/mL, V = 2350 mL, K = 500000 mL/g, C_o = 0.4 ng/mL, and S_o = 0 ng/g.

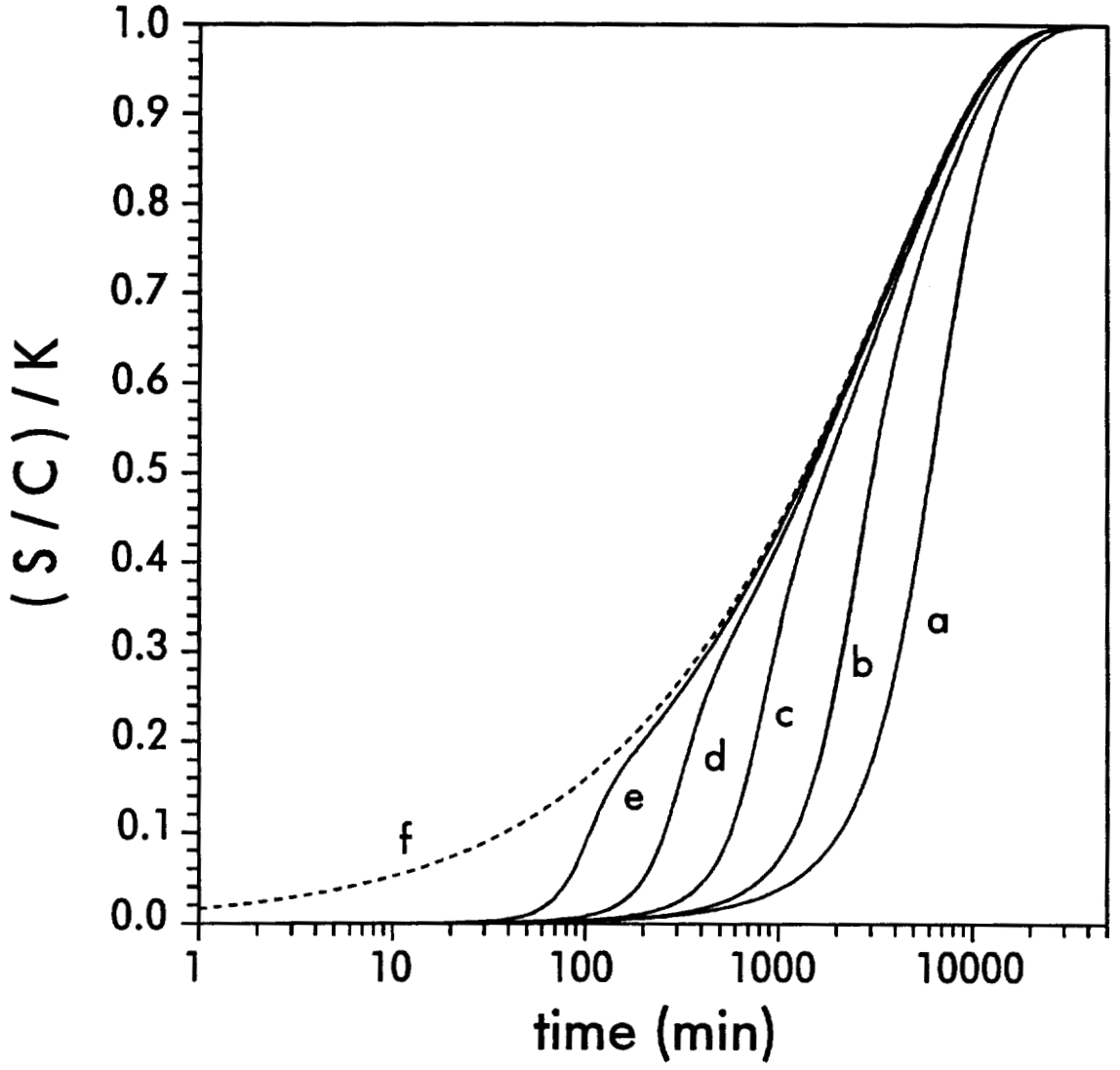

Figure 5.9. Sorbent mass dependence of the $(S/C)/K$ curves as predicted by the dual resistance model. Values of m are 0.1, 0.3, 1.0, 3.0, and 10 for curves a-e, respectively. Curve f was obtained with m = 10 g and $\xi = \infty$. Curves a-e used ξ = 1.0. Other input parameters: $D_{eff}/R^2 = 10^{-5}$ min^{-1}, R = 0.01 cm, ρ_b = 0.558 g/mL, V = 2350 mL, K = 500000 mL/g, C_o = 0.4 ng/mL, and S_o = 0 ng/g.

The completeness of a sorption reaction should not be measured by the fractional approach to equilibrium, defined as M_t/M_e where M_t is the mass exchanged between the aqueous and solid phases at time t and M_e is the corresponding amount at equilibrium. Rather, the value of $(S/C)/K$ is a far better predictor (Figure 5.10). The value of $(S/C)/K$ always lags behind M_t/M_e and can still be quite low even when the value of M_t/M_e nears 1.0. Indeed, when sorption is strong, further decreases in C can have little effect on M_t/M_e, but can have a large effect on S/C.

Experimental

Amberlite XAD-7, a moderately hydrophilic macroreticular sorbent composed of a methylmethacrylate polymer, was obtained from Rohm & Haas Co. (Philadelphia, PA). The structural density and porosity of XAD-7 are 1.24 g/mL and ~0.55, respectively (ρ_b = 0.558 g/mL). XAD-7 is characterized by a surface area of 450 m^2/g and a pore size of ~80 Å (*40*). The sorbent was cleaned before use in the general manner suggested by others (*41-42*). First, the beads were washed with deionized water to remove residual NaCl and Na_2CO_3. The beads were then sieved into six size fractions. Each size fraction was further cleaned by soxhlet extraction with methanol, acetone, and diethyl ether for 24 hours each. Residual ether was subsequently removed by washing with deionized water.

The adsorbates used in this study were 1,2-dichlorobenzene (DCB), 1,2,4-trichlorobenzene (TrCB), and 1,2,4,5-tetrachlorobenzene (TeCB). Each compound was obtained from Chem Service (West Chester, PA) and was used without further purification. These compounds are good model adsorbates because their sorption properties span a relatively wide range. The octanol-water partition coefficients of these compounds span 1.5 orders of magnitude (log K_{ow} = 3.38, DCB; 4.09, TrCB; 4.80, TeCB (*43-44*)). In addition, these compounds are easily and efficiently analyzed in water samples by the purging with whole column cryotrapping method with electron capture detection (*45*).

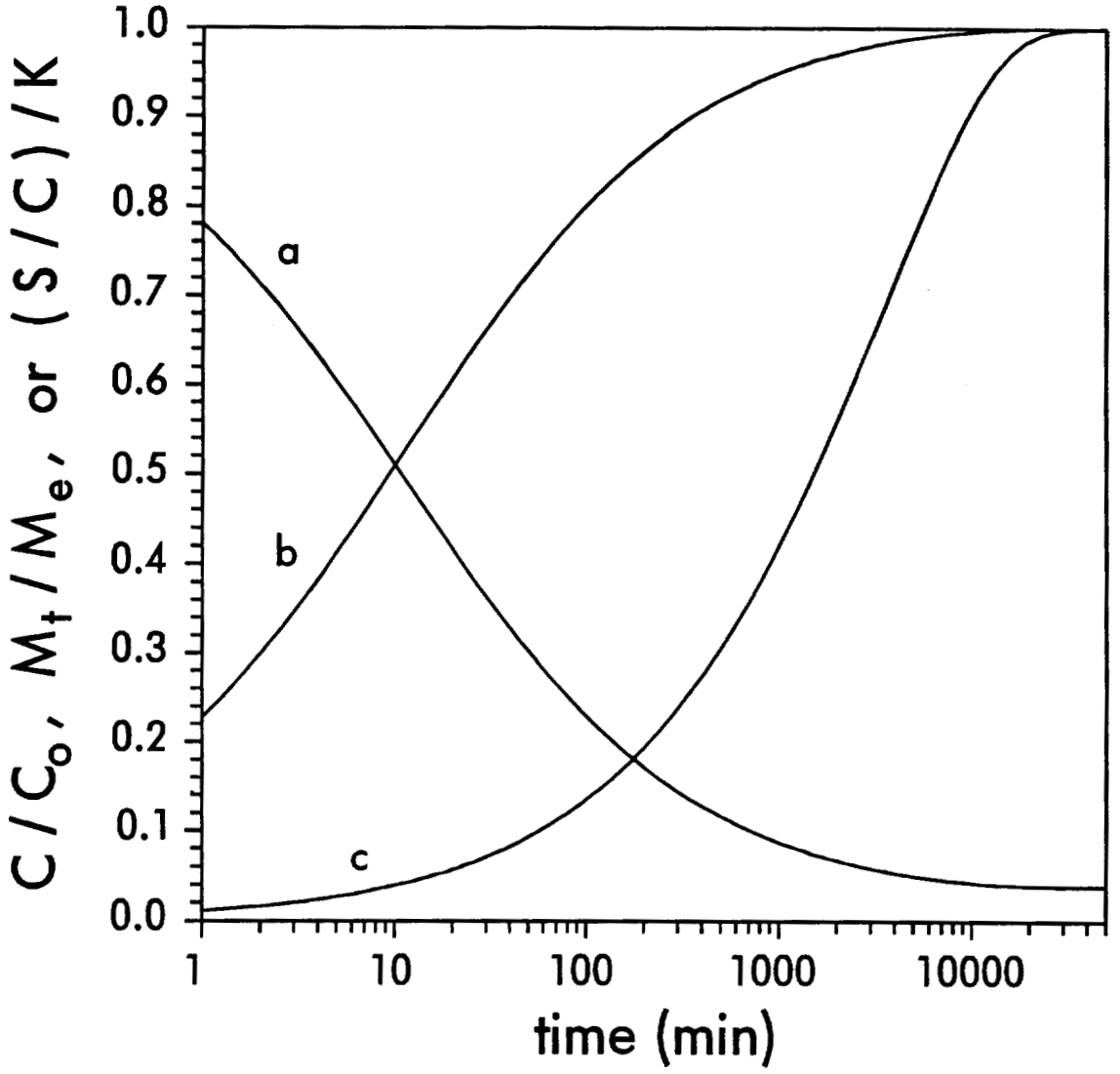

Figure 5.10. Normalized predictions of the intraparticle diffusion model. Curve a represents C/C_o. Curve b is M_t/M_e. Curve c is $(S/C)/K$. Input parameters: $D_{eff}/R^2 = 10^{-5}$ min^{-1}, $m = 0.117$ g, $V = 2350$ mL, $K = 500000$ mL/g, $C_o = 0.4$ ng/mL, and $S_o = 0$ ng/g.

Values of D_m were estimated by the method of Hayduk and Laudie (44).

Time Scale Experiments. To obtain an estimate of the time scale of the sorption reaction, a series of batch sorption studies were conducted. These experiments were performed in 14 mL screw-cap septum vials (Pierce, Rockford, IL). Vials were charged with 25 mg of one of the smaller size fractions of XAD-7 (R = 0.0176 cm or 0.0203 cm). Fifteen mL of prepurged, deionized water was added ("14 mL" vials actually hold over 15 mL). Each suspension was then spiked with one of the model adsorbates. Three different analyte concentrations for each particle size were used. Four replicates of each experiment were prepared, to be analyzed at different equilibration times. Vials were agitated on a custom-built shaker to provide efficient mixing. Experiments were conducted at ambient laboratory temperature and allowed to equilibrate for between 1 and 67 days. Upon analysis, results from experiments with the same equilibration time and particle size but different initial concentrations were used to calculate apparent isotherms and S/C values. Solid phase concentrations were calculated by difference. Observed S/C values for different equilibration times were then fitted to the analytical intraparticle diffusion model using a nonlinear least squares technique.

Continuous Batch Experiments. A set of batch sorption experiments was conducted in large vessels, thereby allowing the aqueous phase to be sampled intermittently without significantly disturbing the rate of reaction. These experiments also provided better time resolution than was achieved in the time scale experiments. Clear glass acid bottles able to hold ~2.5 L of solution were used as reaction vessels. Each screw cap was lined with Teflon and fitted with a sampling tube. The 1/16th inch stainless steel sampling tube passed through the screw cap via a 1/8th inch Swagelok bulkhead fitting. The bulkhead fitting was screwed through a tapped hole in the cap and securely sealed in place. The sampling apparatus was designed such that a liquid sample could be removed without reducing the pressure in the reaction vessel or removing the cap; N_2 gas was allowed to pass into the headspace at the same time as liquid was being

removed via the sampling tube. The end of the sampling tube that resided in the solution was covered with a fine mesh stainless steel screen to prevent the tube from plugging with sorbent.

The sorption kinetics of each of the three model adsorbates was studied at two different temperatures and with two different particle size fractions. Each experiment used 0.117 g of XAD-7 and 2350 mL of prepurged, deionized water. Particle size distributions for these experiments were measured with an optical microscope and are shown in Figure 5.11. Mean values of R for these size fractions were 0.0256 cm and 0.0319 cm. The temperature of each reaction was precisely controlled with a water bath. Experiments were conducted at $4.0 \pm 0.5^{\circ}C$ and $34 \pm 1^{\circ}C$. Mixing was achieved magnetically. Glass-encased stir bars were used to minimize sorption to the stirrer. Each experiment was spiked with 745 ng of DCB, 933 ng of TrCB, or 633 ng of TeCB. All experiments were allowed to run for approximately 30 days.

Control experiments were also conducted without sorbent to correct for sorption to the reaction vessel and to assess analyte stability. A partition coefficient K_{rv} (mL) was used to correct for adsorption to the reaction vessel

$$K_{rv} = \frac{M_{rv}}{C} \tag{5.17}$$

where M_{rv} (ng) is the mass adsorbed to the bottle walls. The available glass surface area is incorporated into the value of K_{rv}. Sorption equilibrium with the reaction vessel was assumed to be instantaneous. In effect, instantaneous sorption to the reaction vessel increases the apparent volume of the solution. Consideration of the Henry's law constants for each of the adsorbates revealed that loss of analytes to the headspace was limited to less than 0.7 percent.

Each experiment was fitted to the five previously-discussed mechanistic sorption models using nonlinear least squares techniques. The film diffusion, particle abrasion, and dual resistance models all used analytical methods. Fits for the intraparticle diffusion and coupled diffusion/abrasion models were

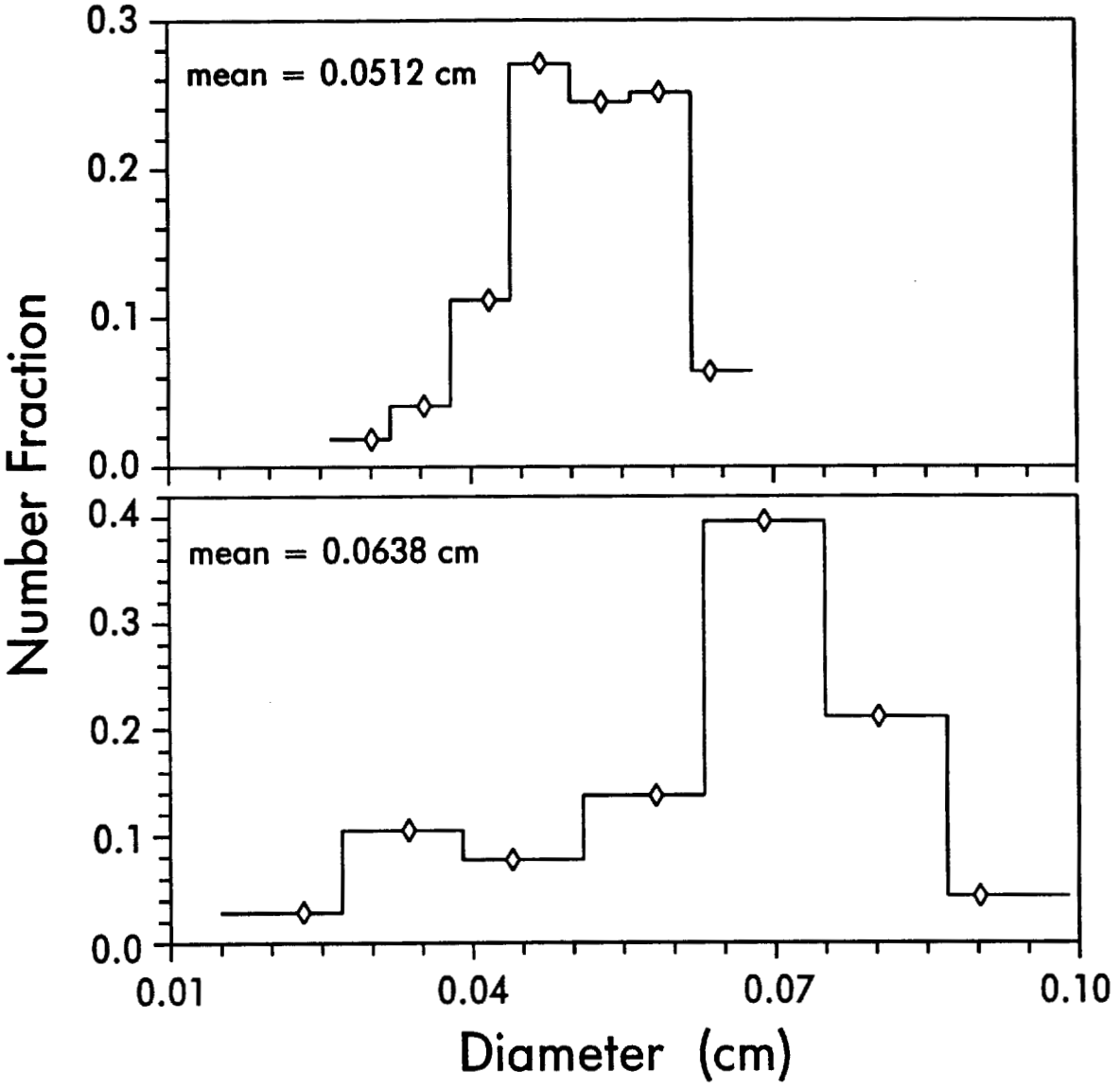

Figure 5.11. Experimentally measured particle size distributions used in the numerical modeling of the continuous batch experiments.

performed numerically. For the numerical models, a spatial discretization of 1501 nodes/particle was used to minimize numerical error. All models accounted for sorption to the reaction vessel. Correction for the removal of analyte mass from the system via sampling was incorporated into all except the dual resistance model. Neglection of the mass lost to sampling did not significantly affect the results in that one case. The downhill simplex method was used for 2-parameter fits; 1-parameter fits were performed with Brent's method of inverse parabolic interpolation (*46*).

Results and Discussion

Time Scale Experiments. Values of S/C were calculated as a function of time for each of the batch vial experiments. The purpose of these experiments was to assess general time scales for the sorption reaction. The trends were clear. Equilibrium was achieved most quickly for DCB: approximately three days were required. Between 10 and 20 days were required for TrCB, while TeCB needed about a month to reach full sorption equilibrium. This is consistent with an intraparticle diffusive rate limitation for sorption. Assuming a diffusive rate control, the values of mK/V used in these experiments were large enough that values of $(S/C)/K$ should represent the characteristics of intraparticle diffusion rather than film diffusion, even if the latter were the rate-controlling mechanism (Figure 5.9). Assuming pore diffusion to be the predominant mechanism of intraparticle transport, values of D_{eff} are expected to vary with K according to

$$D_{eff} = \frac{D_m n}{\tau(\rho_b K + n)} \tag{5.18}$$

where n is the porosity (dimensionless) and τ is the particle tortuosity (dimensionless). The value of tortuosity is usually between 2 and 10 (*33*) and can be approximated as $1/n$ (*21*).

The S/C data were fitted with the intraparticle diffusion model to determine estimates of K and D_{eff} for each compound. Data from each particle size were fitted both separately and as a group (R = 0.019 cm). Figure 5.12 illustrates the experimental data and the best-fit curves when the data are grouped. The correlation between D_{eff} and D_m/K is shown in Figure 5.13. Assuming that n is much less than $\rho_b K$, equation (5.18) predicts a slope of 1.0 and an intercept of -0.27 for this log-log plot. The slope and intercept obtained by linear regression of the data are 0.93 and -0.16, respectively. The results of the time scale experiments, therefore, are consistent with intraparticle diffusion. While the mixing rate obtained in the vials may not have been sufficient to keep film diffusion from limiting the sorption rate, the analysis of S/C data provided estimates of the rate of intraparticle diffusion.

Continuous Batch Experiments. Several days to weeks were required for sorption equilibrium to be achieved in each continuous batch experiment. Every experiment attained equilibrium within an elapsed time of 30 days. Experiments without sorbent showed no competing loss processes other than sorption to the vessel; these data were used to calculate K_{rv} values for each compound and at each temperature. Sorbed concentrations were calculated by difference. Partition coefficients were calculated using the final aqueous concentrations of each experiment. Values of K for different particle size fractions were averaged in all but one case. Figures 5.14 through 5.25 illustrate the data and the best-fit model predictions for each experiment. In general, the predictions of the abrasion and diffusion/abrasion models were very similar. To avoid confusion, the predictions of the diffusion/abrasion model were not included in these plots.

For each compound, the rate of adsorption depended upon both the particle size and the solution temperature. For a given temperature, experiments using the larger particle size fraction required a longer period of time to reach equilibrium. Experiments conducted at 4°C were slower than those run at 34°C. Each of these observations are consistent with a rate-limitation by film or intraparticle diffusion. Furthermore, the cold experiments

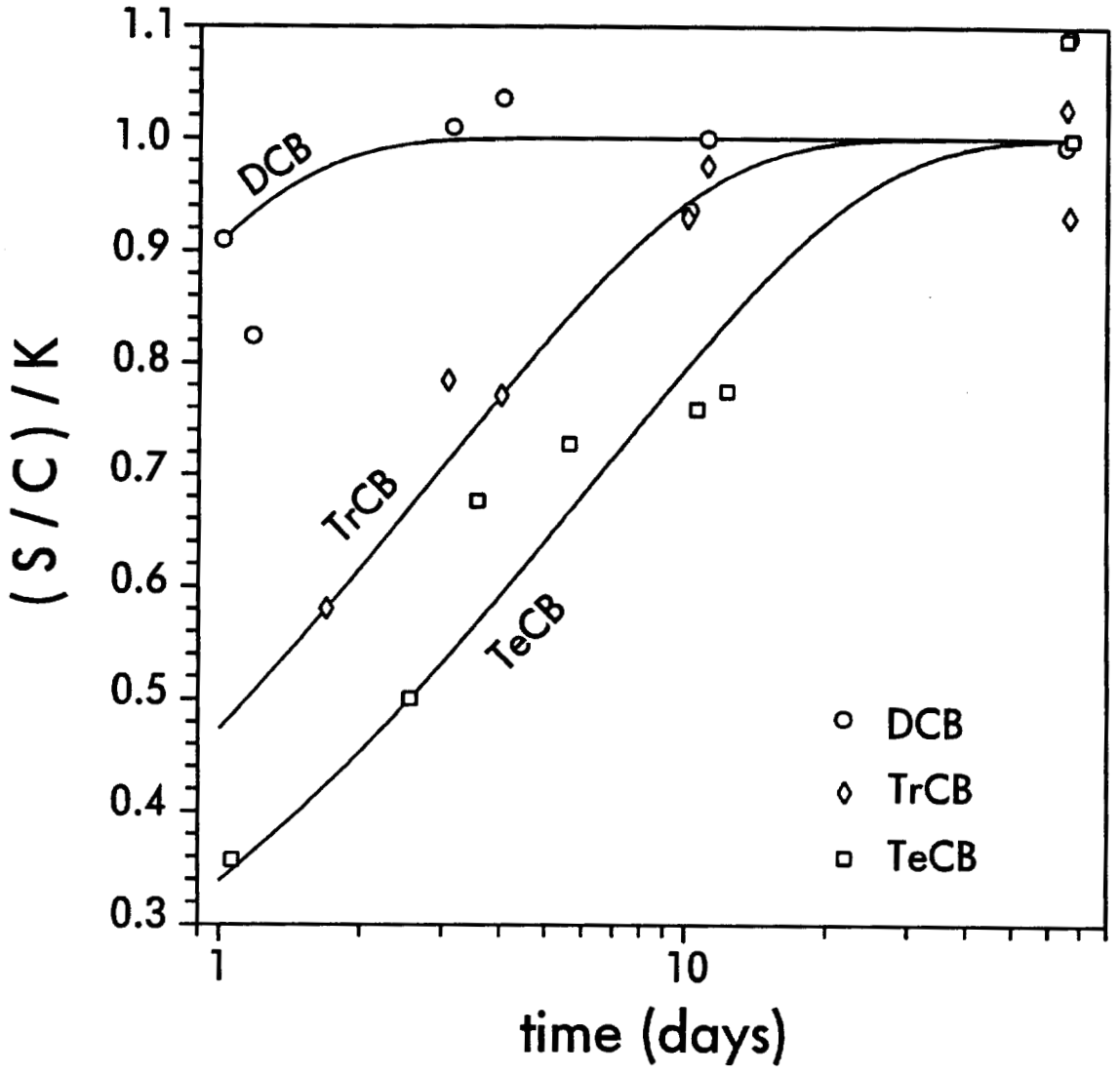

Figure 5.12. Best fits of the time scale data with the intraparticle diffusion model for each of the chlorobenzenes.

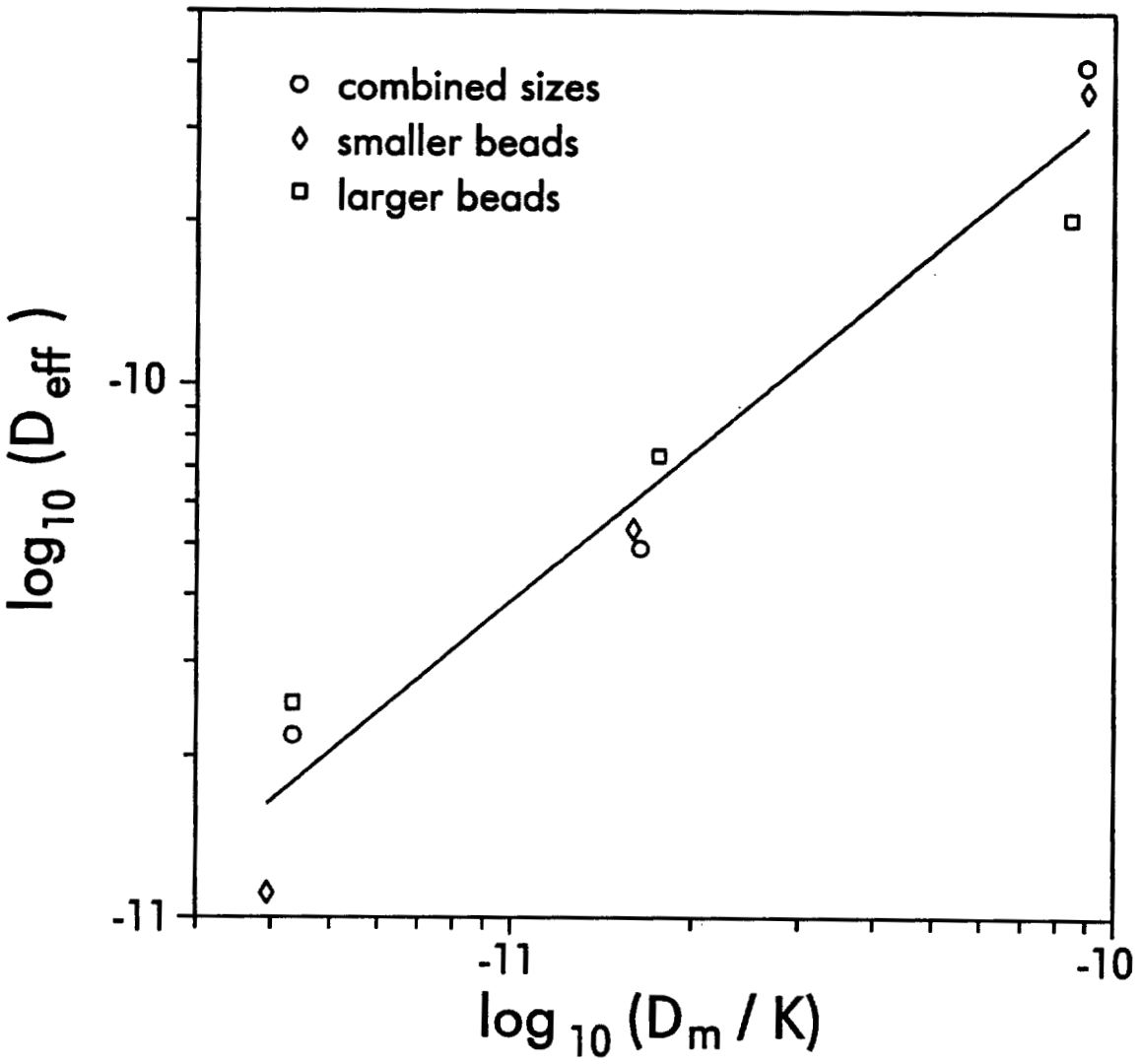

Figure 5.13. Correlation between the fitted values of D_{eff} (cm^2/s) and K (mL/g) for the time scale experiments, corrected for the dependence of D_{eff} on D_m (cm^2/s). The best-fit parameters for the individual data sets and the combined data set were included in the regression. Slope = 0.93, intercept = -0.16.

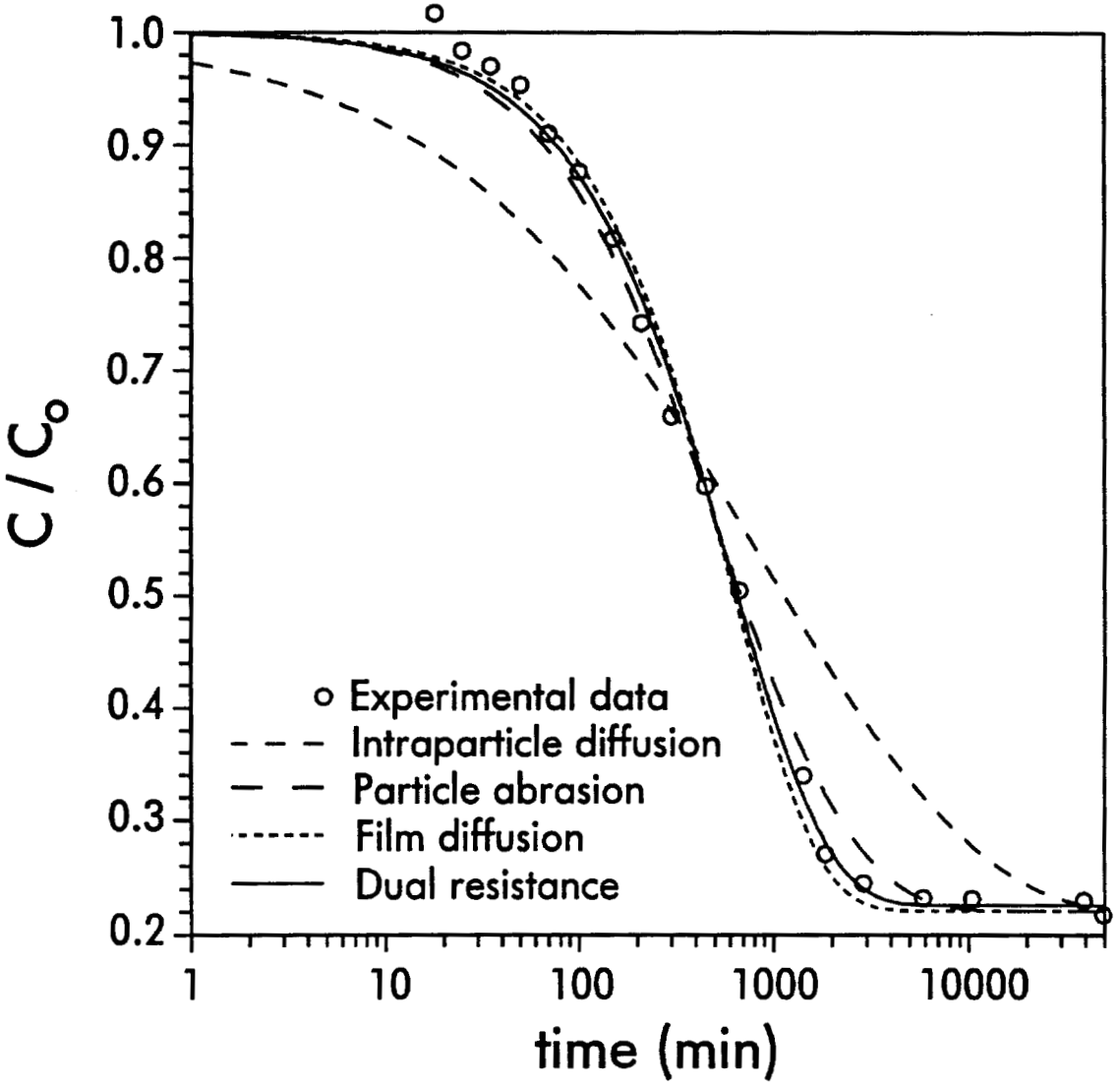

Figure 5.14. Optimized model fits for 1,2-dichlorobenzene and the large beads at 34°C. Input parameters: m = 0.117 g, V = 2350 mL, K = 86920 mL/g, K_{rv} = 614 mL, C_o = 0.2512 ng/mL, S_o = 0 ng/g, ρ_b = 0.558 g/mL, n = 0.55.

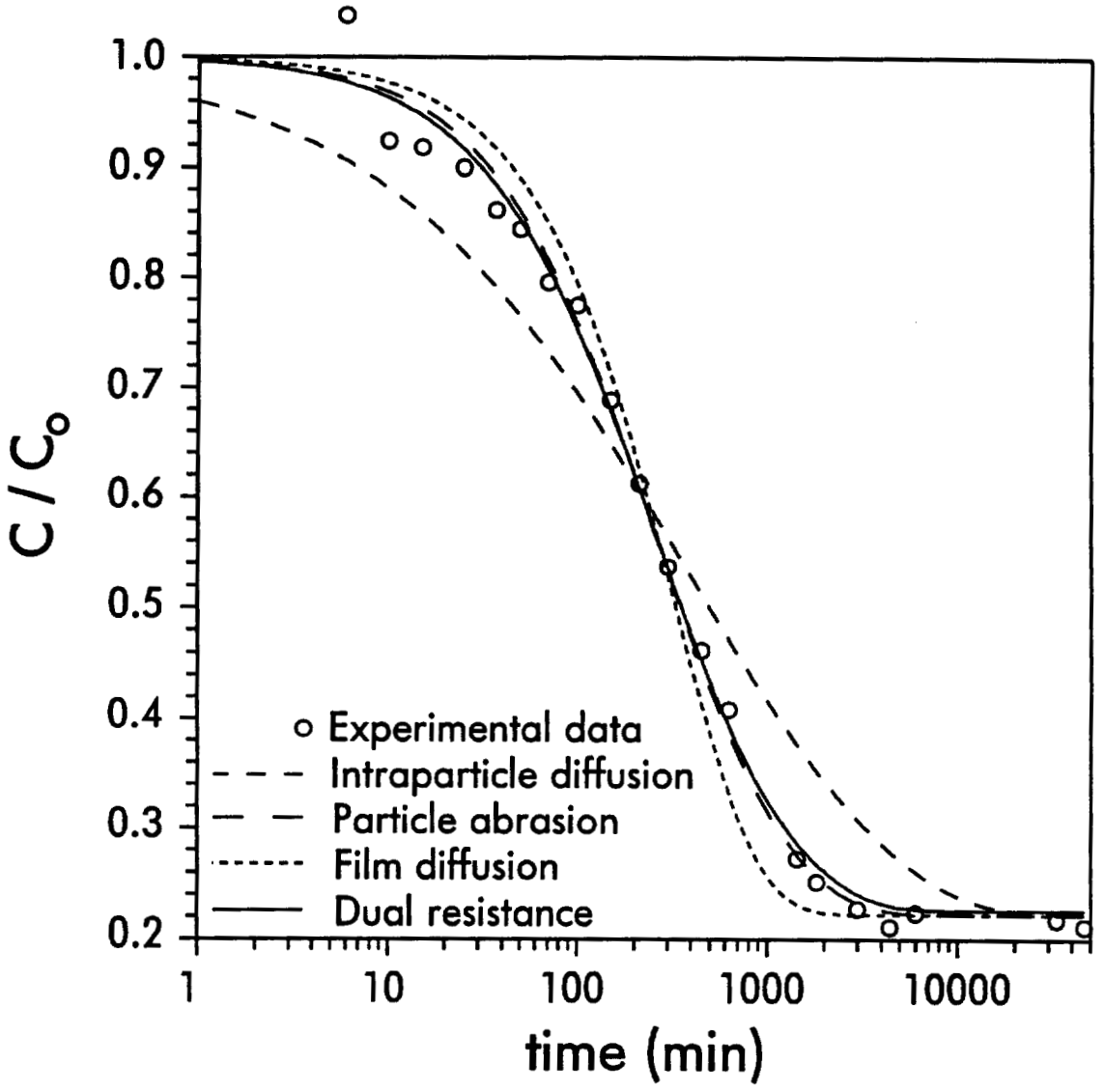

Figure 5.15. Optimized model fits for 1,2-dichlorobenzene and the small beads at 34°C. Input parameters: m = 0.117 g, V = 2350 mL, K = 86920 mL/g, K_{rv} = 614 mL, C_o = 0.2512 ng/mL, S_o = 0 ng/g, ρ_b = 0.558 g/mL, n = 0.55.

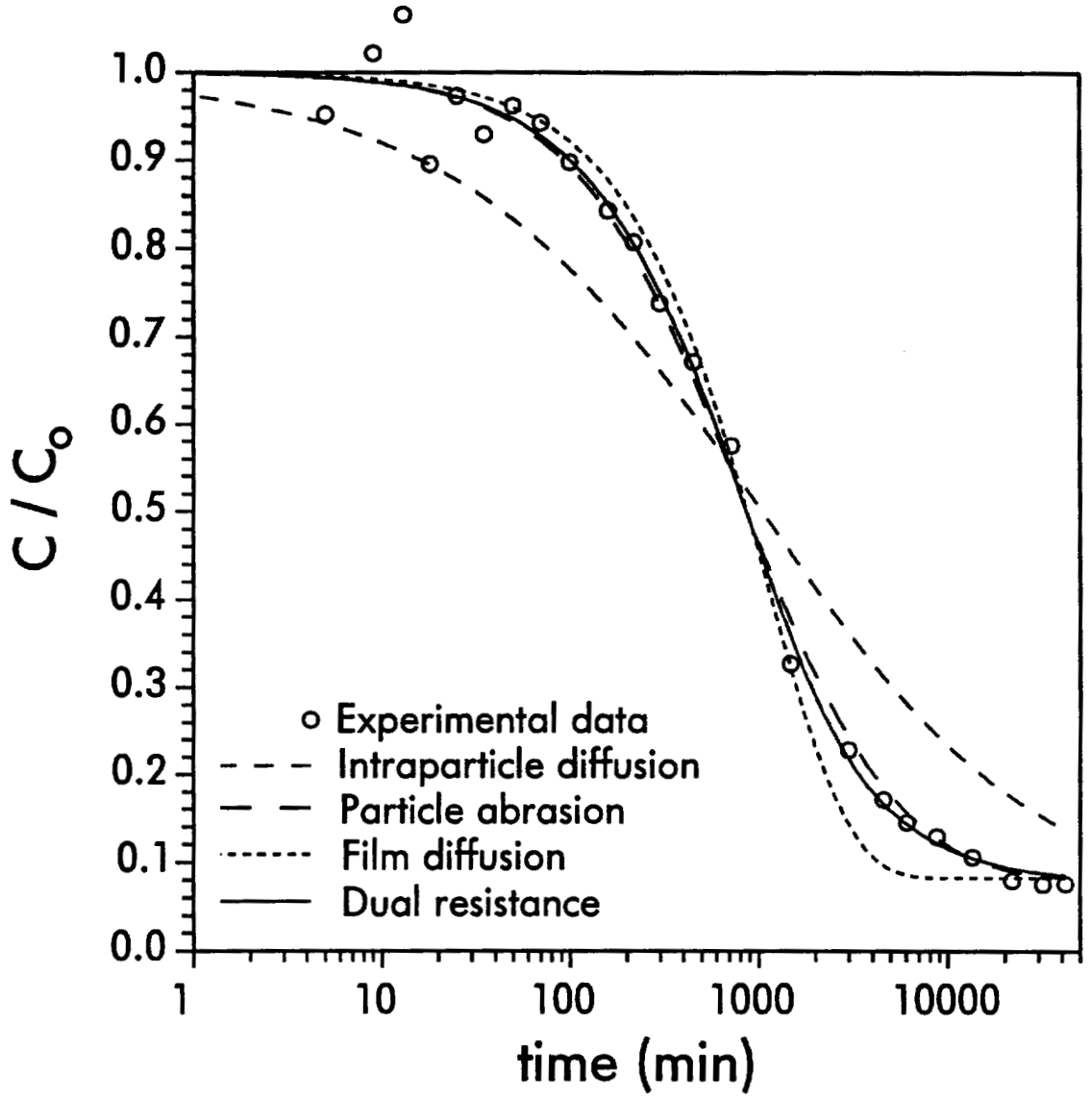

Figure 5.16. Optimized model fits for 1,2-dichlorobenzene and the large beads at 4°C. Input parameters: m = 0.117 g, V = 2350 mL, K = 277400 mL/g, K_{rv} = 656 mL, C_o = 0.2477 ng/mL, S_o = 0 ng/g, ρ_b = 0.558 g/mL, n = 0.55.

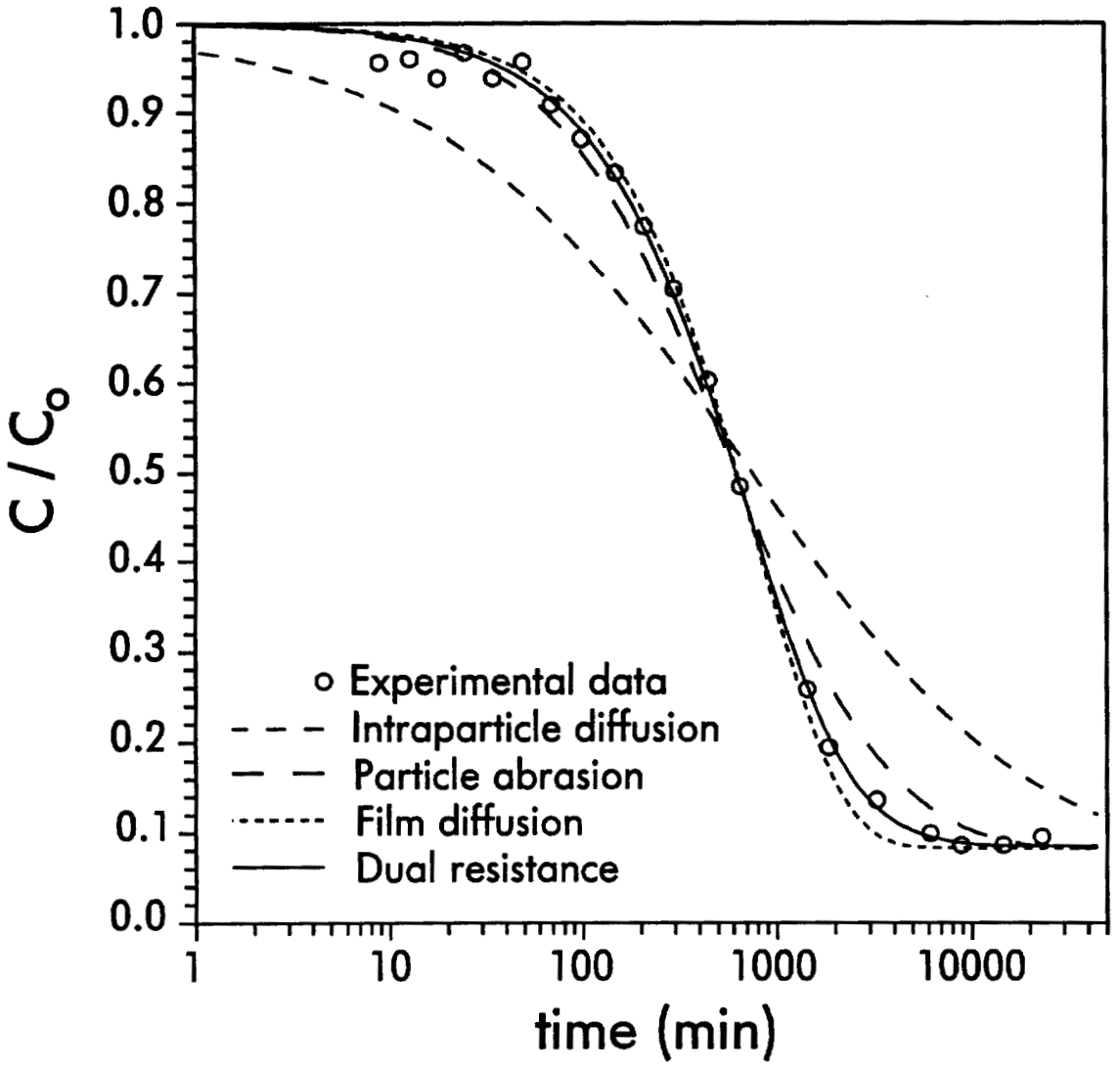

Figure 5.17. Optimized model fits for 1,2-dichlorobenzene and the small beads at 4°C. Input parameters: m = 0.117 g, V = 2350 mL, K = 277400 mL/g, K_{rv} = 656 mL, C_o = 0.2477 ng/mL, S_o = 0 ng/g, ρ_b = 0.558 g/mL, n = 0.55.

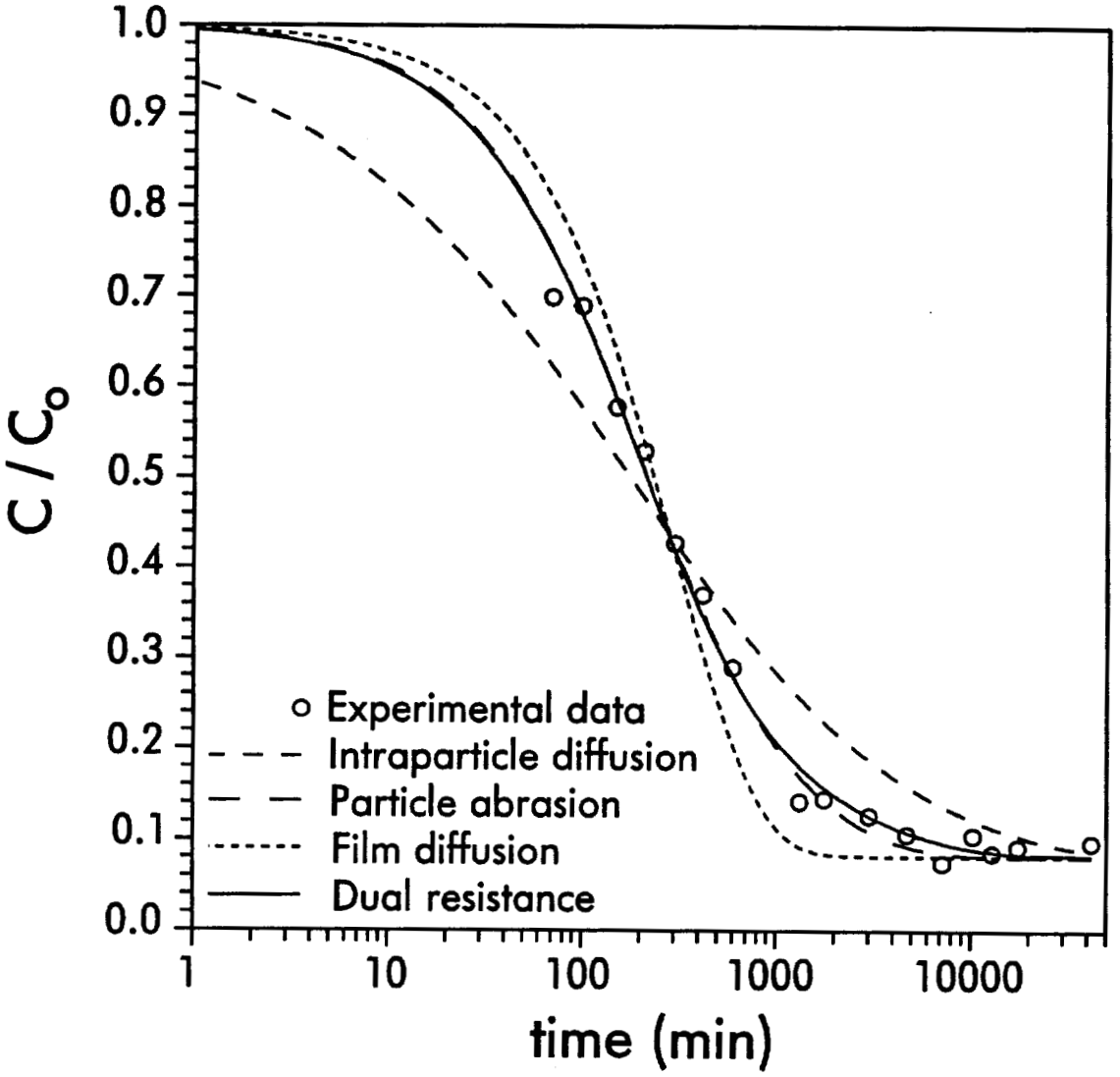

Figure 5.18. Optimized model fits for 1,2,4-trichlorobenzene and the large beads at 34°C. Input parameters: m = 0.117 g, V = 2350 mL, K = 323500 mL/g, K_{rv} = 1101 mL, C_o = 0.2704 ng/mL, S_o = 0 ng/g, ρ_b = 0.558 g/mL, n = 0.55.

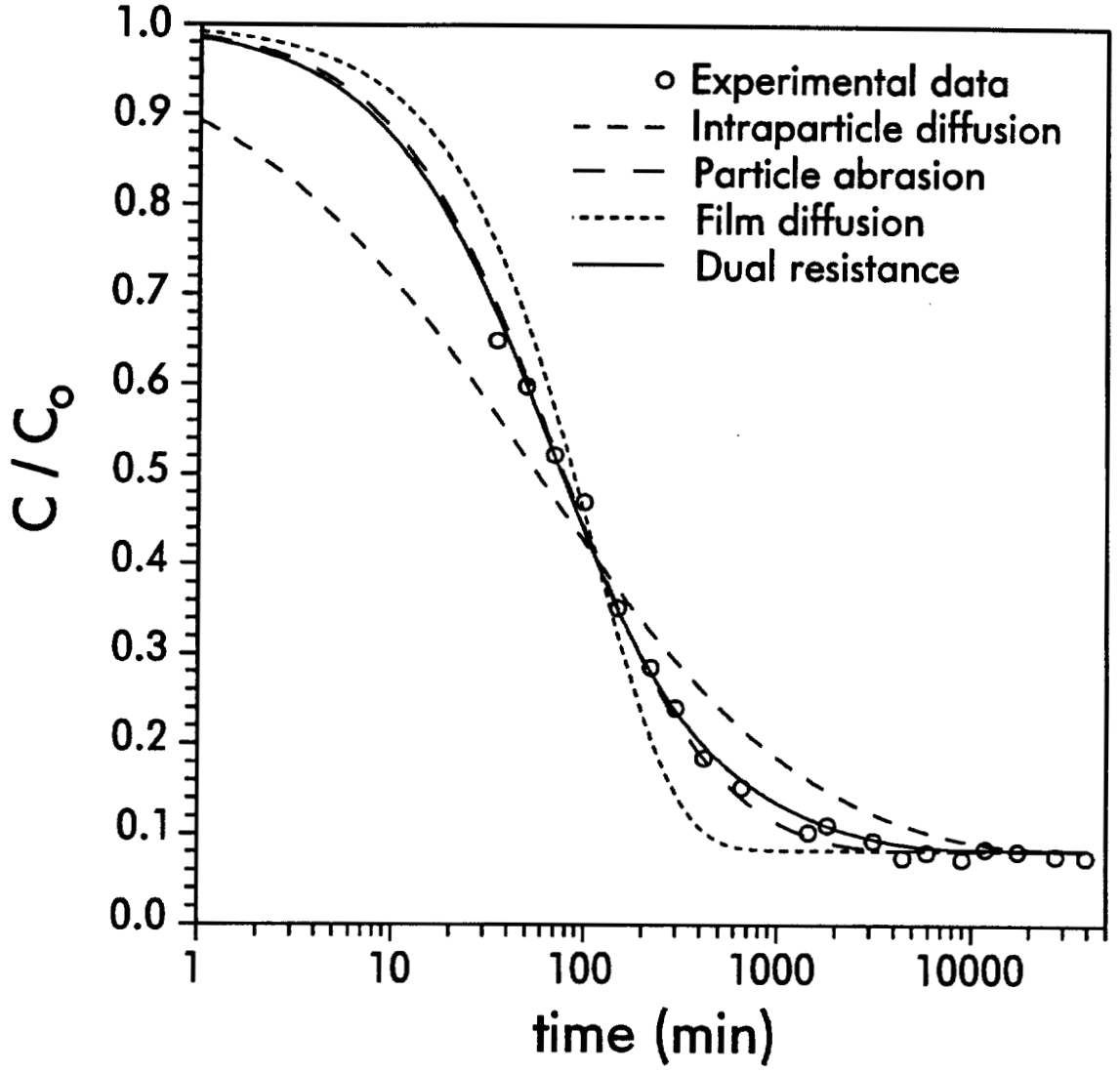

Figure 5.19. Optimized model fits for 1,2,4-trichlorobenzene and the small beads at 34°C. Input parameters: m = 0.117 g, V = 2350 mL, K = 323500 mL/g, K_{rv} = 1101 mL, C_o = 0.2704 ng/mL, S_o = 0 ng/g, ρ_b = 0.558 g/mL, n = 0.55.

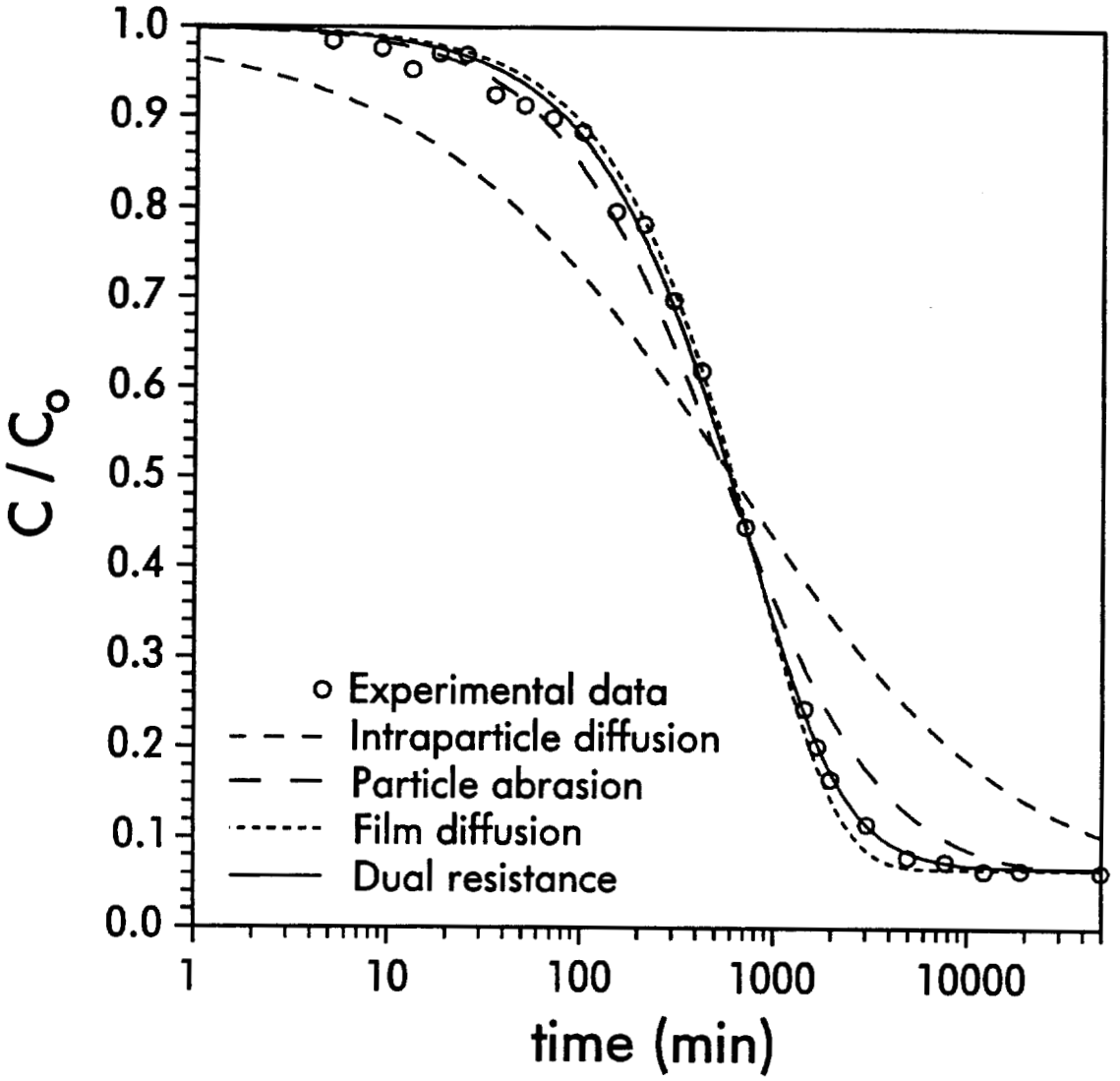

Figure 5.20. Optimized model fits for 1,2,4-trichlorobenzene and the large beads at 4°C. Input parameters: m = 0.117 g, V = 2350 mL, K = 411400 mL/g, K_{rv} = 1125 mL, C_o = 0.2685 ng/mL, S_o = 0 ng/g, ρ_b = 0.558 g/mL, n = 0.55.

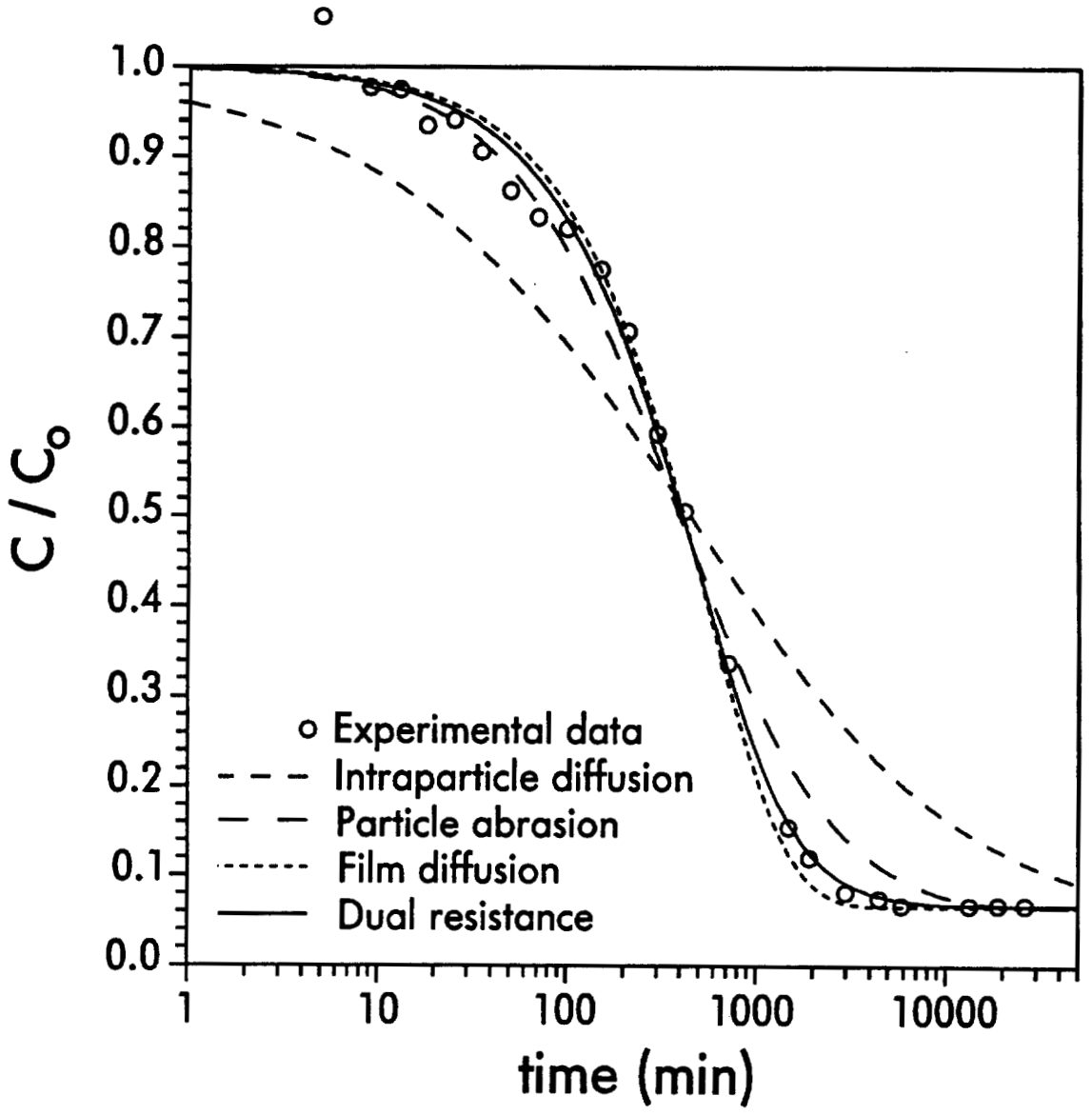

Figure 5.21. Optimized model fits for 1,2,4-trichlorobenzene and the small beads at 4°C. Input parameters: m = 0.117 g, V = 2350 mL, K = 411400 mL/g, K_{rv} = 1125 mL, C_o = 0.2685 ng/mL, S_o = 0 ng/g, ρ_b = 0.558 g/mL, n = 0.55.

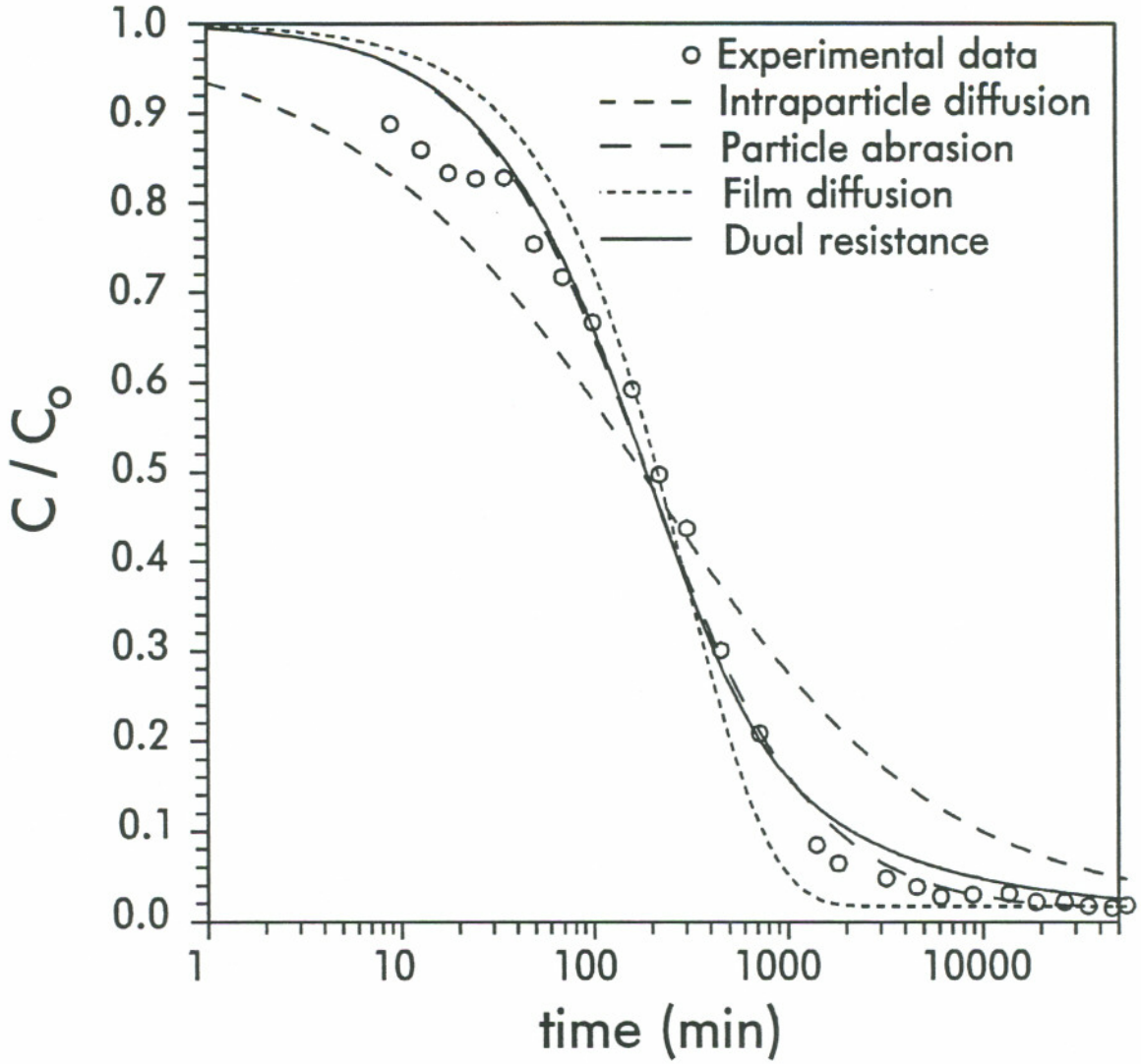

Figure 5.22. Optimized model fits for 1,2,4,5-tetrachlorobenzene and the large beads at 34°C. Input parameters: m = 0.117 g, V = 2350 mL, K = 1137000 mL/g, K_{rv} = 0 mL, C_o = 0.2698 ng/mL, S_o = 0 ng/g, ρ_b = 0.558 g/mL, n = 0.55.

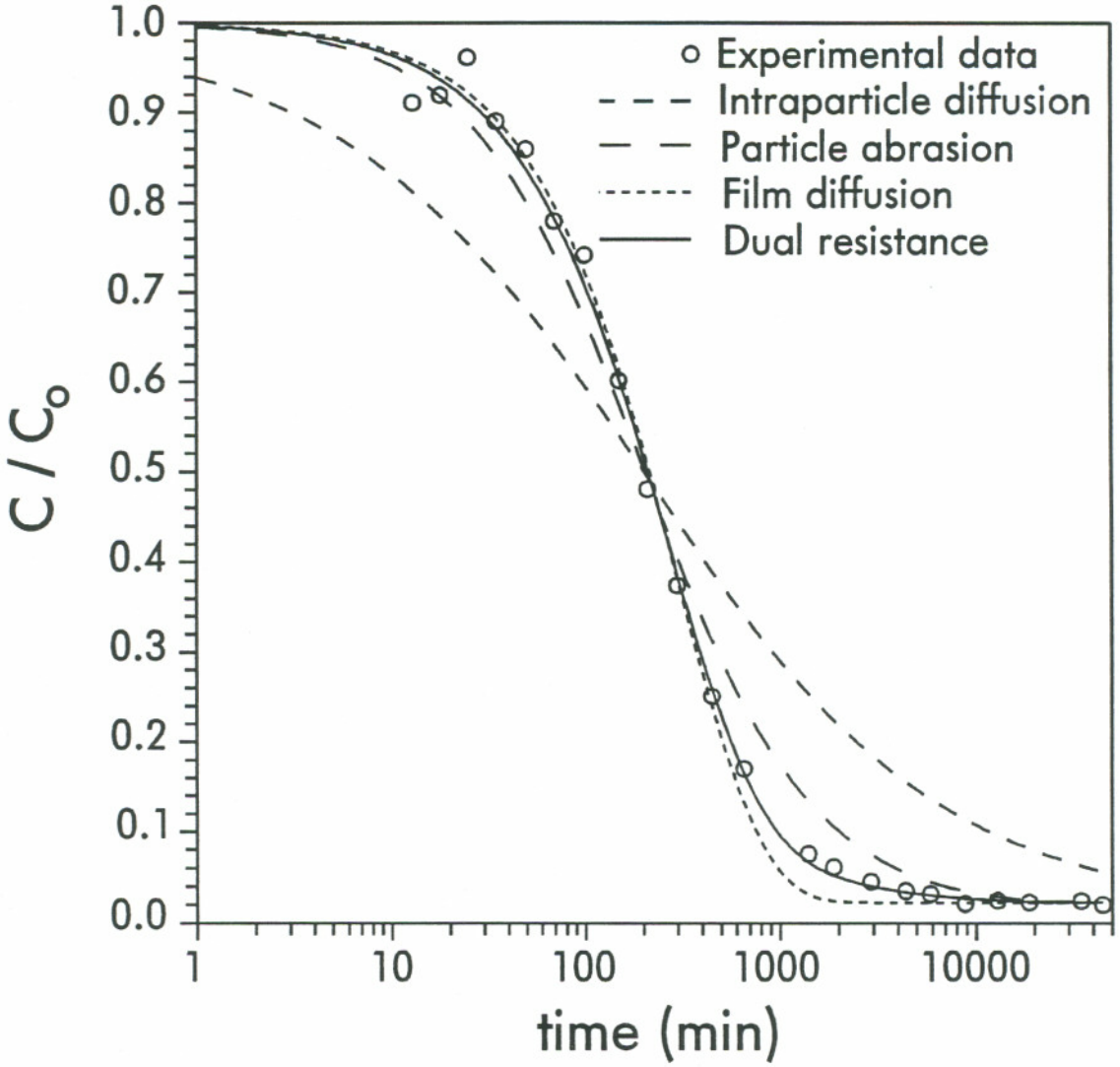

Figure 5.23. Optimized model fits for 1,2,4,5-tetrachlorobenzene and the small beads at 34°C. Input parameters: m = 0.117 g, V = 2350 mL, K = 1474000 mL/g, K_{rv} = 1690 mL, C_o = 0.1567 ng/mL, S_o = 0 ng/g, ρ_b = 0.558 g/mL, n = 0.55.

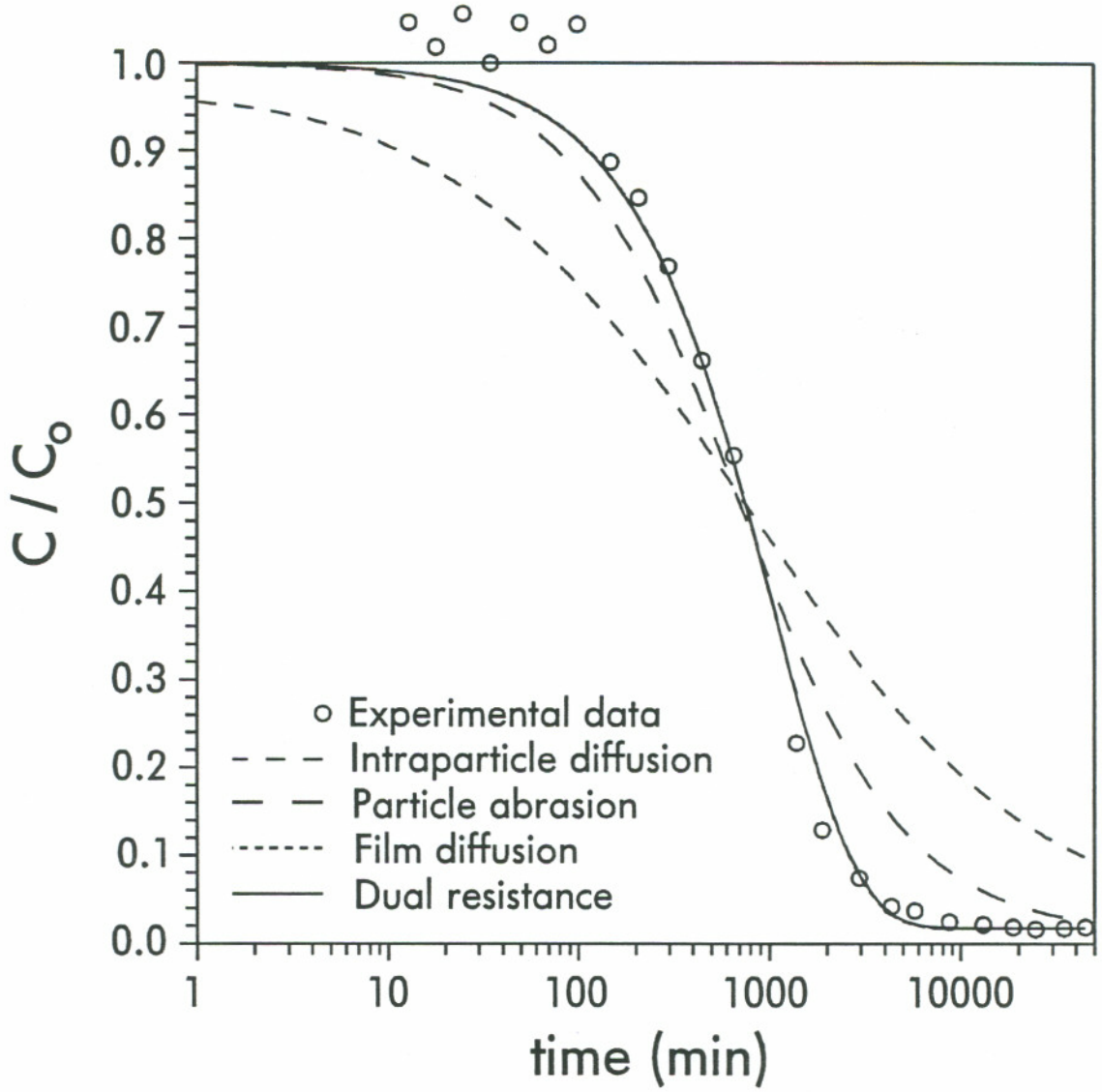

Figure 5.24. Optimized model fits for 1,2,4,5-tetrachlorobenzene and the large beads at 4°C. Input parameters: m = 0.117 g, V = 2350 mL, K = 1996000 mL/g, K_{rv} = 1753 mL, C_o = 0.1543 ng/mL, S_o = 0 ng/g, ρ_b = 0.558 g/mL, n = 0.55.

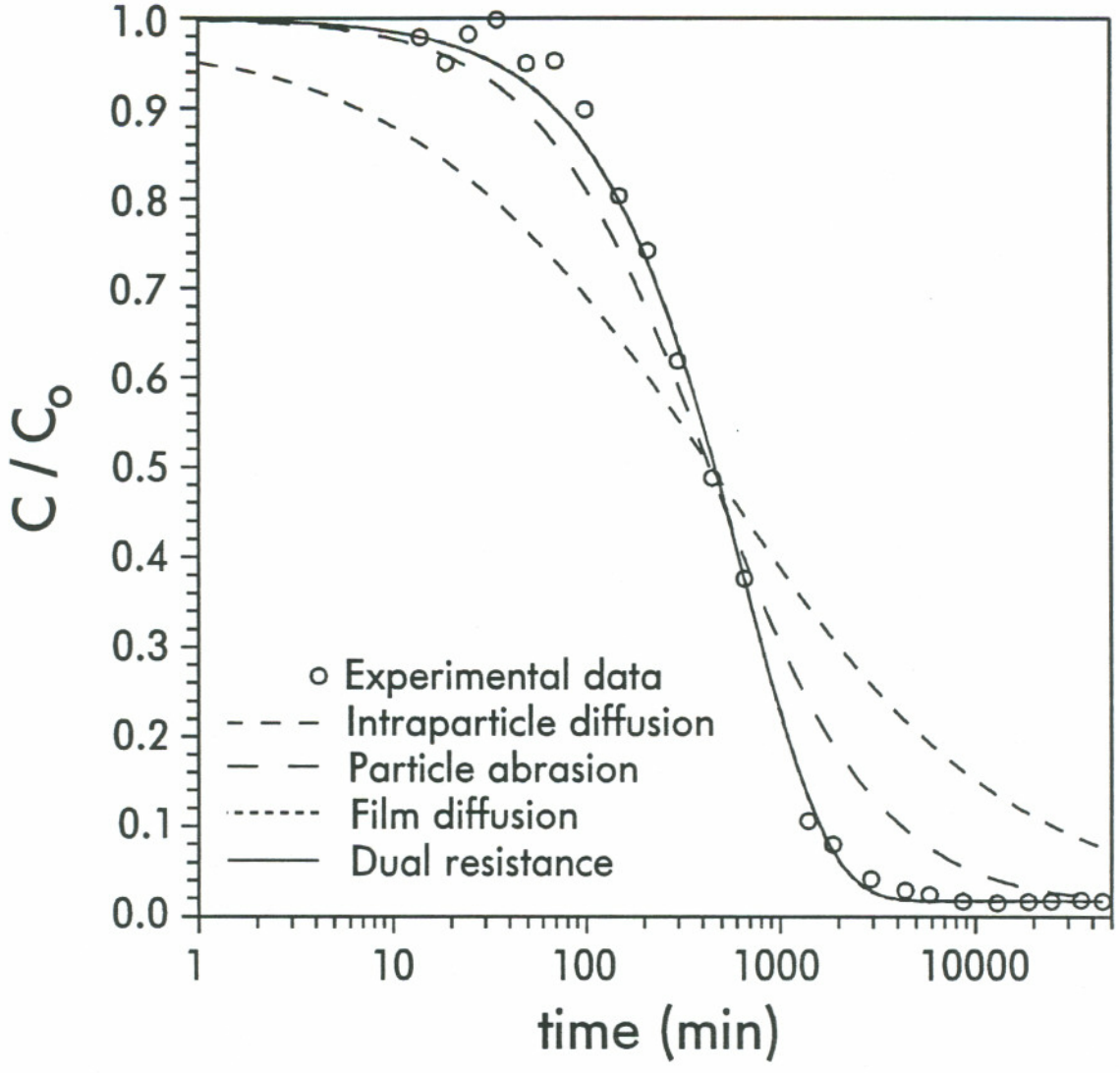

Figure 5.25. Optimized model fits for 1,2,4,5-tetrachlorobenzene and the small beads at 4°C. Input parameters: m = 0.117 g, V = 2350 mL, K = 1996000 mL/g, K_{rv} = 1753 mL, C_o = 0.1543 ng/mL, S_o = 0 ng/g, ρ_b = 0.558 g/mL, n = 0.55.

run with small particles always exhibited a slower uptake rate than did the warm experiments using the larger particle size fraction. With respect to intraparticle diffusion, the colder temperature would decrease D_{eff} values and thereby slow the kinetics. The smaller particle size would partially offset the effect of a decreased D_{eff}. The temperature change from 4 to 34°C increases the partition coefficient, thereby increasing the final fractional uptake by some small amount. An increase in the final fractional uptake would speed up the initial phase of intraparticle transport for these values of mK/V. This somewhat counterintuitive behavior is caused by a greater effective concentration gradient in the early phase of adsorption. It is difficult to assess the net effect of a decrease in both temperature and particle size on the intraparticle transport rate. In contrast, the experimental observation is clearly consistent with the predictions of the film diffusion model. The relative difference between D_m values at 4 and 34°C is larger than the relative difference in the two particle radii. By equation (5.4), a slower uptake rate would result at the lower temperature. In addition, because the increased partition coefficient dictates that more analyte must be transported into the solid phase, the process takes intrinsically longer at 4°C than it does at 34°C.

A comparison of each of the best-fit plots reveals that some of the models were better able than others to predict the observed sorption kinetics. The experimental data were not described well by intraparticle diffusion alone. The characteristic slope of the intraparticle diffusion model is much too shallow to fit the observed data. At the other extreme, the steep characteristic slope of the film diffusion model is a much closer fit for 8 of the 12 experiments. For the other experiments, neither the film nor the intraparticle diffusion models provided an accurate fit. The first order particle abrasion and the diffusion/abrasion models matched the data fairly well in about half of the experiments. In order to fit that data, however, the abrasion models predicted *complete* particle abrasion by the end of each experiment, a prediction that is inconsistent with experimental observations. Abrasion probably did play some

role in these experiments, but it could not have been the sole rate-limiting process.

Of all of the models assessed in this study, the dual resistance model consistently produced the closest fit to the experimental data. Systematic over- or underpredictions were exhibited for only one of the fits (Figure 5.22), and those deviations were not dramatic. Of course, the dual resistance model has two fitting parameters, k_f and D_{eff}, and is therefore inherently more flexible than the film diffusion, particle abrasion, or intraparticle diffusion models. If the exchange of analyte between phases in this system is diffusion-limited, however, then it is reasonable to use a model that represents both of the probable diffusion processes rather than one that presupposes the dominance of one process over the other. As conditions change, the predominant rate-limitation may shift from film to intraparticle diffusion, or vice versa.

The optimized values of k_f and D_{eff} from the dual resistance model and their estimated 95% confidence limits are given in Table 5.1 for each of the experiments. The optimized k_f values are in good agreement with those previously reported for both diffusion-limited ion exchange (*31*) and adsorption onto activated carbon (*47-50*). The value of k_f is directly related to the hydrodynamic film thickness δ (equation 5.5), which is a function of mixing rate and temperature. Consequently, correlation of these k_f values with previously published values may lend support for the use of the dual resistance model, but it does not validate the mechanism. Calculated values of the film thickness and the dimensionless number ξ are presented in Table 5.2. Film thicknesses are on the order of 11 μm, or about 1/25th of the particle radius. Variations in δ are most likely due to differing mixing rates. Values of ξ indicate that, for most of the experiments, film diffusion was more important than intraparticle diffusion in determining the sorption rate. Mixing in the reaction vessels was vigorous, but apparently not rapid enough to overcome the resistance of film diffusion. Because these experiments were dominated by film diffusion, the optimized values of D_{eff} were not very precise. Therefore, the D_{eff} values could not be

Table 5.1. Optimized k_f and D_{eff} Values for the Dual Resistance Model.

compound	temp (°C)	R (cm)	K (mL/g)	k_f x 1000 (cm/s) best	(low - high)	log (D_{eff}) (cm^2/s) best	(low - high)
DCB	34	0.03188	86920	3.82	(3.08 - 4.74)	-8.785	(-9.196 - -7.355)
DCB	34	0.02559	86920	8.67	(7.37 - 10.27)	-9.255	(-9.381 - -9.116)
DCB	4	0.03188	277400	3.00	(2.51 - 3.59)	-10.07	(-10.294 - -9.787)
DCB	4	0.02559	277400	2.80	(2.60 - 3.00)	-9.661	(-9.849 - -9.421)
TrCB	34	0.03188	323500	16.26	(14.09 - 18.94)	-9.722	(-9.842 - -9.592)
TrCB	34	0.02559	323500	38.97	(35.35 - 43.21)	-9.524	(-9.590 - -9.454)
TrCB	4	0.03188	411400	4.06	(3.82 - 4.32)	-9.536	(-9.706 - -9.328)
TrCB	4	0.02559	411400	4.76	(4.28 - 5.28)	-9.593	(-9.878 - -9.167)
TeCB	34	0.03188	1137000	10.99	(8.83 - 13.86)	-10.94	(-11.168 - -10.675)
TeCB	34	0.02559	1474000	10.21	(9.52 - 10.96)	-10.05	(-10.311 - -9.687)
TeCB	4	0.03188	1996000	3.20	(2.70 - 3.80)	-6.613	(-10.464 - -1.098)
TeCB	4	0.02559	1996000	4.18	(3.87 - 4.52)	-6.431	(-9.957 - -1.144)

Table 5.2. Calculated Film Thicknesses and Reaction Rate Ratios for the Dual Resistance Model.

compound	temp (°C)	R (cm)	D_m (cm^2/s)	δ (μm) best	δ (μm) (low - high)	ξ best	ξ (low - high)
DCB	34	0.03188	1.04×10^{-5}	27.26	(21.93 - 33.81)	1.53	(0.05 - 4.89)
DCB	34	0.02559	1.04×10^{-5}	12.00	(10.13 - 14.10)	8.23	(5.08 - 13.03)
DCB	4	0.03188	4.37×10^{-6}	14.58	(12.18 - 17.43)	7.27	(3.16 - 14.56)
DCB	4	0.02559	4.37×10^{-6}	15.64	(14.56 - 16.79)	2.12	(1.13 - 3.50)
TrCB	34	0.03188	9.54×10^{-6}	5.87	(5.04 - 6.77)	15.15	(9.72 - 23.24)
TrCB	34	0.02559	9.54×10^{-6}	2.45	(2.21 - 2.70)	18.45	(14.27 - 23.81)
TrCB	4	0.03188	4.02×10^{-6}	9.91	(9.31 - 10.54)	1.94	(1.13 - 3.04)
TrCB	4	0.02559	4.02×10^{-6}	8.45	(7.61 - 9.39)	2.08	(0.70 - 4.45)
TeCB	34	0.03188	8.87×10^{-6}	8.07	(6.40 - 10.04)	48.70	(21.00 - 102.5)
TeCB	34	0.02559	8.87×10^{-6}	8.69	(8.09 - 9.32)	3.57	(1.44 - 6.98)
TeCB	4	0.03188	3.74×10^{-6}	11.68	(9.86 - 13.86)	3.76×10^{-4}	(0 - 3.16)
TeCB	4	0.02559	3.74×10^{-6}	8.94	(8.28 - 9.66)	2.59×10^{-4}	(0 - 0.94)

accurately probed for insight into the relative importance of intraparticle pore diffusion and intraparticle surface diffusion. In general, D_{eff} values were in the same range as those determined by the time scale experiments.

Implications. These experiments support a diffusive rate limitation for the adsorption of organics on macroreticular sorbents such as XAD-7. The collection, concentration, and subsequent desorption of analytes using columns of such sorbents will be affected by rate-limited sorption processes. The prediction of collection efficiencies must account for diffusion-limited transport.

Extrapolating the results of these experiments to natural systems, it is unlikely that mixing in surface waters is vigorous enough to eliminate the resistance of film diffusion. For small particles or particles with an open, porous structure, intraparticle diffusion is probably not slow enough to control the exchange rate. Organic sorption kinetics for such systems would be controlled by film diffusion. Particles that are completely nonporous are not subject to intraparticle diffusion, but will exhibit film diffusion kinetics. For porous particles that are heavily coated with organic matter, intraparticle diffusion may be heavily retarded, causing the resistance of film diffusion to be less important with respect to intraparticle transport. In general, however, the description of sorption kinetics in surface waters must include a component of film diffusion. If information is available concerning the nature of the particulate matter, a dual resistance model would probably provide the best predictions of rate-limited sorption.

Summary and Conclusions

The characteristics of five different mechanistic models of rate-limited sorption were examined and compared. Experiments were conducted to determine the kinetics of adsorption for a set of chlorinated benzenes on the sorbent XAD-7 in a batch system. Days to weeks were required to achieve sorption equilibrium. Each model was fitted to the experimental data using nonlinear least squares techniques. The ability of each model to describe the

observed uptake was assessed. Rate-control by particle abrasion or by intraparticle diffusion alone was ruled out. The ability of particle abrasion to increase the sorption rate should be considered in batch systems, but it did not control the rate in these experiments. The dual resistance model, coupling both film and intraparticle diffusion, consistently was able to fit the observed data with a high degree of accuracy. The dependence of the sorption rate on particle size and temperature suggested a diffusive rate limitation. Fits of the data with the dual resistance model showed that film diffusion was the dominant rate-limiting mechanism, with intraparticle diffusion contributing an additional minor resistance. Film diffusion will be an important mechanism of rate-limited sorption for suspended particles in surface waters.

Glossary

C	aqueous concentration of analyte (ng/mL)
C_o	initial aqueous concentration of analyte (ng/mL)
C_s	aqueous concentration of analyte at the particle surface (ng/mL)
D_{eff}	effective diffusion coefficient (cm^2/s)
D_m	molecular diffusion coefficient in water (cm^2/s)
F_e	fraction of equilibrium sites in the two-site model
g_n	roots of an equation needed for the intraparticle diffusion and dual resistance models
K	aqueous partition coefficient (mL/g)
k_{ab}	first order abrasion rate constant (min^{-1})
k_d	first order sorption rate constant (min^{-1})
k_f	film mass-transfer coefficient (cm/s)
K_{ow}	octanol-water partition coefficient
K_{rv}	partition coefficient for sorption to the reaction vessel (mL)
m	total mass of sorbent (g)
M_e	analyte mass exchanged between aqueous and solid phases at equilibrium

M_{rv}	analyte mass sorbed to the reaction vessel (ng)
M_t	analyte mass exchanged between phases at time t
M_t/M_e	fractional approach to equilibrium
n	particle porosity (dimensionless)
r	radial distance (cm)
R	radius of sorbent particle (cm)
S	uniform sorbed concentration (ng/g)
S_o	initial sorbed concentration (ng/g)
$S(r)$	total volumetric concentration of analyte in the particulate phase at a radial distance r (ng/mL)
t	time (min)
V	volume of solution (mL)
α_c	dimensionless number related to the final fractional uptake in the intraparticle diffusion and dual resistance models
δ	hydrodynamic film thickness (cm)
η	fractional radial distance
ξ	dimensionless number that relates the film diffusion rate to the intraparticle diffusion rate
ρ_b	bulk density of porous sorbent (g/mL)
τ	particle tortuosity (dimensionless)
ψ	dimensionless number that relates the abrasion rate to the intraparticle diffusion rate
Ω_n	term in the analytical solution to the dual resistance model

Registry No. 1,2-Dichlorobenzene, 95-50-1; 1,2,4-Trichlorobenzene, 120-82-1; 1,2,4,5-Tetrachlorobenzene, 95-94-3.

Literature Cited

(1) Mackay, D. M.; Cherry, J. A. *Environ. Sci. Technol.* **1989**, *23*, 630-636.

(2) McCarthy, J. F.; Jimenez , B. D.; Barbee, T. *Aquat. Toxicol.* **1985**, *7*, 15-24.

(3) Steinberg, S. M.; Pignatello, J. J.; Sawhney, B. L. *Environ. Sci. Technol.* **1987**, *21*, 1201-1208.

(4) Rijnaarts, H. H. M.; Bachmann, A.; Jumelet, J. C.; Zehnder, A. J. B. *Environ. Sci. Technol.* **1990**, *24*, 1349-1354.

(5) Mihelcic, J. R.; Luthy, R. G. *Environ. Sci. Technol.* **1991**, *25*, 169-177.

(6) Karickhoff, S. W. In *Contaminants and Sediments*; Baker, R. A., Ed.; Ann Arbor Science: Ann Arbor, MI, 1980; vol. 2, pp.193-205.

(7) Karickhoff, S. W. *J. Hydraul. Eng.* **1984**, *110*, 707-735.

(8) Karickhoff, S. W.; Morris, K. R. *Environ. Toxicol. Chem.* **1985**, *4*, 469-479.

(9) Coates, J. T.; Elzerman, A. W. *J. Contam. Hydrol.* **1986**, *1*, 191-210.

(10) Miller, C. T.; Weber, W. J. *J. Contam. Hydrol.* **1986**, *1*, 243-261.

(11) Pavlostathis, S. G.; Mathavan, G. N. *Environ. Sci. Technol.* **1992**, *26*, 532-538.

(12) Chiou, C. T.; Peters, L. J.; Freed, V. H. *Science* **1979**, *206*, 831-832.

(13) Karickhoff, S. W. *Chemosphere* **1981**, *10*, 833-846.

(14) Schwarzenbach, R.; Westall, J. *Environ. Sci. Technol.* **1981**, *15*, 1360-1367.

(15) Chiou, C. T.; Schmedding, D. W.; Manes, M. *Environ. Sci. Technol.* **1982**, *16*, 4-10.

(16) Chiou, C. T.; Porter, P. E.; Schmedding, D. W. *Environ. Sci. Technol.* **1983**, *17*, 227-231.

(17) Chiou, C. T.; Shoup, T. D. *Environ. Sci. Technol.* **1985**, *19*, 1196-1200.

(18) Chiou, C. T.; Shoup, T. D.; Porter, P. E. *Org. Geochem.* **1985**, *8*, 9-14.

(19) Leenheer, J. A.; Ahlrichs, J. L. *Soil Sci. Soc. Amer. Proc.* **1971**, *35*, 700-705.

(20) Rao, P. S. C.; Jessup, R. E. In *Chemical Mobility and Reactivity in Soil Systems*; Nelson, D. W., Tanji, K. K., Elrick, D. E., Eds.; Am. Soc. Agron.: Madison, WI, 1983; pp. 183-201.

(21) Wu, S.-C.; Gschwend, P. M. *Environ. Sci. Technol.* **1986**, *20*, 717-725.

(22) Bouchard, D. C.; Wood, A. L.; Campbell, M. L.; Nkedi-Kizza, P.; Rao, P. S. C. *J. Contam. Hydrol.* **1988**, *2*, 209-223.

(23) Brusseau, M. L.; Rao, P. S. C. *Chemosphere* **1989**, *18*, 1691-1706.

(24) Podoll, R. T.; Irwin, K. C.; Parish, H. J. *Chemosphere* **1989**, *18*, 2399-2412.

(25) Brusseau, M. L.; Jessup, R. E.; Rao, P. S. C. *Environ. Sci. Technol.* **1991**, *25*, 134-142.

(26) Ball, W. P.; Roberts, P. V. *Environ. Sci. Technol.* **1991**, *25*, 1237-1249.

(27) Boyd, G. E.; Adamson, A. W.; Meyers, L. S. *J. Am. Chem. Soc.* **1947**, *69*, 2836-2848.

(28) Helfferich, F.; Plesset, M. S. *J. Chem. Phys.* **1958**, *28*, 418-424.

(29) Plesset, M. S.; Helfferich, F.; Franklin, J. N. *J. Chem. Phys.* **1958**, *29*, 1064-1069.

(30) Helfferich, F. *J. Phys. Chem.* **1962**, *66*, 39-44.

(31) Huang, T.-C.; Li, K.-Y. *Ind. Eng. Chem. Fundam.* **1973**, *12*, 50-55.

(32) Sparks, D. L. *Kinetics of Soil Chemical Processes*; Academic Press: San Diego, CA, 1989.

(33) Satterfield, C. N. *Mass Transfer in Heterogeneous Catalysis*; R. E. Krieger Pub. Co.: Malabar, FL, 1981.

(34) Eagle, S.; Scott, J. W. *Ind. Eng. Chem.* **1950**, *42*, 1287-1294.

(35) Edeskuty, F. J.; Amundson, N. R. *Ind. Eng. Chem.* **1952**, *44*, 1698-1703.

(36) Furusawa, T.; Smith, J. M. *Ind. Eng. Chem. Fundam.* **1973**, *12*, 197-203.

(37) Nkedi-Kizza, P.; Brusseau, M. L.; Rao, P. S. C.; Hornsby, A. G. *Environ. Sci. Technol.* **1989**, *23*, 814-820.

(38) Brusseau, M. L.; Jessup, R. E.; Rao, P. S. C. *Environ. Sci. Technol.* **1990**, *24*, 727-735.

(39) Crank, J. *The Mathematics of Diffusion*, 2nd ed.; Clarendon: Oxford, England, 1975; pp. 89-96.

(40) Rohm and Haas, Co. *Amberlite XAD-7*, Technical Bulletin IE-204/72-78, Philadelphia, PA, 1981.

(41) Junk, G. A. In *Organic Pollutants in Water*; Suffet, I. H., Malaiyandi, M., Eds.; Advances in Chemistry 214; American Chemical Society: Washington, DC, 1987; pp. 201-246.

(42) Gibs, J.; Brenner, L.; Cognet, L.; Suffet, I. H. In *Organic Pollutants in Water*; Suffet, I. H., Malaiyandi, M., Eds.; Advances in Chemistry 214; American Chemical Society: Washington, DC, 1987; pp. 267-294.

(43) Verschueren, K. *Handbook of Environmental Data on Organic Chemicals*; Van Nostrand Reinhold: New York, NY, 1983, 2nd edn.

(44) Lyman, W. J.; Reehl, W. F.; Rosenblatt, D. H. *Handbook of Chemical Property Estimation Methods*; American Chemical Society: Washington, DC, 1990; ch. 1.

(45) Rounds, S. A. Ph.D. Thesis, Oregon Graduate Institute, 1992, ch. 4.

(46) Press, W. H.; Flannery, B. P.; Teukolsky, S. A.; Vetterling, W. T. *Numerical Recipes: The Art of Scientific Computing*; Cambridge University Press: New York, NY, 1989.

(47) Mathews, A. P. In *Fundamentals of Adsorption*; Liapis, A. I., Ed.; Engineering Foundation: New York, NY, 1987; pp. 345-354.

(48) Van Lier, W. C. In *Fundamentals of Adsorption*; Liapis, A. I., Ed.; Engineering Foundation: New York, NY, 1987; pp. 599-610.

(49) Smith, E. H.; Weber, W. J. *Environ. Sci. Technol.* **1989**, *23*, 713-722.

(50) Traegner, U. K.; Suidan, M. T. *Water Res.* **1989**, *23*, 267-273.

CHAPTER VI

Summary

General

Models of diffusion-limited intraparticle transport were developed, tested, and assessed for their ability to describe rate-limited sorption in atmospheric and aqueous systems. Investigations of gas/particle sorption kinetics for airborne particles and for particle-laden filters were limited to the use of an intraparticle diffusion model. The desorption of *n*-alkanes and PAHs from a heavily-loaded filter provided experimental data for the analysis of intraparticle diffusion as a rate-limiting mechanism in the atmosphere. For sorbent suspensions in aqueous systems, four diffusion-based models were compared. The similarity of first order chemical reaction and two-site models to those based on diffusion was assessed. Particle abrasion was presented as a competing mechanism. Adsorption experiments were conducted to test the possible rate-limiting mechanisms of sorption in aqueous sorbent suspensions.

Gas/Particle Sorption Kinetics

Models of diffusion-limited intraparticle transport were developed to describe gas/particle sorption kinetics for airborne and filter-bound particulate material. To approximately describe particles that are not fully porous, a porous shell/solid core model was proposed. Sorption reaction time scales were predicted using a theoretical description of sorption-retarded, gaseous,

intraparticle pore diffusion. According to that description, gas/particle partitioning equilibrium with airborne particles was predicted to be rapid for compounds typically determined in atmospheric samples. Particles that have a thin porous outer shell were predicted to approach equilibrium faster than those that are fully porous. For sorption reactions on/in particle-laden filters, adsorption and desorption processes were characterized by the diffusion reaction time scale T_D and the mass transfer time scale T_M. Given a change in the influent gas-phase concentration, the most volatile compounds were predicted to re-achieve equilibrium quickly. Predictions of sorption reactions on/in filters showed that adsorption and desorption were rapid enough to significantly alter the measured gas/particle distribution ratios of a wide range of compounds during a typical sampling event.

An experiment was conducted to test the predictions of the filter-based intraparticle diffusion model. Particles from a roadway tunnel were collected on a filter. Particle-associated organic compounds were subsequently desorbed over time in a laboratory experiment by passing clean N_2 through the filter at a controlled rate, humidity, and temperature. Desorbed analytes were collected and their concentrations were determined. The experimental data for a set of *n*-alkanes and PAHs were fitted to the intraparticle diffusion model using a nonlinear least squares technique. For most of the compounds, the fitted predictions of the model closely matched the desorption data; no systematic errors were evident.

Optimized partition coefficients K_p and effective diffusion coefficients D_{eff} were determined. These values of K_p agreed well with those reported by others, and also correlated well with values of the subcooled liquid vapor pressure. The fitted D_{eff} values correlated with K_p in the manner expected from theory. However, the absolute magnitudes of the D_{eff} values were roughly 10^6 times smaller than expected. The slower than expected desorption rates are proposed to result from the coupling of several processes: diffusion through or within a liquid-like organic film; diffusion through the solid phase; and sorption-retarded,

gaseous diffusion within micropores. The fitted effective diffusion coefficients are a measure of the effects of all rate-limiting processes. The presence of dead-end pores also may have contributed to the slow desorption. In addition, particle aggregation or preferential flow through the filter might have increased the effective diffusion length and thereby artificially lowered the fitted values of D_{eff}. An analysis of adsorption and desorption sampling artifacts showed that slow sorption kinetics could not prevent the expression of such artifacts. The ability of sorption kinetics to limit the magnitude of sampling artifacts was shown to be most important for compounds of intermediate volatility and depended upon the total sampling time.

If preferential flow through the filter was negligible, then the small optimized values of D_{eff} result in diffusion reaction time scales that are longer than those predicted by gaseous intraparticle diffusion alone. In contrast to the initial predictions, full gas/particle partitioning equilibrium with airborne particulate matter would rarely be achieved for most compounds typically determined in atmospheric samples. Long range atmospheric transport and depositional processes may be significantly affected by rate-limited gas/particle partitioning.

Aqueous Sorption Kinetics

An investigation of sorption kinetics in aqueous systems was performed to gain insight into the most important rate-limiting mechanisms. The characteristics of five different mechanistic models of rate-limited sorption in aqueous batch systems were examined and compared. The models included in this study were: film diffusion, first order particle abrasion, intraparticle diffusion, coupled intraparticle diffusion and abrasion, and coupled film and intraparticle diffusion (dual resistance). In four of these models, the sorption rate is controlled by a diffusive process. The particle abrasion model is an approximate representation of how the competing process of particle breakage can affect observed reaction rates in batch systems.

Models based on first order chemical reaction kinetics are commonly used to represent rate-limited sorption. For linear sorption isotherms, the first order reaction model was shown to be identical to the film diffusion model. Two-site or bicontinuum models can be used successfully to describe diffusion-limited sorption, but lack the predictive confidence of a mechanistic model. First order and two-site models do not require information concerning the physical properties of the sorbent, but the rate "constants" obtained are not necessarily constant and may not provide insight into the rate-controlling mechanisms.

The kinetics for the adsorption of a set of chlorinated benzenes to a model sorbent (XAD-7) was investigated in the laboratory. Each of the five mechanistic models were fitted to the experimental data using nonlinear least squares techniques. The film diffusion model fitted most of the experiments fairly well, but systematic errors were apparent in at least half of the fits. The particle abrasion model fitted some of the data well, but was ruled out because it predicted the complete destruction of the sorbent beads, a prediction that was inconsistent with experimental observations. Intraparticle diffusion alone was a poor predictor of the experimental data. The coupled diffusion/abrasion model gave best-fit predictions dominated by particle abrasion. The dual resistance model consistently outperformed all of the other tested models; all but one of the experiments was fitted with a high degree of accuracy and no observable systematic errors.

In the context of the dual resistance model, the experimental data were found to be particularly influenced by the resistance of film diffusion. The relative importance of film and intraparticle diffusion in the dual resistance model was estimated using the dimensionless number ξ (also known as the Biot number, Bi). For ξ values of ~ 10 or less, film diffusion is expected to be the dominant rate-limiting process. In contrast, for conditions under which ξ is above 100, intraparticle diffusion will control the rate. Film diffusion was the predominant rate-controlling mechanism in almost every experiment. Assuming that intraparticle transport is dominated by pore diffusion, the value of ξ is

expected to depend only on the properties of the sorbent. In these experiments, however, intraparticle surface diffusion probably contributed to the internal transport rate. Hydrodynamic film thicknesses for the conditions of these experiments were calculated to be roughly 11 μm, or about 1/25th of the particle radius.

Intraparticle diffusion will be the dominant rate-controlling process only for sorbent suspensions in which the particles are large or the mixing rate is particularly rapid. The results of these experiments indicate that quite vigorous mixing would be required to completely eliminate the resistance of film diffusion. If mixing is particularly violent, however, particle abrasion can significantly affect the sorption rate. In natural systems such as rivers, lakes, or oceans, mixing rates are probably not rapid enough to eliminate the resistance of film diffusion. Therefore, film diffusion is proposed to be an important component of rate-limited sorption in natural waters. Because first order reaction models are mathematically identical to those of film diffusion, transport models that account for sorption kinetics with a first order model should perform well when film diffusion controls the sorption rate.

Analytical Method Development

In the course of the aqueous kinetic investigations, the purge with whole column cryotrapping method for the determination of volatile organic compounds in aqueous samples was adapted for use with an electron capture detector. An in-line, temperature-programmed, cold-zone water trap was used to desiccate the purge gas. The water trap was essential in preventing the GC column from plugging with ice and in removing the chromatographic interference of water. Di-, tri-, and tetrachlorobenzenes in aqueous samples were quickly and efficiently determined by this method. Detection limits were quite low, ranging from 0.01 ng/mL for 1,2-dichlorobenzene to 0.0006 ng/mL for 1,2,4,5-tetrachlorobenzene in a 5 mL sample. The purge with whole column

cryotrapping method was also shown to be a potentially useful method for the determination of semi-volatile compounds such as pentachlorobenzene.

Further Work

Gas/Particle Partitioning and Kinetics. When the goal of an investigation is to develop predictive, mechanistic tools to describe an observed behavior, additional information concerning that process at the microscopic level is always valuable. In the case of gas/particle interactions, information concerning the physical nature of atmospheric particulate matter would be particularly useful. Measurement of particle surface areas, densities, and porosities would aid in the determination of α values for use with the model developed in this study. Alternatively, that information could be used to develop a different model of rate-limited sorption that more accurately accounts for particle shape and surface area. Investigations into the nature and role of the organic film that has been proposed to coat parts of some atmospheric particles would further the understanding of both the kinetics and equilibrium position of sorption reactions in atmospheric systems.

Aqueous Sorption Kinetics. To test the assertion that film diffusion is an important rate-controlling mechanism for sorption in natural systems, experiments should be carried out with actual sediment suspensions. The dependence of the observed kinetics on the mixing rate and the particle size would help to determine the relative importance of film diffusion. Any process that can be used to control the hydrodynamic film thickness might help determine the rate-limitations of film diffusion. Novel experimental designs will be necessary to isolate the individual rate-controlling mechanisms. Useful suggestions might be found in the ion-exchange or chemical engineering literature. For example, a short-bed, flow-through system such as that used by Boyd *et al.* (*1*) might be useful in controlling the hydrodynamic film thickness. Alternatively, any of the flow, stirred-flow, or interruption techniques described by Sparks (2) might be helpful.

Analytical Method Development. If further experiments are pursued to extend the purge with whole column cryotrapping method to the analysis of semi-volatile compounds, then efforts should be concentrated on increasing the water trap and transfer line throughput and/or the purging efficiency of those compounds. The overall purging efficiencies of penta- and hexachlorobenzene were much lower than expected in experiments conducted to date. These compounds are characterized by Henry's law constants that are high enough for this method to be viable. Retention of these compounds in the water trap should be investigated with respect to the phase II temperature and purge time. A shorter water trap column could be tried. In addition, if this method is to be used for routine analysis, it must be automated. This method lends itself to control by a computer. Snap valves could be replaced with solenoid valves. Purge times could be programmed. Automation would make the method less labor-intensive and more reproducible.

Literature Cited

(1) Boyd, G. E.; Adamson, A. W.; Myers L. S. *J. Am. Chem. Soc.* **1947**, *69*, 2836-2848.

(2) Sparks, D. L. *Kinetics of Soil Chemical Processes;* Academic Press: San Diego, CA, 1989.

APPENDIX A

Filter Desorption Experiments Data

Experimental data from the filter desorption study (Chapter Three) are presented in this appendix. Tables A.1 and A.2 contain the downstream gas-phase concentrations (A_{out}, ng/m^3) measured for each of the *n*-alkanes and PAHs. Tables A.3 and A.4 present the fractional approach to equilibrium (M_t/M_e) data for each of the compounds. The flow rates measured throughout the experiment are listed in Table A.5. The specifications of the 6-bin particle size distribution are listed in Table A.6.

Table A.1. Downstream Gas-phase Concentration Data (ng/m^3): *n*-alkanes.

time (min)	124	374	739	1239	1992	2992	4881	10102	21246	39848
volume (m^3)	0.474	1.432	2.852	4.848	7.760	11.59	19.12	35.41	67.69	131.5
compound										
hexadecane	79.5792	37.3125	22.3485	16.8050	12.0603	9.1786	5.9391	1.7378	1.0162	0.2753
octadecane	82.1595	69.0242	62.8402	39.8017	38.0048	24.5046	14.1812	8.0967	5.5577	1.0908
nonadecane	84.3638	76.9179	73.1258	59.0418	54.3519	41.8488	29.4797	24.8632	10.5271	2.5255
eicosane	72.7712	61.3959	65.6343	56.3080	61.8519	53.2778	39.6017	31.4473	22.8031	5.9200
heneicosane	44.5563	40.8553	50.9774	39.6237	50.6817	42.9878	34.4849	31.8372	27.7124	11.5168
docosane	15.4313	31.3962	25.3174	21.2050	28.1176	25.6800	19.5273	19.2610	19.1245	9.6202
tricosane	10.7692	11.5658	11.1624	8.7383	10.3732	10.9854	6.7488	6.8850	5.2735	2.2138
tetracosane	10.1085	4.2695	2.2925	2.9760	3.5585	3.7219	4.5112	3.3223	2.3947	1.6411
pentacosane	0.0000	1.4575	-0.9976	3.2062	1.1784	1.8015	0.8308	2.1245	1.6388	1.2983

Table A.2. Downstream Gas-phase Concentration Data (ng/m^3): PAHs.

time (min)	124	374	739	1239	1992	2992	4881	10102	21246	39848
volume (m^3)	0.474	1.432	2.852	4.848	7.760	11.59	19.12	35.41	67.69	131.5
compound										
acenaphthene	2.5247	0.3474	0.1972	0.1120	0.1169	0.0833	0.0600	0.0355	0.0250	0.0008
acenaphthylene	7.1598	1.4240	0.7483	0.5484	0.4861	0.2433	0.2550	0.1295	0.1044	0.0230
benz(a)anthracene	4.0335	2.8733	0.0477	1.7618	1.7589	2.3409	1.1373	1.1219	0.8957	0.6044
chrysene	0.0000	3.8559	0.8319	2.6671	3.1888	4.6893	2.0928	1.9184	2.2270	1.4145
fluoranthene	8.7475	13.7090	18.0958	12.9222	15.1973	13.7391	9.3255	7.2360	5.6288	1.8587
fluorene	10.8087	2.6698	0.7190	0.4690	0.2752	0.3115	0.1197	0.1004	0.0774	0.0215
9-fluorenone	19.8994	18.3999	12.0392	6.2182	5.1157	3.3650	1.9979	1.1893	0.6279	0.2042
2-methylphenanthrene	17.0213	17.6079	14.8437	8.7877	7.8750	4.9883	2.6434	2.6316	1.6686	0.4323
phenanthrene	84.2764	63.7309	37.7968	18.0952	11.9023	6.8145	3.7159	2.3144	1.4185	0.5406

Table A.3. Fractional Approach to Equilbrium Data: *n*-alkanes.

time (min)	124	374	739	1239	1992	2992	4881	10102	21246	39848
volume (m^3)	0.474	1.432	2.852	4.848	7.760	11.59	19.12	35.41	67.69	131.5
compound										
hexadecane	0.1135	0.2211	0.3165	0.4174	0.5231	0.6288	0.7633	0.8485	0.9471	1.0000
octadecane	0.0332	0.0897	0.1658	0.2335	0.3279	0.4080	0.4990	0.6116	0.7646	0.8240
nonadecane	0.0178	0.0506	0.0968	0.1492	0.2196	0.2909	0.3896	0.5699	0.7211	0.7928
eicosane	0.0102	0.0276	0.0551	0.0883	0.1416	0.2018	0.2899	0.4414	0.6589	0.7706
heneicosane	0.0043	0.0122	0.0268	0.0428	0.0726	0.1058	0.1583	0.2631	0.4438	0.5923
docosane	0.0010	0.0053	0.0103	0.0163	0.0279	0.0417	0.0625	0.1068	0.1938	0.2804
tricosane	0.0005	0.0017	0.0034	0.0053	0.0085	0.0130	0.0184	0.0303	0.0485	0.0635
tetracosane	0.0005	0.0010	0.0013	0.0020	0.0032	0.0047	0.0085	0.0145	0.0231	0.0347
pentacosane	0.0000	0.0001	0.0000	0.0004	0.0005	0.0009	0.0013	0.0032	0.0062	0.0108

Table A.4. Fractional Approach to Equilbrium Data: PAHs.

time (min)	124	374	739	1239	1992	2992	4881	10102	21246	39848
volume (m^3)	0.474	1.432	2.852	4.848	7.760	11.59	19.12	35.41	67.69	131.5
compound										
acenaphthene	0.2612	0.3339	0.3951	0.4439	0.5182	0.5878	0.6864	0.8128	0.9886	1.0000
acenaphthylene	0.1872	0.2625	0.3211	0.3815	0.4596	0.5110	0.6168	0.7332	0.9191	1.0000
benz(a)anthracene	0.0044	0.0107	0.0109	0.0189	0.0307	0.0512	0.0709	0.1128	0.1792	0.2677
chrysene	0.0000	0.0019	0.0025	0.0052	0.0099	0.0190	0.0271	0.0430	0.0795	0.1255
fluoranthene	0.0039	0.0161	0.0401	0.0642	0.1056	0.1547	0.2202	0.3304	0.5000	0.6108
fluorene	0.1201	0.1800	0.2039	0.2259	0.2446	0.2726	0.2937	0.3320	0.3906	0.4228
9-fluorenone	0.0329	0.0945	0.1541	0.1975	0.2494	0.2944	0.3469	0.4146	0.4853	0.5308
2-methylphenanthrene	0.0195	0.0602	0.1110	0.1533	0.2087	0.2547	0.3027	0.4062	0.5361	0.6027
phenanthrene	0.0477	0.1206	0.1846	0.2278	0.2691	0.3003	0.3336	0.3787	0.4333	0.4745

Table A.5. Flow Rates for the Filter Desorption Experiment.

time (min)	flow rate (mL/min)	time (min)	flow rate (mL/min)	time (min)	flow rate (mL/min)
37	3715	5912	4093	21652	3873
74	3798	6937	2824	22650	3929
104	3931	7047	4136	22883	3787
124	3905	7327	2698	23101	3923
214	3955	8403	2783	24301	3481
254	3743	8771	2684	25724	2903
314	3765	9807	3217	26998	3048
374	3780	10102	3120	27367	1739
434	3747	10214	3366	27427	627
504	3697	11157	3409	28344	4124
664	3982	11319	2201	28541	3953
739	3988	11379	2146	28750	3916
1239	3992	11429	2119	28802	3977
1262	3883	12729	2153	29794	3050
1507	3820	13113	2718	29974	3689
1652	3787	14190	2705	30291	3732
1767	3990	15627	2529	31414	3790
1992	3904	17059	2500	31604	3817
2642	3845	18362	2505	32860	3371
2782	3821	18498	3932	33136	3251
2992	3778	18838	3903	34146	3309
3107	3901	19793	3705	35606	2659
3530	3872	20133	3682	37064	2674
4624	4037	20278	3822	37451	4336
4881	3986	21198	3782	38404	4362
5444	3770	21246	3602	38607	4234
5619	3671	21386	3553	38879	4323
5744	4057	21529	3896	39848	4339

Table A.6. Particle Size Distribution.

diameter (μm)	volume fraction
0.02702	0.00747
0.10881	0.09749
0.29804	0.42704
0.75205	0.18864
1.89608	0.14503
4.35896	0.13433

APPENDIX B

Filter Desorption Experiments Computer Programs

Two of the most important computer programs used in the filter desorption study are presented in this appendix. Both were written in FORTRAN. These programs were compiled and used on an IBM RISC System/6000 (model 320) workstation. The memory requirements are not prohibitively large. Therefore, these programs could be implemented on a personal computer. These programs are rather computationally intensive, however, and the time required to run these programs could limit their application on a PC. The first program, *FILT4RES*, calculates breakthrough curves. The downstream gas-phase concentration (A_{out}), average sorbed concentration, and fractional approach to equilibrium (M_t/M_e) are all calculated versus time and volume for a given set of input. The second program, *FILT9SIM*, is the two-parameter optimization routine used to find best-fit values of the partition coefficient K_p and the effective diffusion coefficient D_{eff}. Input for both programs is read from files. Separate files are needed for general input, experimental M_t/M_e data, flow rates, and the particle size distribution. Note that the number of nodes/particle must be an odd number for the numerical integration to be performed accurately. Both programs are thoroughly commented; I/O should be self-explanatory.

Filter-based Intraparticle Diffusion Model: Breakthrough Curve.

```
      Program FILT4RES
c
c     This program will calculate data for the exchange of organic
c       compounds between particulate matter trapped on/in an air
c       sampling filter and the gas passing through that filter.
c       The mechanism for the exchange process is intraparticle
c       diffusion.  The following boundary conditions and
c       assumptions are made:
c
c         1.  Particles are spherical.
c         2.  Particles have a nonporous, nonsorbing inner core
c              surrounded by a porous, sorbing shell.  The percent
c              volume that is porous is set by the user.
c         3.  The bulk concentration of analyte in the gas phase is
c              uniform.
c         4.  Particles initially contain a uniform concentration of
c              analyte.
c         5.  Sorption is reversible and follows a linear isotherm,
c              defined as Kp = (F/TSP)/A.
c         6.  Kp and Deff are spatially invariant.
c         7.  Local equilibrium holds in the micropores of the particles.
c
c     The particle size distribution is read in from a file called
c       "partdist.dat" and is of the format:
c             diameter (um),  volume fraction
c       The number of sizes in the distribution is noted on the first
c       line of that file.
c
c     The flow rate through the filter is allowed to be variable in
c       this program.  Flow rate data is read in from another input
c       file called "flowrate.dat" and is in the format:
c             cumulative time (min),  flow rate (mL/min)
c       The number of flow rates is noted on the first line of the file.
c       The cumulative time is the time at which the flow rate changes.
c
c     This program will also read in some experimental data and
c       calculate the sum of the squared residuals between the
c       calculated and experimental data.
c
      real*8 A, alpha, Aout, bedmass, Blast, Deff, depth, dt, dtsave, dx
      real*8 epsilon, exchange, flag, flowrate, frac, gamma, initmass
      real*8 Kp, mass, masstot, maxdt, number, pb, pi, pmasstot
      real*8 pormass, poros, ps, residual, Savg, sumj, T4, test, time
      real*8 total, volume, avgS(100), B(6,50), f(6), f2(6), MtMe(2,10)
      real*8 period(85), radius(6), rate(85), theta(6), tyme(10)
      real*8 T1(6,50,3), T3(6,50),u(100,6,51),ut(100,6,51), volfract(6)
      integer*4 i, j, n, grid, nlayer, nrates, nsizes, p, v, t
      character*12 file1, file2, datfile, name*40
c
      Common /CRUN1/ Deff, dt, dx, epsilon, f, f2, flowrate, gamma
      Common /CRUN2/ grid, nsizes, pb, poros, radius
      Common /CRUN3/ Kp, T1, T3, T4, theta
c
      External CRUNCH
c     External FLUSH
c
      pi = 2.0D0 * DACOS(0.0D0)
c
c     Explanation of variable names:
c     A is the influent analyte concentration in the air (ng/cu.m.).
c     alpha is the fraction of a particle's volume which is porous.
c     Aout is the conc. of analyte in the effluent gas (ng/cu.m.)
c     avgS(n) is the average sorbed concentration of the analyte
c       (ng/cu.m.) in layer n of the filter.
c     B(i,j) is the vector on the right hand side of the matrix equation
c     bedmass is the mass of particulate matter on the filter (ug).
c     Blast is the value of B for the last row.
```

```
c     datfile is the file holding the experimental data.
c     Deff is the effective diffusion coefficient (sq.cm./sec.).
c     depth is the radial distance which is porous (um).
c     dt is the time interval between computations (minutes).
c     dtsave is a saved value of the time step (min).
c     dx is the dimensionless distance between grid points.
c     epsilon is Kp/(pb*1D12) + the sum of f2(i)*(grid-1).
c     exchange is the total amount of analyte mass exchanged between
c       the gas phase and the particulate phase at equilibrium (ng).
c     f(i) is f2(i) w/o the dependence on flowrate or dt.
c     f2(i) is volfract(i)*bedmass*dx/(nlayer*ps*(1-alpha*poros)
c       *1.0D12*flowrate*dt).
c     file1 is the name of the input file.
c     file2 is the name of the output file.
c     flowrate is the flowrate of air through the filter (cu.m./min).
c     frac is the fractional approach to equilibrium, Mt/Me.
c     gamma is a factor which is (1-alpha)**(1/3).  It is also equal
c       to the ratio:  radius of the inner core / particle radius.
c     grid is the number of grid points in each particle.
c     i is the index for the particle size fraction.
c     initmass is the mass of the analyte associated with the
c       particulate phase at the beginning of the simulation (ng).
c     j is the index for the grid point of interest.
c     Kp is the atmospheric partition coefficient.
c       Kp = (F/TSP)/A (cu.m./ug)
c     mass is the mass of particles of a particular size (ug).
c     masstot is the calculated value of bedmass (ug).  If there is
c       a difference between bedmass and masstot it is due to a
c       discrepancy in the values of volfract(i) such that they do not
c       sum to 1.0.
c     maxdt is the maximum time step allowed (min.)
c     MtMe() is the array which holds the calculated and experimental
c       data that is compared.
c     n is the current layer of the filter.
c     name is the analyte name.
c     nlayer is the number of layers in the filter.
c     nrates is the number of flow rates used.
c     nsizes is the number of particle sizes.
c     number is the actual number of particles in a given size range.
c     p is the index for the time period.
c     pb is the estimated bulk density of the particles (g/cu.cm.).
c     period(p) is the time (minutes) at which the flow rate changes
c       from rate(p) to rate(p+1).
c     pi is the irrational number 3.14159.....
c     pmasstot is the total mass of porous material (ug).
c     pormass is the total mass of the porous fraction of all particles
c       having a certain size (ug).
c     poros is the porosity = 1 - pb/ps
c     ps is the dry sorbent density (g/cu.cm.)
c     radius(i) is the mean radius of a particle (um).
c     rate(p) is the flow rate (mL/min) for the time between period(p-1)
c       and period(p).
c     residual is the sum of the squared residuals.
c     S is the total volumetric concentration of analyte in the
c       particulate phase (ng/cu.m.).
c     Savg is the average sorbed concentration of analyte (ng/cu.m.)
c     T1, T3, and T4 are the arrays which hold the coefficient
c       matrix and the L and U decompositions of that matrix.
c       T1(i,j) handles the tridiagonal part of the matrix.
c       T3 is the bottom row, except for the last column.
c       T4 is the coefficient in the last row, last column.
c     theta(i) is 2(delta x)**2/(delta tao)
c     time is in minutes.
c     total is the number of particles on the filter.
c     u(n,i,j) saves the values of ut(n,i,j).
c     ut(n,i,j) is the matrix of u values (u = x*S).
c     v is a printing index which allows data to be printed to a file
c       approximately once for each cubic meter of gas that flows
c       through the filter.
```

```
c     volfract(i) is the volume fraction of particles from the total
c       distribution which fall in the size range whose mean radius
c       is radius(i).  Data is in the file partdist.dat.
c     volume is the vol. of air which has passed thru the filter (cu.m.)
c     x is the dimensionless radial distance (=r/R)
c     sumj, test, etc. are all dummy variables which are used
c       to temporarily save values of interest.
c
c     Read in the values of Deff, Kp, A, bedmass, initmass, etc.
      Write (*,10) 'FILT4RES',
     z  'A Simulation of Gas/Particle Sorption Kinetics on/in Filters',
     z  'Composite Particles',
     z  'Inner Nonporous Core / Porous Outer Shell',
     z  'Stewart A. Rounds','November, 1990'
10    Format (/36X,A/12X,A/31X,A/20X,A//32X,A/32X,A//)
      Write (*,20) 'name of input file:  '
      Read (*,20) file1
20    Format (A)
c
      open (3,file=file1)
      Read (3,20) name
      Read (3,*) Kp
      Read (3,*) Deff
      Read (3,*) A
      Read (3,*) initmass
      Read (3,*) bedmass
      Read (3,*) alpha
      Read (3,*) pb
      Read (3,*) ps
      Read (3,*) nlayer
      Read (3,*) grid
      Read (3,*) dt
      Read (3,*) maxdt
      Read (3,20) datfile
      Read (3,20) file2
      close (3)
c
c     Read in the volume distribution of the particles.
c       The size data is given as the diameter, not the radius.
      open (3,file='partdist.dat')
      read (3,*) nsizes
      do 25 i=1,nsizes
        read(3,*) radius(i),volfract(i)
        radius(i) = radius(i) / 2.0D0
25      continue
      close (3)
c
c     Read in the flow rate and time period data.
      open (3,file='flowrate.dat')
      Read (3,*) nrates
      do 30 p=1,nrates
        Read (3,*) period(p), rate(p)
30    continue
      close (3)
c
c     Read in the experimental data.
      open (3,file=datfile)
      do 32 i=1,10
        Read (3,*) tyme(i), MtMe(1,i)
32    continue
      close (3)
c
c     Calculate the porosity of the porous section.
      poros = 1.0D0 - pb / ps
c
c     Calculate gamma.
      gamma = (1.0D0 - alpha)**(1.0D0/3.0D0)
c
c     Print the relevant data to a file.
```

```
      open (4,file=file2)
      Write (4,20) name
      Write (4,35) 'macroscopic Kp = ',Kp,' cu.m./ug'
c
c     Calculate the corrected value of Kp.  This calculation corrects
c       the entered value of Kp for the fraction of the particulate
c       mass which is porous.  This is done because the measured value
c       of Kp is calculated using the total particulate mass.  In
c       this model, the inner core of the particles does not sorb
c       because it is not porous.  Therefore, the amount of mass which
c       is actually involved in the sorption process is less than the
c       total particulate mass.
c
      Kp = Kp * (1.0D0 - alpha * poros) / (alpha * (1.0D0 - poros))
c
      Write (4,35) 'microscopic Kp = ',Kp,' cu.m./ug'
      Write (4,35) 'Deff = ',Deff,' sq.cm./sec'
      Write (4,36) 'A = ',A,' ng/cu.m.'
      Write (4,35) 'initially sorbed analyte mass = ',initmass,' ng.'
      Write (4,35) 'mass of particulate phase = ',bedmass,' ug.'
      Write (4,37) 'porous fraction = ',alpha
      Write (4,36) 'bulk density of porous section = ',pb,' g/cu.cm.'
      Write (4,36) 'dry density of nonporous section = ',ps,' g/cu.cm.'
      Write (4,37) 'porosity of porous section = ',poros
      Write (4,38) 'particle sizes = ',nsizes
      Write (4,38) 'number of flow rates = ',nrates
      Write (4,38) 'number of layers in filter = ',nlayer
      Write (4,38) 'nodes / particle = ',grid
      Write (4,35) 'initial time step = ',dt,' min.'
      Write (4,35) 'maximum time step = ',maxdt,' min.'
      Write (4,35) 'end of simulation = ',period(nrates),' min.'
35    Format (A,E12.6,A)
36    Format (A,F9.5,A)
37    Format (A,F9.5)
38    Format (A,I3)
c
c     Print the particle mass and number distributions to the file.
      write (4,40) 'Particle Mass and Number Distribution Data:',
     z  'Radius (um)   Shell (um)     Number   ',
     z  '  Mass (ug)        Porous Mass (ug)'
40    format (//A//A,3X,A/)
      masstot = 0.0D0
      pmasstot = 0.0D0
      total = 0.0D0
      do 50 i=1,nsizes
        mass = volfract(i) * bedmass
        masstot = masstot + mass
        number = mass * 0.75D6 / (pi * radius(i) *radius(i) * radius(i)
     z           * ps * (1.0D0 - alpha * poros))
        total = total + number
        depth = radius(i) * (1.0D0 - gamma)
        pormass = mass * alpha * (1.0D0-poros) / (1.0D0 - alpha * poros)
        pmasstot = pmasstot + pormass
        write (4,45) radius(i),depth,number,mass,pormass
45      format (F10.6,4X,F10.6,3X,E11.5,5X,F11.4,9X,F11.4)
50    continue
      write (4,52) 'Totals:', total, masstot, pmasstot
52    format (/A,19X,E12.5,5X,F11.4,9X,F11.4/)
      write (4,53) 'Each layer of the filter contains 1/',nlayer,
     z    ' of the total particulate mass.'
53    format (A,I3,A/)
c
      write (*,54) 'Working . . .'
54    format (/A/)
c
c     Set the grid spacing.
      dx = (1.0D0 - gamma) / (grid - 1.0D0)
      do 60 i=1,nsizes
        f(i) = volfract(i) * bedmass * dx / (nlayer *
```

```
     z          ps * (1.0D0 - alpha * poros) * 1.0D12)
60    continue
c
c     Initialize the ut array.  Recall that u=x*S.
c       u and ut are in units of ng/cu.m.
      Do 75 n = 1,nlayer
        Do 70 i = 1,nsizes
          Do 65 j = 1,grid
            ut(n,i,j) = (dx*(j-1)+gamma) *initmass *pb *1.0D12 /pmasstot
65        Continue
70      Continue
75    Continue
c
c     Initialize time, p, flowrate, frac, v, volume, dt, exchange.
      time = 0.0D0
      p = 1
      flowrate = rate(1) / 1.0D6
      frac = 0.0D0
      t = 1
      residual = 0.0D0
      v = 0
      volume = 0.0D0
      if (dt .gt. period(1)) dt = period(1)
      if (dt .gt. maxdt) dt = maxdt
      dtsave = dt
      exchange = A * pmasstot * (Kp + poros / (pb * 1.0D12)) - initmass
c
c     Initialize epsilon, theta and f2(i).  Set up the coefficient
c       matrix and perform an L-U decomposition.
      CALL CRUNCH
c
c     Start the simulation.
      write (4,78) 'Time (min.)   Volume (cu.m.)   Aout (ng/cu.m.)',
     z    '    Average S (ng/ml)     Mt/Me'
78    format (/A,A/)
80    Aout = A
c
c     Initialize the u array.
      do 105 n=1,nlayer
        do 100 i=1,nsizes
          do 90 j=1,grid
            u(n,i,j) = ut(n,i,j)
90        continue
100     continue
105   continue
c
c     Loop through each of the layers of the filter.
110   do 300 n = 1,nlayer
c
c       Loop through the particle size distribution.
c       Set up the B vector.
        do 130 i = 1,nsizes
          B(i,1) = (1.0D0 + (gamma-dx)/(gamma+dx)) * ut(n,i,2)
     z             - (2.0D0 - theta(i)) * ut(n,i,1)
          do 120 j = 2,(grid - 1)
            B(i,j) = ut(n,i,j-1)-(2-theta(i))*ut(n,i,j)+ut(n,i,j+1)
120       continue
130     continue
        Blast = Aout
        do 150 i = 1,nsizes
          Blast = Blast + f2(i) * (gamma * ut(n,i,1) + ut(n,i,grid))
          do 140 j = 2,(grid - 1)
            Blast = Blast + f2(i) * (dx * (j-1) + gamma)
     z               * (3 + (-1)**j) * ut(n,i,j)
140       continue
150     continue
        Blast = Blast / epsilon
c
c       Forward substitution:
```

```
        do 170 i = 1,nsizes
          ut(n,i,1) = B(i,1)
          do 160 j = 2,(grid-1)
            ut(n,i,j) = B(i,j) - T1(i,j,1) * ut(n,i,j-1)
160       continue
170     continue
        ut(n,1,grid) = Blast
        do 190 i = 1,nsizes
          do 180 j = 1,(grid-1)
            ut(n,1,grid) = ut(n,1,grid) - T3(i,j) * ut(n,i,j)
180       continue
190     continue
c
c       Backward substitution:
        ut(n,1,grid) = ut(n,1,grid) / T4
        do 210 i = nsizes,1,-1
          j = grid - 1
          ut(n,i,j) = (ut(n,i,j) + ut(n,1,grid)) / T1(i,j,2)
          do 200 j = (grid-2),1,-1
            ut(n,i,j) = (ut(n,i,j)-T1(i,j,3)*ut(n,i,j+1))/T1(i,j,2)
200       continue
210     continue
c
c       Calculate the bulk effluent concentration.
        Aout = ut(n,1,grid) / (poros + pb * Kp * 1.0D12)
c
c       Update the values of ut(n,i,grid).
        do 220 i = 2,nsizes
          ut(n,i,grid) = ut(n,1,grid)
220     continue
300   continue
c
c     Check the effect of the current time step.
      test = (A - Aout) * dt * flowrate / exchange
      if ((test .gt. 0.04) .and. (dt .gt. 0.000001)) then
        dt = dt / 1.5D0
        dtsave = dt
        Aout = A
        do 340 n=1,nlayer
          do 330 i=1,nsizes
            do 320 j=1,grid
              ut(n,i,j) = u(n,i,j)
320         continue
330       continue
340     continue
        CALL CRUNCH
        goto 110
      endif
c
c     Increment the time.
      time = time + dt
c
c     Update the fractional approach to equilibrium.
      frac = frac + ((A-Aout) * dt * flowrate) / exchange
c
c     Calculate average sorbed concentrations.
      Savg = 0.0D0
      do 380 n = 1,nlayer
        avgS(n) = 0.0D0
        do 370 i = 1,nsizes
          sumj = gamma * ut(n,i,1) + ut(n,i,grid)
          do 360 j = 2,(grid - 1)
            sumj = sumj + (3+(-1)**j) * (dx*(j-1)+gamma) * ut(n,i,j)
360       continue
          avgS(n) = avgS(n) + volfract(i) * dx * sumj
370     continue
        Savg = Savg + avgS(n)
380   continue
      Savg = Savg / (nlayer * 1.0D6)
```

```
c
      volume = volume + dt * flowrate
      if ((volume .gt. v) .or. (time .eq. period(nrates))) then
        write (4,390) time, volume, Aout, Savg, frac
390     format (F10.2,5X,F12.5,6X,E12.5,7X,E12.5,6X,F8.5)
        v = INT(volume) + 1
c
c       Flush the print buffer.
c       Call FLUSH(4)
      endif
c
      if (time .eq. tyme(t)) then
        residual = residual + (frac - MtMe(1,t))**2.0D0
        MtMe(2,t) = frac
        t = t + 1
      endif
c
      if (time .lt. period(nrates)) then
        flag = 0
        if (time .eq. period(p)) then
          p = p + 1
          flowrate = rate(p) / 1.0D6
          flag = 1
          dt = dtsave
        elseif ((test .lt. 0.001) .and. (dt .ne. maxdt)) then
          dt = dt * 1.5D0
          if (dt .gt. maxdt) dt = maxdt
          flag = 1
        endif
        dtsave = dt
        if ((time + dt) .gt. period(p)) then
          dt = period(p) - time
          flag = 1
        endif
        if (flag .eq. 1) CALL CRUNCH
        goto 80
      endif
c
      Write (4,400) 'Mt/Me Data:',
     z   'Time (min)     Mt/Me (expt)     Mt/Me (calc)'
400   Format (//A//A)
      Write (4,410) (tyme(j), (MtMe(i,j), i=1,2), j=1,10)
410   Format (10(F10.2,7X,F7.5,10X,F7.5/))
      Write (4,420) 'Sum of squared residuals = ',residual
420   Format (A,E16.9)
      close (4)
      end
c
c
      SUBROUTINE CRUNCH
c
c     Set up the coefficient matrix and perform an L-U decomposition.
c
      Real*8 Deff, dt, dx, epsilon, flowrate, gamma, Kp, pb, poros, T4
      Real*8 f(6), f2(6), radius(6), T1(6,50,3), T3(6,50), theta(6)
      Integer*4 i, j, grid, nsizes
      Common /CRUN1/ Deff, dt, dx, epsilon, f, f2, flowrate, gamma
      Common /CRUN2/ grid, nsizes, pb, poros, radius
      Common /CRUN3/ Kp, T1, T3, T4, theta
c
      epsilon = 1.0D0 / (pb * Kp * 1.0D12 + poros)
      do 668 i=1,nsizes
        f2(i) = f(i) / (flowrate * dt)
        epsilon = epsilon + f2(i)
        theta(i) = 2.0D0*dx*dx*radius(i)*radius(i) / (Deff*dt*6.0D9)
668   continue
c
      do 680 i=1,nsizes
        T1(i,1,1) = 0.0D0
```

```
        T1(i,1,2) = 2.0D0 + theta(i)
        T1(i,1,3) = -1.0D0 - (gamma - dx) / (gamma + dx)
        do 670 j = 2,(grid-2)
          T1(i,j,1) = -1.0D0
          T1(i,j,2) = 2.0D0 + theta(i)
          T1(i,j,3) = -1.0D0
670     continue
        T1(i,grid-1,1) = -1.0D0
        T1(i,grid-1,2) = 2.0D0 + theta(i)
        T1(i,grid-1,3) = 0.0D0
680   continue
c
      do 690 i = 1,nsizes
        T3(i,1) = f2(i) * gamma / epsilon
        do 685 j = 2,(grid-1)
          T3(i,j) = f2(i) * (dx*(j-1)+gamma) * (3+(-1)**j) / epsilon
685     continue
690   continue
c
c     L-U Decomposition:
c     Use Thomas Algorithm for T1.
      do 696 i=1,nsizes
        do 695 j = 2,(grid-1)
          T1(i,j,1) = T1(i,j,1) / T1(i,j-1,2)
          T1(i,j,2) = T1(i,j,2) - T1(i,j,1) * T1(i,j-1,3)
695     continue
696   continue
c
c     Decompose T3.
      do 701 i=1,nsizes
        T3(i,1) = T3(i,1) / T1(i,1,2)
        do 700 j = 2,(grid-1)
          T3(i,j) = (T3(i,j) - T3(i,j-1) * T1(i,j-1,3)) / T1(i,j,2)
700     continue
701   continue
c
c     Set up and decompose T4.
      T4 = 1.0D0
      do 705 i = 1,nsizes
        T4 = T4 + T3(i,grid-1)
705   continue
c
      return
      end
```

Filter-based Intraparticle Diffusion Model: Two-parameter Optimization.

```
      PROGRAM FILT9SIM

c     Finds the best combination of Kp and Deff values that are needed
c     to fit experimental filter desorption data using the program
c     FILT4RES as a fitting function.

c     The search method is the downhill simplex method.  This method is
c     described in Numerical Recipes by Press, Flannery, Teukolsky, and
c     Vetterling, Cambridge University Press, 1986, chapter 10.  Much of
c     the code is taken directly from that chapter.  The search method
c     is contained in the subroutine AMOEBA.

c     This optimization routine uses logarithmic values as the search
c     indices for the two fitting parameters, Kp and Deff.

      Integer ndim
      Parameter (ndim=2)

      Real*8 Vect(ndim+1,ndim), Val(ndim+1), FUNK, ftol
      Real*8 Kstart, Kend, Kinc, Dstart, Dend, Dinc
      Integer*4 i, iter, row, col, nrows, ncols

      Common /set1/ Kstart, Kend, Dstart, Dend, nrows, ncols

      External SETUP
      External FUNK
      External AMOEBA
      External FLUSH

      Data ftol /0.0000001/

c     Title.
      Write (*,5) 'FILT9SIM','Non-Linear Least Squares Analysis',
     z  'Downhill Simplex Method','- Stewart A. Rounds -',
     z  'December 12, 1991'
5     Format (/36X,A//24X,A/29X,A/30X,A/32X,A/)

      CALL SETUP

      Write (4,80) nrows, ncols
80    Format (/,'SIMPLEX search over ',I3,' rows and ',I3,' columns.')
      Write (4,85) Kstart, Kend
85    Format ('Starting Kp = ',E13.5,'   Ending Kp = ',E13.5)
      Write (4,86) Dstart, Dend
86    Format ('Starting Deff = ',E13.5,'   Ending Deff = ',E13.5)

c     For each starting point:
c     - Set the starting positions for beginning the search.
c     - Call AMOEBA to find the minimum.
c     - Report the number of iterations, the tolerance level, the
c         ending vertices, and the function values at those vertices.

      Kinc = (LOG10(Kend) - LOG10(Kstart)) / (nrows-1)
      Dinc = (LOG10(Dend) - LOG10(Dstart)) / (ncols-1)
      Do 160 row = 1,nrows
        Do 150 col = 1,ncols
          Vect(1,1) = LOG10(Kstart) + (row-1)*Kinc
          Vect(2,1) = Vect(1,1) + Kinc/3.0D0
          Vect(3,1) = Vect(1,1)

          Vect(1,2) = LOG10(Dstart) + (col-1)*Dinc
          Vect(2,2) = Vect(1,2)
          Vect(3,2) = Vect(1,2) + Dinc/3.0D0

          Write (4,90) 'Starting positions:'
90        Format (/A)
          Write (4,95)
```

```
95        Format (10X,'Vertex #1      Vertex #2      Vertex #3')
          Write (4,100) (10**Vect(I,1), I=1,3)
100       Format ('Kp:   ',3(3X,E12.5))
          Write (4,101) (10**Vect(I,2), I=1,3)
101       Format ('Deff: ',3(3X,E12.5))
          Write (4,104) '  Kp(macro)    Kp(micro)',
     z                  '      Deff         alpha        resid'
104       Format (/A,A)

c         Flush the print buffer.
          Call FLUSH(4)

c         Find the best fit for Kp and Deff.
          Call AMOEBA(Vect,Val,ndim,ftol,FUNK,iter)

          Write (4,140) iter,ftol
140       Format (/,' Search ended after ',I5,' iterations.',
     z         '  Tolerance:  ',F11.9)
          Write (4,95)
          Write (4,100) (10**Vect(I,1), I=1,3)
          Write (4,101) (10**Vect(I,2), I=1,3)
          Write (4,145) (Val(I), I=1,3)
145       Format ('resid:',3(2X,E13.6))
          Write (5,147) (10**Vect(I,1),10**Vect(I,2),Val(I),I=1,3)
147       Format (2(3(E15.7)/),3(E15.7))

c         Flush the print buffers.
          Call FLUSH(4)
          Call FLUSH(5)

150     Continue
160   Continue

      close (4)
      close (5)
      end

c *********************************************************************

      SUBROUTINE SETUP

c     This subroutine reads the input data from the necessary files,
c       opens the output files, and does some preliminary calculations.

c     The particle size distribution is read in from a file called
c       "partdist.dat" and is of the format:
c             diameter (um),  volume fraction
c       The number of sizes in the distribution is noted on the first
c       line of that file.

c     The flow rate through the filter is allowed to be variable in
c       this program.  Flow rate data is read in from another input
c       file called "flowrate.dat" and is in the format:
c             cumulative time (min),  flow rate (mL/min)
c       The number of flow rates is noted on the first line of the file.
c       The cumulative time is the time at which the flow rate changes.

      real*8 A, alpha, bedmass, Dend, depth, Dstart, dtinit, dx, gamma
      real*8 initmass, Kend, Kstart, mass, masstot, maxdt, number
      real*8 pb, pi, pmasstot, pormass, poros, ps, total
      real*8 f(6), MtMe(10), period(85), radius(6), rate(85)
      real*8 tyme(10), volfract(6)
      integer*4 i, grid, ncols, nlayer, nrates, nrows, nsizes
      character*12 file1, file2, file3, datfile, name*40

      Common /set1/ Kstart, Kend, Dstart, Dend, nrows, ncols
      Common /Param1/ A, alpha, bedmass, dtinit, initmass, maxdt
      Common /Param2/ MtMe, period, pmasstot, ps, rate, tyme
      Common /Param3/ volfract, nlayer, nrates
```

```
      Common /CRUN1/ dx, f, gamma, pb, poros, radius, grid, nsizes

c     Variable name descriptions.
c       See the function FUNK for most of the descriptions.
c     tyme(t) is the time of interest for the experimental data (min).
c     MtMe(t) is the value of Mt/Me for the desorption at tyme(t).

      pi = 2.0D0 * DACOS(0.0D0)

      Write (*,10) 'FILTER4',
     z  'A Simulation of Gas/Particle Sorption Kinetics on/in Filters',
     z  'Composite Particles',
     z  'Inner Nonporous Core / Porous Outer Shell',
     z  'Stewart A. Rounds','August 25, 1991'
10    Format (/37X,A/12X,A/31X,A/20X,A//32X,A/32X,A/)
      Write (*,20) 'Name of input file:  '
20    Format (A)
      Read (*,20) file1

      open (3,file=file1)
      Read (3,20) name
      Read (3,*) A
      Read (3,*) initmass
      Read (3,*) bedmass
      Read (3,*) alpha
      Read (3,*) pb
      Read (3,*) ps
      Read (3,*) nlayer
      Read (3,*) grid
      Read (3,*) dtinit
      Read (3,*) maxdt
      Read (3,*) nrows, ncols
      Read (3,*) Kstart, Kend
      Read (3,*) Dstart, Dend
      Read (3,20) datfile
      Read (3,20) file2
      Read (3,20) file3
      close (3)

c     Read in the volume distribution of the particles.
c       The size data is given as the diameter, not the radius.
      open (3,file='partdist.dat')
      read (3,*) nsizes
      do 25 i=1,nsizes
        read(3,*) radius(i),volfract(i)
        radius(i) = radius(i) / 2.0D0
25      continue
      close (3)

c     Read in the flow rate and time period data.
      open (3,file='flowrate.dat')
      Read (3,*) nrates
      do 28 i=1,nrates
        Read (3,*) period(i), rate(i)
28    continue
      close (3)

c     Read in the experimental times and Mt/Me data.
      open (3,file=datfile)
      do 30 i = 1,10
        read (3,*) tyme(i), MtMe(i)
30    continue
      close (3)

c     Calculate the porosity of the porous section.
      poros = 1.0D0 - pb / ps

c     Calculate gamma.
      gamma = (1.0D0 - alpha)**(1.0D0/3.0D0)
```

```
c     Print the relevant data to a file.
      open (4,file=file2)
      open (5,file=file3)

      Write (4,20) name
      Write (4,36) 'A = ',A,' ng/cu.m.'
      Write (4,35) 'initially sorbed analyte mass = ',initmass,' ng.'
      Write (4,35) 'mass of particulate phase = ',bedmass,' ug.'
      Write (4,37) 'porous fraction = ',alpha
      Write (4,36) 'bulk density of porous section = ',pb,' g/cu.cm.'
      Write (4,36) 'dry density of nonporous section = ',ps,' g/cu.cm.'
      Write (4,37) 'porosity of porous section = ',poros
      Write (4,38) 'particle sizes = ',nsizes
      Write (4,38) 'number of flow rates = ',nrates
      Write (4,38) 'number of layers in filter = ',nlayer
      Write (4,38) 'nodes / particle = ',grid
      Write (4,35) 'initial time step = ',dtinit,' min.'
      Write (4,35) 'maximum time step = ',maxdt,' min.'
      Write (4,35) 'end of simulation = ',period(nrates),' min.'
35    Format (A,E12.6,A)
36    Format (A,F9.5,A)
37    Format (A,F14.10)
38    Format (A,I3)

c     Print the particle mass and number distributions to the file.
      write (4,40) 'Particle Mass and Number Distribution Data:',
     z  'Radius (um)   Shell (um)     Number   ',
     z  '  Mass (ug)        Porous Mass (ug)'
40    format (//A//A,3X,A/)
      masstot = 0.0D0
      pmasstot = 0.0D0
      total = 0.0D0
      do 50 i=1,nsizes
        mass = volfract(i) * bedmass
        masstot = masstot + mass
        number = mass * 0.75D6 / (pi * radius(i) *radius(i) * radius(i)
     z           * ps * (1.0D0 - alpha * poros))
        total = total + number
        depth = radius(i) * (1.0D0 - gamma)
        pormass = mass * alpha * (1.0D0-poros) / (1.0D0 - alpha * poros)
        pmasstot = pmasstot + pormass
        write (4,45) radius(i),depth,number,mass,pormass
45      format (F10.6,4X,F10.6,3X,E11.5,5X,F11.4,9X,F11.4)
50    continue
      write (4,51) 'Totals:', total, masstot, pmasstot
51    format (/A,19X,E12.5,5X,F11.4,9X,F11.4/)

      write (4,52) 'Notes:  The Kp used as a search index in this',
     z ' optimization is the macroscopic','        value of the',
     z ' partition coefficient, the value that is normalized to',
     z '        the total particulate mass.'
52    format (/A,A/A,A/A)

      write (4,53) 'Each layer of the filter contains 1/',nlayer,
     z    ' of the total particulate mass.'
53    format (/A,I3,A/)

      write (*,54) 'Working . . .'
54    format (/A/)

c     Set the grid spacing.
      dx = (1.0D0 - gamma) / (grid - 1.0D0)
      do 60 i=1,nsizes
        f(i) = volfract(i) * bedmass * dx / (nlayer *
     z          ps * (1.0D0 - alpha * poros) * 1.0D12)
60    continue

      return
      end
```

```
c ***********************************************************************

      DOUBLE PRECISION FUNCTION FUNK(V)

c     This function will calculate data for the exchange of organic
c       compounds between particulate matter trapped on/in an air
c       sampling filter and the gas passing through that filter.
c       The mechanism for the exchange process is intraparticle
c       diffusion.  The following boundary conditions and
c       assumptions are made:

c       1.  Particles are spherical.
c       2.  Particles have a nonporous, nonsorbing inner core
c            surrounded by a porous, sorbing shell.  The percent
c            volume that is porous is set by the user.
c       3.  The bulk concentration of analyte in the gas phase is
c            uniform.
c       4.  Particles initially contain a uniform concentration of
c            analyte.
c       5.  Sorption is reversible and follows a linear isotherm,
c            defined as Kp = (F/TSP)/A.
c       6.  Kp and Deff are spatially invariant.
c       7.  Local equilibrium holds in the micropores of the particles.

c     This value which this function returns is the sum of the square
c       of the residuals between calculated and experimental results.
c       This sum is the function that must be minimized.

      real*8 A, alpha, Aout, bedmass, Blast, Deff, dt, dtinit, dtsave
      real*8 dx, epsilon, exchange, flag, flowrate, frac, gamma
      real*8 initmass, Kp, maxdt, pb, pmasstot, poros, ps, T4, test
      real*8 time, B(6,50), f(6), f2(6), MtMe(10), period(85), radius(6)
      real*8 rate(85), T1(6,50,3), T3(6,50), theta(6), tyme(10)
      real*8 u(60,6,51), ut(60,6,51), V(2), volfract(6)
      integer*4 i, j, n, grid, nlayer, nrates, nsizes, p, t

      Common /Param1/ A, alpha, bedmass, dtinit, initmass, maxdt
      Common /Param2/ MtMe, period, pmasstot, ps, rate, tyme
      Common /Param3/ volfract, nlayer, nrates
      Common /CRUN1/ dx, f, gamma, pb, poros, radius, grid, nsizes
      Common /CRUN2/ Deff, dt, epsilon, f2, flowrate
      Common /CRUN3/ Kp, T1, T3, T4, theta

      External CRUNCH
      External FLUSH

c     Explanation of variable names:
c     A is the influent analyte concentration in the air (ng/cu.m.).
c     alpha is the fraction of a particle's volume which is porous.
c     Aout is the conc. of analyte in the effluent gas (ng/cu.m.)
c     B(i,j) is the vector on the right hand side of the matrix equation
c     bedmass is the mass of particulate matter on the filter (ug).
c     Blast is the value of B for the last row.
c     Deff is the effective diffusion coefficient (sq.cm./sec.).
c     depth is the radial distance which is porous (um).
c     dt is the time interval between computations (minutes).
c     dtinit is the initial time step.
c     dtsave is a saved value of the time step (min).
c     dx is the dimensionless distance between grid points.
c     epsilon is Kp/(pb*1D12) + the sum of f2(i)*(grid-1).
c     exchange is the total amount of analyte mass exchanged between
c       the gas phase and the particulate phase at equilibrium (ng).
c     f(i) is f2(i) w/o the dependence on flowrate or dt.
c     f2(i) is volfract(i)*bedmass*dx/(nlayer*ps*(1-alpha*poros)
c       *1.0D12*flowrate*dt).
c     file1 is the name of the input file.
c     file2 is the name of the output file.
c     flowrate is the flowrate of air through the filter (cu.m./min).
c     frac is the fractional approach to equilibrium, Mt/Me.
```

```
c     gamma is a factor which is (1-alpha)**(1/3).  It is also equal
c       to the ratio:  radius of the inner core / particle radius.
c     grid is the number of grid points in each particle.
c     i is the index for the particle size fraction.
c     initmass is the mass of the analyte associated with the
c       particulate phase at the beginning of the simulation (ng).
c     j is the index for the grid point of interest.
c     Kp is the atmospheric partition coefficient.
c       Kp = (F/TSP)/A (cu.m./ug)
c     mass is the mass of particles of a particular size (ug).
c     masstot is the calculated value of bedmass (ug).  If there is
c       a difference between bedmass and masstot it is due to a
c       discrepancy in the values of volfract(i) such that they do not
c       sum to 1.0.
c     maxdt is the maximum time step allowed (min.)
c     n is the current layer of the filter.
c     name is the analyte name.
c     nlayer is the number of layers in the filter.
c     nrates is the number of flow rates used.
c     nsizes is the number of particle sizes.
c     number is the actual number of particles in a given size range.
c     p is the index for the time period.
c     pb is the estimated bulk density of the particles (g/cu.cm.).
c     period(p) is the time (minutes) at which the flow rate changes
c       from rate(p) to rate(p+1).
c     pi is the irrational number 3.14159.....
c     pmasstot is the total mass of porous material (ug).
c     pormass is the total mass of the porous fraction of all particles
c       having a certain size (ug).
c     poros is the porosity = 1 - pb/ps
c     ps is the dry sorbent density (g/cu.cm.)
c     radius(i) is the mean radius of a particle (um).
c     rate(p) is the flow rate (mL/min) for the time between period(p-1)
c       and period(p).
c     S is the total volumetric concentration of analyte in the
c       particulate phase (ng/cu.m.).
c     T1, T3, and T4 are the arrays which hold the coefficient
c       matrix and the L and U decompositions of that matrix.
c       T1(i,j) handles the tridiagonal part of the matrix.
c       T3 is the bottom row, except for the last column.
c       T4 is the coefficient in the last row, last column.
c     theta(i) is 2(delta x)**2/(delta tao)
c     time is in minutes.
c     total is the number of particles on the filter.
c     u(n,i,j) saves the values of ut(n,i,j).
c     ut(n,i,j) is the matrix of u values (u = x*S).
c     volfract(i) is the volume fraction of particles from the total
c       distribution which fall in the size range whose mean radius
c       is radius(i).  Data is in the file partdist.dat.
c     x is the dimensionless radial distance (=r/R)
c     test, etc. are all dummy variables which are used
c       to temporarily save values of interest.

c     Set the two values of interest.
      Kp = 10**V(1)
      Deff = 10**V(2)

c     The Kp used as a search index in this optimization is the macro-
c       scopic value of the partition coefficient, the value that is
c       normalized to the total particulate mass.
c     Calculate the microscopic value of Kp:
      Kp = Kp * (1.0D0 - alpha * poros) / (alpha * (1.0D0 - poros))

c     Initialize the ut array.  Recall that u=x*S.
c       u and ut are in units of ng/cu.m.
      Do 75 n = 1,nlayer
        Do 70 i = 1,nsizes
          Do 65 j = 1,grid
            ut(n,i,j) = (dx*(j-1)+gamma) *initmass *pb *1.0D12 /pmasstot
```

```
65        Continue
70      Continue
75    Continue

c     Initialize time, p, flowrate, frac, t, FUNK, dt, dtsave, exchange.
      time = 0.0D0
      p = 1
      flowrate = rate(1) / 1.0D6
      frac = 0.0D0
      t = 1
      FUNK = 0.0D0
      dt = dtinit
      if (dt .gt. period(1)) dt = period(1)
      if (dt .gt. maxdt) dt = maxdt
      dtsave = dt
      exchange = A * pmasstot * (Kp + poros / (pb * 1.0D12)) - initmass

c     Initialize epsilon, theta and f2(i).  Set up the coefficient
c       matrix and perform an L-U decomposition.
      CALL CRUNCH

c     Start the simulation.
80    Aout = A

c     Initialize the u array.
      do 105 n=1,nlayer
        do 100 i=1,nsizes
          do 90 j=1,grid
            u(n,i,j) = ut(n,i,j)
90        continue
100     continue
105   continue

c     Loop through each of the layers of the filter.
110   do 300 n = 1,nlayer

c       Loop through the particle size distribution.
c       Set up the B vector.
        do 130 i = 1,nsizes
          B(i,1) = (1.0D0 + (gamma-dx)/(gamma+dx)) * ut(n,i,2)
     z             - (2.0D0 - theta(i)) * ut(n,i,1)
          do 120 j = 2,(grid - 1)
            B(i,j) = ut(n,i,j-1)-(2-theta(i))*ut(n,i,j)+ut(n,i,j+1)
120       continue
130     continue
        Blast = Aout
        do 150 i = 1,nsizes
          Blast = Blast + f2(i) * (gamma * ut(n,i,1) + ut(n,i,grid))
          do 140 j = 2,(grid - 1)
            Blast = Blast + f2(i) * (dx * (j-1) + gamma)
     z              * (3 + (-1)**j) * ut(n,i,j)
140       continue
150     continue
        Blast = Blast / epsilon

c       Forward substitution:
        do 170 i = 1,nsizes
          ut(n,i,1) = B(i,1)
          do 160 j = 2,(grid-1)
            ut(n,i,j) = B(i,j) - T1(i,j,1) * ut(n,i,j-1)
160       continue
170     continue
        ut(n,1,grid) = Blast
        do 190 i = 1,nsizes
          do 180 j = 1,(grid-1)
            ut(n,1,grid) = ut(n,1,grid) - T3(i,j) * ut(n,i,j)
180       continue
190     continue
```

```
c       Backward substitution:
        ut(n,1,grid) = ut(n,1,grid) / T4
        do 210 i = nsizes,1,-1
          j = grid - 1
          ut(n,i,j) = (ut(n,i,j) + ut(n,1,grid)) / T1(i,j,2)
          do 200 j = (grid-2),1,-1
            ut(n,i,j) = (ut(n,i,j)-T1(i,j,3)*ut(n,i,j+1))/T1(i,j,2)
200       continue
210     continue

c       Calculate the bulk effluent concentration.
        Aout = ut(n,1,grid) / (poros + pb * Kp * 1.0D12)

c       Update the values of ut(n,i,grid).
        do 220 i = 2,nsizes
          ut(n,i,grid) = ut(n,1,grid)
220     continue
300   continue

c     Check the effect of the current time step.
      test = (A - Aout) * dt * flowrate / exchange
      if ((test .gt. 0.04) .and. (dt .gt. 0.000001)) then
        dt = dt / 1.5D0
        dtsave = dt
        Aout = A
        do 340 n=1,nlayer
          do 330 i=1,nsizes
            do 320 j=1,grid
              ut(n,i,j) = u(n,i,j)
320         continue
330       continue
340     continue
        CALL CRUNCH
        goto 110
      endif

c     Increment the time.
      time = time + dt

c     Update the fractional approach to equilibrium.
      frac = frac + ((A-Aout) * dt * flowrate) / exchange

      if (time .eq. tyme(t)) then
        FUNK = FUNK + (frac - MtMe(t))**2.0D0
        t = t + 1
      endif

      if (time .lt. period(nrates)) then
        flag = 0
        if (time .eq. period(p)) then
          p = p + 1
          flowrate = rate(p) / 1.0D6
          flag = 1
          dt = dtsave
        elseif ((test .lt. 0.001) .and. (dt .ne. maxdt)) then
          dt = dt * 1.5D0
          if (dt .gt. maxdt) dt = maxdt
          flag = 1
        endif
        dtsave = dt
        if ((time + dt) .gt. period(p)) then
          dt = period(p) - time
          flag = 1
        endif
        if (flag .eq. 1) CALL CRUNCH
        goto 80
      endif

c     Print the values to the output file.
```

```
      Write (4,400) 10**V(1), Kp, Deff, alpha, FUNK
400   Format (E12.5,4(1X,E12.5))
      Call FLUSH(4)

      return
      end

c *********************************************************************

      SUBROUTINE CRUNCH

c     Set up the coefficient matrix and perform an L-U decomposition.

      Real*8 Deff, dt, dx, epsilon, flowrate, gamma, Kp, pb, poros, T4
      Real*8 f(6), f2(6), radius(6), T1(6,50,3), T3(6,50), theta(6)
      Integer*4 i, j, grid, nsizes

      Common /CRUN1/ dx, f, gamma, pb, poros, radius, grid, nsizes
      Common /CRUN2/ Deff, dt, epsilon, f2, flowrate
      Common /CRUN3/ Kp, T1, T3, T4, theta

      epsilon = 1.0D0 / (pb * Kp * 1.0D12 + poros)
      do 668 i=1,nsizes
        f2(i) = f(i) / (flowrate * dt)
        epsilon = epsilon + f2(i)
        theta(i) = 2.0D0*dx*dx*radius(i)*radius(i) / (Deff*dt*6.0D9)
668   continue

      do 680 i=1,nsizes
        T1(i,1,1) = 0.0D0
        T1(i,1,2) = 2.0D0 + theta(i)
        T1(i,1,3) = -1.0D0 - (gamma - dx) / (gamma + dx)
        do 670 j = 2,(grid-2)
          T1(i,j,1) = -1.0D0
          T1(i,j,2) = 2.0D0 + theta(i)
          T1(i,j,3) = -1.0D0
670     continue
        T1(i,grid-1,1) = -1.0D0
        T1(i,grid-1,2) = 2.0D0 + theta(i)
        T1(i,grid-1,3) = 0.0D0
680   continue

      do 690 i = 1,nsizes
        T3(i,1) = f2(i) * gamma / epsilon
        do 685 j = 2,(grid-1)
          T3(i,j) = f2(i) * (dx*(j-1)+gamma) * (3+(-1)**j) / epsilon
685     continue
690   continue

c     L-U Decomposition:
c     Use Thomas Algorithm for T1.
      do 696 i=1,nsizes
        do 695 j = 2,(grid-1)
          T1(i,j,1) = T1(i,j,1) / T1(i,j-1,2)
          T1(i,j,2) = T1(i,j,2) - T1(i,j,1) * T1(i,j-1,3)
695     continue
696   continue

c     Decompose T3.
      do 701 i=1,nsizes
        T3(i,1) = T3(i,1) / T1(i,1,2)
        do 700 j = 2,(grid-1)
          T3(i,j) = (T3(i,j) - T3(i,j-1) * T1(i,j-1,3)) / T1(i,j,2)
700     continue
701   continue

c     Set up and decompose T4.
      T4 = 1.0D0
      do 705 i = 1,nsizes
```

```
        T4 = T4 + T3(i,grid-1)
705   continue

      return
      end

c *********************************************************************

      SUBROUTINE AMOEBA(P,Y,NDIM,FTOL,FUNC,ITER)

c     Multidimensional minimization of the function FUNC(X) where X is
c     an NDIM-dimensional vector, by the downhill simplex method of
c     Nelder and Mead.  Input is a matrix P whose NDIM+1 rows are NDIM-
c     dimensional vectors which are the vertices of the starting
c     simplex.  [Logical dimensions of P are P(NDIM+1,NDIM)].  Also
c     input is FTOL, the fractional convergence tolerance to be achieved
c     in the function value.  On output, P contains the coordinates of
c     NDIM+1 new points all within FTOL of a minimum function value, Y
c     contains the function values at those points, and ITER gives the
c     number of iterations taken.

      INTEGER*4 ITMAX, ND
      REAL*8 ALPHA, BETA, GAMMA
      PARAMETER (ALPHA=1.0, BETA=0.5, GAMMA=2.0, ITMAX=5000, ND=2)

c     ALPHA, BETA, and GAMMA are three parameters which define the
c     expansions and contractions.  ITMAX is the maximum allowed number
c     of iterations.  ND is the number of dimensions.  This is awkward,
c     but I want to try to match array sizes on function calls.

      INTEGER*4 I, IHI, ILO, INHI, ITER, J, MPTS, NDIM
      REAL*8 FTOL, FUNC, P(NDIM+1,NDIM), PBAR(ND), PR(ND), PRR(ND)
      REAL*8 RTOL, Y(NDIM+1), YPR, YPRR
      EXTERNAL FUNC

      MPTS=NDIM+1
      ITER=0

c     Evaluate the function FUNC at each of the vertices.

      DO 8 I=1,MPTS
        DO 7 J=1,NDIM
          PR(J)=P(I,J)
7       CONTINUE
        Y(I)=FUNC(PR)
8     CONTINUE

c     First, determine which point has the highest (worst) value,
c     the next-highest, and the lowest (best) value by looping over the
c     points in the simplex.

10    ILO=1
      IF (Y(1).GT.Y(2)) THEN
        IHI=1
        INHI=2
      ELSE
        IHI=2
        INHI=1
      ENDIF
      DO 20 I=1,MPTS
        IF (Y(I).LT.Y(ILO)) ILO=I
        IF (Y(I).GT.Y(IHI)) THEN
          INHI=IHI
          IHI=I
        ELSE IF (Y(I).GT.Y(INHI)) THEN
          IF (I.NE.IHI) INHI=I
        ENDIF
20    CONTINUE
```

```
c     Compute the fractional range from highest to lowest and return
c     if satisfactory.

      RTOL=2.0D0*ABS(Y(IHI)-Y(ILO))/(ABS(Y(IHI))+ABS(Y(ILO)))
      IF (RTOL.LT.FTOL) RETURN

      IF (ITER.EQ.ITMAX) THEN
        WRITE (*,*) 'Amoeba exceeding maximum iterations.'
        RETURN
      ENDIF

c     Begin a new iteration.  Compute the vector average of all points
c     except the highest, i.e. the center of the "face" of the simplex
c     across from the high point.  We will subsequently explore along
c     the ray from the high point through that center.

      ITER=ITER+1
      DO 30 J=1,NDIM
        PBAR(J)=0.0D0
30    CONTINUE
      DO 50 I=1,MPTS
        IF (I.NE.IHI) THEN
          DO 40 J=1,NDIM
            PBAR(J)=PBAR(J)+P(I,J)
40        CONTINUE
        ENDIF
50    CONTINUE

c     Extrapolate by a factor ALPHA through the face, i.e. reflect the
c     simplex from the high point.

      DO 60 J=1,NDIM
        PBAR(J)=PBAR(J)/NDIM
        PR(J)=(1.+ALPHA)*PBAR(J)-ALPHA*P(IHI,J)
60    CONTINUE

c     Evaluate the function at the reflected point.

      YPR=FUNC(PR)
      IF (YPR.LE.Y(ILO)) THEN

c       Gives a result better than the best point, so try an additional
c       extrapolation by a factor GAMMA.

        DO 70 J=1,NDIM
          PRR(J)=GAMMA*PR(J)+(1.-GAMMA)*PBAR(J)
70      CONTINUE

c       ... and check out the function there.

        YPRR=FUNC(PRR)
        IF (YPRR.LT.Y(ILO)) THEN

c         The additional extrapolation succeeded, and the high point
c         is replaced.

          DO 80 J=1,NDIM
            P(IHI,J)=PRR(J)
80        CONTINUE
          Y(IHI)=YPRR
        ELSE

c         The additional extrapolation failed, but we can still use
c         the reflected point.

          DO 90 J=1,NDIM
            P(IHI,J)=PR(J)
90        CONTINUE
          Y(IHI)=YPR
```

```
        ENDIF
      ELSEIF (YPR.GE.Y(INHI)) THEN

c     The reflected point is worse than the second-highest.

        IF (YPR.LT.Y(IHI)) THEN

c         If it's better than the highest, then replace the highest.

          DO 100 J=1,NDIM
            P(IHI,J)=PR(J)
100       CONTINUE
          Y(IHI)=YPR
        ENDIF

c       Look for an intermediate lower point.  In other words, perform
c       a contraction of the simplex along one dimension.  Then evaluate
c       the function.

        DO 110 J=1,NDIM
          PRR(J)=BETA*P(IHI,J)+(1.-BETA)*PBAR(J)
110     CONTINUE
        YPRR=FUNC(PRR)

        IF (YPRR.LT.Y(IHI)) THEN

c         Contraction gives an improvement, so accept it.

          DO 120 J=1,NDIM
            P(IHI,J)=PRR(J)
120       CONTINUE
          Y(IHI)=YPRR

        ELSE

c         Can't seem to get rid of that high point.  Better contract
c         around the lowest (best) point.

          DO 140 I=1,MPTS
            IF (I.NE.ILO) THEN
              DO 130 J=1,NDIM
                PR(J)=0.5*(P(I,J)+P(ILO,J))
                P(I,J)=PR(J)
130           CONTINUE
              Y(I)=FUNC(PR)
            ENDIF
140       CONTINUE
        ENDIF

      ELSE

c       We arrive here if the original reflection gives a middling
c       point.  Replace the old high point and continue.

        DO 150 J=1,NDIM
          P(IHI,J)=PR(J)
150     CONTINUE
        Y(IHI)=YPR
      ENDIF
      GOTO 10

      END
```

APPENDIX C

Aqueous Adsorption Experiments Data

Experimental data obtained from the aqueous adsorption studies (Chapter Five) are presented in this appendix. Data are given as both C (ng/mL) and C/C_o versus time (min). Tables C.1 through C.4 are for 1,2-dichlorobenzene; C.5 through C.8 are for 1,2,4-trichlorobenzene; C.9 through C.12 are for 1,2,4,5-tetrachlorobenzene. The first two tables for each compound present the data from experiments run at 34°C; the last two give the data for experiments run at 4°C. Odd numbered tables present data from experiments that used the large particle size fraction. Even numbered tables give the data from those that used the small particle size fraction.

Table C.1. Adsorption Data: 1,2-dichlorobenzene, 34°C, large beads.

time (min)	C/C_o	C (ng/mL)
18	1.0167	0.2554
25	0.9837	0.2471
35	0.9699	0.2436
50	0.9535	0.2395
70	0.9105	0.2287
100	0.8770	0.2203
150	0.8177	0.2054
210	0.7424	0.1865
300	0.6593	0.1656
450	0.5973	0.1500
670	0.5046	0.1268
1425	0.3393	0.0852
1845	0.2706	0.0680
2895	0.2451	0.0616
5835	0.2321	0.0583
10408	0.2312	0.0581
39095	0.2298	0.0577
49244	0.2173	0.0546

Table C.2. Adsorption Data: 1,2-dichlorobenzene, 34°C, small beads.

time (min)	C/C_o	C (ng/mL)
6	1.0383	0.2608
10	0.9235	0.2320
15	0.9177	0.2305
25	0.9000	0.2261
37	0.8617	0.2165
50	0.8447	0.2122
70	0.7962	0.2000
100	0.7750	0.1947
150	0.6884	0.1729
212	0.6129	0.1540
300	0.5369	0.1349
450	0.4616	0.1160
630	0.4082	0.1026
1440	0.2724	0.0684
1830	0.2513	0.0631
2975	0.2268	0.0570
4420	0.2108	0.0530
6005	0.2231	0.0561
33175	0.2176	0.0547
46166	0.2111	0.0530

Table C.3. Adsorption Data: 1,2-dichlorobenzene, 4°C, large beads.

time (min)	C/C_o	C (ng/mL)
5	0.9525	0.2359
9	1.0222	0.2532
13	1.0670	0.2643
18	0.8958	0.2219
25	0.9733	0.2411
35	0.9297	0.2303
50	0.9622	0.2383
70	0.9429	0.2336
100	0.8978	0.2224
160	0.8439	0.2090
220	0.8080	0.2001
300	0.7389	0.1830
450	0.6712	0.1663
720	0.5750	0.1424
1475	0.3274	0.0811
2970	0.2289	0.0567
4565	0.1716	0.0425
6030	0.1455	0.0361
8735	0.1289	0.0319
13415	0.1061	0.0263
21835	0.0799	0.0198
31755	0.0754	0.0187
41815	0.0762	0.0189

Table C.4. Adsorption Data: 1,2-dichlorobenzene, 4°C, small beads.

time (min)	C/C_o	C (ng/mL)
9	0.9557	0.2367
13	0.9598	0.2377
18	0.9382	0.2324
25	0.9666	0.2394
35	0.9380	0.2323
50	0.9564	0.2369
70	0.9087	0.2251
100	0.8710	0.2157
150	0.8336	0.2065
210	0.7742	0.1918
300	0.7049	0.1746
450	0.6025	0.1493
654	0.4843	0.1200
1440	0.2583	0.0640
1860	0.1946	0.0482
3275	0.1365	0.0338
6165	0.0992	0.0246
8880	0.0858	0.0212
14580	0.0859	0.0213
23045	0.0953	0.0236

Table C.5. Adsorption Data:
1,2,4-trichlorobenzene, 34°C, large beads.

time (min)	C/C_o	C (ng/mL)
70	0.6991	0.1890
100	0.6895	0.1864
151	0.5776	0.1561
210	0.5291	0.1430
302	0.4273	0.1155
420	0.3701	0.1001
600	0.2898	0.0784
1330	0.1420	0.0384
1775	0.1447	0.0391
3025	0.1267	0.0342
4725	0.1067	0.0289
7200	0.0747	0.0202
10320	0.1052	0.0284
12950	0.0858	0.0232
17520	0.0927	0.0251
41885	0.0976	0.0264

Table C.6. Adsorption Data:
1,2,4-trichlorobenzene, 34°C, small beads.

time (min)	C/C_o	C (ng/mL)
35	0.6489	0.1754
50	0.5985	0.1618
70	0.5224	0.1412
100	0.4700	0.1271
150	0.3525	0.0953
223	0.2855	0.0772
300	0.2405	0.0650
420	0.1854	0.0501
660	0.1523	0.0412
1458	0.1026	0.0277
1830	0.1107	0.0299
3153	0.0933	0.0252
4470	0.0746	0.0202
5945	0.0805	0.0218
9030	0.0729	0.0197
11883	0.0845	0.0229
17503	0.0818	0.0221
27455	0.0765	0.0207
39263	0.0750	0.0203

Table C.7. Adsorption Data: 1,2,4-trichlorobenzene, 4°C, large beads.

time (min)	C/C_o	C (ng/mL)
5	0.9838	0.2641
9	0.9760	0.2621
13	0.9522	0.2557
18	0.9701	0.2605
25	0.9691	0.2602
35	0.9243	0.2482
50	0.9126	0.2450
70	0.8983	0.2412
100	0.8836	0.2372
150	0.7970	0.2140
210	0.7826	0.2101
300	0.6979	0.1874
420	0.6192	0.1662
715	0.4451	0.1195
1452	0.2441	0.0655
1692	0.2022	0.0543
1980	0.1660	0.0446
3045	0.1156	0.0310
4950	0.0788	0.0212
7730	0.0740	0.0199
12262	0.0640	0.0172
18922	0.0647	0.0174
49352	0.0629	0.0169

Table C.8. Adsorption Data: 1,2,4-trichlorobenzene, 4°C, small beads.

time (min)	C/C_o	C (ng/mL)
5	1.0579	0.2840
9	0.9774	0.2624
13	0.9749	0.2617
18	0.9351	0.2511
25	0.9415	0.2528
35	0.9067	0.2434
50	0.8628	0.2317
70	0.8338	0.2239
100	0.8212	0.2205
151	0.7759	0.2083
210	0.7074	0.1899
300	0.5927	0.1591
420	0.5056	0.1357
720	0.3372	0.0905
1500	0.1551	0.0416
1920	0.1203	0.0323
2985	0.0816	0.0219
4465	0.0751	0.0202
5850	0.0671	0.0180
13385	0.0673	0.0181
18865	0.0675	0.0181
26275	0.0680	0.0183

Table C.9. Adsorption Data: 1,2,4,5-tetrachlorobenzene, 34°C, large beads.

time (min)	C/C_o	C (ng/mL)
9	0.8885	0.2397
13	0.8600	0.2320
18	0.8338	0.2249
25	0.8274	0.2232
35	0.8285	0.2235
50	0.7542	0.2035
70	0.7171	0.1935
100	0.6668	0.1799
160	0.5922	0.1598
220	0.4974	0.1342
305	0.4375	0.1180
455	0.3011	0.0812
720	0.2085	0.0563
1410	0.0849	0.0229
1825	0.0644	0.0174
3210	0.0480	0.0130
4605	0.0384	0.0104
6080	0.0274	0.0074
8905	0.0298	0.0080
13653	0.0309	0.0083
18810	0.0219	0.0059
26260	0.0217	0.0059
34800	0.0173	0.0047
46110	0.0153	0.0041
54895	0.0184	0.0050

Table C.10. Adsorption Data: 1,2,4,5-tetrachlorobenzene, 34°C, small beads.

time (min)	C/C_o	C (ng/mL)
13	0.9109	0.1427
18	0.9193	0.1440
25	0.9616	0.1507
35	0.8907	0.1396
50	0.8600	0.1348
70	0.7801	0.1222
100	0.7422	0.1163
150	0.6015	0.0942
210	0.4807	0.0753
300	0.3749	0.0587
450	0.2510	0.0393
655	0.1702	0.0267
1400	0.0756	0.0118
1885	0.0609	0.0095
2915	0.0453	0.0071
4395	0.0351	0.0055
5860	0.0318	0.0050
8840	0.0214	0.0034
12955	0.0247	0.0039
18780	0.0227	0.0036
34695	0.0242	0.0038
44690	0.0202	0.0032

Table C.11. Adsorption Data: 1,2,4,5-tetrachlorobenzene, 4°C, large beads.

time (min)	C/C_o	C (ng/mL)
13	1.0454	0.1613
18	1.0176	0.1570
25	1.0548	0.1627
35	0.9994	0.1542
50	1.0447	0.1612
70	1.0205	0.1574
100	1.0432	0.1609
150	0.8872	0.1369
210	0.8473	0.1307
300	0.7688	0.1186
450	0.6621	0.1021
660	0.5540	0.0855
1395	0.2282	0.0352
1890	0.1292	0.0199
2965	0.0735	0.0113
4355	0.0416	0.0064
5755	0.0367	0.0057
8730	0.0240	0.0037
13060	0.0209	0.0032
18805	0.0182	0.0028
24590	0.0158	0.0024
34635	0.0168	0.0026
44925	0.0180	0.0028

Table C.12. Adsorption Data: 1,2,4,5-tetrachlorobenzene, 4°C, small beads.

time (min)	C/C_o	C (ng/mL)
14	0.9789	0.1510
19	0.9504	0.1466
25	0.9827	0.1516
35	0.9983	0.1540
50	0.9500	0.1466
70	0.9527	0.1470
100	0.8993	0.1387
150	0.8039	0.1240
210	0.7427	0.1146
300	0.6186	0.0954
450	0.4878	0.0753
660	0.3761	0.0580
1400	0.1058	0.0163
1870	0.0798	0.0123
2930	0.0416	0.0064
4410	0.0290	0.0045
5850	0.0244	0.0038
8670	0.0168	0.0026
13005	0.0150	0.0023
18755	0.0164	0.0025
24580	0.0172	0.0027
34865	0.0183	0.0028
44940	0.0171	0.0026

APPENDIX D

Aqueous Adsorption Experiments Computer Programs

Five of the computer programs used to model the aqueous sorption kinetics discussed in Chapter Five are listed in this appendix. The programs are: *AQFRES* for the first order reaction model (external film diffusion model), *AQABRES* for the first order particle abrasion model, *DIFFUSE9* for the intraparticle diffusion model, *AQBRES* for the coupled intraparticle diffusion and particle abrasion model, and *DUALDIFF* for the coupled external film diffusion and intraparticle diffusion model. Each of these programs calculate C (ng/mL), S (ng/g), and C/C_o versus time (min) when given a set of input data. Not included in this appendix are the corresponding one- or two-parameter search routines that were used to find best-fit values of the appropriate kinetic parameter(s) from each model. Those search routines are readily available elsewhere and were referenced in Chapter Five.

Each of these programs were written in FORTRAN. The analytical models (*AQFRES, AQABRES, DIFFUSE9,* and *DUALDIFF*) were compiled and run on a personal computer using the Microsoft FORTRAN Compiler (v. 4.01). Due to enormous memory requirements and speed considerations, the numerical model (*AQBRES*) was compiled and run on an IBM RISC System/6000 workstation (model 320). All input is read from files. Each program requires a general input file for parameters such as the partition coefficient and the mass

of sorbent. In addition, a separate file containing experimental concentration data is needed for all programs except *DIFFUSE9*. That intraparticle diffusion program was not used for fitting experimental data; *AQBRES* was used for that purpose (w/ k_{ab} = 0). The numerical model *AQBRES* is the only one of these models that was designed to use a polydisperse particle size distribution; the particle number distribution is read in from another file. Note that the number of nodes/particle in *AQBRES* must be an odd number for the numerical integration to be performed accurately. Each program is thoroughly commented; I/O should be self-explanatory.

First Order Reaction Model

```
      PROGRAM AQFRES
c
c     This program will calculate first order uptake data for
c       organic compounds into particles in water.
c
c     The bulk concentration of analyte in the aqueous phase is
c       uniform.
c     Particles initially contain a uniform concentration of analyte.
c     Sorption is reversible and follows a linear isotherm.
c
c     This program will read in experimental data and calculate
c       the sum of the squared residuals between the calculated and
c       the experimental data.  The format of that file is:
c         time, aqueous concentration, volume withdrawn, code
c       time is in minutes, concentration is in ng/mL, volume is in
c         mL, and code tells whether or not the point will be used
c         or ignored in the computation of the residual (0 = ignore,
c         1 = use).
c       The number of points is noted on the first line of the file.
c
c     This version also can account for some sorption to the reaction
c       vessel, using instantaneous equilibrium denoted by
c           Krv = Mrv / C
c       Mrv is the mass of analyte sorbed to the reaction vessel.
c       Krv has units of volume.  Krv=0 for no sorption to the vessel.
c
      real*8 beadmass, C, Ci, Cinit, Csorb, expo, factor, index, K, Krv
      real*8 k1, oldt, Resid, S, Si, spike, time, Conc(2,26), tyme(26)
      integer*4 code(26), i, j, t, npts, volinit, volume, volsamp(26)
      character*12 datfile, in1, name*40, out1
c
c     Explanation of variable names:
c     beadmass is the mass of sorbent (g).
c     C is the analyte concentration in the water (ng/ml).
c     code() is a code used in the calculation of the residual.
c       code() = 0 means ignore the point, 1 means use the point.
c     Csorb is the uniform analyte concentration initially in the
c       particles -->> S=function(Csorb).
c     Conc() is the array which holds the experimental
c       concentrations that are compared.
c     datfile is the file containing the experimental data.
c     in1 is the primary input file.
c     K is the aqueous partition coefficient.  K = S/C, (ml/g)
```

```
c     Krv is the partition coefficient for the reaction vessel.
c       Krv = Mrv / C, (mL)
c     name is the analyte name.
c     npts is the number of experimental points.
c     out1 is the name of the output file.
c     spike is the initial spike of analyte (ng).
c     time is in minutes.
c     tyme() is an array holding the times of experimental interest.
c     volinit is the initial volume of the reaction (mL).
c     volsamp() is the volume removed from the vessel for sampling (mL).
c     volume is the volume of aqueous solution (mL).
c
c     Title.
      Write (*,10) 'AQFRES','First Order Sorption Kinetics',
     z  'Stewart A. Rounds','March 9, 1992'
10    Format (37X,A/26X,A/32X,A/34X,A//)
c
c     Read in the input values.
      Write (*,20) ' name of input file:  '
      Read (*,20) in1
20    Format (A)
c
      open (1,file=in1)
      Read (1,20) name
      Read (1,*) k1
      Read (1,*) K
      Read (1,*) spike
      Read (1,*) beadmass
      Read (1,*) volinit
      Read (1,*) Krv
      Read (1,*) Csorb
      Read (1,20) datfile
      Read (1,20) out1
      close (1)
c
c     Read in the experimental data.
      open (3,file=datfile)
      read (3,*) npts
      do 27 i=1,npts
        read (3,*) tyme(i), Conc(1,i), volsamp(i), code(i)
27    continue
      close (3)
c
c     Initialize.
      t = 1
      Cinit = spike / (volinit + Krv)
      oldt = 0.0D0
      Ci = Cinit
      Si = K * Csorb
      volume = volinit
      Resid = 0.0D0
c
c     Print the relevant data to a file.
      open (4,file=out1)
c
      Write (4,20) name
      Write (4,31) 'macroscopic K = ',K,' ml/g'
      Write (4,31) 'first order reaction rate = ',k1,' /min'
      Write (4,31) 'spike = ',spike,' ng'
      Write (4,33) 'mass of beads = ',beadmass,' g'
      Write (4,36) 'initial volume = ',volinit,' ml'
      Write (4,31) 'solids concentration = ',beadmass/volinit,' g/ml'
      Write (4,31) 'K(reaction vessel) = ',Krv,' mL'
      Write (4,31) 'Cinit = ',Cinit,' ng/ml'
      Write (4,31) 'Csorb = ',Csorb,' ng/ml'
      Write (4,30) 'file for experimental data = ',datfile
30    Format (A,A)
31    Format (A,E12.6,A)
33    Format (A,F8.5,A)
```

```
36    Format (A,I5,A)
c
      write (*,54) ' Working . . .'
54    format (/A/)
      write (4,64) '   Time (min)       C (ng/ml)',
     z             '       S (ng/g)          C/Co'
64    format (/A,A/)
c
c     Start the simulation.
      index = -0.02
80    index = index + 0.02
      time = 10**index
      if (time .gt. tyme(t)) then
        time = tyme(t)
        index = log10(time)
      endif
c
      factor = volume + Krv + beadmass * K
      expo = -k1 * factor * (time - oldt) / (volume + Krv)
      C = beadmass * Si + (volume + Krv) * Ci
      C = C + beadmass * (K * Ci - Si) * dexp(expo)
      C = C / factor
      S = Si + (volume + Krv) * (Ci - C) / beadmass
c
      write (4,150) time, C, S, C/Cinit
150   format (2X,3(E12.6,4X),E12.6)
c
      if (time .eq. tyme(t)) then
        if (code(t) .gt. 0.5) then
          Resid = Resid + (C - Conc(1,t))**2.0D0
        endif
        Conc(2,t) = C
        volume = volume - volsamp(t)
        t = t + 1
        oldt = time
        Ci = C
        Si = S
      endif
c
      if (time .lt. tyme(npts)) goto 80
c
      Write (4,500) 'Data Comparison:',
     z   'Time (min)     Conc. (expt)     Conc. (calc)     Code'
500   Format (//A//A)
      Write (4,510) (tyme(j), (Conc(i,j), i=1,2), code(j), j=1,npts)
510   Format (F10.2,5X,E12.6,5X,E12.6,6X,I1)
      Write (4,520) 'Code:  0 = ignore, 1 = use',
     z   'Sum of squared residuals = ', Resid
520   Format (/A/A,E16.9)
c
      close (4)
      end
```

First Order Particle Abrasion Model

```
      PROGRAM AQABRES
c
c     This program will calculate first order uptake data for
c       organic compounds into particles in water.
c
c       The bulk concentration of analyte in the aqueous phase is
c         uniform.
c       Particles initially contain a uniform concentration of analyte.
c       Sorption is reversible and follows a linear isotherm.
c
c     This program will read in experimental data and calculate
c       the sum of the squared residuals between the calculated and
c       the experimental data.  The format of that file is:
c         time, aqueous concentration, volume withdrawn, code
c       time is in minutes, concentration is in ng/mL, volume is in
c         mL, and code tells whether or not the point will be used
c         or ignored in the computation of the residual (0 = ignore,
c         1 = use).
c       The number of points is noted on the first line of the file.
c
c     This version also can account for some sorption to the reaction
c       vessel, using instantaneous equilibrium denoted by
c           Krv = Mrv / C
c       Mrv is the mass of analyte sorbed to the reaction vessel.
c       Krv has units of volume.  Krv=0 for no sorption to the vessel.
c
      real*8 beadmass, C, Ci, Cinit, Csorb, f, index, K, kab, Krv, oldf
      real*8 oldt, Resid, S, So, spike, time, Conc(2,26), tyme(26)
      integer*4 code(26), i, j, t, npts, volinit, volume, volsamp(26)
      character*12 datfile, in1, name*40, out1
c
c     Explanation of variable names:
c     beadmass is the mass of sorbent (g).
c     C is the analyte concentration in the water (ng/ml).
c     code() is a code used in the calculation of the residual.
c       code() = 0 means ignore the point, 1 means use the point.
c     Csorb is the uniform analyte concentration initially in the
c       particles -->> S=function(Csorb).
c     Conc() is the array which holds the experimental
c       concentrations that are compared.
c     datfile is the file containing the experimental data.
c     in1 is the primary input file.
c     K is the aqueous partition coefficient.  K = S/C, (ml/g)
c     Krv is the partition coefficient for the reaction vessel.
c       Krv = Mrv / C, (mL)
c     name is the analyte name.
c     npts is the number of experimental points.
c     out1 is the name of the output file.
c     spike is the initial spike of analyte (ng).
c     time is in minutes.
c     tyme() is an array holding the times of experimental interest.
c     volinit is the initial volume of the reaction (mL).
c     volsamp() is the volume removed from the vessel for sampling (mL).
c     volume is the volume of aqueous solution (mL).
c
c     Title.
      Write (*,10) 'AQABRES','First Order Abrasion Kinetics',
     z  'Stewart A. Rounds','March 5, 1992'
10    Format (37X,A/26X,A/32X,A/34X,A//)
c
c     Read in the input values.
      Write (*,20) ' name of input file:  '
      Read (*,20) in1
20    Format (A)
c
      open (1,file=in1)
      Read (1,20) name
```

```
      Read (1,*) kab
      Read (1,*) K
      Read (1,*) spike
      Read (1,*) beadmass
      Read (1,*) volinit
      Read (1,*) Krv
      Read (1,*) Csorb
      Read (1,20) datfile
      Read (1,20) out1
      close (1)
c
c     Read in the experimental data.
      open (3,file=datfile)
      read (3,*) npts
      do 27 i=1,npts
        read (3,*) tyme(i), Conc(1,i), volsamp(i), code(i)
27    continue
      close (3)
c
c     Initialize.
      t = 1
      Cinit = spike / (volinit + Krv)
      oldt = 0.0D0
      Ci = Cinit
      So = K * Csorb
      volume = volinit
      Resid = 0.0D0
c
c     Print the relevant data to a file.
      open (4,file=out1)
c
      Write (4,20) name
      Write (4,31) 'macroscopic K = ',K,' ml/g'
      Write (4,31) 'first order abrasion rate = ',kab,' /min'
      Write (4,31) 'spike = ',spike,' ng'
      Write (4,33) 'mass of beads = ',beadmass,' g'
      Write (4,36) 'initial volume = ',volinit,' ml'
      Write (4,31) 'solids concentration = ',beadmass/volinit,' g/ml'
      Write (4,31) 'K(reaction vessel) = ',Krv,' mL'
      Write (4,31) 'Cinit = ',Cinit,' ng/ml'
      Write (4,31) 'Csorb = ',Csorb,' ng/ml'
      Write (4,30) 'file for experimental data = ',datfile
30    Format (A,A)
31    Format (A,E12.6,A)
33    Format (A,F8.5,A)
36    Format (A,I5,A)
c
      write (*,54) ' Working . . .'
54    format (/A/)
      write (4,64) '   Time (min)       C (ng/ml)',
     z             '       S (ng/g)          C/Co'
64    format (/A,A/)
c
c     Start the simulation.
      index = -0.02
80    index = index + 0.02
      time = 10**index
      if (time .gt. tyme(t)) then
        time = tyme(t)
        index = log10(time)
      endif
c
      oldf = volume +Krv +beadmass *K *(1.0D0 -dexp(-3.0D0*kab*oldt))
      f = volume +Krv +beadmass *K *(1.0D0 -dexp(-3.0D0 *kab *time))
      C = beadmass *So*(dexp(-3.0D0*kab*oldt) -dexp(-3.0D0*kab*time))
      C = (C + Ci * oldf) / f
      S = K * C + (So - K * C) * dexp(-3.0D0 * kab * time)
c
      write (4,150) time, C, S, C/Cinit
```

```
150   format (2X,3(E12.6,4X),E12.6)
c
      if (time .eq. tyme(t)) then
        if (code(t) .gt. 0.5) then
          Resid = Resid + (C - Conc(1,t))**2.0D0
        endif
        Conc(2,t) = C
        volume = volume - volsamp(t)
        t = t + 1
        oldt = time
        Ci = C
      endif
c
      if (time .lt. tyme(npts)) goto 80
c
      Write (4,500) 'Data Comparison:',
     z   'Time (min)     Conc. (expt)     Conc. (calc)     Code'
500   Format (//A//A)
      Write (4,510) (tyme(j), (Conc(i,j), i=1,2), code(j), j=1,npts)
510   Format (F10.2,5X,E12.6,5X,E12.6,6X,I1)
      Write (4,520) 'Code:  0 = ignore, 1 = use',
     z   'Sum of squared residuals = ', Resid
520   Format (/A/A,E16.9)
c
      close (4)
      end
```

Analytical Intraparticle Diffusion Model

```
      Program DIFFUSE9
c
c     This program will calculate uptake data for the intraparticle
c     diffusion of organic compounds into spherical particles which are
c     suspended in a well-stirred solution.
c
c     Assumptions of model:
c      1.  Particles are spherical.
c      2.  Particles are internally homogeneous.
c      3.  Concentration of solute in the bulk solution is always
c          uniform.
c      4.  Particles are initially free of solute.
c      5.  Particles are all of the same size.
c      6.  The partition coefficient and the effective diffusion
c          coefficient are spatially invariant.
c      7.  Sorption is controlled by linear isotherms.
c      8.  Sorption is reversible.
c      9.  Within the particles, local equilibrium holds.
c
c     The analytical solution used here can be found in:
c      Crank, J., The Mathematics of Diffusion, 2nd ed., Clarendon
c        Press, Oxford, 93-96 (1975).
c
      real*8 alpha, beta, C, Co, Kp, q(0:200)
      real*8 S, solids, time
      real*8 q1, q2, q3, test, pi, diff1, diff2, fraction, nexterm
      real*8 gam1, gam2, eerfc, x, funct
      integer i,j
      character name*50, in1*12, out1*12
c
c     Define variables:
c     alpha is a dimensionless constant equal to 1/(solids * Kp).
c     beta is Deff/radius^2 (1/min)
c     C is the aqueous conc. of solute, ng/ml.
c     Co is the initial aqueous conc. of solute, ng/ml.
c     Deff is the effective diffusion coefficient, cm^2/sec.
c     fraction is Mt/Me.
c     Kp is the partition coefficient (ml/g).
c     pi is the irrational number pi.
c     q(i) are the roots of the equation:
c       tan(q(i)) = (3 * q(i)) / (3 + alpha * q(i) * q(i))
c     radius is the particle radius, cm.
c     S is the sorbed conc. of solute, ng/g.
c     solids is the sorbent to water ratio (g/ml).
c     time is the time of simulation, minutes.
c
      pi = 2*dacos(0.0D0)
c
c     Read in the needed parameters from the user.
      Write(*,10) 'DIFFUSE9','Analytical Solution for Intraparticle',
     z  ' Diffusion','Monodisperse Particle Size Distribution',
     z  'Stewart A. Rounds','March 10, 1992'
10    format(///32X,A//12X,A,A/16X,A//27X,A/28X,A//)
c
      Write(*,20) 'Name of input file:  '
20    format(1X,A\)
      Read(*,25) in1
25    format (A)
c
      open (1,file=in1)
      Read (1,25) name
      Read (1,*) Co
      Read (1,*) Kp
      Read (1,*) beta
c     beta = Deff/(radius*radius) in units of 1/min.
      Read (1,*) solids
      Read (1,25) out1
```

```
      close (1)
c
      time = 1.0D0
      alpha = 1.0/(solids*Kp)
      gam1 = (dsqrt(1.0D0 + 4.0D0*alpha/3.0D0) + 1.0D0)/2.0D0
      gam2 = gam1 - 1.0D0
c
      open (6,file=out1)
c
c     Write input data to the output file:
      Write(6,105) name
105   format(1X,A)
      Write(6,106) 'Initial concentration:  ',Co,' ng/ml'
106   format(1X,A,F10.5,A)
      Write(6,107) 'Partition coefficient:  ',Kp,' ml/g'
107   format(1X,A,F10.1,A)
      Write(6,108) 'Deff / (radius squared):  ',beta,' /min'
108   format(1X,A,D11.4,A)
      Write(6,109) 'Sorbent to water ratio:  ',solids,' g/ml'
109   format(1X,A,F11.8,A)
      Write(6,110) 'alpha = 1/(solids*Kp) = ',alpha
110   format(1X,A,F11.8)
c
      Write(6,112) 'Intraparticle Diffusion Model:  Analytical Solution'
112   format(/1X,A/)
      Write(6,115) 'Time (min.)','C (ng/ml)','S (ng/g)','C/Co','Mt/Me'
115   format(/4X,A,5X,A,6X,A,6X,A,7X,A/)
      Write(6,117) (time - time), Co
117   format(1X,F15.3,3X,F11.5)
c
      Write(*,120) 'Working . . . '
120   format(/1X,A/)
      q(0)=1
      do 300 i=1,200
        q1 = q(i-1) + pi
c
        do 200 j=1,1000
          q2 = q1
          diff1 = 3 * q1 / (3 + alpha * q1 * q1) - dtan(q1)
          if (j .eq. 1) then
            diff2 = diff1
            q3 = q2
            q1 = q1 + 0.2
          else
            q1 = q2 - (diff1 * (q3 - q2)) / (diff2 - diff1)
c
c         this is the secant method of linear extrapolation
c
          endif
          test = dabs(q1 - q2)
          if (test .lt. 1.0E-11) goto 250
          if (dabs(diff2) .gt. dabs(diff1)) then
            diff2 = diff1
            q3 = q2
          endif
200       continue
250     q(i)=q1
        Write(*,275) 'Root number = ',i
275     format('+',A,I3)
300     continue
c
      do 500 i=1,1E5
        fraction = 1.0D0
        do 400 j=1,201
          if (j .NE. 201) then
            nexterm = (dexp(-beta*q(j)*q(j)*time)*6*alpha*
     z          (alpha+1))/(9+9*alpha+q(j)*q(j)*alpha*alpha)
            fraction = fraction - nexterm
            test = nexterm/fraction
```

```
            if (test .lt. 1E-7) goto 410
          else
            x = 3.0D0 * gam1 * dsqrt(beta * time) / alpha
            funct = eerfc(x)
            fraction = 1.0D0 - gam1 * funct / (gam1 + gam2)
            x = -3.0D0 * gam2 * dsqrt(beta * time) / alpha
            funct = eerfc(x)
            fraction = (fraction - gam2 * funct / (gam1 + gam2))
     z         * (1.0D0 + alpha)
          endif
400       continue
c
410     C = Co * (1.0D0 - fraction + fraction/(1.0D0 + solids*Kp))
        S = (Co - C)/solids
        write (*,424) 'time = ',time,' minutes   Mt/Me = ',fraction
        write (6,460) time, C, S, C/Co, fraction
424     format ('+',A,F15.3,A,F10.8)
460     format (1X,F15.3,3X,F11.5,3X,F11.3,3X,F8.6,3X,F8.6)
c
        if (time .eq. 50000.0D0) goto 600
        time = time * 1.2D0
        if (time .gt. 50000.0D0) time = 50000.0D0
500     continue
600   close (6)
      end
c
c
      DOUBLE PRECISION FUNCTION EERFC(x)
c
c     This function will generate values of
c       e erfc(z) = exp(z*z) * erfc(z)
c
c     The code for the complementary error function was found in:
c     Press, W.H., B.P. Flannery, S.A. Teukolsky, and W.T. Vetterling,
c        Numerical Recipes, Cambridge University Press, N.Y., 198?,
c        pp. 155-165.
c
      real*8 x, erfc, Z, T
c
      Z = DABS(x)
      T = 1.0 / (1.0 + 0.5*Z)
      erfc = T*DEXP(-Z*Z-1.26551223+T*(1.00002368+T*(0.37409196+
     z   T*(0.09678418+T*(-0.18628806+T*(0.27886807+T*(-1.13520398+
     z   T*(1.48851587+T*(-0.82215223+T*0.17087277)))))))))
      if (x .LT. 0.0) then
        erfc = 2.0 - erfc
      endif
c
      eerfc = dexp(x*x) * erfc
      end
```

Coupled Intraparticle Diffusion and Particle Abrasion Model

```
      Program AQBRES
c
c     This program will calculate uptake data for the intraparticle
c       diffusion of organic compounds into spherical particles
c       suspended in water according to the following conditions:
c
c       1.  Particles are spherical.
c       2.  Particles have a nonporous, nonsorbing inner core
c            surrounded by a porous, sorbing shell.  The percent
c            volume that is porous is set by the user.
c       3.  The bulk concentration of analyte in the aqueous phase is
c            uniform.
c       4.  Particles initially contain a uniform concentration of
c            analyte within their micropores.
c       5.  Sorption is reversible and follows a linear isotherm.
c       6.  K and Deff are spatially invariant.
c       7.  Local equilibrium holds in the micropores of the particles.
c
c     The particle size distribution is input from another file.
c       That file is of the format:
c              diameter (cm),  number fraction
c       The number of sizes in the distribution is noted on the first
c       line of that file.
c
c     This program will also read in experimental data and calculate
c       the sum of the squared residuals between the calculated and
c       the experimental data.  The format of that file is:
c         time, aqueous concentration, volume withdrawn, code
c       time is in minutes, concentration is in ng/mL, volume is in
c         mL, and code tells whether or not the point will be used
c         or ignored in the computation of the residual (0 = ignore,
c         1 = use).
c       The number of points is noted on the first line of the file.
c
c     This version also can account for some sorption to the reaction
c       vessel, using instantaneous equilibrium denoted by
c           Krv = Mrv / C
c       Mrv is the mass of analyte sorbed to the reaction vessel.
c       Krv has units of volume.  Krv=0 for no sorption to the vessel.
c
c     This version also allows for "breakage" of the particles.  In
c       this formulation, the outer layers are allowed to wear off
c       according to a first order rate law.  Defining the number of
c       3-node shells that can be worn off as Nt, the first order
c       decrease in Nt is
c         Nt = NINT(N0 * EXP(-brate * time))
c       where the rate constant is brate (1/min), NINT() is a rounding
c       function, and N0 is the initial number of shells that can be
c       worn off (N0 = (grid - 3)/2).
c       Therefore, if sigma is the outermost node at time t,
c         sigma = 2 * NINT(((grid - 3) / 2) * exp(-brate*time)) + 3
c
      real*8 abmax, alpha, avgS, beadmass, Blast, brate, C, Cinit
      real*8 Csave, Csorb, deff, depth, dt, dtsave, dx, epsilon, eta
      real*8 gamma, K, Krv, mass, masstot, maxdt, mindt, number, omega
      real*8 pb, pi, pmasstot, pormass, poros, ps, residual, spike
      real*8 sumj, T4, temp, test, time, total, utemp
      real*8 B(7,2000), Conc(2,26), f(7), factor(7), numfract(7)
      real*8 radius(7), T1(7,2000,3), T3(7,2000), theta(7)
      real*8 tyme(26), u(7,2001), ut(7,2001), volfract(7)
      integer*4 code(26), flag, grid, i, j, Nt1, Nt2, npts, oldsig
      integer*4 sigma, sizes, stest, t, volume, volsamp(26)
      character*12 datfile, in1, in2, name*40, out1
c
      Common /CRUN1/ deff, dt, dx, epsilon, eta, f, factor, gamma, K
      Common /CRUN2/ Krv, omega, pb, poros, radius, grid, sigma, sizes
      Common /CRUN3/ theta, T1, T3, T4, volume
```

```
c
      External CRUNCH
c
      pi = 2.0D0 * DACOS(0.0D0)
c
c     Explanation of variable names:
c     abmax is the maximum time step allowed by abrasion.
c     alpha is the fraction of a particle's volume which is porous.
c     avgS is the average sorbed conc.
c     B(i,j) is the vector on the right hand side of the matrix equation
c     beadmass is the mass of sorbent (g).
c     Blast is the value of B for the last row.
c     brate is the first order breakage rate (1/min).
c     C is the analyte concentration in the water (ng/ml).
c     Cinit is the initial analyte concentration in the water (ng/ml).
c     code() is a code used in the calculation of the residual.
c       code() = 0 means ignore the point, 1 means use the point.
c     Csorb is the uniform analyte concentration initially in the
c       micropores of the particles -->> S=function(Csorb).
c     Conc() is the array which holds the calculated and experimental
c       concentrations that are compared.
c     datfile is the file containing the experimental data.
c     deff is the effective diffusion coefficient (sq.cm./sec.).
c     depth is the radial distance which is porous (cm)
c     dt is the time interval between computations (minutes).
c     dtsave is a saved value of the time step (min).
c     dx is the dimensionless distance between grid points.
c     epsilon is 1/((pb*K+poros)*omega) + (omega+eta)*(sum factor(i)).
c     eta is needed to correct for sorption to worn-off shells.
c       For the math, see CRUNCH.
c     f(i) is volfract(i)*beadmass*dx /(ps*(1-alpha*poros)).
c     factor(i) is f(i) / (volume + Krv).
c     gamma is a factor which is = (1-alpha)**(1/3).  It is also equal
c       to the ratio:  radius of the inner core / particle radius.
c     grid is the number of grid points in each particle.
c     i is the index for the particle size fraction.
c     in1 is the primary input file.
c     in2 is the file containing the size distribution data.
c     j is the index for the grid point of interest.
c     K is the aqueous partition coefficient.
c       K = S/C, (ml/g)
c     Krv is the partition coefficient for the reaction vessel.
c       Krv = Mrv / C, (mL)
c     mass is the mass of particles of a particular size (g/ml)
c     masstot is the calculated value of the solids concentration
c       (g/ml).  The only difference between beadmass/volume and
c       masstot is the fact that the sum of all volfract(i) may not
c       exactly equal 1.0.
c     maxdt is the maximum time step allowed (min.)
c     mindt is the minimum time step allowed (min.)
c     name is the analyte name.
c     npts is the number of experimental points.
c     Nt1 and Nt2 are abradable shell numbers used as tests.
c     number is the actual number of particles in a given size range.
c     numfract(i) is the number fraction of particles in size range i.
c     oldsig is the value of sigma before breakage.
c     omega is gamma + dx*(sigma-1)
c     out1 is the name of the output file.
c     pb is the estimated bulk density of the particles (g/cu.cm.).
c     pi is the irrational number 3.14159.....
c     pmasstot is the total mass of porous material (g/ml)
c     pormass is the total mass of the porous fraction of all particles
c       having a certain size (g/ml)
c     poros is the porosity = 1 - pb/ps
c     ps is the dry sorbent density (g/cu.cm.)
c     radius(i) is the mean radius of a particle (cm).
c     residual is the sum of the squared residuals.
c     sigma is the outermost grid point of the particles.
c     sizes is the number of particle sizes.
```

```
c     spike is the initial spike of analyte (ng).
c     stest is a test for changes in sigma.
c     T1, T3, and T4 are the arrays which hold the coefficient
c       matrix and the L and U decompositions of that matrix.
c       T1(i,j) handles the tridiagonal part of the matrix.
c       T3 is the bottom row, except for the last column.
c       T4 is the coefficient in the last row, last column.
c     theta(i) is 2(delta x)**2/(delta tao)
c     time is in minutes.
c     total is the total number of particles / ml.
c     tyme() is an array holding the times of experimental interest.
c     volfract(i) is the volume fraction (and the mass fraction) of
c       particles from the total distribution which fall in the size
c       range whose mean radius is radius(i).
c     volsamp() is the volume removed from the vessel for sampling (mL).
c     volume is the volume of aqueous solution (mL).
c     Csave, sumj, temp, test are all dummy variables which
c       are used to temporarily save values of interest.
c
c     Read in the values of deff, K, spike, Csorb, etc.
      Write (*,10) 'AQBRES',
     z  'A Simulation of Aqueous Sorption Kinetics',
     z  'Composite Particles:  Inner Nonporous Core / ',
     z  'Porous Outer Shell','First Order Wear Rate',
     z  'Stewart A. Rounds','February 15, 1992'
10    Format (/37X,A/20X,A/9X,A,A/30X,A//32X,A/32X,A//)
      Write (*,20) 'name of input file:  '
      Read (*,20) in1
20    Format (A)
c
      open (1,file=in1)
      Read (1,20) name
      Read (1,*) K
      Read (1,*) deff
      Read (1,*) spike
      Read (1,*) beadmass
      Read (1,*) volume
      Read (1,*) brate
      Read (1,*) Krv
      Read (1,*) Csorb
      Read (1,*) alpha
      Read (1,*) pb
      Read (1,*) ps
      Read (1,*) grid
      Read (1,*) dt
      Read (1,*) mindt
      Read (1,*) maxdt
      Read (1,20) datfile
      Read (1,20) in2
      Read (1,20) out1
      close (1)
c
c     Read in the number distribution of the particles.
c       The size data is given as the diameter, not the radius.
      open (3,file=in2)
      read (3,*) sizes
      temp = 0.0D0
      do 25 i=1,sizes
        read(3,*) radius(i), numfract(i)
        radius(i) = radius(i) / 2.0D0
        temp = temp + numfract(i) * radius(i) * radius(i) * radius(i)
25    continue
      close (3)
c
c     Calculate the volume distribution of the particles.
      do 26 i=1,sizes
        volfract(i) = numfract(i) * radius(i)*radius(i)*radius(i) /temp
26    continue
c
```

```
c     Read in the experimental data.
      open (3,file=datfile)
      read (3,*) npts
      do 27 i=1,npts
        read (3,*) tyme(i), Conc(1,i), volsamp(i), code(i)
27    continue
      close (3)
c
c     Calculate the initial concentration.
      Cinit = spike / (volume + Krv)
c
c     Calculate the porosity of the porous section.
      poros = 1.0D0 - pb / ps
c
c     Calculate gamma.
      gamma = (1.0D0 - alpha)**(1.0D0/3.0D0)
c
c     Print the relevant data to a file.
      open (4,file=out1)
      Write (4,20) name
      Write (4,31) 'macroscopic K = ',K,' ml/g'
c
c     Calculate the microscopic value of K.  This calculation accounts
c       for the fact that the macroscopic value of K is normalized to
c       the total particulate mass while the microscopic value of K is
c       based only on the particulate mass which is porous.
c
      K = K * (1.0D0 - alpha * poros) / (alpha * (1.0D0 - poros))
      Write (4,31) 'microscopic K = ',K,' ml/g'
      Write (4,31) 'Deff = ',deff,' sq.cm./sec'
      Write (4,31) 'spike = ',spike,' ng'
      Write (4,33) 'mass of beads = ',beadmass,' g'
      Write (4,36) 'initial volume = ',volume,' ml'
      Write (4,31) 'solids concentration = ',beadmass/volume,' g/ml'
      Write (4,31) 'wear rate = ',brate,' /minute'
      Write (4,31) 'K(reaction vessel) = ',Krv,' mL'
      Write (4,31) 'Cinit = ',Cinit,' ng/ml'
      Write (4,31) 'Csorb = ',Csorb,' ng/ml'
      Write (4,34) 'porous fraction = ',alpha
      Write (4,33) 'bulk density of porous section = ',pb,' g/cu.cm.'
      Write (4,33) 'dry density of nonporous section = ',ps,' g/cu.cm.'
      Write (4,34) 'porosity of porous section = ',poros
      Write (4,32) 'particle sizes = ',sizes
      Write (4,32) 'initial nodes / particle = ',grid
      Write (4,35) 'initial time step = ',dt,' min.'
      Write (4,35) 'minimum time step = ',mindt,' min.'
      Write (4,35) 'maximum time step = ',maxdt,' min.'
      Write (4,35) 'end of simulation = ',tyme(npts),' min.'
      Write (4,30) 'file for experimental data = ',datfile
      Write (4,30) 'file for size distribution = ',in2
30    Format (A,A)
31    Format (A,E12.6,A)
32    Format (A,I4)
33    Format (A,F8.5,A)
34    Format (A,F8.5)
35    Format (A,F14.7,A)
36    Format (A,I5,A)
c
c     Print the particle mass and number distributions to the file.
      write(4,37) 'Initial Particle Mass and Number Distribution Data:',
     z  'Radius (cm)','Shell (cm)','Number/ml',
     z  'Mass (g/ml)','Porous Mass (g/ml)'
37    format (//2X,A//A,3X,A,4X,A,5X,A,5X,A/)
      masstot = 0.0D0
      pmasstot = 0.0D0
      total = 0.0D0
      do 39 i=1,sizes
        mass = volfract(i) * beadmass / volume
        masstot = masstot + mass
```

```
        number = mass * 0.75D0 / (pi * radius(i) * radius(i) *
     z             radius(i) * ps * (1.0D0 - alpha * poros))
        total = total + number
        depth = radius(i) * (1.0D0 - gamma)
        pormass = mass *alpha *(1.0D0 - poros) /(1.0D0 - alpha*poros)
        pmasstot = pmasstot + pormass
        write (4,38) radius(i),depth,number,mass,pormass
38      format (F10.6,4X,F10.6,3X,E11.5,4X,E12.6,8X,E12.6)
39    continue
      write (4,41) 'Totals:', total, masstot, pmasstot
41    format (/A,19X,E12.5,4X,E12.6,8X,E12.6/)
c
      write (*,43) 'Working . . .'
43    format (/A/)
      write (4,44) '   Time (min)       C (ng/ml)       S (ng/g)',
     z             '      nodes        C/Co'
44    format (/A,A/)
c
c     Set the grid spacing and f(i).
      dx = (1.0D0 - gamma) / (grid - 1.0D0)
      do 50 i=1,sizes
        f(i) = volfract(i) *beadmass *dx / (ps *(1.0D0 - alpha *poros))
50    continue
c
c     Initialize the ut array.  Recall that u=x*Sstar
c     u and ut are in units of ng/ml
      do 60 i = 1,sizes
        do 55 j = 1,grid
          ut(i,j) = (dx*(j-1)+gamma) * (Csorb * (poros + pb*K))
55      continue
60    continue
c
c     Calculate the maximum initial time step allowed by abrasion.
      if (brate .gt. 0.0D0) then
        abmax = -1.0D0 * LOG(1.0D0 - (2.0D0 /(grid - 3.0D0))) / brate
      endif
c
c     Initialize time, t, residual, C, dt, dtsave, sigma.
      time = 0.0D0
      t = 1
      residual = 0.0D0
      C = Cinit
      sigma = grid
      stest = 2 * NINT(((grid - 3) / 2) * EXP(-brate*dt)) + 3
      if ((sigma - stest) .gt. 3) then
        dt = abmax
        if (dt .lt. mindt) mindt = dt
      endif
      if (dt .gt. tyme(1)) dt = tyme(1)
      if (dt .gt. maxdt) dt = maxdt
      dtsave = dt
c
c     Initialize theta(), factor(), and epsilon.  Set up the
c       coefficient matrix and perform an L-U decomposition.
      CALL CRUNCH
c
c     Start the simulation.
80    Csave = C
c
c     Initialize the u array.
      do 100 i=1,sizes
        do 90 j=1,sigma
          u(i,j) = ut(i,j)
90      continue
100   continue
c
c     Loop through the particle size distribution.
c     Set up the B vector.
110   do 130 i = 1,sizes
```

```
        B(i,1) = (1.000 + (gamma-dx)/(gamma+dx)) * ut(i,2)
     z                  - (2 - theta(i)) * ut(i,1)
        do 120 j = 2,(sigma - 1)
          B(i,j) = ut(i,j-1) - (2-theta(i)) * ut(i,j) + ut(i,j+1)
120     continue
130   continue
      Blast = C
      do 150 i = 1,sizes
        sumj = gamma * ut(i,1) + (omega + eta) * ut(i,sigma)
        do 140 j = 2,(sigma - 1)
          sumj = sumj + (dx * (j-1) + gamma) * (3 + (-1)**j) * ut(i,j)
140     continue
        Blast = Blast + factor(i) * sumj
150   continue
      Blast = Blast / epsilon
c
c     Forward substitution:
      do 170 i = 1,sizes
        ut(i,1) = B(i,1)
        do 160 j = 2,(sigma-1)
          ut(i,j) = B(i,j) - T1(i,j,1) * ut(i,j-1)
160     continue
170   continue
      ut(1,sigma) = Blast
      do 190 i = 1,sizes
        do 180 j = 1,(sigma-1)
          ut(1,sigma) = ut(1,sigma) - T3(i,j) * ut(i,j)
180     continue
190   continue
c
c     Backward substitution:
      ut(1,sigma) = ut(1,sigma) / T4
      do 210 i = sizes,1,-1
        ut(i,sigma-1) = (ut(i,sigma-1) + ut(1,sigma)) / T1(i,sigma-1,2)
        do 200 j = (sigma-2),1,-1
          ut(i,j) = (ut(i,j) - T1(i,j,3) * ut(i,j+1)) / T1(i,j,2)
200     continue
210   continue
c
c     Calculate the new bulk concentration.
      C = ut(1,sigma) / ((poros + pb*K) * omega)
c
c     Check the effect of the current time step.
      test = (C - Csave) / (Conc(1,npts) - Cinit)
      if ((test .gt. 0.04) .and. (dt .gt. mindt)) then
        dt = dt / 1.5D0
        if (dt .lt. mindt) dt = mindt
        C = Csave
        do 220 i=1,sizes
          do 215 j=1,sigma
            ut(i,j) = u(i,j)
215       continue
220     continue
        CALL CRUNCH
        goto 110
      endif
c
c     Update the values of ut(i,sigma), i>1; ut(i,j), j>sigma.
      do 230 i = 2,sizes
        ut(i,sigma) = ut(1,sigma)
230   continue
      do 240 i = 1,sizes
        do 235 j = (sigma+1),grid
          ut(i,j) = (gamma + dx * (j-1)) * ut(1,sigma) / omega
235     continue
240   continue
c
c     Increment the time.
      time = time + dt
```

```
c
c     Calculate average sorbed concentrations.
      avgS = 0.0D0
      do 450 i = 1,sizes
        sumj = gamma * ut(i,1) + ut(i,grid)
        do 440 j = 2, (grid - 1)
          sumj = sumj + (3+(-1)**j) * (dx*(j-1) + gamma) * ut(i,j)
440     continue
        avgS = avgS + volfract(i) * dx * sumj
450   continue
      avgS = avgS / (ps * (1 - alpha * poros))
c
      write (4,455) time, C, avgS, sigma, C/Cinit
455   format (2X,3(E12.6,4X),I5,4X,E12.6)
c
c     Calculate the maximum time step allowed by abrasion.
      if (brate .gt. 0.0D0) then
        abmax = 1.0D0 - (2.0D0 / (grid - 3.0D0)) * EXP(brate * time)
        abmax = -1.0D0 * LOG(abmax) / brate
      endif
c
      flag = 0
      if (time .eq. tyme(t)) then
        if (code(t) .gt. 0.5) then
          residual = residual + (C - Conc(1,t))**2.0D0
        endif
        Conc(2,t) = C
        volume = volume - volsamp(t)
        t = t + 1
        flag = 2
        dt = dtsave
      elseif ((test .lt. 0.002) .and. (dt .ne. maxdt)) then
        Nt1 = NINT(((grid - 3) / 2) * EXP(-brate * time))
        Nt2 = NINT(((grid - 3) / 2) * EXP(-brate * (time + dt*1.5)))
        if ((Nt1 - Nt2) .lt. 1.5) then
          dt = dt * 1.5D0
          if (dt .gt. maxdt) dt = maxdt
          flag = 1
        elseif ((2 * Nt1 - 3) .lt. sigma) then
          dt = abmax
          if (dt .gt. maxdt) dt = maxdt
          flag = 1
        endif
      endif
c
      if (time .lt. tyme(npts)) then
        dtsave = dt
        if ((time + dt) .gt. tyme(t)) then
          dt = tyme(t) - time
          if (flag .lt. 0.5) flag = 1
        endif
c
c       Test for particle "breakage."  Adjust the aqueous concentration
c         and the values of the ut array.
        stest = 2 * NINT(((grid - 3) / 2) * EXP(-brate*time)) + 3
        if (stest .lt. sigma) then
          if (flag .gt. 1.5) CALL CRUNCH
          oldsig = sigma
          sigma = stest
          utemp = epsilon * ut(1,oldsig)
          do 475 i = 1,sizes
            sumj = 0.0D0
            do 470 j = sigma,(oldsig-1)
              sumj = sumj + (gamma + dx*(j-1)) * (3+(-1)**j) * ut(i,j)
470         continue
            utemp = utemp + factor(i) * sumj
475       continue
          CALL CRUNCH
          ut(1,sigma) = utemp / epsilon
```

```
          C = ut(1,sigma) / ((pb * K + poros) * omega)
c
c         Update the values of ut(i,sigma), i>1; ut(i,j), j>sigma.
          do 480 i = 2,sizes
            ut(i,sigma) = ut(1,sigma)
480       continue
          do 485 i = 1,sizes
            do 483 j = (sigma+1),grid
              ut(i,j) = (gamma + dx * (j-1)) * ut(1,sigma) / omega
483         continue
485       continue
c
c         Calculate average sorbed concentrations.
          avgS = 0.0D0
          do 495 i = 1,sizes
            sumj = gamma * ut(i,1) + ut(i,grid)
            do 490 j = 2, (grid - 1)
              sumj = sumj + (3+(-1)**j) * (dx*(j-1) + gamma) * ut(i,j)
490         continue
            avgS = avgS + volfract(i) * dx * sumj
495       continue
          avgS = avgS / (ps * (1 - alpha * poros))
c
          write (4,455) time, C, avgS, sigma, C/Cinit
          flag = 0
        endif
c
        if (flag .gt. 0.5) CALL CRUNCH
        goto 80
      endif
c
      Write (4,500) 'Data Comparison:',
     z   'Time (min)     Conc. (expt)     Conc. (calc)     Code'
500   Format (//A//A)
      Write (4,510) (tyme(j), (Conc(i,j), i=1,2), code(j), j=1,npts)
510   Format (F10.2,5X,E12.6,5X,E12.6,6X,I1)
      Write (4,520) 'Code:  0 = ignore, 1 = use',
     z   'Sum of squared residuals = ',residual
520   Format (/A/A,E16.9)
c
      close (4)
      end
c
c
      SUBROUTINE CRUNCH
c
c     Set up the coefficient matrix and perform an L-U decomposition.
c
      real*8 deff, dt, dx, epsilon, eta, f(7), factor(7), gamma, K
      real*8 Krv, omega, poros, pb, radius(7), theta(7)
      real*8 T1(7,2000,3), T3(7,2000), T4
      integer*4 grid, i, j, sigma, sizes, volume
c
      Common /CRUN1/ deff, dt, dx, epsilon, eta, f, factor, gamma, K
      Common /CRUN2/ Krv, omega, pb, poros, radius, grid, sigma, sizes
      Common /CRUN3/ theta, T1, T3, T4, volume
c
      omega = gamma + dx * (sigma - 1)
      eta = 0.0D0
      if ((grid - sigma) .gt. 1.5) then
        do 640 j = (sigma+1),(grid-1)
          eta = eta + ((gamma + dx * (j-1))**2) * (3 + (-1)**j)
640     continue
        eta = ((eta + 1.0D0) / omega) + omega
      endif
      epsilon = 0.0D0
      do 650 i=1,sizes
        factor(i) = f(i) / (volume + Krv)
        epsilon = epsilon + factor(i)
```

```
650   continue
      epsilon = (omega + eta)* epsilon + (1.0D0 /((pb*K+poros)* omega))
c
      do 680 i=1,sizes
        theta(i) = 2 * dx * dx * radius(i)*radius(i) / (deff*dt*6.0D1)
        T1(i,1,1) = 0.0D0
        T1(i,1,2) = 2.0D0 + theta(i)
        T1(i,1,3) = -1.0D0 - (gamma-dx)/(gamma+dx)
        do 670 j = 2,(sigma-2)
          T1(i,j,1) = -1.0D0
          T1(i,j,2) = 2.0D0 + theta(i)
          T1(i,j,3) = -1.0D0
670     continue
        T1(i,sigma-1,1) = -1.0D0
        T1(i,sigma-1,2) = 2.0D0 + theta(i)
        T1(i,sigma-1,3) = 0.0D0
680   continue
c
      do 690 i = 1,sizes
        T3(i,1) = factor(i) * gamma / epsilon
        do 685 j = 2,(sigma-1)
          T3(i,j) = factor(i) * (dx*(j-1)+gamma) * (3+(-1)**j) /epsilon
685     continue
690   continue
c
c     L-U Decomposition:
c     Use Thomas Algorithm for T1.
      do 696 i=1,sizes
        do 695 j = 2,(sigma-1)
          T1(i,j,1) = T1(i,j,1) / T1(i,j-1,2)
          T1(i,j,2) = T1(i,j,2) - T1(i,j,1) * T1(i,j-1,3)
695     continue
696   continue
c
c     Decompose T3.
      do 701 i=1,sizes
        T3(i,1) = T3(i,1) / T1(i,1,2)
        do 700 j = 2,(sigma-1)
          T3(i,j) = (T3(i,j) - T3(i,j-1) * T1(i,j-1,3)) / T1(i,j,2)
700     continue
701   continue
c
c     Set up and decompose T4.
      T4 = 1.0D0
      do 705 i = 1,sizes
        T4 = T4 + T3(i,sigma-1)
705   continue
c
      return
      end
```

Coupled External Film Diffusion and Intraparticle Diffusion Model (Dual Resistance Model)

```
      Program DUALDIFF
c
c     This program will calculate uptake data for the intraparticle
c     diffusion of organic compounds into spherical particles which are
c     suspended in a well-stirred solution.  Diffusion across an
c     external boundary layer of thickness delta is included.
c
c     Assumptions of model:
c      1.  Particles are spherical.
c      2.  Particles are internally homogeneous.
c      3.  Concentration of solute in the bulk solution is always
c          uniform.
c      4.  Particles are initially free of solute.
c      5.  Particles are all of the same size.
c      6.  The partition coefficient and the effective diffusion
c          coefficient are spatially invariant.
c      7.  Sorption is controlled by linear isotherms.
c      8.  Sorption is reversible.
c      9.  Within the particles, local equilibrium holds.
c
c     The analytical solution used here can be found in:
c      Huang, T-C. and K-Y Li, "Ion Exchange Kinetics for Calcium
c        Radiotracer in a Batch System," Ind. Eng. Chem. Fundam.,
c        vol. 12, 1973, pp. 50-55.
c
      real*8 alpha, beadmass, beta, C, Co, Deff, denom, F1, F2
      real*8 fraction, ftol, gcrit, g1, g2, g(2000), HUANG, index
      real*8 K, kf, Krv, nexterm, numer, pb, pi, radius, Resid
      real*8 S, spike, test, time, xi, Conc(2,26), tyme(26)
      integer*4 code(26), i, iter, j, jcrit, last
      integer*4 npts, t, volinit, volume, volsamp(26)
      character*12 name*40, in1, out1, datfile
c
      Common /Param1/ alpha, xi
c
      External ZBRENT
      External HUANG
c
c     Define variables:
c     alpha is a dimensionless constant equal to volume/(beadmass*K).
c     beadmass is the mass of sorbent (g).
c     beta is Deff/radius^2 (1/min)
c     C is the aqueous conc. of solute, ng/ml.
c     Co is the initial aqueous conc. of solute, ng/ml.
c     Deff is the effective diffusion coefficient, cm^2/sec.
c     fraction is Mt/Me.
c     g(i) are the roots of an equation (see reference).
c     K is the partition coefficient (ml/g).
c     kf is the film mass transfer coefficient (cm/sec).
c     Krv is the partition coefficient that corrects for sorption
c       to the reaction vessel (mL).
c     pb is the bulk density of the sorbent (g/mL).
c     pi is the irrational number pi.
c     radius is the particle radius, cm.
c     S is the sorbed conc. of solute, ng/g.
c     spike is the amount of analyte injected (ng).
c     time is the time of simulation, minutes.
c     volume is the volume of solution (mL).
c     xi is the dimensionless number:
c       xi = radius*kf/(pb*K*Deff)
c
      pi = 2*dacos(0.0D0)
c
c     Read in the needed parameters from the user.
      Write(*,10) 'DUALDIFF',
```

```
     z  'Analytical Solution for Dual Resistance Model',
     z  'Monodisperse Particle Size Distribution',
     z  'Stewart A. Rounds','March 17, 1992'
10    format(///31X,A//13X,A/16X,A//27X,A/28X,A//)
c
      Write(*,20) 'Name of input file:  '
20    format(1X,A\)
      Read(*,25) in1
25    format (A)
c
      open (1,file=in1)
      Read (1,25) name
      Read (1,*) kf
      Read (1,*) K
      Read (1,*) Deff
      Read (1,*) radius
      Read (1,*) pb
      Read (1,*) spike
      Read (1,*) beadmass
      Read (1,*) volinit
      Read (1,*) Krv
      Read (1,25) datfile
      Read (1,25) out1
      close (1)
c
c     Read in the experimental data.
      open (3,file=datfile)
      read (3,*) npts
      do 27 i=1,npts
        read (3,*) tyme(i), Conc(1,i), volsamp(i), code(i)
27    continue
      close (3)
c
c     Initialize.
      t = 1
      volume = volinit + Krv
      Co = spike / (volinit + Krv)
      alpha = volume / (beadmass * K)
      beta = 60.0D0 * Deff / (radius * radius)
      xi = radius * kf / (pb * K * Deff)
      Resid = 0.0D0
      ftol = 0.00001D0
c
      open (6,file=out1)
c
c     Write input data to the output file:
      Write (6,105) name
      Write (6,106) 'kf = ',kf,' cm/sec'
      Write (6,106) 'K = ',K,' mL/g'
      Write (6,106) 'Deff = ',Deff,' sq.cm./sec'
      Write (6,106) 'spike = ',spike,' ng'
      Write (6,106) 'spike (effective) = ',Co * volinit,' ng'
      Write (6,106) 'Krv = ',Krv,' mL'
      Write (6,107) 'V = ',volinit,' mL'
      Write (6,107) 'V (effective) = ',volume,' mL'
      Write (6,106) 'Co = ',Co,' ng/mL'
      Write (6,106) 'm = ',beadmass,' g'
      Write (6,106) 'Sorbent to water ratio:  ',beadmass/volinit,' g/mL'
      Write (6,106) 'alpha = 1/(solids*K) = ',alpha,' '
      Write (6,106) 'beta = ',beta,' /min'
      Write (6,106) 'xi = ',xi,' '
      Write (6,104) 'file for experimental data = ',datfile
104   format (A,A)
105   format (A)
106   format (A,E12.5,A)
107   format (A,I5,A)
c
      Write(6,112) 'Dual Resistance Model:  Analytical Solution'
112   format(/A)
```

```
      Write(6,115) 'Time (min.)','C (ng/ml)','S (ng/g)','C/Co','Mt/Me'
115   format(/3X,A,5X,A,6X,A,6X,A,6X,A,7X,A/)
      Write(6,117) (time - time), Co
117   format(F15.3,3X,F11.5)
c
      Write(*,120) 'Working . . . '
120   format(/1X,A/)
c
c     Calculate the critical g value.
      last = 0
      gcrit = 0.0D0
      jcrit = 0
      if (xi .lt. 1.0D0) then
        gcrit = dsqrt(3.0D0 * xi / ((1.0D0 - xi) * alpha))
        if (gcrit .lt. (pi/2.0D0)) then
          jcrit = 1
          g1 = 1.00000000001D0 * gcrit
          g2 = 0.9999999999990 * (pi / 2.0D0)
          F1 = HUANG(g1)
          F2 = HUANG(g2)
          if ((F1 * F2) .lt. 0.0D0) then
            Call ZBRENT(HUANG,g1,g2,F1,F2,ftol,iter)
          else
            Write (*,120) 'Critical root not found.'
            stop
          endif
          g(1) = g2
          last = 1
          Write (*,275) 'Root number = ',last,'   iterations = ',iter
275       format ('+',A,I4,A,I4)
        endif
      endif
c
c     Start the simulation.
      index = -0.02
310   index = index + 0.02
      time = 10**index
      if (time .gt. tyme(t)) then
        time = tyme(t)
        index = log10(time)
      endif
c
      fraction = 1.0D0
      do 400 j=1,2000
        if (j .gt. last) then
          g1 = 1.00000000001D0 * (j - jcrit - 0.5D0) * pi
          g2 = 0.999999999999D0 * (j - jcrit + 0.5D0) * pi
          if ((g1 .lt. gcrit) .and. (g2 .gt. gcrit)) then
            if (jcrit .lt. 0.5) then
              g2 = 0.9999999999990 * gcrit
              jcrit = 1
            else
              g1 = 1.00000000001D0 * gcrit
            endif
          endif
          F1 = HUANG(g1)
          F2 = HUANG(g2)
          if ((F1 * F2) .lt. 0.0D0) then
            Call ZBRENT(HUANG,g1,g2,F1,F2,ftol,iter)
          else
            if ((g1 - gcrit) .gt. 10) then
              g(j) = g(j-1) + pi
              iter = 0
            else
              Write (*,120) 'Problem finding root.'
              stop
            endif
          endif
          g(j) = g2
```

```
          last = j
          Write (*,275) 'Root number = ',j,'   iterations = ',iter
        endif
        numer = 6.0D0*xi*xi*(1.0D0+alpha)*dexp(-beta*time*g(j)*g(j))
        denom = xi*xi *(9.0D0 + alpha * g(j) * g(j) + 9.0D0 / alpha)
        denom = denom - xi * g(j) * g(j) * (6.0D0 + alpha)
        denom = denom + alpha * g(j) * g(j) * g(j) * g(j)
        nexterm = numer / denom
        fraction = fraction - nexterm
        test = nexterm / fraction
        if (abs(test) .lt. 1.0D-7) goto 410
400   continue
c
410   write (*,424) 'time = ',time,' min.   Mt/Me = ',fraction,
     z    '    # of terms = ',j
424   format ('+',A,F15.3,A,F10.8,A,I4)
      C = Co * (1.0D0 - fraction * (1.0D0 / (1.0D0 + alpha)))
      S = (Co - C) * volume / beadmass
      if (j .eq. 2001) then
        write (6,461) time, C, S, C/Co, fraction
      else
        write (6,460) time, C, S, C/Co, fraction
      endif
460   format (F15.3,3X,F11.5,3X,F11.3,3X,F8.6,3X,F8.6)
461   format (F15.3,3X,F11.5,3X,F11.3,3X,F8.6,3X,F8.6,' *')
c
      if (time .eq. tyme(t)) then
        if (code(t) .gt. 0.5) then
          Resid = Resid + (C - Conc(1,t))**2.0D0
        endif
        Conc(2,t) = C
        t = t + 1
      endif
c
      if (time .lt. tyme(npts)) goto 310
c
      Write (6,500) 'Data Comparison:',
     z   'Time (min)     Conc. (expt)     Conc. (calc)     Code'
500   Format (//A//A)
      Write (6,510) (tyme(j), (Conc(i,j), i=1,2), code(j), j=1,npts)
510   Format (F10.2,5X,E12.6,5X,E12.6,6X,I1)
      Write (6,520) 'Code:  0 = ignore, 1 = use',
     z   'Sum of squared residuals = ', Resid
520   Format (/A/A,E16.9)
c
      close (6)
      end
c
c ***************************************************************************
c
      DOUBLE PRECISION FUNCTION HUANG(g)
c
      Real*8 calc1, calc2, g, alpha, xi
      Common /Param1/ alpha, xi
c
      calc1 = (3.0D0 * xi - alpha * g * g)
      calc1 = calc1 / (3.0D0 * xi + (xi - 1.0D0) * alpha * g * g)
      calc2 = dtan(g) / g
      HUANG = calc1 - calc2
      return
      end
c
c ***************************************************************************
c
      SUBROUTINE ZBRENT(FUNC,A,B,FA,FB,TOL,ITER)
c
c     Using Brent's method, find the root of a function FUNC known to
c     lie between A and B, whose function values are FA and FB,
c     respectively.  The root is returned as B, and will be accurate
```

```
c     to within an absolute error of TOL.  This routine
c     has been modified by SAR for use with a bracketing routine.
c
      INTEGER*4 ITER, ITMAX
      REAL*8 A, B, C, D, E, EPS, FA, FB, FC, FUNC
      REAL*8 P, Q, R, S, TOL, TOL1, XM
c
      PARAMETER (ITMAX = 100, EPS = 3.0D-8)
c
c     ITMAX is the maximum number of iterations, and EPS is a
c     representation of the machine floating point precision.
c
      FC=FB
      DO 11 ITER=0,ITMAX
        IF(FB*FC.GT.0.0D0) THEN
c
c         Rename A, B, C, and adjust bounding interval D.
c
          C=A
          FC=FA
          D=B-A
          E=D
        ENDIF
        IF(ABS(FC).LT.ABS(FB)) THEN
          A=B
          B=C
          C=A
          FA=FB
          FB=FC
          FC=FA
        ENDIF
        TOL1 = 2.0D0 * EPS * ABS(B) + 0.5D0 * TOL
        XM=0.5D0*(C-B)
c
c       Convergence check.
c
        IF (ABS(XM).LE.TOL1 .OR. FB.EQ.0.0D0) RETURN
        IF (ABS(E).GE.TOL1 .AND. ABS(FA).GT.ABS(FB)) THEN
c
c         Attempt the inverse quadratic interpolation.
c
          S=FB/FA
          IF (A.EQ.C) THEN
            P=2.0D0*XM*S
            Q=1.0D0-S
          ELSE
            Q=FA/FC
            R=FB/FC
            P=S*(2.0D0*XM*Q*(Q-R)-(B-A)*(R-1.0D0))
            Q=(Q-1.0D0)*(R-1.0D0)*(S-1.0D0)
          ENDIF
c
c         Check whether in bounds.
c
          IF (P.GT.0.0D0) Q=-Q
          P=ABS(P)
          IF (2.0D0*P .LT. MIN(3.0D0*XM*Q-ABS(TOL1*Q),ABS(E*Q))) THEN
c
c           Accept the interpolation.
c
            E=D
            D=P/Q
          ELSE
c
c           Interpolation failed, use bisection.
c
            D=XM
            E=D
          ENDIF
```

```
        ELSE
c
c         Bounds decreasing too slowly, use bisection.
c
          D=XM
          E=D
        ENDIF
c
c       Move last best guess to A.
c
        A=B
        FA=FB
c
c       Find the new value of the trial root.
c
        IF (ABS(D) .GT. TOL1) THEN
          B=B+D
        ELSE
          B=B+SIGN(TOL1,XM)
        ENDIF
        FB=FUNC(B)
11    CONTINUE
c
      WRITE (6,12) 'ZBRENT exceeding maximum iterations.'
12    FORMAT (A)
      RETURN
      END
```

VITA

The author was born in Evanston, Illinois in 1963. He spent most of his childhood in Evanston before moving with the family to Rockford, Illinois in 1976. He attended high school at Rockford Guilford High, graduating in 1981. During his formative years, his life was dominated by school and Boy Scouts. Besides his parents, the most influential people in his life were his Scoutmasters, Sam E. Sibley in Evanston and James Boeger in Rockford. The author became an Eagle Scout in 1980. From 1981 to 1984, summer vacations were spent on the staff of Philmont Scout Ranch, a backpacking high adventure base operated by the Boy Scouts in the mountains of northeastern New Mexico. Stewart graduated with honors from the University of Illinois (Urbana) in 1985 with a B.S. degree in chemistry. Upon graduation from U of I, the author spent an interesting summer doing research for a large chemical company, E. I. du Pont de Nemours & Co., Inc. in Wilmington, Delaware.

Stewart became a student at OGI in the Fall of 1985. He was awarded a National Science Foundation Graduate Fellowship in the Spring of 1986. Softball, Ultimate frisbee, and Student Council were added to his list of activities in 1986. Enjoyable stints of field work were performed in Yakima and in Seattle, Washington. As the unknowing copilot of the OGI/ESE flight team, the author participated in an experiment proving the inefficient flight aerodynamics of the departmental pickup truck. He successfully defended his thesis proposal in September of 1987. After serving as President of Student Council during the 1987-1988 academic year, the author resigned from the Council to devote all of his time to research. With preliminary research results, he won a Graduate Student Research Paper award in 1989 from the Environmental Chemistry Division of the American Chemical Society. He married his wife, Bernadine Bonn, in 1989. With his wife, he wrote and published a computer program (*DREAM*, 1990) that calculates groundwater flow for simple systems. He completed the requirements for the degree of Ph.D. in April of 1992.

Immediate post-graduate plans include finishing version 2.0 of *DREAM* and version 1.0 of *STREAM* (another computer program that calculates groundwater streamlines for simple systems), finding an interesting job in Portland, rediscovering Boy Scouts as an adult leader, and looking for a softball team that needs a good shortstop.

Bonn, B. A.; Rounds, S. A. *DREAM - Analytical Groundwater Flow Programs,* Lewis Publishers: Chelsea, MI, 1990.

Larson, R. A; Rounds, S. A. "Photochemistry in Aqueous Surface Layers: 1-Naphthol," In *Photochemistry of Environmental Aquatic Systems;* Zika, R. G., Cooper, W. J., Eds.; ACS Symposium Series 327; American Chemical Society: Washington, DC, 1987; pp. 206-214.

Bonn, B. A.; Rounds, S. A. "An Eulerian Approach for Calculating Streamlines," *Proceedings of the Fourth International Conference on Solving Ground Water Problems with Models;* National Water Well Association: Dublin, OH, 1989; pp. 49-67.

Rounds, S. A.; Bonn, B. A. "DREAM: A Menu-Driven Program that Calculates Drawdown, Streamlines, Velocity and Water Level Elevation," *Proceedings of the Fourth International Conference on Solving Ground Water Problems with Models;* National Water Well Association: Dublin, OH, 1989; pp. 329-350.

Rounds, S. A.; Pankow, J. F. "Application of a Radial Diffusion Model to Describe Gas/Particle Sorption Kinetics," *Environ. Sci. Technol.* **1990**, *24*, 1378-1386.

Rounds, S. A.; Pankow, J. F. "Direct Sample-to-Column Purging with Whole Column Cryotrapping (P/WCC) for the Determination of Volatile Organic Compounds in Water," In *Monitoring Water in the 1990s: Meeting New Challenges, ASTM 1102;* Hall, J. R., Glysson, G. D., Eds.; American Society for Testing and Materials: Philadelphia, PA, 1991.

Rounds, S. A.; Tiffany, B. A.; Pankow, J. F. "Description of Gas/Particle Sorption Kinetics with an Intraparticle Diffusion Model: Filter Desorption Experiments," submitted to *Environ. Sci. Technol.* **1992.**

Rounds, S. A.; Pankow, J. F. "Determination of Chlorinated Benzenes in Water by Purging Directly to a Capillary Column with Whole Column Cryotrapping and Electron Capture Detection," submitted to *J. High Res. Chromatog.* **1992.**